Volcanogenic floods in Iceland

An assessment of hazards and risks at Öræfajökull and on the Markarfljót outwash plain

Volcanogenic floods in Iceland

An assessment of hazards and risks at Öræfajökull and on the Markarfljót outwash plain

Edited by Emmanuel Pagneux, Magnús T. Gudmundsson,
Sigrún Karlsdóttir and Matthew J. Roberts

Cover design: IMO
Cover photo: Glacial outburst flood caused by the summit eruption of Eyjafjallajökull Volcano on April 14 2010 © Haukur Hlíðkvist Ómarsson
Layout: IMO

ISBN 978-9979-9975-7-3

Icelandic Meteorological Office
Bústaðavegur 7–9, 108 Reykjavik, Iceland
Web: en.vedur.is
Tel.: +354 522 6000

Institute of Earth Sciences, University of Iceland
Sturlugata 7, 101 Reykjavik, Iceland
Web: earthice.hi.is
Tel.: +354 525 4492

Department of Civil Protection and Emergency Management, National Commissioner of the Icelandic Police
Skúlagata 21, 101 Reykjavik, Iceland
Web: almannavarnir.is
Tel.: +354 444 2500

Printed in Iceland by Svansprent

Paper
Munken Polar 120/240 gsm

Recommended citations
Book:
Pagneux, E., Gudmundsson, M. T., Karlsdóttir, S., & Roberts, M. J. (Eds.) (2015). Volcanogenic floods in Iceland: An assessment of hazards and risks at Öræfajökull and on the Markarfljót outwash plain. Reykjavík: IMO, IES-UI, NCIP-DCPEM.

Individual chapters (example):
Roberts, M. J., & Gudmundsson, M. T. (2015). Öræfajökull Volcano: Geology and historical floods. In E. Pagneux, M. T. Gudmundsson, S. Karlsdóttir, & M. J. Roberts (Eds.), *Volcanogenic floods in Iceland: An assessment of hazards and risks at Öræfajökull and on the Markarfljót outwash plain* (pp. 17–44). Reykjavík: IMO, IES-UI, NCIP-DCPEM.

Authors

Eiríkur Gíslason	*Icelandic Meteorological Office, Process and Research Division*
Magnús T. Gudmundsson	*Nordic Volcanological Center, Institute of Earth Sciences, University of Iceland*
Ásdís Helgadóttir	*Icelandic Meteorological Office, Process and Research Division*
Þórdís Högnadóttir	*Nordic Volcanological Center, Institute of Earth Sciences, University of Iceland*
Esther H. Jensen	*Icelandic Meteorological Office, Process and Research Division*
Sigrún Karlsdóttir	*Icelandic Meteorological Office, Dir. General Office*
Eyjólfur Magnússon	*Nordic Volcanological Center, Institute of Earth Sciences, University of Iceland*
Emmanuel Pagneux	*Icelandic Meteorological Office, Process and Research Division*
Viðir Reynisson	*South Iceland Police, General Division*
Matthew J. Roberts	*Icelandic Meteorological Office, Warnings and Forecasting Division*

Project funding

The project was funded by the Icelandic Avalanche and Landslide Fund, the National Power Company, and the Icelandic Road and Coastal Administration.

Acknowledgements

The Editorial Board gratefully acknowledges the scholars and experts below who reviewed the book chapters and provided valuable feedback to their authors.

Dr. Stéphanie Defossez	*Associate Professor. University Montpellier 3, School of Human and Environmental Sciences, France*
Dr. Kristín M. Hákonardóttir	*Fluid dynamics, Verkís Consulting Engineers, Iceland*
Trausti Jónsson, Msc.	*Senior scientist, risk expert at Icelandic Meteorological Office*
Pr. Frédéric Leone	*University Montpellier 3, School of Human and Environmental Sciences, France*
Dr. Philip Marren	*Senior lecturer in physical Geography, University of Chester, Geography and Development Studies, UK*
Pr. Andrew J. Russell	*Newcastle University, School of Geography, Politics and Sociology, UK*
Dr. Haraldur Sigþórsson	*Head of Security Planning Department, Facilitation and Coordination Division, Icelandic Transport Authority*
Dr. Tómas Jóhannesson	*Senior scientist, glaciological research at Icelandic Meteorological Office*
Dr. Chris Waythomas	*Project chief at USGS, Water Resources Division program on Hydrologic Hazards and Processes at Alaska Volcano Observatory, USA*

TABLE OF CONTENTS

I. VOLCANOGENIC FLOODS IN ICELAND: AN EXPLORATION OF HAZARDS AND RISKS

Emmanuel Pagneux [*], Sigrún Karlsdóttir [*], Magnús T. Gudmundsson [**], Matthew J. Roberts [*] and Viðir Reynisson [***] [1]

[*] *Icelandic Meteorological Office*
[**] *Nordic Volcanological Centre, Institute of Earth Sciences, University of Iceland*
[***] *National Commissioner of the Icelandic Police, Department of Civil Protection and Emergency Management*

1. Introduction

This publication presents the results from an exploratory project on the risk assessment of glacial outburst floods (jökulhlaups) caused by volcanic eruptions in Iceland. Such floods result from the interaction of hot freshly erupted lava, tephra or hot gases with glacier ice and snow on the slopes of volcanoes.

Jökulhlaups related to volcanic activity, caused both directly by volcanic eruptions and indirectly through geothermal activity, are one of the main volcanogenic hazards in Iceland (Gudmundsson *et al.*, 2008). Over half of all Icelandic eruptions occur in ice covered volcanoes, resulting either directly or indirectly in jökulhlaups (Larsen *et al.*, 1998; Larsen, 2002). The magnitude and frequency of these events is variable. During the 19th and first half of the 20th century, major jökulhlaups were frequent, not least due to conditions at Grímsvötn, the most active volcano. In Grímsvötn, a large, geothermally sustained subglacial lake issued periodic floods with peak discharges of tens of thousands of cubic meters per second about once every 10 years, with some of these events being directly caused by eruptions (e.g. Björnsson, 2003). A source of truly catastrophic jökulhlaups throughout settlement history has been the Katla volcano, where the recurrence time of eruptions is about 50 years. The largest of these eruptions have caused rapidly rising floods with a maximum discharge 100–300,000 m^3/s (e.g. Tómasson, 1996; Larsen, 2000; Elíasson *et al.*, 2006).

The largest hazard and risk to life in volcanogenic floods occurs on populated slopes of large, steep-sided ice-clad volcanoes. This particular environment is found in Iceland on the foothills of Eyjafjallajökull, Snæfellsjökull and Öræfajökull volcanoes. The most severe events have occurred at Öræfajökull, which erupted in 1362 and 1727. On both occasions the eruptions and the associated floods lead to destruction, devastation and loss of life (Thorarinsson, 1958). In the last 20 years, volcanic unrest has resulted in several jökulhlaups that have caused significant damage, including Vatnajökull in 1996 (Haraldsson, 1997; Björnsson, 2003) and Eyjafjallajökull in 2010 (Þorkelsson, 2012; Magnússon *et al.*, 2012; Snorrason *et al.*, 2012). As half of the Icelandic volcanic systems considered active in the Holocene period are covered by ice (Figure I-1), and despite an expected reduction in ice cover due to climate change (Jóhannesson *et al.*, 2012), the threat posed by volcanogenic floods will persist for at least one or two centuries.

[1] Now at South Iceland Police, General Division

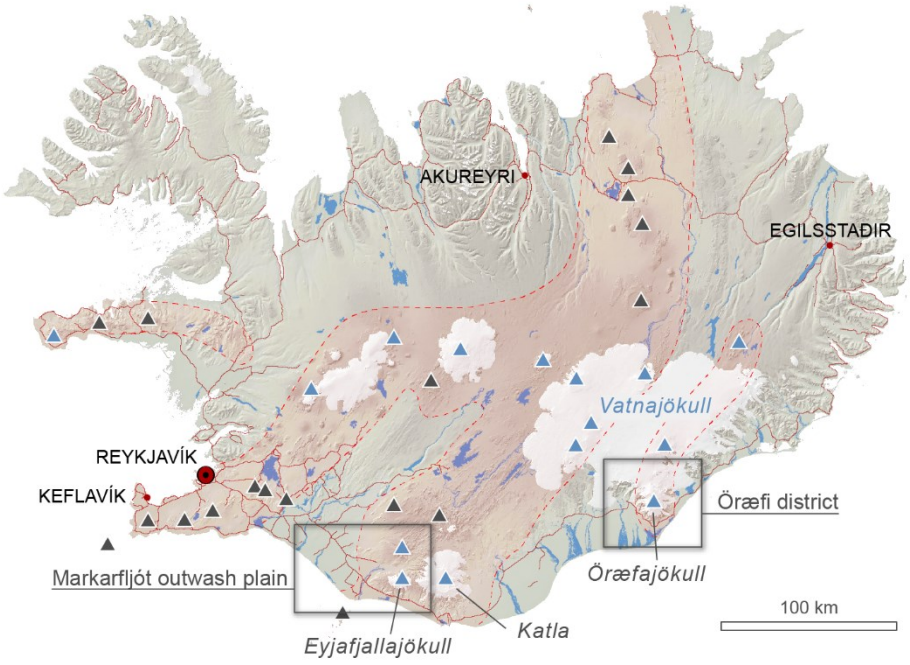

Figure I-1: Extent of the Icelandic volcanically active zones (semi-transparent red area bordered by a dashed line). The centres of the active volcanic systems are shown as triangles, coloured either in blue (ice-covered volcanoes) or black (ice-free). Location of the Markarfljót outwash plain and Öræfi district, the two areas studied in the project, is also shown.

2. Project description

2.1. The Icelandic volcanic risk assessment programme

The present project belongs to *Gosvá*, a national collaborative research programme on the assessment of volcanic hazard risks in Iceland led by the Icelandic Meteorological Office (IMO). The programme's steering committee is composed of representatives from IMO, the Institute of Earth Sciences (IES, University of Iceland), the Department of Civil Protection and Emergency Management of the National Commissioner of the Icelandic Police (NCIP-DCPEM), the Soil Conservation Service of Iceland (SCSI), and the Icelandic Road and Coastal Administration (IRCA).

Three additional projects have been conducted as part of the first phase of the programme: (i) An appraisal of the current knowledge of eruptive activity and potential volcanic hazards; (ii) an initial risk assessment of large explosive eruptions; and (iii) an initial risk assessment of volcanic eruptions that may cause extensive damage to property (i.e. eruptions in the vicinity of urban areas and international airports).

2.2. Financial support

This assessment project was funded mainly by the National Avalanche and Landslide Fund, with additional financial contributions from IRCA and the National Power Company.

2.3. Areas studied

The study was undertaken on the Markarfljót outwash plain and in the Öræfi district (Figure I-1), two regions of Iceland that have been subjected to volcanogenic floods in the last millennium. In the Markarfljót outwash plain (Figure I-2), the present project can be seen as a continuation of the extensive effort dedicated to the assessment of floods caused by eruptions of Katla (the volcano underlying Mýrdalsjökull) and Eyjafjallajökull performed in the years 2002–2005 (Guðmundsson and Gylfason, 2005). In the Öræfi district, this project is the first attempt to assess together the magnitude and impact of jökulhlaups on the inhabited slopes of Öræfajökull Volcano, situated west and south from the caldera (Figure I-3).

2.4. An exploration of both flood hazards and flood risks

Both the magnitude of volcanogenic floods and their impact were investigated in the project. Potential adverse consequences received particular attention, with the present project being the first attempt in Iceland to systematically map flood-damage potential as well as spatio-temporal patterns in population exposure. As regards the magnitude of floods, flood timings and routing, the methodologies set out in previous Katla and Eyjafjallajökull hazard assessments were applied (Guðmundsson and Gylfason, 2005; Guðmundsson and Högnadóttir, 2005).

Investigation of other direct volcanic hazards such as ash fall, lava flow, and gas emission are not part of the study presented here. Similar assessment of such hazards, which could have acute, far-reaching effects, is expected to be carried out in other phases of *Gosvá*. These hazards could also influence decisions about when and where to evacuate people at risk.

Exploring both flood hazards and flood risks is in line with the goals of the Icelandic authorities, which are committed to a comprehensive, self-standing regulation on the assessment and management of flood risks, comparable in its scope to the Icelandic regulation on avalanche risks (Arnalds *et al.*, 2004).

2.4.1. The International Strategy for Disaster Risk Reduction

Iceland is signatory to the Hyogo Framework for Action 2005-2015 (United Nations, 2005) and Sendai Framework for Disaster Risk Reduction 2015–2030 (United Nations, 2015). The International Strategy for Disaster Risk Reduction of the United Nations (UNISDR), to which the two above-mentioned frameworks apply, is the base for all the risk assessment projects that have been conducted by the Icelandic Meteorological Office on behalf of the Icelandic government.

2.4.2. The EU Floods Directive

The European Directive on the Assessment and Management of Flood Risks (European Parliament and Council, 2007) has at present not been implemented in Iceland. However, the comprehensive nature of the directive made it a framework well suited to structure the project as a coherent workflow of investigations, manifest in this book as a suite of thematic chapters (Table I-1; Figure I-4).

2.4.3. Acceptable risk

It is expected that recommendations on a legally binding acceptable risk will be formulated during the second phase of the volcanic risk programme, to be started in 2016. A new step towards a normalised, comprehensive risk assessment of volcanogenic floods in Iceland would be reached should the Icelandic Parliament validate such an approach.

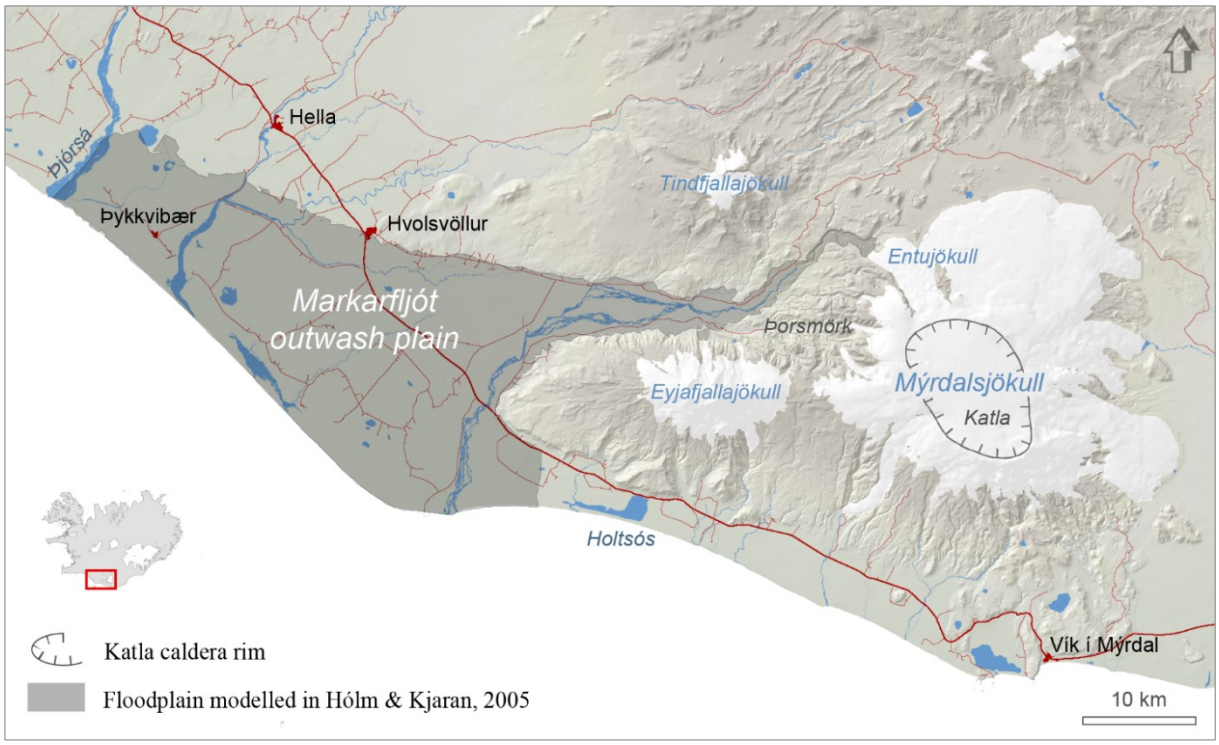

Figure I-2: Markarfljót outwash plain. The grey area shows the extent of a hypothetical 300,000m^3/s flood originating from the caldera of Katla Volcano (Hólm and Kjaran, 2005).

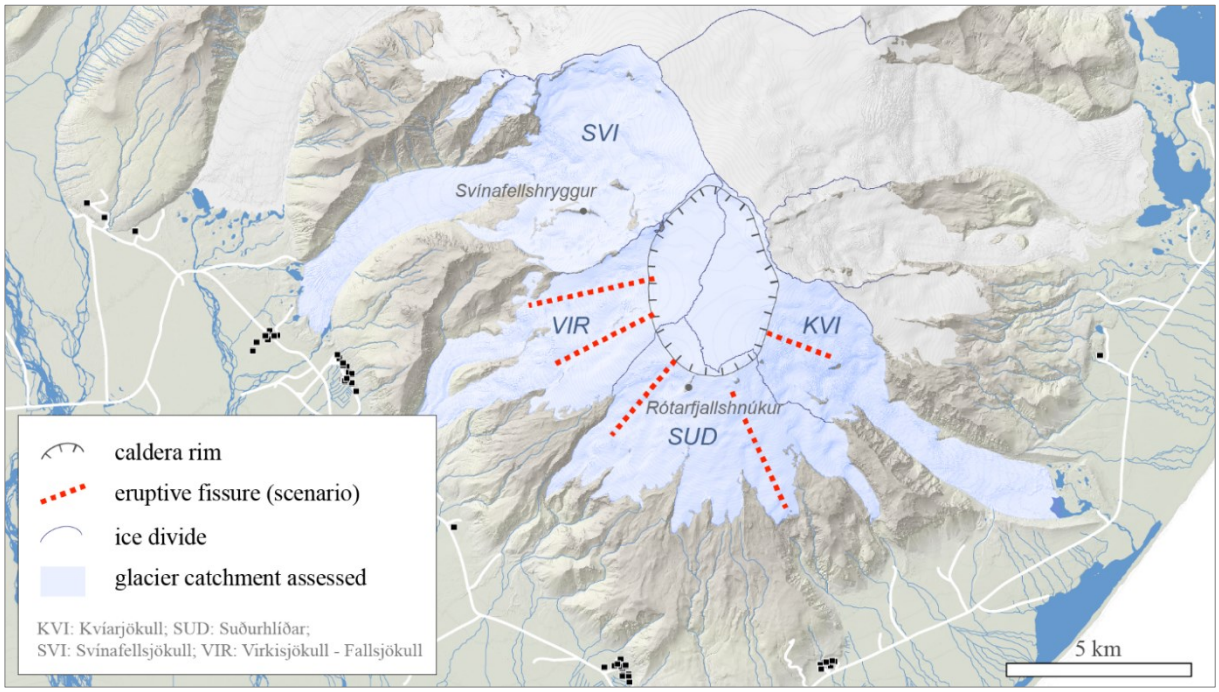

Figure I-3: Öræfajökull volcano (See Figure I-1 for general location). The glacier catchments examined in the project are shown in light blue, settlements as black dots. From chapter IV (Helgadóttir et al., 2015).

Table I-1: Correspondence between (i) the chapters featured in the book and (ii) the EU Floods Directive (2007/60/EC) phases.

Book		**2007/60/EC Directive**		
Chapters	*Subject(s) covered*	*Phase*	*Article (Alineas)*	*Key topic(s)*
II	Geology and historical floods	Preliminary flood risk assessment	4.2 (b)	Past floods and known impacts
III	Melting scenarios	Flood hazard maps and flood risk maps	6.3 (a,b)	Medium and low probability event scenarios
IV	Hydraulic simulations		6.4 (a,b,c)	Flood extent, water depths, flow velocities
V	Damage potential		6.4 (d)	Other useful information
VI	Population exposure		6.5 (a)	Indicative number of inhabitants potentially affected
VII	Evacuation time modelling	Flood risk management plans	7	Reduction of potential adverse consequences

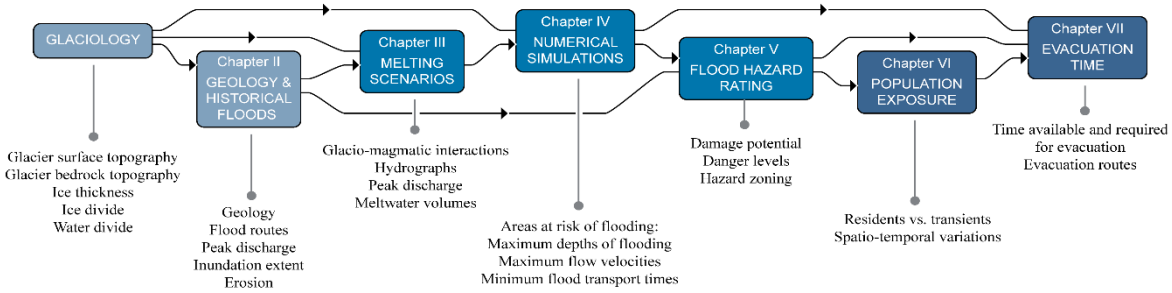

Figure I-4: Project workflow. Each chapter of the book covers a specific domain of investigation and links to the other chapters as a predecessor or as a follower.

3. Chapter overviews

Brief summaries of the subjects covered in the chapters are given below. Main findings are outlined in a separate section.

Chapter II. Öræfajökull Volcano: Geology and historical floods

A description of the geology of the Öræfajökull region and of the geomorphic impacts of volcanogenic floods caused by Öræfajökull eruptions in 1362 and 1727 CE is given in Chapter II (Roberts and Gudmundsson, 2015). Of the two known historical floods, the 1727 jökulhlaup is better documented, allowing estimates of the timing, size, and extent of the flood. These inferences are applied to the 1362 jökulhlaup, for which contemporary documentation is lacking. Using available descriptions, field observations, aerial photographs, and modern-day analogues, the duration, extent, composition, and maximum discharge of the jökulhlaups during these two events is approximated. The insight gained on the routing and maximum discharge of volcanogenic floods from Öræfajökull, is applied in Chapters III and IV.

Chapter III. Öræfajökull Volcano: Eruption melting scenarios

Chapter III (Gudmundsson *et al.*, 2015) assesses the ice melting to be expected during eruptions in Öræfajökull central volcano. Three main types of melting scenarios are

considered: (i) Caldera eruptions (ice thickness up to 500 m), (ii) flank eruptions (ice thickness <100 m), and (iii) surface melting by pyroclastic density currents in Plinian eruptions. Models of melting for thick ice (>200 m) and thin ice (<200 m) are presented based on empirical evidence and thermo-dynamic considerations. These models are applied to the slopes of Öræfajökull and serve as a basis in hazard assessment for events with peak discharges ranging from 10^4 m^3/s (flank eruptions) to 10^5 m^3/s (large caldera eruptions).

Chapter IV. Öræfajökull Volcano: Numerical simulations of eruption-induced jökulhlaups using the SAMOS flow model

Chapter IV (Helgadóttir *et al.*, 2015) identifies regions around Öræfajökull Volcano that would be liable to flooding during a subglacial eruption. Jökulhlaups are simulated as viscous fluids using the SAMOS 2D avalanche model (Zwinger *et al.*, 2003). Simulations are made for jökulhlaups caused by a caldera eruption, flank eruptions, and pyroclastic density currents using the melting scenarios developed in Chapter III. Information produced on inundation extent, maximum depths of flooding, maximum flow speeds and minimum surface transport times is used in the of rating flood hazards (Chapter V), assessment of the populations exposed to floods (Chapter VI), and modelling of evacuation time (Chapter VII).

Chapter V. Öræfi district and Markarfljót outwash plain: Rating of flood hazards

In Chapter V (Pagneux and Roberts, 2015), a provisional method for rating of flood hazards is proposed, followed by the designation of flood hazard zones in the Markarfljót outwash plain and the Öræfi district. The presence of life-threatening debris and the temperature of floodwater are considered, along with information on depths of flooding and/or flow velocities given in Chapter IV and Holm and Kjaran (2005). The aim of the study is to provide authorities with spatial information on flood danger levels and flood damage potential in the two study areas.

Chapter VI. Öræfi district and Markarfljót outwash plain: Spatio-temporal patterns in population exposure to volcanogenic floods

In Chapter VI (Pagneux, 2015a), a spatio-temporal exploration of population exposure is performed in the Markarfljót outwash plain and in the Öræfi district. Inventory of the populations exposed to floods is performed for night time, using daily overnights estimates weighted with road traffic data as an indicator. The main objective of the assessment is to provide authorities with a realistic estimate, at different periods of the year and at particular locations within the two studied areas, of the likely number of residents and guests potentially in the path of a flood or those that would be stranded due to flooding. Results of the assessment in the Öræfi district are used in Chapter VII to estimate the time required for a full evacuation of the areas liable to be flooded.

Chapter VII. Öræfajökull: Evacuation time modelling of areas prone to volcanogenic floods

An evacuation time model and evacuation routes for areas exposed to floods due to eruptive activity of Öræfajökull Volcano are presented in Chapter VII (Pagneux, 2015b). The aim of the study is to provide the authorities in charge of the emergency response with critical baseline estimates for the development of an effective flood evacuation plan.

4. Main findings

4.1. Öræfajökull

Öræfajökull is an ice-covered stratovolcano that has been and will remain a source of hazardous jökulhlaups in the event of an eruption:

1) The recurrence time of eruptions in the last several thousand years is in the range 500–1000 years.

2) The two known eruptions since settlement, in 1362 CE and 1727 CE caused major jökulhlaups that had a large impact on the lowlands through flooding, formation of sandur plains (outwash deltas) and large quantities of ice blocks that took years or decades to melt. The magnitude of the 1362 jökulhlaup was of order 100,000 m^3/s, whereas the 1727 flood was about half that size.

3) Volcanogenic jökulhlaups can be of three types, depending on source:

- Floods resulting from eruption in the caldera, where the ice is up to 500 m thick. Large eruptions can melt of order 100,000 m^3/s. Jökulhlaups can be expected from Virkisjökull-Falljökull or Kvíárjökull.
- Floods resulting from fissure eruptions on the upper flanks where the ice is 50–100 m thick. Expected melting in eruptions is in the range 1,000–10,000 m^3/s. Jökulhlaups of this type can happen anywhere on the slopes from Virkisjökull in the west to Hrútárjökull in the east.
- Floods resulting from hot (300–600°C) pyroclastic density currents in large explosive eruptions (as occurred in 1362 CE). The discharge may be in the range 1,000–20,000 m^3/s. Such jökulhlaups can occur anywhere on the slopes from Svínafellsjökull in the west to Hrútárjökull in the east.

4) Jökulhlaups caused by volcanic activity can be hyperconcentrated, carrying large quantities of sediment and ice down to the lowlands.

5) Jökulhlaups can be very swift, reaching the lowlands in as little as 20–30 minutes from the onset of an eruption.

6) A large part of the lowland between the rivers Skaftafellsá and Breiðá (340 km^2) is susceptible to flooding because of volcanogenic jökulhlaups descending the western and southern slopes of Öræfajökull.

7) Jökulhlaups from Öræfajökull can cause complete destruction or unrepairable damage to dwellings and outbuildings almost anywhere in sectors at risk of flooding. The potential impact of major floods on the local economy is therefore high.

8) If the largest of the potential floods assessed in this study where to happen **without warning and evacuation**, it is estimated that up to 130 people could be in severe danger and potentially lose their lives, with a further 240–250 people isolated due to destruction of sections of the road network. Proper monitoring and early warning systems with regularly updated response plans are therefore essential for the area around Öræfajökull.

9) During summer time, tourists represent the vast majority (up to 90 %) of the population staying overnight in areas susceptible to flooding or at risk of isolation.

10) Full evacuation of the populated areas cannot be achieved in less than 30–35 minutes.

4.2. Markarfljót outwash plain

Results of investigations into damage potential and population exposure are outlined next. Information on flood history, melting scenarios, propagation times and possible inundation extent can be found in Guðmundsson and Gylfason (2005).

1) Jökulhlaups can cause extensive damage to structures. The potential for complete destruction of inhabited buildings is possible over a very large portion of land (330 km^2), that covers the outwash plain almost from Entujökull Glacier down to road 255 (Akureyjarvegur).

2) More than one thousand people are located in the flood inundation zone and therefore at risk during the summer season when the number of tourists is highest, distributed over some 720 km^2 of land.

3) Partial destruction of the road network could leave about 600 people isolated in Fljótshlíð, Þórsmörk recreational area and in the lowlands flanking Eyjafjallajökull Volcano to the northwest, west and south-west.

4) Tourists and other temporary visitors represent up to 40% of the people in areas susceptible to flooding or at risk of isolation.

5. Recommendations

5.1. Management of flood risks

5.1.1. Monitoring and early warning

Maintaining risk at acceptably low levels during an eruption cannot be achieved without proper long-term monitoring of precursory signs of volcanic activity. An effective system of monitoring, early warning and regularly updated response plans is required for timely evacuation of the inhabited lowlands in the two regions.

Markarfljót: A system of early warning is already in place but it should be considered whether gaps or blind spots still exist.

Öræfajökull: Work on identifying and correcting possible weaknesses in the current monitoring system should be carried out and additions made as needed.

5.1.2. Land use and spatial planning

In order to increase the resilience of a region, actions to minimize the exposure to hazard need to be an integrated part of all land-use planning. It is beyond the scope of this project to address this issue. However, the full benefits of the assessment can only be achieved if it is ensured that the planning legislation and regulation take full account of the volcanic hazard and in particular the hazards from jökulhlaups.

5.1.3. Awareness raising and education

The continued expansion of tourism-related activities in the two volcanic areas is resulting in an increased number of people in close proximity to sites where volcanogenic flooding is possible. Ongoing awareness campaigns, both for residents and tourists, should form part of strategies for reducing volcanic risks.

5.2. Further research

The potential locations for volcanogenic floods in Iceland include many of the larger rivers issuing from glaciers in the volcanic zones. Further work is needed for many of these areas. This should include:

- Geological mapping of deposits and erosion from older floods to establish better magnitudes and recurrence times, and better assess flood damage potential.
- Extension of the existing results on melting potential for ice-covered regions to eruptions in western Vatnajökull, where historical records indicate repeated occurrence of jökulhlaups.
- Exploration of the melting potential for other areas, and on the basis of the volcanic history, assess the recurrence times and probabilities of volcanogenic jökulhlaups for different rivers.
- Further studying of the various scenarios of ice melting in subglacial eruptions, through both experimental and theoretical approaches. Better understanding is needed on e.g. the melting potential of pyroclastic density currents and effusive eruptions under thick ice.

Work, similar to that presented here on spatio-temporal patterns in population exposure and evacuation time modelling needs to be carried out for regions potentially at risk from other ice-covered volcanoes. It is expected that various local and regional factors will play a major role and further research is needed to assess these potential complications.

At Öræfajökull, post- and syn-eruptive floods should be further investigated, including:

- Flooding due to melting of snow and ice by lava or pyroclastic density currents on the eastern flanks of the volcano.
- Lahars caused by intense rainfall over tephra on the flanks of the volcano following an explosive eruption. Such lahars could occur anywhere on the volcano, irrespective of primary jökulhlaup paths.

Concerning jökulhlaup propagation modelling, the following issues should receive attention:

- Ice-block deposition is prevalent during volcanogenic floods. Further studies of the size and spatial distribution of ice-blocks from past eruptions is needed to help identify regions of high damage-potential.
- The sensitivity of propagation times to flow properties such as solid content (tephra, other debris), solid proportion and grain size, should be studied further. Such studies would allow for more accurate flood routing and better assessment of properties of past floods on the basis of their deposits.

6. References

Arnalds, Þ., Jónasson, K., & Sigurðsson, S. (2004). Avalanche hazard zoning in Iceland based on individual risk. *Annals of Glaciology, 38*, 285–290.

Björnsson, H. (2003). Subglacial lakes and jökulhlaups in Iceland. *Global and Planetary Change, 35*, 255–271.

Elíasson, J., Larsen, G., Gudmundsson, M. T., & Sigmundsson, F. (2006). Probabilistic model for eruptions and associated flood events in the Katla caldera, Iceland. *Computational Geosciences, 10*, 179–200.

European Parliament, & Council. (2007). Directive 2007/60/EC of the European Parliament and of the Council of 23 October 2007 on the assessment and management of flood risks. *Official Journal L288*, 27–34. Retrieved from http://eur-lex.europa.eu/legal-content/EN/TXT/PDF/?uri=CELEX:32007L0060&from=EN

Gudmundsson, M. T., & Högnadóttir, Þ. (2005). Ísbráðnun og upptakarennsli jökulhlaupa vegna eldgosa í Eyjafjallajökli og vestanverðum Mýrdalsjökli. (Ice melting and discharge of jökulhlaups due to eruptions in Eyjafjallajökull and the western part of Mýrdalsjökull). In M. T. Guðmundsson, & Á. G. Gylfason (Eds.), *Hættumat vegna eldgosa og hlaupa frá vestanverðum Mýrdalsjökli og Eyjafjallajökli (Hazard assessment of volcanic eruptions and glacial outbursts for Eyjafjallajökull and the western outwash plain of Mýrdalsjökull)* (pp. 159–180). Reykjavík: Ríkislögreglustjórinn, Háskólaútgáfan.

Gudmundsson, M. T., Högnadóttir, Þ., & Magnússon, E. (2015). Öræfajökull: Eruption melting scenarios. In E. Pagneux, M. T. Gudmundsson, S. Karlsdóttir, & M. J. Roberts (Eds.), *Volcanogenic floods in Iceland: An assessment of hazards and risks at Öræfajökull and on the Markarfljót outwash plain* (pp. 45–72). Reykjavík: IMO, IES-UI, NCIP-DCPEM.

Gudmundsson, M. T., Larsen, G., Höskuldsson, Á., & Gylfason, Á. G. (2008). Volcanic hazards in Iceland. *Jökull*, 58, 251–258.

Guðmundsson, M. T., & Gylfason, Á. G. (Eds.). (2005). *Hættumat vegna eldgosa og hlaupa frá vestanverðum Mýrdalsjökli og Eyjafjallajökli.* Reykjavík: Ríkislögreglustjórinn, Háskólaútgáfan.

Haraldsson, H. (Ed.). (1997). *Vatnajökull - Gos og hlaup 1996 (Vatnajökull — Eruption and Jökulhlaup 1996).* Reykjavík: The Icelandic Public Road Administration.

Helgadóttir, Á., Pagneux, E., Roberts, M. J., Jensen, E. H., & Gíslason, E. (2015). Öræfajökull Volcano: Numerical simulations of eruption-induced jökulhlaups using the SAMOS flow model. In E. Pagneux, M. T. Gudmundsson, S. Karlsdóttir, & M. J. Roberts (Eds.), *Volcanogenic floods in Iceland: An assessment of hazards and risks at Öræfajökull and on the Markarfljót outwash plain* (pp. 73–100). Reykjavík: IMO, IES-UI, NCIP-DCPEM.

Hólm, S. L., & Kjaran, S. P. (2005). Reiknilíkan fyrir útbreiðslu hlaupa úr Entujökli (Hydraulic model of floods from Entujökull). In M. T. Guðmundsson, & Á. G. Gylfason (Eds.), *Hættumat vegna eldgosa og hlaupa frá vestanverðum Mýrdalsjökli og Eyjafjallajökli (Hazard assessment of volcanic eruptions and glacial outbursts for Eyjafjallajökull and the western outwash plain of Mýrdalsjökull)* (pp. 197–210). Reykjavík: National Commissioner of Police.

Jóhannesson, T., Aðalgeirsdóttir, G., Ahlstrøm, A., Andreassen, L. M., Beldring, S., Björnsson, H., Crochet, P., Einarsson, B., Elvehøy, H., Guðmundsson, S., Hock, R., Machguth, H., Melvold, K., Pálsson, F., Radić, V., Sigurðsson, O., and Thorsteinsson, T. (2012). Hydropower, snow and ice. In T. Thorsteinsson, & H. Björnsson (Eds.), *Climage change and energy systems. Impacts, risks and adaptation in the Nordic and Baltic countries* (pp. 91–111). Copenhagen: Nordic Council of Ministers.

Larsen, G. (1998). Eight centuries of periodic volcanism at the center of the Iceland hot spot revelaed by glacier tephrastatigraphy. *Geology, 26*, 943-946.

Larsen, G. (2000). Holocene eruptions within the Katla volcanic system, south Iceland: Characteristics and environmental impact. *Jökull, 49*, 1–28.

Larsen, G. (2002). A brief overview of eruptions from ice-covered and ice-capped volcanic systems in Iceland during the past 11 centuries: frequency, periodicity and implications. In J. L. Smellie, & M. G. Chapman (Eds.), *Volcano Ice Interactions on Earth and Mars* (pp. 81–90). London: Geological Society.

Magnússon, E., Gudmundsson, M. T., Sigurdsson, G., Roberts, M. J., Höskuldsson, F., & Oddsson, B. (2012). Ice-volcano interactions during the 2010 Eyjafjallajökull eruption, as revealed by airborne radar. *J. Geophys. Res., 117, B07405*. doi:10.1029/2012JB009250

Pagneux, E. (2015a). Öræfi district and Markarfljót outwash plain: Spatio-temporal patterns in population exposure to volcanogenic floods. In E. Pagneux, M. T. Gudmundsson, S. Karlsdóttir, & M. J. Roberts (Eds.), *Volcanogenic floods in Iceland: An assessment of hazards and risks at Öræfajökull and on the Markarfljót outwash plain* (pp. 123–140). Reykjavík: IMO, IES-UI, NCIP-DCPEM.

Pagneux, E. (2015b). Öræfajökull: Evacuation time modelling of areas prone to volcanogenic floods. In E. Pagneux, M. T. Gudmundsson, S. Karlsdóttir, & M. J. Roberts (Eds.), *Volcanogenic floods in Iceland: An assessment of hazards and risks at Öræfajökull and on the Markarfljót outwash plain* (pp. 141–164). Reykjavík: IMO, IES-UI, NCIP-DCPEM.

Pagneux, E., & Roberts, M. J. (2015). Öræfi district and Markarfljót outwash plain: Rating of flood hazards. In E. Pagneux, M. T. Gudmundsson, S. Karlsdóttir, & M. J. Roberts (Eds.), *Volcanogenic floods in Iceland: An assessment of hazards and risks at Öræfajökull and on the Markarfljót outwash plain* (pp. 101–122). Reykjavík: IMO, IES-UI, NCIP-DCPEM.

Roberts, M. J., & Gudmundsson, M. T. (2015). Öræfajökull Volcano: Geology and historical floods. In E. Pagneux, M. T. Gudmundsson, S. Karlsdóttir, & M. J. Roberts (Eds.), *Volcanogenic floods in Iceland: An assessment of hazards and risks at Öræfajökull and on the Markarfljót outwash plain* (pp. 17–44). Reykjavík: IMO, IES-UI, NCIP-DCPEM.

Snorrason, Á., Einarsson, B., Pagneux, E., Hardardóttir, J., Roberts, M., Sigurðsson, O., Thórarinsson, Ó., Crochet, P., Jóhannesson, T., and Thorsteinsson, T. (2012). Floods in Iceland. In Z. W. Kundzewicz (Ed.), *Changes in flood risk in Europe* (pp. 257–276). IAHS Special Publication 10.

Thorarinsson, S. (1958). The Öræfajökull eruption of 1362. *Acta Naturalia Islandica, 2*(4), 100.

Tómasson, H. (1996). The Jökulhlaup from Katla in 1918. *Annals of Glaciology, 22*, 249–254.

United Nations. (2005). *Hyogo Framework for Action 2005-2015: Building the resilience of Nations and Communities to Disasters.* Geneva: The United Nations Office for Disaster Risk Reduction.

United Nations. (2015). *Sendai Framework for disaster Reduction 2015 - 2030.* Geneva: The United Nations Office for Disaster Risk Reduction.

Zwinger, T., Kluwick, A., & Sampl, P. (2003). Simulation of Dry-Snow Avalanche Flow over Natural Terrain. In K. Hutter, & N. Kirchner (Eds.), *Dynamic Response of Granular and Porous Materials under Large and Catastrophic Deformations* (Vol. 11, pp. 161–194). Heidelberg: Springer.

Þorkelsson, B. (Ed.). (2012). *The 2010 Eyjafjallajökull eruption, Iceland. Report to ICAO.* Reykjavík: Icelandic Meteorological Office.

II. ÖRÆFAJÖKULL VOLCANO: GEOLOGY AND HISTORICAL FLOODS

Matthew J. Roberts * and Magnús T. Gudmundsson **

** Icelandic Meteorological Office*
***Nordic Volcanological Centre, Institute of Earth Sciences, University of Iceland*

1. Introduction and scope

Glacial outburst floods (jökulhlaups[1]) are a potent hazard in the proximal and distal regions of an erupting subglacial volcano (Tilling, 1989; Roberts, 2005; Gudmundsson *et al.*, 2008). Besides meltwater, volcanogenic jökulhlaups comprise fragmented ice and primary and secondary volcaniclastic material (Major and Newhall, 1989; Tómasson, 1996). Such fluid-sediment mixtures can produce a variety of flow properties, ranging from turbulent, Newtonian discharge to cohesionless, hyper-concentrated torrents (Maizels, 1989). Moreover, volcanogenic jökulhlaups descending from steep, erodible slopes often produce sediment-laden flows by entraining debris dynamically (e.g. Naranjo *et al.*, 1986; Waythomas, 2015).

In 1362 CE, and again in 1727 CE, an explosive eruption at Öræfajökull — an ice-capped stratovolcano located on the southern coast of Iceland — resulted in a massive, short-lived jökulhlaup that caused fatalities and extensive damage to farmland (Thorarinsson, 1958). The Plinian eruption of 1362 is considered paroxysmal, equivalent to six on the volcano explosivity index (VEI) (Gudmundsson *et al.*, 2008), and the largest explosive eruption in Europe since Mount Vesuvius erupted in 79 CE. The following eruption of Öræfajökull, 365 years later in 1727, is thought to have been VEI ~4 in magnitude. Eyewitness accounts of the 1727 jökulhlaup depicts a scene where floodwater rushed from high on the side of Öræfajökull to the adjacent floodplain (sandur) within tens of minutes (Thorarinsson, 1958 and references therein). During both historical floods, water burst from two sets of combined glaciers: Falljökull and Virkisjökull (herein referred to as Falljökull) and Kotárjökull, and Rótarfjallsjökull (herein referred to as Kotárjökull), as shown in Figure II-1. There is also credible evidence of jökulhlaup activity on the southern flanks of the ice-cap (Höskuldsson, personal communication, October 2015), including a possible pre-historical route via Kvíárjökull (Thorarinsson, 1958; Iturrizaga, 2008). Remarkably, both historical floods deposited blocks of glacial ice on the sandur that took decades to melt. In several cases, these stranded masses were renamed as glaciers as they melted amongst jökulhlaup deposits (Sigurðsson and Williams, 2008).

Despite the documented severity and lasting geomorphic imprint of the 1362 and 1727 jökulhlaups, there is scant information about the routing and extent of these floods. Using published descriptions, field observations, aerial photographs, and modern-day analogues, we reconstruct the 1362 and 1727 jökulhlaups. The goal is to constrain the duration, extent, composition, and maximum discharge of the two floods. The results

[1] Note that the terms jökulhlaup and flood are used interchangeably in this chapter when describing lahar-type flows from Öræfajökull.

provide new insight into the routing and maximum discharge of volcanogenic floods from Öræfajökull, thereby contributing toward hazard assessment in the region (Helgadóttir *et al.*, 2015, Chapter IV) and (Pagneux and Roberts, 2015, Chapter V).

A geological overview of Öræfajökull is presented next, summarising the stratigraphy, ice cover, and Holocene eruptive activity of the volcano. This is followed by descriptions of the 1362 and 1727 jökulhlaups. The chapter concludes by considering hazard-related issues, including (i) floodwater routing, timing, and extent; (ii) flow properties; (iii) maximum discharge; and (iv) modern-day comparisons.

2. Geological overview

The Öræfajökull volcano is located about 50 km southeast of the active rift zone in Iceland forming, together with Esjufjöll and Snæfell, a 120 km long, discontinuous volcanic flank zone (Sæmundsson, 1979; Björnsson and Einarsson, 1990; Sigmundsson, 2006). Öræfajökull is the highest volcano in Iceland, rising from sea level to over 2,100 m to form Iceland's highest peak, Hvannadalshnjúkur (~2110 m AMSL) (Figures II-1 and II-2). The mountain massif of Öræfajökull is elongated slightly, with a north-south base diameter of 25 km, while the east-west basal diameter is about 20 km.

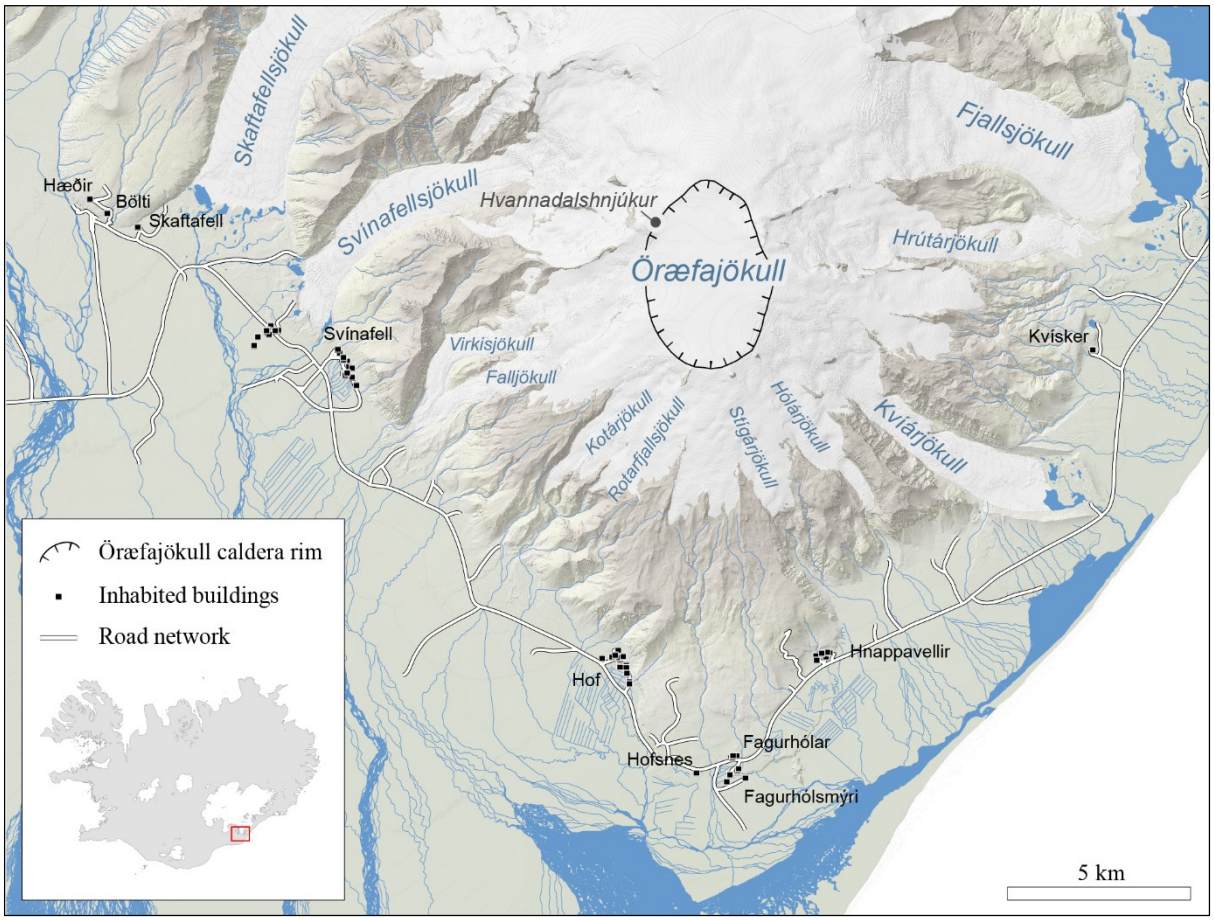

Figure II-1: Location of Öræfajökull, an ice-capped stratovolcano in south-east Iceland. The summit of the ice cap, Hvannadalshnjúkur, is ~2110 m AMSL and the highest point in Iceland. Radio-echo sounding measurements from the surface of the ice cap show that ice within the caldera is up to 540 m thick (Magnússon et al., 2012b). The magnitude of the 1362 eruption may have caused deepening and widening of the volcano's caldera. Both historical eruptions occurred either within the caldera or on its rim; however, in 1362 most flooding came from Falljökull, implying that the eruption site was within the caldera.

A 14 km^2 summit caldera exists in the southern part of the massif (Figures II-1 and II-2). The ice-covered upper part of Öræfajökull is the southernmost region of Vatnajökull, connected to the main ice-cap at Hermannaskarð. Valley glaciers from the extensively eroded northern part of Öræfajökull have progressively carved overdeepened valleys, resulting in up to 550-m-thick valley glaciers such as Svínafells-jökull (Figures II-1 and II-2; Magnússon *et al.*, 2012b).

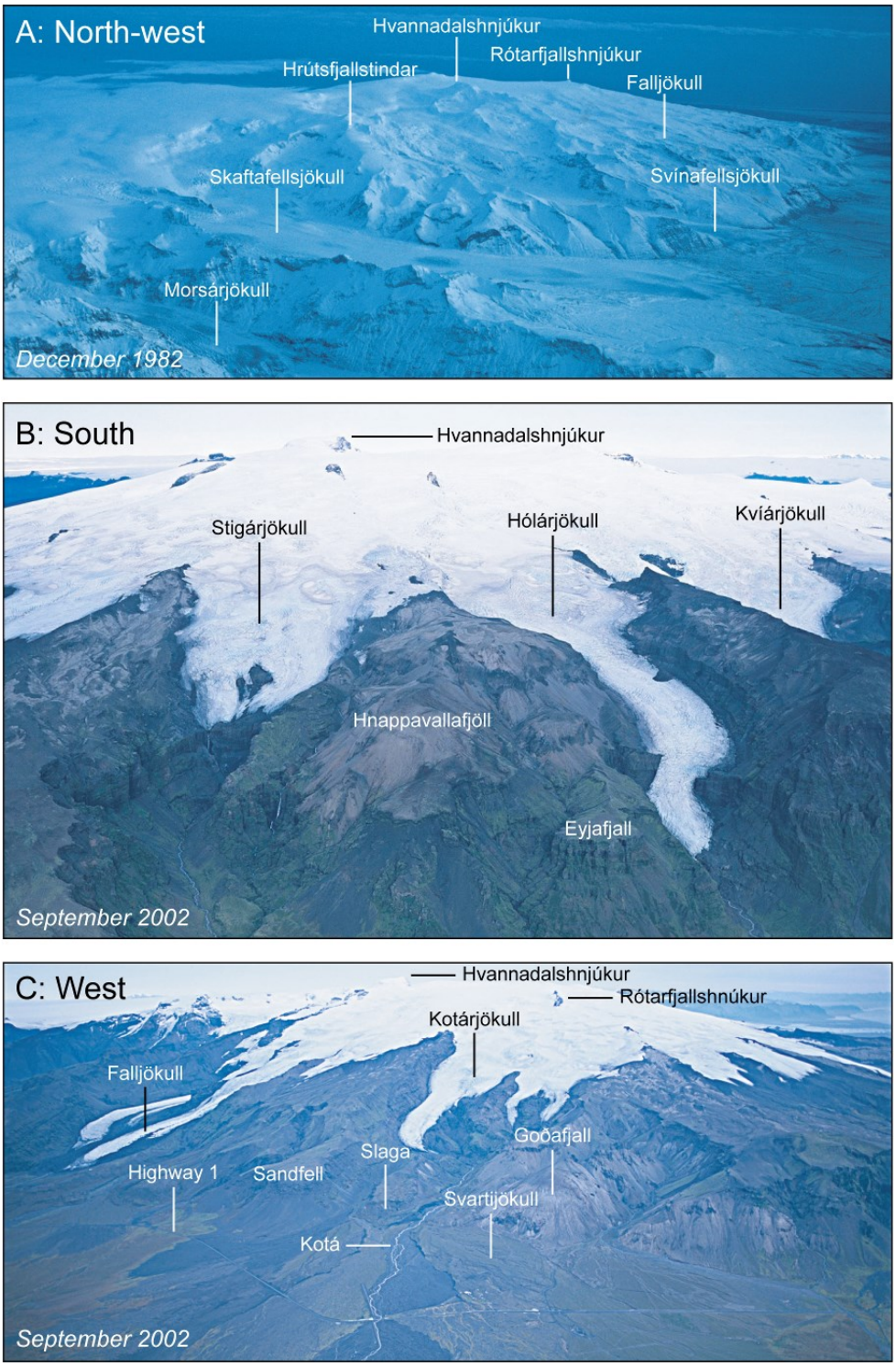

Figure II-2: Oblique aerial photographs of Öræfajökull. (A) View from the north-west; (B) southern flank; and (C) western flank. Photographer: O. Sigurðsson.

2.1. Stratigraphy

The oldest rocks are found in the northern part of the Öræfajökull massif, with the volcanic strata becoming progressively younger on the volcano's southern side. A boundary occurs roughly along a line between Svínafellsjökull, Tjaldskarð and Fjallsjökull. To the north of this line the rocks are predominantly from the Matuyama magnetic chron (2.58–0.78 Ma) or older, as deduced from pronounced magnetic lows in aeromagnetic surveys (Jónsson *et al.*, 1991) and confirmed by stratigraphic mapping and radiometric dating (Helgason, 2007; Helgason and Duncan, 2001). South of the divide is the presently active Öræfajökull stratovolcano, comprising normally magnetized rocks from the Brunhes chron (<0.78 Ma). The oldest dated rocks found near the base of Svínafell have an Ar-Ar age of 0.76 Ma (Helgason and Duncan, 2001; Helgason, 2007).

Thorarinsson (1958) published chemical analyses of the 1362 tephra from Öræfajökull; he also described the overall morphology and geology of the volcano. Torfason (1985) compiled a geological map of southeast Iceland, including Öræfajökull. Later stratigraphy work was undertaken by Helgason and Duncan (2001, 2013) on the northern parts of the massif. The petrology of Öræfajökull was considered by Prestvik (1982), whereas Stevenson *et al.* (2006) analysed the physical volcanology of a large Pleistocene rhyolitic lava flow on the southeast side of the volcano. Jakobsson *et al.* (2008) classified the Öræfajökull central volcano as belonging to the transitional alkalic series, together with other volcanoes in the Öræfajökull-Snæfell flank zone. Other notable studies include that of Gudmundsson (1998) who used tephrochronology to study the Holocene volcanic history of Öræfi. Björnsson (1988) published the first results of radio-echo soundings from a north-south traverse and measured the depth of the 14 km^2 summit caldera. Magnússon *et al.* (2012b) performed an extensive radio-echo survey on Öræfajökull, deriving ice thickness for the caldera and the upper and lower areas of the valley glaciers; the study's results are summarised in § 2.2.

Some of the nunataks on the caldera rim are made of rhyolites. Rhyolite formations are also found on the lower southwest slopes and on the eastern side where the Vatnafjöll ridge to the north of Kvíárjökull is made partly of a massive rhyolitic lava flow (Stevenson *et al.*, 2006). For the most part, the lower slopes consist of hyaloclastites and lava flows of basaltic to intermediate composition. In summary, eruptions contributing to the growth of the edifice are thought to have occurred mainly during glacial periods. This is also apparent in the form of the lower slopes of Öræfajökull, which are steeper than the upper slopes, suggesting partial confinement by glacial ice during extended periods over the volcano's existence.

2.2. Ice cover

The upper parts of Öræfajökull, south of Hermannaskarð, have a mean slope angle of 15 degrees, with glacial ice covering most of the volcano above about 1000 m AMSL. The summit plateau between Hvannadalshnjúkur, Snæbreið and Hnappar has an elevation of 1800–1850 m AMSL. The plateau is the surface expression of the 14 km^2 summit caldera, containing 3.9 km^3 of ice at depths of up to 540 m in the caldera centre (Magnússon *et al.*, 2012b). Ice flows out of the caldera in all directions, although mostly westwards to Falljökull and southeast to Kvíárjökull.

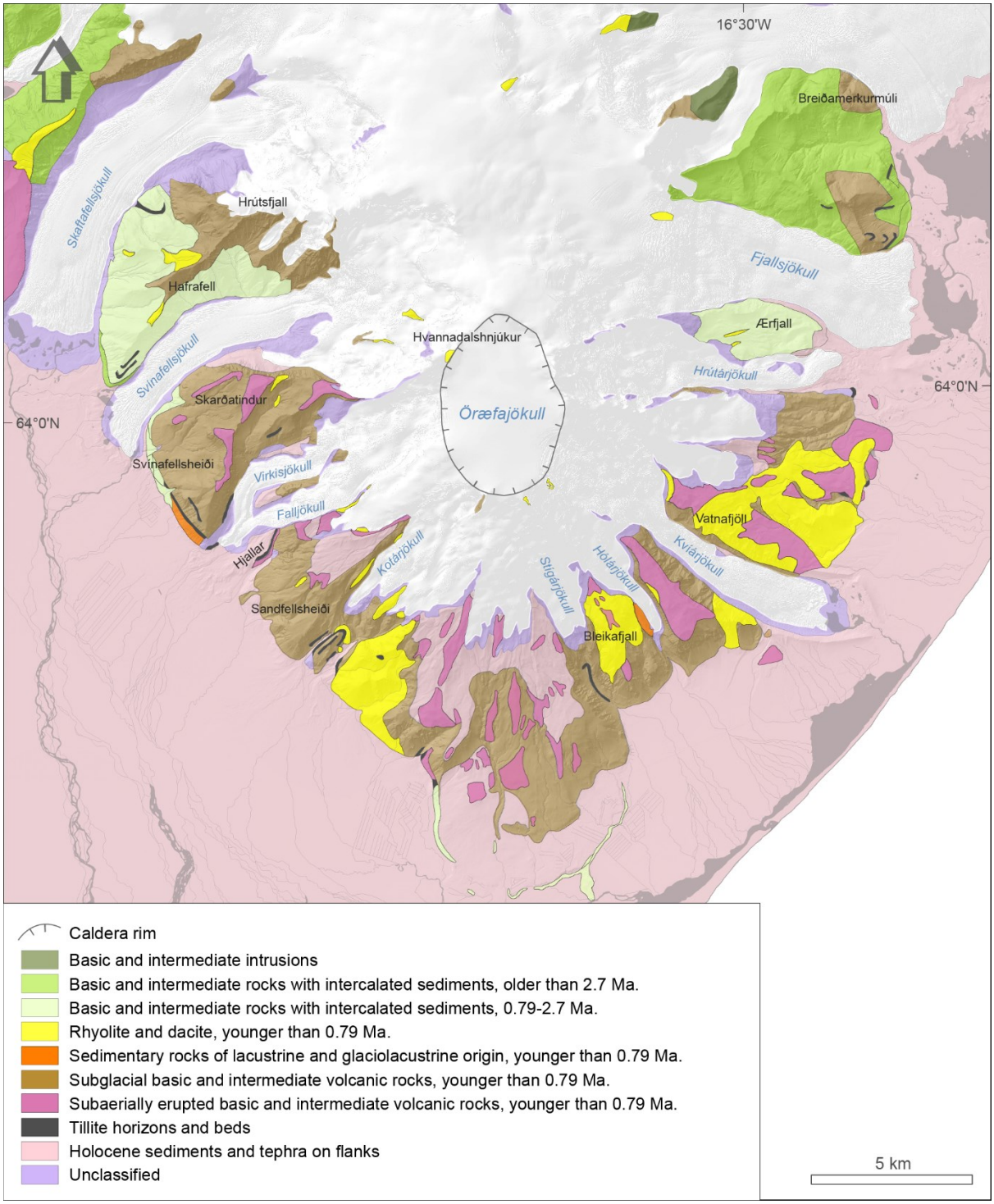

Figure II-3: Geological map of Öræfajökull (modified from Torfason, 1985).

A small area near the southwest margin of the caldera drains to Kotárjökull. Radio-echo soundings reveal that the lowest bedrock points are where Falljökull and Kviárjökull drain out of the caldera. These low points are 270–290 m higher than the base of the caldera.

The steep-sloping ice falls of Falljökull and Kviárjökull result in ice thicknesses of 50–100 m. Thicker ice exists near to the termini of the valley glaciers, some of which have eroded deep bedrock troughs (Magnússon *et al.*, 2012b).

2.3. Volcanic production rate and Holocene activity

The total volume of rocks above sea level south of Hermannaskarð is about 370 km^3. The volume of ice in the same area is 25–30 km^3. Of the 370 km^3 massif, it appears that roughly half the volume belongs to the present volcano, younger than 0.79 Ma. A rough, lower bound for the production rate of the volcano may be obtained by assuming that the present edifice has been built incrementally during this period. Consequently, the rate of volume growth is about quarter of a cubic kilometre every thousand years. However, the long-term mean eruption rate must have been considerably higher given the erosive effects of repeated glaciations and jökulhlaups.

The two historic eruptions of 1362 and 1727 are discussed in more detail later, but the first one is considered to be the largest explosive eruption in Iceland in the last 1100 years. Selbekk and Trønnes (2007) described rhyolitic tephra from 1362 as fine-grained vesicular glass, indicative of fast magma ascent to form a Plinian eruption plume. Rhyolitic tephra fell over large parts of Iceland during the 1362 eruption, although the main area of deposition was oriented out to sea, with a dispersal axis towards the east-southeast (Thorarinsson, 1958). Thorarinsson (1958) estimated the bulk volume of freshly fallen tephra at 10 km^3. Deposits of pyroclastic density currents have been found on the slopes and lowlands to the south and southwest of the volcano (Höskuldsson and Thordarson, 2006, 2007).

Holocene volcanic activity before the 1362 eruption was modest, with two minor lava flows on the east side of the volcano. One is on the lowlands west of Kvíárjökull while the other is higher up on the slopes in Vatnafjöll on the north side of Kvíárjökull. Tephrochronology of soils around Öræfajökull has been studied, suggesting that a few, relatively small rhyolitic eruptions occurred during the period (Guðmundsson, 1998). Thus, apart from the 1362 eruption, activity in Öræfajökull has been modest in Holocene times. It has been proposed that a trachyandesite lava-flow by the northern side of Kotárjökull, on the eastern side of Mount Slaga, is an ice-confined lava, emplaced during the 1727 eruption (Forbes *et al.*, 2014). This location is also the same area where floodwater burst from Kotárjökull in 1727 (§ 5.3).

3. Jökulhlaups due to eruptions of Öræfajökull

Since Norsemen first settled Iceland in the late 9th Century CE, there are two written accounts of volcanic activity at Öræfajökull. Before the 1362 eruption the ice-cap was known as Knappafellsjökull, but in the aftermath of the eruption the name was changed to Öræfajökull in recognition of the devastation wreaked by the eruption (Thorarinsson, 1958). Before 1362, the lowlands flanking Öræfajökull hosted fertile grazing land, which supported at least 40 farms in a regional settlement known formerly as Litlahérað (Ives, 1991 and references therein).

Deposits from pyroclastic density currents have been identified in the lowlands as belonging to the 1362 eruption. Tephra fall was prevalent during both historical eruptions, particularly in 1362. Excavations of relic dwellings to the immediate south and west of the volcano show that, during the onset of 1362 eruption, several pyroclastic surges occurred (Höskuldsson and Thordarson, 2007), followed by extensive fall-out of rhyolitic ash (Thorarinsson, 1958). A wider examination of the region (Höskuldsson, 2012), reveals that pyroclastic density currents from the 1362 eruption reached a distance of over 10 km from the centre of the caldera (Gudmundsson *et al.*, 2008). In this chapter, only deposits due to jökulhlaups are considered; however it should be borne in mind that tephra-related hazards were probably responsible for the apparent total destruction of Litlahérað.

4. Methods

Several methods were used to reconstruct the timing, routing, and geomorphic impact of the 1362 and 1727 jökulhlaups. The sequence of events for both jökulhlaups was pieced together mainly from published sources, as explained in § 4.1. Similarly, palaeo-estimates of subaerial floodwater routing and floodwater extent at maximum discharge were derived from published sources, as well as an examination of aerial photographs (§ 4.2). The same mosaic of images was used to map coarse-scale flood deposits and features (§ 4.3). The following sub-sections outline the methodological details of each approach.

4.1. Historical accounts

The pioneering monograph by Thorarinsson (1958) is the foremost resource about the 1362 jökulhlaup; this source is used extensively here. Detailed first-hand accounts of the 1727 jökulhlaup exist (Thorarinsson, 1958 and references therein), and they are used here to infer how the 1362 jökulhlaup developed. Likewise, qualitative comparisons are made with volcanogenic jökulhlaup in Iceland from 1918 onwards (§ 10).

4.2. Geomorphic mapping

A digital surface model (DSM) and high-resolution aerial photographs were used to identify and map flood deposits to the west and south of Öræfajökull. The DSM was derived from an airborne LIDAR survey of the region, performed during the summers of 2011 and 2012. The horizontal and vertical accuracy of the initial scan was <0.5 m. These measurements were used to create a DSM that depicted surface features exceeding 1 m^2 in area. The DSM was also used to measure the depth of kettle-holes and to extract cross-sectional profiles. In this context, the estimated vertical accuracy of the model is <0.5 m. For details of the LIDAR survey and data handling, see Jóhannesson *et al.* (2013).

Flood deposits and erosional features were studied during fieldwork that was carried out in 2003, 2005, and 2006 (Figure II-4). Features including kettle-holes, boulder clusters, and terraces were mapped using a *Trimble Pathfinder* backpack-mounted GPS.

A differential correction was applied to the data using continuous measurements from a fixed GPS site in Reykjavík (baseline distance: ~247 km). The calculated accuracy of the results is ~0.7 m horizontally and ~1.3 m vertically. Geomorphic features were identified from aerial photographs (§ 4.3) using established criteria for the recognition of jökulhlaup deposits (Maizels, 1993, 1997; Russell and Marren, 1999; Marren, 2005; Russell *et al.*, 2005) (Table II-1).

Figure II-4: Field assessment of jökulhlaup deposits. (A) Collection of bulk samples of sediment from the Kotá fan on 18 March 2003 (§ 5.3). (B) Boulder survey to the west of Falljökull on 27 August 2006. Note the person for scale.

Table II-1: Criteria for the recognition of jökulhlaup deposits (after Marren 2005, p. 233).

Criteria indicative of high-magnitude flooding	Sedimentary characteristics
Hyperconcentrated flow:	*Poor sorting; massive; reverse grading; poor imbrication; floating clasts; traction carpets.*
Debris flow:	*Very poor sorting; massive; may show correlation between maximum particle size and bed thickness.*
Strongly uniform palaeo-flow:	*Indicative of a lack of reworking by falling-stage flows.*
Thick, inversely graded (upward coarsening) units:	*Inversely graded units in coarse sediment thicker than ~2 m. Formed under rising-stage conditions.*
Large-scale gravel foresets:	*Thick (>2 m) cross-bedded coarse gravel. Formed in expansion or pendant bars and in mega-dunes.*
Ice-block features:	*Steep-walled and inverse conical kettle-holes; circular 'rimmed' kettles; obstacle marks and tails; hummocky terrain.*
Rip-up clasts:	*Blocks of subglacial diamict, bedrock, or river-bank sediment uprooted and deposited out-of-place.*
Large-scale geomorphic features:	*Hummocky terrain; mega-scale bars and terraces; boulder fields; palaeo wash-limits.*

4.3. Analysis of aerial photographs

Using Thorarinsson's (1958) delineation of flood routes, aerial photographs from *Loftmyndir ehf.* were used to classify surface features indicative of flooding in 1362 and 1727. The imagery was made available in geo-referenced format at a pixel resolution of <1 m. Combining the images with the DSM enabled a detailed geomorphological view of the region, allowing erosional and depositional features to be classified using *ArcGIS 10*. Aerial photographs from the National Land Survey of Iceland were also used to aid field investigations in 2005 and 2006.

5. Course of events

As well as considering the geomorphic legacy of prehistoric jökulhlaups, this section describes the development of the 1362 and 1727 jökulhlaups. As described in § 3, pyroclastic density currents would have been prevalent during eruptions of Öræfajökull. Partial collapse of the eruption plume could have triggered pyroclastic density currents, which would have scoured large zones of the ice-cap, causing significant and pervasive ice-melt (e.g., Naranjo *et al.*, 1986). In fact, anecdotal accounts of the 1362 eruption describe every gully awash with floodwater (Thorarinsson, 1958). Thermal and mechanical erosion of the ice-cap by the passage of pyroclastic density currents could account for the deposition of some jökulhlaup deposits; however this is not addressed here. For further details about tephra deposition, see Thorarinsson (1958) and Höskuldsson (2012).

5.1. Prehistoric jökulhlaups

According to Thorarinsson (1958) a prehistoric jökulhlaup burst from Kvíárjökull at a lateral breach known as Kambskarð in the terminal moraines (see also Iturrizaga, 2008) (Figure II-5). Sketchy accounts exist of the 1362 jökulhlaup draining partly from Kvíárjökull, but Thorarinsson disputed this. He argued that tephra fall from the eruption caused significant and widespread melting of the ice-cap, thereby causing a jökulhlaup that cascaded across the surface of Kvíárjökull. The Stórugrjót outwash fan to the immediate west of Kvíárjökull extends into the sea. Thorarinsson believed that Stórugrjót is prehistoric as it underlies the terminal

moraine of Kvíárjökull, which is thought widely to have formed ~500 BCE (Thorarinsson, 1956). West of Kvíárjökull, boulders from the Stórugrjót surface overtop the fringe of a basaltic, postglacial lava flow (Figure II-5). Thorarinsson (1956) claimed that the terminal moraine of Kvíárjökull postdates the aforementioned lava flow. According to Thorarinsson, the lava flow originated to the east of Kvíárjökull; therefore, an eruption occurred at a time when Kvíárjökull was much farther up-valley than the position demarcated by the terminal moraine.

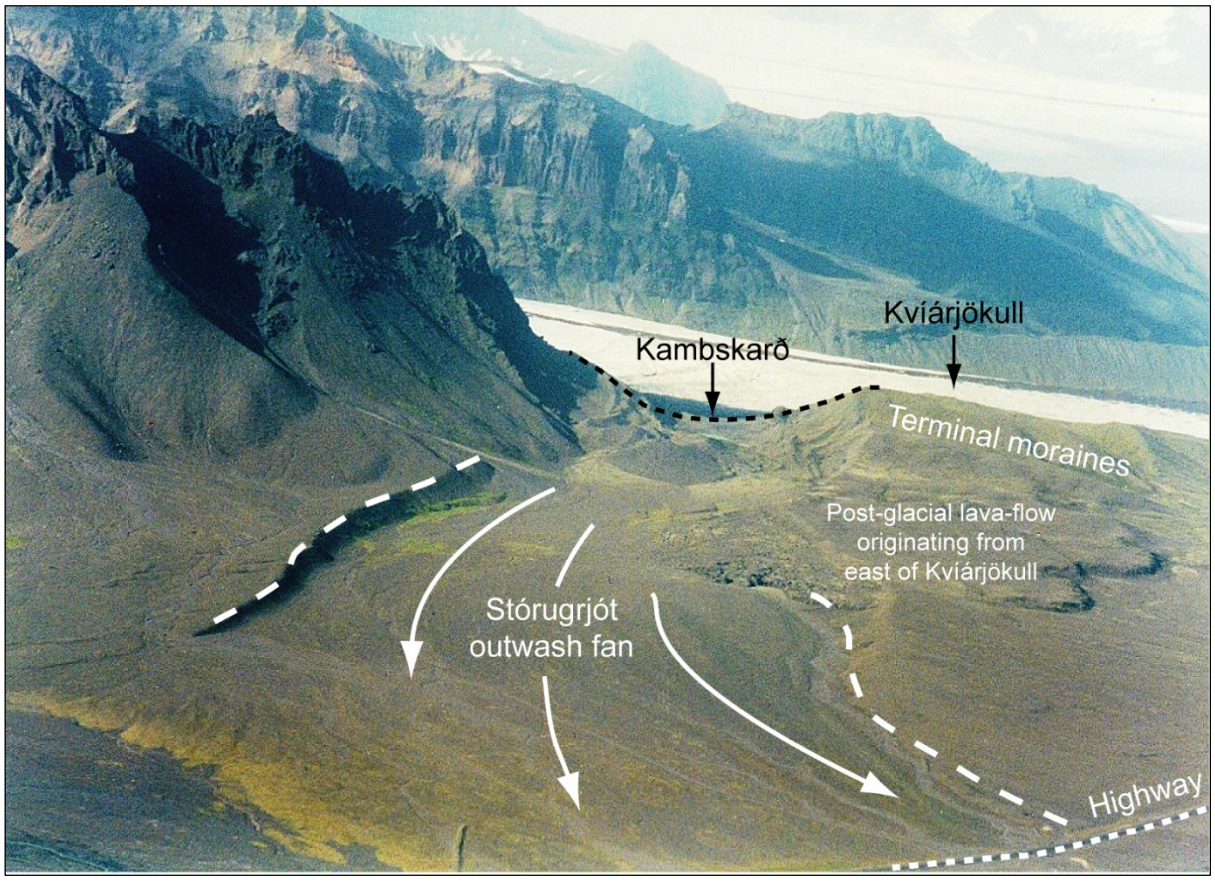

Figure II-5: Oblique, aerial view of Kvíárjökull showing the lateral breach in the terminal moraine and the relic outwash-fan extending from it. Photographer: M. J. Roberts, July 2000.

5.2. 1362 jökulhlaup

As Thorarinsson (1958) acknowledged, contemporary accounts of the 1362 eruption are vague, claiming that the entire settlement was obliterated during the eruption. Likewise other descriptions made decades after the eruption allude to complete destruction of Litlahérað. The only direct reference to the 1362 jökulhlaup is found in the fragmented church annals of Skálholt, written at a monastery in Möðruvellir, Northern Iceland. Thorarinsson's (1958, p. 26) translation of this text is as follows: "*At the same time [as the eruption] there was a glacier burst from Knappafellsjökull [Öræfajökull] into the sea carrying such quantities of rocks, gravel and mud as to form a sandur plain where there had previously been thirty fathoms [~55 m] of water.*"

Thorarinsson (1958) considered that the 1362 eruption began in mid-June and it persisted until the autumn. Flooding, though, was confined mostly to the onset of the eruption and possibly the first 24 hours (*c.f.* Magnússon *et al.*, 2012b). The eruption

created direct hazards of unprecedented magnitude. Melting of ice through rapid heat transfer from magma to ice, most likely within the volcano's ice-filled caldera, would have generated masses of meltwater at a bedrock elevation of ~1600 m AMSL (Gudmundsson *et al.*, 2015, Chapter III). The ensuing jökulhlaup propagated through Falljökull and Kotárjökull before inundating farmland on the western side of Öræfajökull at an initial elevation of ~80 m AMSL and a distance of 10–30 km from the eruption site (Figure II-6). Church annals written in the decades following the eruption depict a colossal flood that swept pieces of the ice-cap across Skeiðarársandur, cutting off all access to the region (Thorarinsson, 1958).

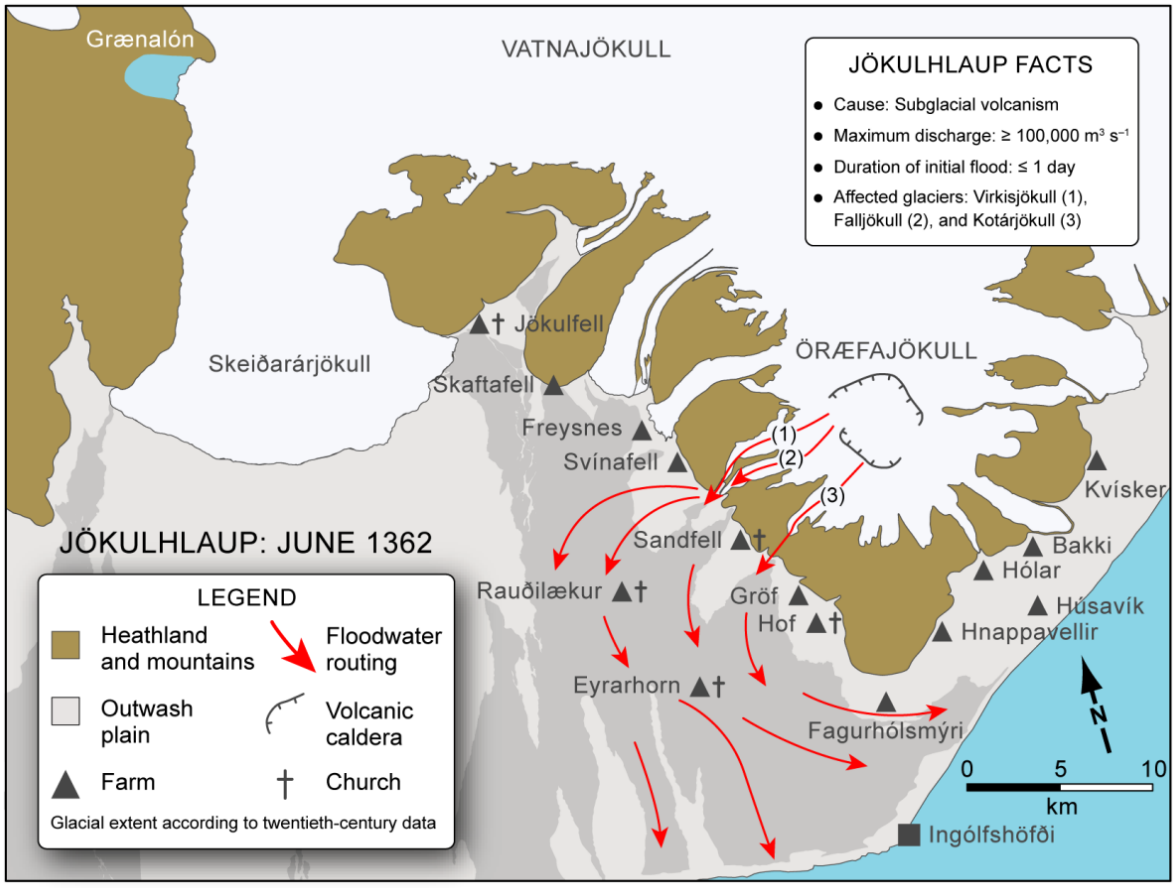

Figure II-6: Postulated routing of floodwater from Öræfajökull during the 1362 eruption (after Thorarinsson, 1958). Note the location of churches and farms along the flood path.

From historical descriptions and geomorphological evidence, Thorarinsson (1958) concluded that the 1362 jökulhlaup burst primarily from Falljökull. Flood deposits, recognisable by the presence of light-coloured rhyolitic tephra, extend over a much larger area than dark-coloured, basaltic deposits from the 1727 eruption (Figure II-7). Moreover, rhyolitic tephra from 1362 comprises coarse silt-sized grains (e.g. Selbekk and Trønnes, 2007), whereas 1727 material is mostly coarse sands and pebbles. To the west and northwest of Falljökull, a boulder-strewn lag of vegetated, water-lain deposits extends to the present-day course of Skaftafellsá (Figure II-7). Outcrops of the same surface continue west beyond Skaftafellsá to the former eastern edge of Skeiðará. Large jökulhlaups from Skeiðarárjökull (e.g. 1861, 1938, and 1996) would have reworked or buried the Öræfajökull deposits, blurring the western extent of the sedimentary record on Skeiðarársandur (Thorarinsson, 1959; Björnsson, 2003).

Clearly, flows to the west and northwest of Falljökull carried large quantities of glacial ice and metre-scale boulders. This is supported by two lines of reasoning: Firstly, the area was renamed at some point after the 1362 eruption as Langafellsjökull, signifying that copious blocks of ice were left on the sandur (Thorarinsson, 1958; Guttormsson, 1993; Sigurðsson and Williams, 2008). Secondly, clusters of angular-shaped rocks lie ~4 km west from Falljökull (e.g. Figure II-4B); projecting 4–5 m above the sandur, these boulders are estimated to weigh more than 500 tonnes and they are inter-bedded with jökulhlaup deposits (Thorarinsson, 1958). Another notable boulder deposit is the smjörsteinn (butter stone) southeast of Svínafell; it is believed that this boulder was transported to its present location by the 1362 jökulhlaup (Thorarinsson, 1958) (Figure II-7). In addition to the breccia of ice blocks, boulders, and juvenile deposits known as Langafellsjökull, three other named deposits have been associated with the 1362 jökulhlaup; these are: Forarjökull, Grasjökull, and Miðjökull, which all contained masses of ice and remained stranded at the foot of Öræfajökull for decades (Thorarinsson, 1958; Sigurðsson and Williams, 2008) (Figure II-7).

In the foreground of Kotárjökull, evidence of the 1362 jökulhlaup is less obvious than at Falljökull. From aerial assessments of palaeo-flood extent and ground-based surveys of sedimentary deposits, it is apparent that most of the 1362 deposits were either buried or washed away by the 1727 jökulhlaup. There are, however, occasional outcrops of lighter sediments within the distal path of the 1727 jökulhlaup; Thorarinsson (1958) described an area east of Kotá as an example (Figure II-7).

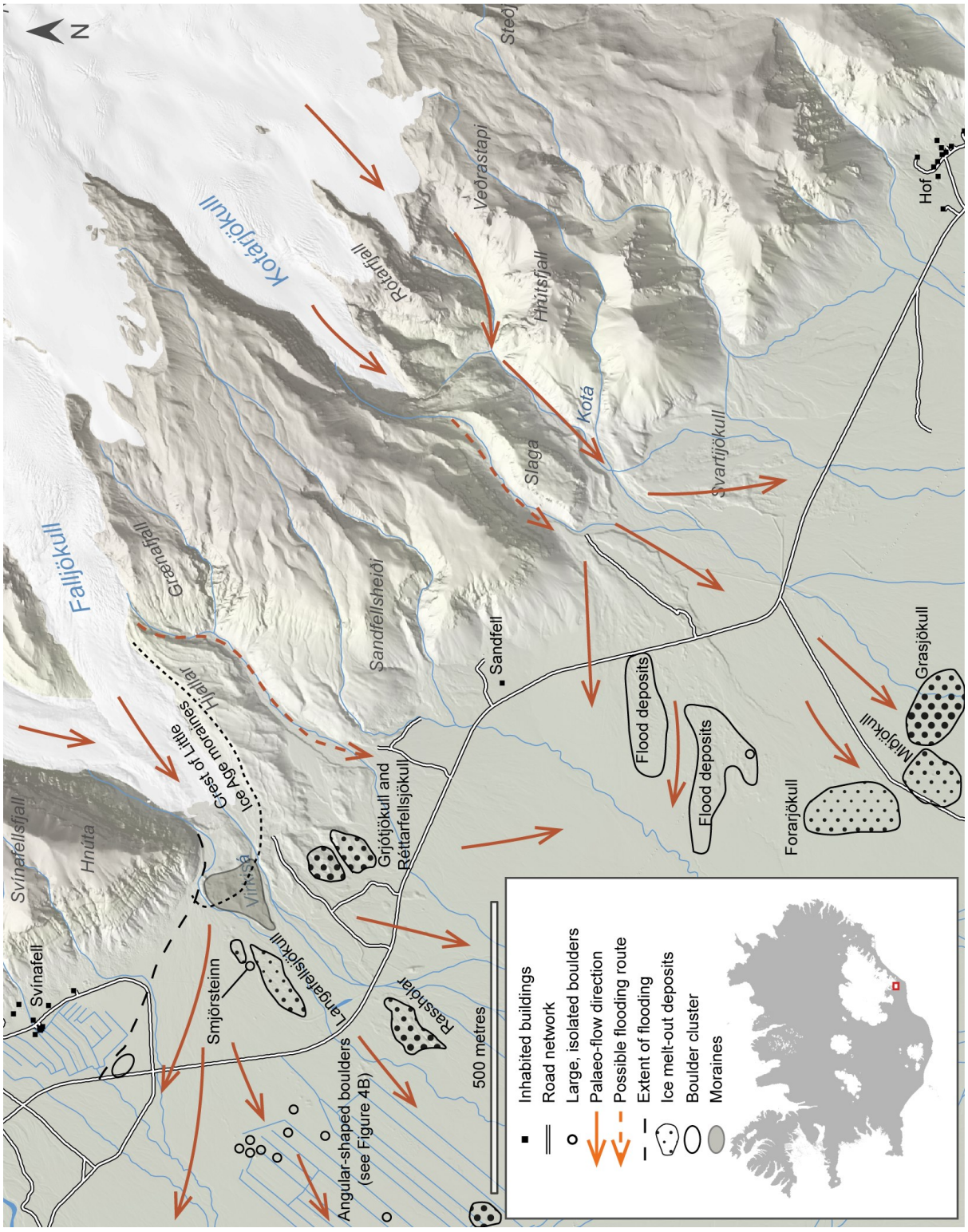

Figure II-7: Extent of jökulhlaup deposits associated with the 1362 eruption of Öræfajökull 1727 jökulhlaup.

5.3. 1727 jökulhlaup

The prelude to the 1727 eruption and the consequent jökulhlaup was described by the rector of Sandfell, Reverend Jón Þorláksson, who documented the course of events over 50 years after the eruption (Olavius, 1780). This description was translated into English by Henderson (1818), with corrections made by Thorarinsson (1958). Whilst holding a sermon at Sandfell on 3 August 1727, the congregation felt earthquakes that became progressively stronger. Damaging earthquakes continued to occur on 4 August and it was noted that booming noises, akin to thunder, radiated from the ice-cap (Háldanarson, 1918). Soon after 09:00 on 4 August, three particularly loud thunderclaps were heard, after which the jökulhlaup began. The jökulhlaup affected Kotárjökull mainly (Háldanarson, 1918), but it is likely that some floodwater drained via Falljökull. Traces of 1362 flood deposits between Sandfell and Hof imply that the 1727 flood inundated roughly the same region, mostly likely covering pre-existing deposits. It can therefore be assumed that the 1727 jökulhlaup from Kotárjökull was comparable in magnitude to the 1362 flood from the same glacier (Thorarinsson, 1958).

The 1727 jökulhlaup caused three fatalities, in addition to the loss of sheep, cows, and horses that were grazing in the path of the initial flood. From Thorarinsson's (1958) translation of accounts, the jökulhlaup occurred as a series of floods, the last of which was by far the greatest. Although the jökulhlaup is thought to have peaked within three to five hours, waning-stage discharge on 11 August from the remains of Kotárjökull was almost too warm for horseback riders to cross. From experience gained at Eyjafjallajökull in 2010 (Magnússon *et al.*, 2012a), such high temperatures are a result of meltwater interacting with advancing lava. As the 1727 jökulhlaup subsided it was clear that Falljökull and Kotárjökull had "*...slid forwards over the plain ground, just like melted metal poured out of a crucible...*" (Thorarinsson, 1958, p. 31). The jökulhlaup was sufficiently large and extensive to allow blocks of glacial ice to reach the sea, in addition to depositing masses of sediment at the foot of the ice-cap.

Decades elapsed before the stranded ice around Sandfell disappeared. When explorers Eggert Ólafsson and Bjarni Pálsson travelled through Öræfi in 1756, they described the terrain between Sandfell and Hof as a jumble of debris-covered ice, ~3 km wide and ~13 km long (Ólafsson, 1974) (Figure II-8). Many pits and ravines were present in the melting ice, making travel through the area difficult. Ólafsson (1974) likened the landscape to the appearance of Skeiðarárjökull, only much lower. The region to the immediate east of Kotá, near to Goðafjall, was named Svartijökull (black glacier) in acknowledgement of the lingering ice (Thorarinsson, 1958; Guttormsson, 1993; Sigurðsson and Williams, 2008); this name remains today. The uppermost surface of Svartijökull is characterised by closely spaced kettle-holes, resulting in hummocky topography (Figure II-8). Angular blocks of palagonite tuff also project through the fan surface, implying simultaneous incorporation and deposition of glacial ice and bedrock from a high-energy, sediment-laden flow (e.g. Maizels, 1989; Russell and Knudsen, 2002). Figure II-9 shows seven surface profiles taken from the DSM of Svartijökull. These profiles depict a highly pitted surface, with some kettle-holes forming inverse conical depressions, whereas others are shallower and edged by a low-amplitude mound of sediment. The former morphology is indicative of in-situ melt-out of buried ice, whereas the later signifies melting of a partially buried block with resultant subaerial deposition of glacial debris (Russell *et al.*, 2005 and references therein). Viewed from above, the field of kettle-holes shows a distinct radial pattern, reflecting flow expansion from the valley between Mount Slaga and Goðafjall (Figure II-8). Additionally, kettle-hole diameters diminish noticeably with increasing distance from the apex of the fan.

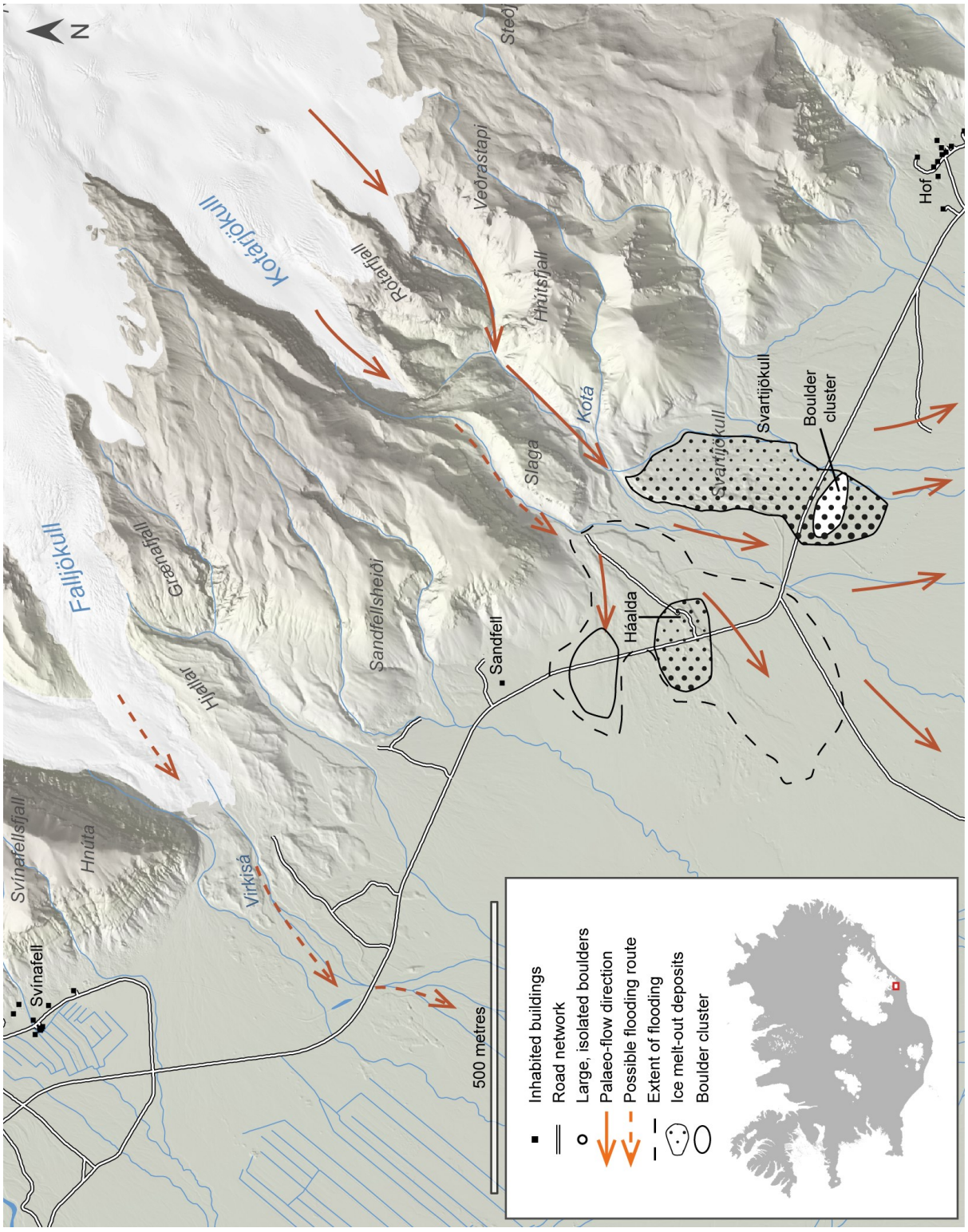

Figure II-8: Extent of jökulhlaup deposits associated with the 1727 eruption of Öræfajökull.

Fluvial terraces incised into the head of Svartijökull show a ~25 m section of sediment in the form of a conformable sequence of interbedded, laterally continuous, water-lain deposits (e.g. Figure II-4A). In places, up to eight nested terraces remain intact. The deposits are dominated by angular, basaltic tephra typically ≤1 cm in diameter, which Thorarinsson (1958) attributed to the 1727 eruption. Thompson and Jones (1986) claimed that the fan contained mostly air-fall pyroclastic deposits. This reasoning was based on the presence of dark, angular fragments of basalt lacking matrix support. However, such massive, homogenous, granular sediment could equally have been deposited under jökulhlaup conditions (Maizels, 1991, 1997; Russell and Knudsen, 1999, 2002). Thompson and Jones (1986) also argued that the distinctive terraces at the head of Svartijökull developed after 1727 as a result of gradual fluvial recovery from the aggradational effects of the jökulhlaup. In contrast, Thorarinsson (1956, 1958) concluded that the terraces formed during the waning-stage of the 1727 jökulhlaup. This is entirely plausible as flooding occurred intermittently over four days (Thorarinsson, 1958). Furthermore the terrace tops show hardly any signs of fluvial reworking, which would be expected if braided streams had flowed over the area for sustained periods. Smaller jökulhlaup could have incised unconsolidated sediments from the main outburst on 4 August 1727, as noted by Dunning *et al.* (2013) for the 2010 eruption of Eyjafjallajökull.

In the foreground of Falljökull, the geomorphic impact of the 1727 jökulhlaup is less prominent. Periods of glacier advance and retreat have extensively reworked flood deposits from 1362 and 1727; moreover the area is vegetated by dwarf birch, which obscures the surface topography. Beyond the periphery of the Little Ice Age (1750–1900 CE) terminal moraines at Falljökull, pitted and boulder-strewn surfaces remain intact (Figure II-7). The moraines themselves and the intervening zone to the ice margin result presumably from glacially reworked flood deposits, particularly those of 1727. For details about modern-day ice retreat at Falljökull, see Bradwell *et al.* (2013) and Hannesdóttir *et al.* (2015).

6. Floodwater routing

Historical accounts and geomorphic evidence substantiate that the 1362 and 1727 eruptions occurred in different locations of Öræfajökull. This is based mainly on the contrasting extent of dark-coloured, basaltic deposits in the river catchments of Falljökull and Kotárjökull (§ 5.3). In the vicinity of Kotá, thick deposits of coarse-grained basaltic tephra are present, whereas this sediment type is less prominent near to Virkisá. The 1362 eruption is thought to have occurred within the caldera; this is supported on two accounts. Firstly, the subglacial catchment of Falljökull extends toward the centreline of the caldera, where ice thickness exceeds 500 m (Magnússon *et al.*, 2012b). Such a quantity of ice, coupled with an eruption of very high mass-discharge rate (Gudmundsson *et al.*, 2015, Chapter III), could account for the volume of water required to deposit large boulders in high-energy, sediment-laden flows kilometres downstream from Falljökull. Secondly, large-scale mechanical break-up of Falljökull, as implied by former dead-ice masses such as Langafellsjökull, necessitates floodwater bursting from the ice surface to effectively sever the lower part of the glacier from the icefall (e.g. Sturm *et al.*, 1986).

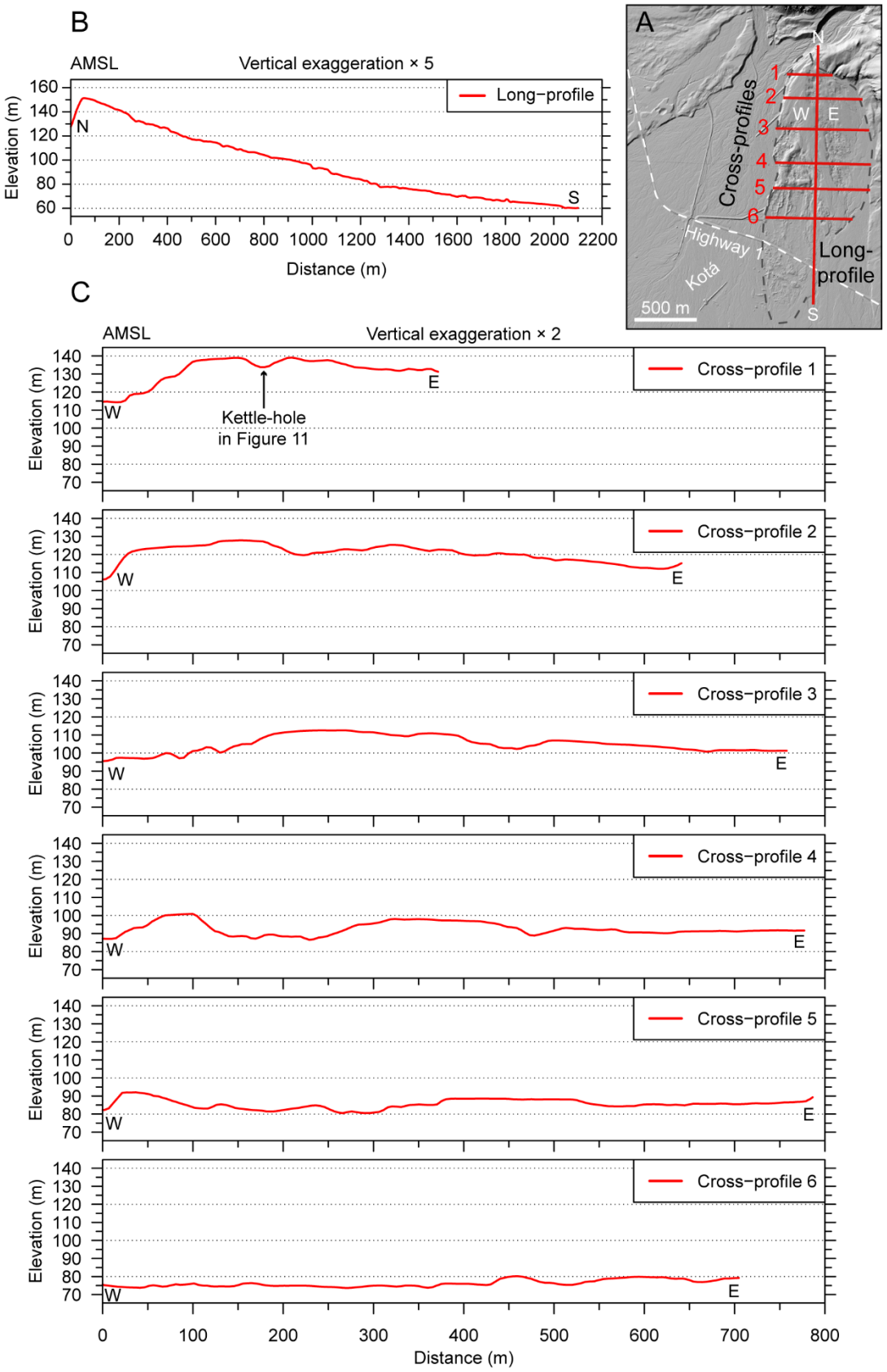

Figure II-9: Longitudinal and transverse profiles of Svartijökull – a mass of hummocky terrain arising from the 1727 jökulhlaup. (A) Map showing profile locations; (B) long-profile; (C) cross-sections depicted in (A). Note the location of Figure II-11 in cross-section 1. Survey data derived from a digital surface model (see § 4.2).

As outlined in § 5.3, the 1727 jökulhlaup was preluded by thunder-like sounds. At Eyjafjallajökull during the summit eruption of 2010, booming sounds emanated from the ice-cap on 15 April, followed immediately by a volcanogenic jökulhlaup (§ 10.5). The sound was attributed to floodwater cascading down the lateral flanks of Gígjökull due to outlets forming high on the glacier (Roberts *et al.*, 2011; Magnússon *et al.*, 2012a). The similarity of the sounds and their timing gives confidence to the idea of subglacial floodwater bursting from the upper slopes of Öræfajökull in 1727. With the benefit of modern-day observations (Roberts, 2005; § 10), subglacial floodwater would have burst preferentially from the thinnest section of Falljökull, which would have been the icefall region (Figure II-10). This, again, implies a floodwater source from within the caldera. It should be noted, however, that Björnsson (2005) disputed a caldera origin for the 1362 eruption, believing instead that the eruption occurred outside the caldera rim in an area of comparatively thinner ice, thus ruling out a high-elevation origin for floodwater. Björnsson (2005) reasoned that an eruption within the caldera would undoubtedly have affected Kvíárjökull. Mapping of bedrock topography in the volcano's caldera by Magnússon *et al.* (2012b) demonstrates that a water source within the subglacial catchment of Falljökull would not necessarily cause flooding down Kvíárjökull. This is an important point to consider in relation to Björnsson's assertions.

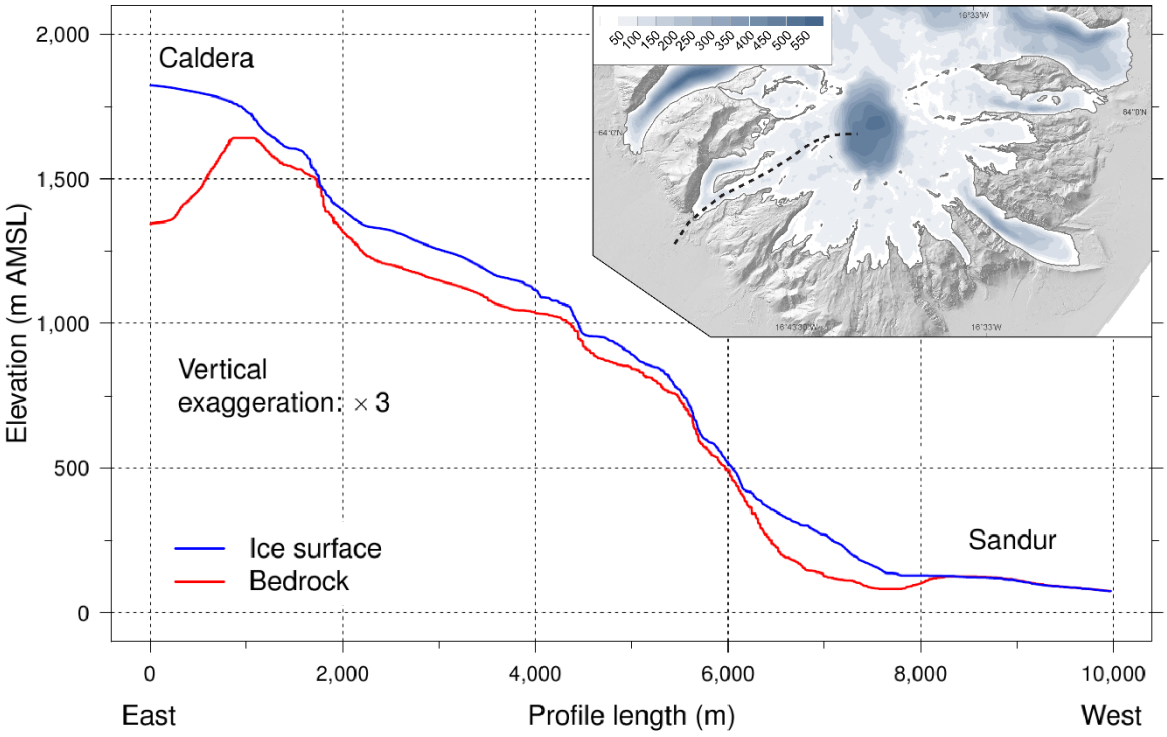

Figure II-10: Northward cross-sectional profile of Falljökull, showing bedrock and ice-surface topography. The inset map shows the extent of the profile on the western flank of Öræfajökull, with shading denoting ice thickness in metres. Bedrock profile data derived from Magnússon et al. (2012b).

Additional insight into the subaerial routing of the 1727 jökulhlaup can be gained from the terrain surrounding Mount Slaga (Figure II-8). The southern part of the region is dominated by the hummocky, steep-sloping surface known as Svartijökull. A boulder-strewn surface to the northwest of Svartijökull also radiates in a down-sandur direction from around the base of Mount Slaga (Figure II-8). This surface, comparable to a debris-flow deposit (Pierson, 2005), appears to represent the initial flood-wave from Öræfajökull, before floodwater focussed on the present-day route of Kotá. It is possible that the boulder-strewn surface also underlies deposits at Svartijökull. The routing of the debris-flow deposit to the north-west of Svartijökull is uncertain. Some of the flow could have been routed between Mount Slaga and Goðafjall, although the adjacent valley between Mount Slaga and Sandfell could have conveyed some of the flow. For this to occur, the Kotá valley must have filled with floodwater, allowing discharge from the western branch of the glacier to descend into the neighbouring valley. This hypothesis is especially plausible if floodwater descended over the surface of Kotárjökull (*c.f.* Roberts *et al.*, 2011).

7. Flood timing and extent

The exact timing of both historical jökulhlaups is difficult to ascertain. Of the two eruptions, only accounts of 1727 contain any detail (§ 5.3). As noted by Thorarinsson (1958), the 1727 eruption began soon after 09:00 on 4 August, and it is thought to have peaked within three to five hours. Nevertheless, the actual duration of the main rise to maximum discharge could have been two to four hours. An hour could have elapsed between the beginning of the subglacial eruption and the onset of flooding from the ice-cap (Gudmundsson *et al.*, 2015, Chapter III). Jökulhlaup deposits from 1727 shed light on the form of the palaeo-hydrograph. Sediments ranging from coarse sands to large, angular boulders were deposited simultaneously within individual, upward-coarsening units such as the Kotá fan; overall such sequences represent large-scale bedding deposited parallel to the slope of the flooded surface. Such deposits would have originated from a pulsating, high-energy flow, limited mainly by sediment supply rather than flood power (Maizels, 1997). The architecture and vertical sedimentary structure of jökulhlaup deposits on the western side of Öræfajökull represent continuous aggradation of sediment during a rapid, linear rise to maximum discharge, akin to a dam burst (*c.f.* Russell *et al.*, 2010).

Scant geomorphic features preserve the downstream extent of the 1362 and 1727 jökulhlaups. As flows expanded from the western flank of Öræfajökull, floodwater would have drained across the eastern side of Skeiðarársandur. In distal regions, mostly sand to cobble-sized sediment would have been deposited from turbulent flows. Despite being laterally extensive, such deposits would either be eroded by Skeiðará or buried by subsequent jökulhlaups on Skeiðarársandur. During the fourteenth century, climate-induced thickening and advance of Skeiðarárjökull forced the drainage of meltwater to the western and eastern edges of the glacier (Björnsson, 2003). Over subsequent centuries Skeiðará would have flowed over distal flood deposits from Öræfajökull. This process would have been particularly effective during large, eruption-related jökulhlaups from Skeiðarárjökull, especially in 1861, 1938, and 1996 (Þórarinsson, 1974; Snorrason *et al.*, 1997).

8. Flow properties

Both the 1362 and 1727 jökulhlaups would have transported masses of freshly erupted material, especially while the eruptions were confined beneath ice (Gudmundsson *et al.*, 2015, Chapter III). As ice blocks became entrained in the developing floods, this would have increased the volume of the jökulhlaups significantly. In this section we review both the rheology and ice-content of the two historic floods.

8.1. Rheology

From existing sedimentological studies at Öræfajökull (Thorarinsson, 1958; Maizels, 1991) and inferences from other volcanogenic floods in Iceland (Tómasson, 1996; Russell *et al.*, 2005; Duller *et al.*, 2008), it is possible to speculate on floodwater composition during the 1362 and 1727 jökulhlaups. Explosive fragmentation during both subglacial eruptions would have created a copious supply of fine-grained volcaniclastic material (Gudmundsson *et al.*, 2015, Chapter III). Combined with fast-flowing water due to steep terrain, sediment would also have been eroded from the entire flood tract, including subglacial pathways. At the onset of flooding, when the amount of floodwater was minor compared to the volume at maximum discharge, sediment concentrations could easily have ranged from hyperconcentrated (40–80% solids by mass) to debris flow conditions (>80% solids by mass). The initial front of both floods would have reached the lowland as a fast-moving, debris-laden wall of muddy material (*c.f.* Russell *et al.*, 2010; Waythomas *et al.*, 2013). Maizels (1991) ascribed debris-flow conditions to matrix-supported clastic deposits at the base of the Kotá fan; the implication being that clasts were supported by a fabric of fine-grained pyroclasts as the 1727 flow emanated from Kotárjökull.

As both the 1362 and 1727 floods continued to rise, water-flood conditions would have prevailed (Maizels, 1991). However, owing to high discharge, steep water-surface slopes, and topographic constrictions, flows would have remained deep and fast enough to produce high shear stresses and strong turbulence (Pierson, 2005). Such conditions would allow for prodigious quantities of sediment transport, ranging from granular- to boulder-sized clasts (*c.f.* Duller *et al.*, 2008).

8.2. Role of ice

The extent of glacial ice on Öræfajökull would have been significantly greater in 1727 than during the 21st Century. In the 1750s, Kvíárjökull is thought to have reached the crest of the terminal moraines (Hannesdóttir *et al.*, 2015), so it is probable that Kotárjökull was advancing also (Guðmundsson *et al.*, 2012). When the 1727 eruption occurred, Kotárjökull was at least 30% more extensive than it was in 2011 (Guðmundsson *et al.*, 2012); this explains why ice-release was so ubiquitous during the 1727 jökulhlaup.

The 1362 and 1727 eruptions were noted for widespread deposition of glacial ice by floodwater (see § 5.2 and 5.3). Densely-clustered kettle holes in the foreground of Falljökull and Kotárjökull are indicative of downstream flow expansion and a corresponding reduction in flood power, leading to ice-block grounding (Baker, 1987; Fay, 2002; Russell and Knudsen, 2002) (Figure II-11). Ice blocks that were buried by rising-stage sediment aggradation led to the formation of circular kettle holes (e.g. Háalda in between Sandfell and Hof), whereas partially buried fragments gave rise to scour-like formations (e.g. lower parts of Svartijökull) (Figure II-8). From eyewitness descriptions of the 1727 jökulhlaup (§ 5.3), large sections of Falljökull and Kotárjökull were broken from Öræfajökull; smaller pieces even reached the coastline, over 18 km away. Grounding of ice blocks during waning-stage flows could have caused floodwater to pond behind an ice dam in regions of flow expansion. Ice blockades, either close to the eruption site, or in the proximal region of Kotá, could account for the series of 1727 floods noted by Thorarinsson (1958) (see § 5.3).

The densely pitted sandur around Kotá affirms to a colossal release of ice from the upper flanks of Öræfajökull. For the 1727 jökulhlaup, mechanical break-up of Kotárjökull by floodwater travelling beneath, along, and on top of the glacier would have readily produced fragmented ice. If the initial flood-wave was a slurry mixture, then the density of the flow itself may have been sufficient to raft tabular sections of Kotárjökull downstream within minutes of the jökulhlaup beginning; this image is consistent with accounts from 1727 (see § 5.3).

Figure II-11: Kettle-hole on the surface of Svartijökull – note the person for scale (photographer: P. Alho, September 2005). The depression formed due to melting of stranded blocks of ice, which were deposited in the region during the 1727 jökulhlaup (Ólafsson, 1974; Thorarinsson, 1958). For the location and dimensions of the kettle-hole, see Figure II-9.

9. Maximum discharge

Historic descriptions of the 1727 jökulhlaup, together with the geomorphic consequences of the 1362 and 1727 eruptions, are clear evidence for a rapid, ephemeral rise to maximum discharge. For instance, Reverend Jón Þorláksson (§ 5.3) recalled that the 1727 jökulhlaup on 4 August peaked within 3–5 hours. Thorarinsson (1958) favoured flooding analogous to volcanogenic jökulhlaups from Katla (Tómasson, 1996), thereby implying a rapid rise to a maximum discharge that would be very high compared to the volume of the jökulhlaup. With this in mind, Thorarinsson (1958) postulated that the 1362 jökulhlaup peaked at $> 1 \times 10^5$ m^3/s.

The 1727 jökulhlaup burst primarily from Kotárjökull, and the extent of flooding was similar to that of 1362 (§ 5.3), however the 1362 jökulhlaup drained foremost from Falljökull (§ 5.2), signifying that the 1727 jökulhlaup was lower in magnitude. From slope-area calculations based on the width of the Kotá valley between Mount Slaga and Goðafjall (Figure II-12) and a corresponding surface velocity of 12.1 m/s, the maximum

discharge of the 1727 jökulhlaup is estimated at ~4×10^4 m^3/s (Figure II-12). Palaeo-discharge estimates are, of course, hindered by the masses of sediment, rock, and glacial ice that are known to have been transported onto the sandur. The maximum discharge from the eruption site (Gudmundsson *et al.*, 2015, Chapter III) is naturally lower than the downstream equivalent, as bulking factors such as sediment and ice need to be considered. For volcanogenic floods from Öræfajökull, a bulking factor as high as ~25% seems reasonable, especially when considering initially hyperconcentrated conditions (§ 6) and exceptional amounts of ice-release (§ 8.2).

Further credence for a rapid rise to maximum discharge comes from a sedimentological interpretation of palaeo-hydrograph form. Large-scale, upward-coarsening units of sand- to cobble-sized deposits (§ 7) demonstrate high-energy flow conditions equivalent to the passage of a lahar (Waythomas *et al.*, 2013). Such sequences could from only under sustained high discharge, resulting in a rising-stage hydro-graph akin to a dam-burst.

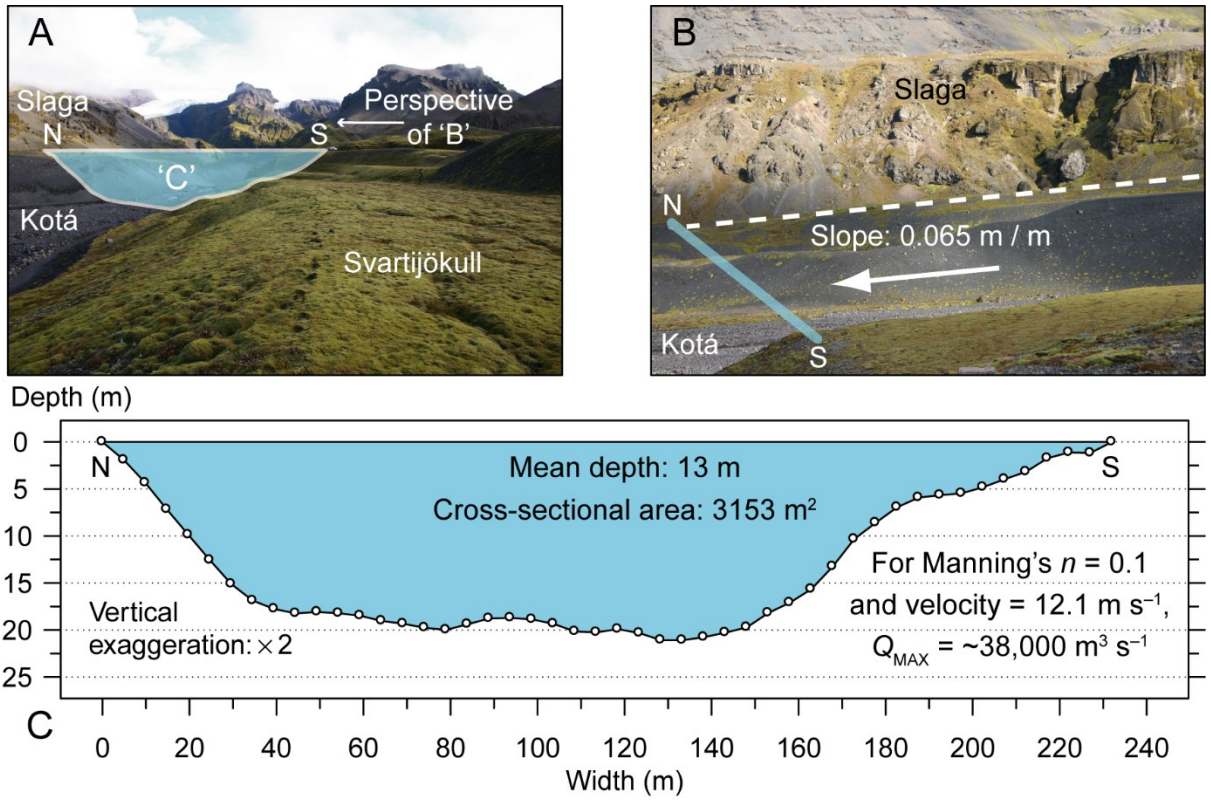

Figure II-12: Reconstructed maximum discharge during the 1727 jökulhlaup from Kotárjökull. (A) Cross-section of the Kotá valley from Mount Slaga to the uppermost surface of Svartijökull (see Figure II-9); (B) calculated slope of the palaeo water-surface; (C) channel cross-section and hydraulic data. Survey data derived from a digital surface model (see § 4.2).

10. Modern-day comparisons

This section highlights occasions when supraglacial flooding has occurred in connection with volcanic activity. The purpose is to use modern-day analogues to better understand how the 1362 and 1727 jökulhlaups developed. Examples are taken from Iceland and Alaska, U.S.A. The Icelandic examples from Eyjafjallajökull and Sólheimajökull are especially relevant, as the affected glaciers are similar in surface profile and ice thickness to the Öræfajökull flood paths.

10.1. Redoubt: 1989–1990 and 2009

The surface of Drift glacier has been disrupted on several occasions by subglacial volcanism at Mount Redoubt in 1989–1990 and 2009 (Trabant *et al.*, 1994; Waythomas *et al.*, 2013). Instead of draining entirely beneath Drift glacier, debris-laden outpourings of floodwater have broken repeatedly through the glacier's surface at high elevation (Trabant *et al.*, 1994). In some locations, glacial ice has been stripped away to bedrock by repeated floods. Distinctive 'ice diamict' deposits have been mapped on the glacier surface and also several kilometres downstream, revealing the extent of supraglacial flooding (Waitt *et al.*, 1994). During the 2009 eruption of Redoubt, floods and pyroclastic flows removed 0.1–0.2 km^3 of ice from Drift Glacier (10–20% of total ice volume) (Waythomas *et al.*, 2013).

10.2. Skeiðarárjökull: 1996

Skeiðarárjökull is a surge-type piedmont glacier draining from the Vatnajökull ice cap. The northern edge of the glacier's water-divide neighbours the Grímsvötn subglacial lake. From 30 September 1996 to early October 1996, a subglacial eruption took place north of Grímsvötn (Gudmundsson *et al.*, 1997). Late on 04 November 1996, 35 days after the start of the eruption, floodwater began to drain from Grímsvötn at a lake-level of 1510 m AMSL. Floodwater exited Grímsvötn through a rapidly expanding subglacial conduit. The initial flood-wave took ~10.5 hours to travel the 50 km distance from Grímsvötn to the edge of Skeiðarárjökull; at peak flow the transit time decreased to about 3 hours (Björnsson, 1998). The jökulhlaup ceased after 40 hours, having released ~3.6 km^3 of floodwater onto Skeiðarársandur (Gudmundsson *et al.*, 1997). During the initial rising stage of the jökulhlaup, floodwater blasted through the surface of Skeiðarárjökull, producing multiple supraglacial outbursts across the terminus (Roberts *et al.*, 2000). In some locations, floodwater burst through ~350 m of ice before reaching the glacier surface. Where floodwater burst through the ice surface close to the margin, large volumes of ice were released (Roberts *et al.*, 2002).

10.3. Sólheimajökull: 1999

Sólheimajökull drains from the Mýrdalsjökull ice cap, which is underlain by the Katla volcano. Sólheimajökull is a 9 km long, non-surging valley glacier, with a surface area of ~78 km^2 and a terminus ~1 km wide. On 10 July 1999, the river issuing from Sólheimajökull (Jökulsá á Sólheimasandi) was abnormally high. People travelling across Sólheimasandur between 14 and 17 July informed local authorities that the river was unusually dark, high, and extremely odorous (Sigurðsson *et al.*, 2000). At 17:00 UTC on 17 July, prolonged seismic tremors were detected from beneath Mýrdalsjökull; this seismicity intensified through the evening, culminating at ~02:00 hours on 18 July. This peak in seismic activity was concomitant with the release of a jökulhlaup from Sólheimajökull (Roberts *et al.*, 2000).

During the jökulhlaup, numerous high-capacity outlets developed across the terminus, western lateral flank and surface of Sólheimajökull (Roberts *et al.*, 2000). Peak discharge at the terminus and 6 km downstream was estimated at ~5,000 m^3/s and 1,940 m^3/s, respectively (Sigurðsson *et al.*, 2000; Russell *et al.*, 2010); these values

indicate marked downstream flow attenuation, analogous to flash-floods in ephemeral regions. Eyewitness accounts from the bridge over Jökulsá á Sólheimasandi suggest that the jökulhlaup persisted for ~6 hours, having peaked within an hour (Sigurðsson *et al.*, 2000).

10.4. Eyjafjallajökull: 2010

Sourced from within the volcano's ice-filled caldera, the April 2010 eruption of Eyjafjallajökull stratovolcano caused repeated jökulhlaups in response to initial subglacial volcanism, followed by phreatomagmatic activity and lava-flow confined by ice (Roberts *et al.*, 2011; Magnússon *et al.*, 2012a). The ice-surface in the summit caldera lies at 1500–1600 m AMSL, with the ice being up to 200 m thick. This ice mass forms Gígjökull – a northward flowing valley glacier. The summit eruption began at 01:15–01.30 UTC on 14 April. By 06:45, stage measurements 1 km from Gígjökull confirmed the onset of flooding. Gauged 18 km downstream from Gígjökull, the initial jökulhlaup reached a discharge of 2,700 m^3/s within 88 minutes of arrival. A smaller, concurrent jökulhlaup also burst from the southern flank of Eyjafjallajökull, carving a 3-km-long trench into the ice surface. On both 14 and 15 April 2010, floodwater descended across the surface and flanks of Gígjökull as it broke through the glacier at an elevation as high as 1400 m AMSL. Such breakout pits formed in several places on the upper reaches of Gígjökull and allowed ice-laden slurries to debouch across the ice-surface (Roberts *et al.*, 2011; Magnússon *et al.*, 2012a).

11. Summary

The stark geomorphic imprints of the 1362 and 1727 jökulhlaups are a testament to the impact of historical volcanism at Öræfajökull. Despite only two confirmed volcanic eruptions during the past thousand years, the landscape in the vicinity of Virkisá and Kotá is almost entirely a consequence of high-magnitude flooding (*c.f.* Duller *et al.*, 2014). In 1362 floodwater was routed primarily via Falljökull, whereas in 1727 floodwater affected Kotárjökull more so, implying different eruption sites within the caldera for the two eruptions. Both historical jökulhlaup were fleeting in nature, rising to maximum discharge in a matter of hours. Although difficult to constrain, the maximum discharge of the 1362 jökulhlaup was on the order of 1×10^5 m^3/s; the peak of the 1727 jökulhlaup, although smaller, was in the region of 4×10^4 m^3/s — a flood discharge equivalent to the height of the November 1996 jökulhlaup from Grímsvötn.

A first-hand account of the 1727 jökulhlaup described floodwater rushing from Falljökull and Kotárjökull, followed by the complete break-up and removal of Kotárjökull. Flooding peaked during the 1727 eruption in a matter of hours; this timeframe necessitates rapid run-off from the eruption site, combined with swift drainage of floodwater to the lowlands. Although onlookers' descriptions of the 1727 jökulhlaup do not refer explicitly to supraglacial outbursts, it is asserted here that such flooding dominated the onset of both the 1362 and 1727 jökulhlaups. From modern-day measurements of subglacial bedrock topography and ice-surface elevation at Öræfajökull, it is evident that floodwater draining from the caldera region would have broken through the ice surface at ~1,500 m AMSL. The implication of this is twofold: Firstly, glaciers such as Falljökull and Kotárjökull would have been severed by fractures conveying floodwater to the ice surface; and secondly, such a process would lead to rapid fragmentation and eventual ice removal, as attested by written accounts. By bypassing subglacial drainage routes, supraglacial outbursts of floodwater would have caused a rapid rise to maximum discharge — a situation akin to a dam-burst. Rapid mechanical disruption of the lower reaches of Falljökull and Kotárjökull would have led to ice-blocks being incorporated constantly into rising-stage flows.

The findings of this chapter provide constraints for estimating the melting potential of Öræfajökull eruptions, as studied in Chapter III by Gudmundsson *et al.* (2015); they are also pertinent to the simulation of volcanogenic floods from Öræfajökull, as explored in Chapter IV by Helgadóttir *et al.* (2015). Furthermore, insights into flood extent, floodwater composition, and the prevalence of ice blocks provides an empirical basis for the rating of flood hazards in the Öræfi region (Pagneux and Roberts, 2015, Chapter V).

12. Acknowledgements

This study was funded by the Icelandic Avalanche Mitigation Fund, the National Power Company, and the Icelandic Road and Coastal Administration. Fieldwork in 2003 was undertaken with funding from the Earthwatch Institute. Fieldwork in 2006 was supported by a grant to Matthew J. Roberts from Kvískerjasjóður. Oddur Sigurðsson provided the photographs for Figure II-2. Emmanuel Pagneux is thanked for assistance with figure preparation. We are grateful to Andrew J. Russell, Trausti Jónsson, Tómas Jóhannesson, Oddur Sigurðsson, and Philip M. Marren for valuable feedback on this chapter.

13. References

Baker, V. R., & Costa, V. R. (1987). Flood power. In L. Mayer, & D. Nash (Eds.), *Catastrophic Flooding* (pp. 1–21). Boston: Allen and Unwin.

Björnsson, H. (1988). Hydrology of ice caps in volcanic regions. *Soc. Sci. Isl., 45*, 139, 21 maps.

Björnsson, H. (1998). Hydrological characteristics of the drainage system beneath a surging glacier. *Nature, 395*, 771–774.

Björnsson, H., & Einarsson, P. (1990). Volcanoes beneath Vatnajökull, Iceland: evidence from radio echo-sounding, earthquakes and jökulhlaups. *Jökull, 40*, 147–168.

Björnsson, S. (2003). Skeiðarársandur og Skeiðará. *Náttúrufræðingurinn, 71*(3–4), 120–128.

Björnsson, S. (2005). Gos í Öræfajökli 1362. *Náttúrufræðingurinn, 73*(3-4), 120–128.

Bradwell, T., Sigurðsson, O., & Everest, J. (2013). Recent, very rapid retreat of a temperate glacier in SE Iceland. *Boreas, 42*, 959–973.

Duller, R. A., Mountney, N. P., Russell, A. J., & Cassidy, N. C. (2008). Architectural analysis of a volcaniclastic jökulhlaup deposit, southern Iceland: sedimentary evidence for supercritical flow. *Sedimentology, 55*, 939–964.

Duller, R. A., Warner, N. H., McGonigle, C., De Angelis, S., Russell, A. J., & Mountney, N. P. (2014). Landscape reaction, response, and recovery following the catastrophic 1918 Katla jökulhlaup, southern Iceland. *Geophysical Research Letters, 41*, 4214–4221.

Dunning, S., Large, A. R., Russell, A. J., Roberts, M. J., Duller, R., Woodward, J., Mériaux, A. S., Tweed, F. S., and Lim, M. (2013). The role of multiple glacier outburst floods in proglacial landscape evolution: the 2010 Eyjafjallajökull eruption Iceland. *Geology, 41*(10), 1123–1126.

Fay, H. (2002). The formation of ice block obstacle marks during the November 1996 glacier outburst flood (jökulhlaup), Skeiðarársandur, Iceland. In I. P. Martini, V. R. Baker, & G. Garzon (Eds.), *Flood and Megaflood Deposits: Recent and Ancient Examples* (pp. 85–97). International Association of Sedimentologists.

Forbes, A. E., Blake, S., Tuffen, H., & Wilson, A. (2014). Fractures in a trachyandesitic lava at Öræfajökull, Iceland, used to infer subglacial emplacement in 1727–8 eruption. *Journal of Volcanology and Geothermal Research, 288*, 8–18.

Gudmundsson, M. T., Högnadóttir, Þ., & Magnússon, E. (2015). Öræfajökull: Eruption melting scenarios. In E. Pagneux, M. T. Gudmundsson, S. Karlsdóttir, & M. J. Roberts (Eds.), *Volcanogenic floods in Iceland: An assessment of hazards and risks at Öræfajökull and on the Markarfljót outwash plain* (pp. 45–72). Reykjavík: IMO, IES-UI, NCIP-DCPEM.

Gudmundsson, M. T., Larsen, G., Höskuldsson, Á., & Gylfason, Á. G. (2008). Volcanic hazards in Iceland. *Jökull, 58*, 251–258.

Gudmundsson, M. T., Sigmundsson, F., & Björnsson, H. (1997). Ice-volcano interaction of the 1996 Gjálp subglacial eruption, Vatnajökull, Iceland. *Nature, 389*, 954–957.

Guðmundsson, H. J. (1998). *Holocene glacier fluctuations and tephrochronology of the Öræfi district, Iceland.* Edinburgh: University of Edinburgh.

Guðmundsson, S., Hannesdóttir, H., & Björnsson, H. (2012). Post-Little Ice Age volume loss of Kotárjökull glacier, SE-Iceland, derived from historical photography. *Jökull, 62*, 97–110.

Guttormsson, H. (1993). *Við rætur Vatnajökuls: byggðir, fjöll og skriðjöklar, Ferðafélag Íslands. Árbók 1993.* Reykjavík: Ferðafélag Íslands.

Hálfdanarson, E. (1918). Frásögn síra Einars Hálfdanarsonar um hlaupið úr Öræfajökli 1727, *Blanda*, *1*, 54-59.

Hannesdóttir, H., Björnsson, H., Pálsson, F., Aðalgeirsdóttir, G., & Guðmundsson, S. (2015). Variations of southeast Vatnajökull ice cap (Iceland) 1650–1900 and reconstruction of the glacier surface geometry at the Little Ice Age maximum. *Geografiska Annaler, Series A, Physical Geography, 97*, 237–264.

Helgadóttir, Á., Pagneux, E., Roberts, M. J., Jensen, E. H., & Gíslason, E. (2015). Öræfajökull Volcano: Numerical simulations of eruption-induced jökulhlaups using the SAMOS flow model. In E. Pagneux, M. T. Gudmundsson, S. Karlsdóttir, & M. J. Roberts (Eds.), *Volcanogenic floods in Iceland: An assessment of hazards and risks at Öræfajökull and on the Markarfljót outwash plain* (pp. 73–100). Reykjavík: IMO, IES-UI, NCIP-DCPEM.

Helgason, J. (2007). Bedrock geological map of Skaftafell, SE-Iceland, scale 1:25,000. Ekra Geological Consulting.

Helgason, J., & Duncan, R. A. (2001). Glacial-interglacial history of the Skaftafell region, southeast Iceland, 0-5 Ma. *Geology, 29*, 179–182.

Helgason, J., & Duncan, R. A. (2013). Stratigraphy, 40Ar–39Ar dating and erosional history of Svínafell, SE-Iceland. *Jökull, 63*, 33–54.

Henderson, E. (1818). *Iceland: Or the Journal of a Residence in that Island, During the Years 1814 and 1815* (Vol. 1). Edinburgh.

Höskuldsson, Á. (2012). Eldgos í Öræfajökli 1362. *Ráðstefna Kvískerjasjóðs 2012, 14 March 2012.* Retrieved 10.15.2015, from URL: http://www.umhverfisraduneyti.is/media/kvisker/Oraefajokull-1362-Kviskerjafundur2012.pdf

Höskuldsson, Á., & Thordarson, T. (2006). Eldgos í Öræfajökli 1362, og myndun gusthlaupa í upphafi eldgoss. *Geoscience Society of Iceland, Spring meeting.* Reykjavík.

Höskuldsson, Á., & Thordarson, T. (2007). The eruption of Oraefajokull 1362 and destruction of the district of Herad, SE-Iceland. *Cities on Volcanoes 5, 19–23 November 2007.* Shimabara: Volcanological Society of Japan.

Iturrizaga, L. (2008). Post-sedimentary Transformation of Lateral Moraines – the Tributary Tongue Basins of the Kviárjökull (Iceland). *Journal of Mountain Science, 5*, 1–16.

Ives, J. D. (1991). Landscape change and human response during a thousand years of climate fluctuations and volcanism: Skaftafell, southeast Iceland. *Pirineos, 137*, 5–50.

Jakobsson, S. P., Jónasson, K., & Sigurðsson, I. A. (2008). The three igneous rock series of Iceland. *Jökull, 58*, 117–138.

Jóhannesson, T., Björnsson, H., Magnússon, E., Guðmundsson, S., Pálsson, F., Sigurðsson, O., Thorsteinsson, T., and Berthier, E. (2013). Ice-volumes changes, bias estimation of mass-balance measurements and changes in subglacial lakes derived by lidar mapping of the surface of Icelandic glaciers. *Annals of Glaciology, 54*(63), 63–74.

Jónsson, G., Kristjansson, L., & Sverrisson, M. (1991). Magnetic surveys of Iceland. *Tectonophysics, 189*, 229–247.

Magnússon, E., Gudmundsson, M. T., Sigurdsson, G., Roberts, M. J., Höskuldsson, F., & Oddsson, B. (2012a). Ice-volcano interactions during the 2010 Eyjafjallajökull eruption, as revealed by airborne radar. *J. Geophys. Res., 117, B07405*.

Magnússon, E., Pálsson, F., Björnsson, H., & Gudmundsson, S. (2012b). Removing the ice cap of Oraefajokull central volcano, SE-Iceland: Mapping and interpretation of bedrock topography, ice volumes, subglacial troughs and implications for hazards assessments. *Jökull, 62*, 131–150.

Maizels, J. K. (1989). Sedimentology, paleoflow dynamics and flood history of jökulhlaup deposits: paleohydrology of Holocene sediment sequences in southern Iceland sandur deposits. *Journal of Sedimentary Petrology, 59*, 204–223.

Maizels, J. K. (1991). The origin and evolution of Holocene sandur deposits in areas of jökulhlaup drainage, south Iceland. In J. K. Maizels, & C. Caseldine (Eds.), *Environmental Change in Iceland: Past and Present* (pp. 267–302). Dordrecht: Kluwer.

Maizels, J. K. (1993). Lithofacies variations within sandur deposits: the role of run-off regime, flow dynamics and sediment supply characteristics. *Sedimentary Geology, 85*, 299–325.

Maizels, J. K. (1997). Jökulhlaup deposits in proglacial areas. *Quaternary Science Reviews, 16*, 793–819.

Major, J. J., & Newhall, G. C. (1989). Snow and ice perturbation during historical volcanic eruptions and the formation of lahars and floods. *Bulletin of Volcanology, 52*, 1–27.

Marren, P. (2005). Magnitude and frequency in proglacial rivers: a geomorphological and sedimentological perspective. *Earth-Science Reviews, 70*, 203–251.

Naranjo, J. L., Sigurdsson, H., Carey, S. N., & Fritz, W. (1986). Eruption of Nevado del Ruiz volcano, Colombia, on 13 November 1985: Tephra fall and lahars. *Science, 233*, 961–963.

Olavius, Ó. (1780). *Oeconomisk Reise igiennem de nordvestlige, norlige, og nordostlige Kanter af Island.* Copenhagen, 602–607 (in Danish)

Ólafsson, E. (1974). *Ferðabók Eggerts Ólafssonar og Bjarna Pálssonar um ferðir þeirra á Íslandi árin 1752–1757.* Reykjavík: Bókaútgáfan Örn og Örlygur.

Pagneux, E., & Roberts, M. J. (2015). Öræfi district and Markarfljót outwash plain: Rating of flood hazards. In E. Pagneux, M. T. Gudmundsson, S. Karlsdóttir, & M. J. Roberts (Eds.), *Volcanogenic floods in Iceland: An assessment of hazards and risks at Öræfajökull and on the Markarfljót outwash plain* (pp. 101–122). Reykjavík: IMO, IES-UI, NCIP-DCPEM.

Pierson, T. C. (2005). Hyperconcentrated flow - transitional processes between water flow and debris flow. In M. Jakob, & H. Oldrich (Eds.), *Debris-Flow Hazards and Related Phenomena* (pp. 159–202). Chichester, UK: Springer/Praxis.

Prestvik, T. (1982). Petrography, chemical characteristics and nomenclature of Öræfajökull rocks. (Bergfræðileg einkenni gosbergs úr Öræfajökli). *Jökull, 32*, 69–76.

Roberts, M. J. (2005). Jökulhlaups: a reassessment of floodwater flow through glaciers. *Reviews of Geophysics, 43*, 1–21.

Roberts, M. J., Russell, A. J., Tweed, F. S., & Knudsen, Ó. (2000). Ice fracturing during jökulhlaups: implications for floodwater routing and outlet development. *Earth Surface Processes and Landforms, 25*, 1429–1446.

Roberts, M. J., Russell, A. J., Tweed, F. S., & Knudsen, Ó. (2002). Controls on the development of supraglacial floodwater outlets during jökulhlaups. In Á. Snorrason, H. P. Finnsdóttir, & M. Moss (Eds.), *Extremes of the Extremes: Extraordinary Floods* (pp. 71–76). International Association of Hydrological Sciences.

Roberts, M. J., Sigurðsson, G., Sigurðsson, O., Pagneux, E., Jóhannesson, T., Zóphóníasson, S., Gudmundsson, M. T., Russell, A. J., Gylfason, Á. G., Höskuldsson, F., and Björnsson, B. B. (2011). The April 2010 Eruption of Eyjafjallajökull Volcano: Glacial flooding and attendant hazards. *IAVCEI Symposium Surface processes in volcanic terrains: the erosion, transport and redeposition of volcaniclastic material and their associated hazards.* Melbourne.

Russell, A. J., & Knudsen, Ó. (1999). An ice-contact rhythmite (turbidite) succession deposited during the November 1996 catastrophic outburst flood (jökulhlaup), Skeiðarárjökull, Iceland. *Sedimentary Geology, 127*, 1–10.

Russell, A. J., & Knudsen, Ó. (2002). The influence of flow stage on the sedimentology and morphology of November 1996 ice-contact jökulhlaup deposits, Skeiðarársandur, Iceland. In I. P. Martini, V. R. Baker, & G. Garzon (Eds.), *Flood and Megaflood Deposits: Recent and Ancient Examples* (pp. 67–83). Wiley-Blackwell.

Russell, A. J., & Marren, P. (1999). Proglacial fluvial sedimentary sequences in Greenland and Iceland: a case study from active proglacial environments subject to jökulhlaups. Skeiðararsandur, Iceland. In A. P. Jones, J. K. Hart, & M. Tucker (Eds.), *The Description and Analysis of Quaternary Stratigraphic Field Sections* (pp. 171–208). Quaternary Research Association.

Russell, A. J., Roberts, M. J., Fay, H., Marren, P., Cassidy, N. J., Tweed, F. S., & Harris, T. D. (2005). Icelandic jökulhlaup impacts: Implications for ice-sheet hydrology. *Geomorphology, 75*, 33–64.

Russell, A. J., Tweed, F., Roberts, M. J., Harris, T. D., Gudmundsson, M. T., Knudsen, O., & Marren, P. M. (2010). An unusual jökulhlaup resulting from subglacial volcanism, Sólheimajökull, Iceland. *Quaternary Science Reviews*, 1363–1381.

Selbekk, R. S., & Trønnes, R. G. (2007). The 1362 AD Öræfajökull eruption, Iceland: Petrology and geochemistry of large-volume homogeneous rhyolite. *Journal of Volcanology and Geothermal Research, 160*, 42–58.

Sigmundsson, F. (2006). *Iceland Geodynamics, Crustal Deformation and Divergent Plate Tectonics.* Chichester, UK: Praxis Publishing - Springer Verlag.

Sigurðsson, O., & Williams, R. S. (2008). *Geographic Names of Iceland's Glaciers: Historic and Modern.* U.S. Geological Survey.

Sigurðsson, O., Zóphóníasson, S., & Ísleifsson, E. (2000). Jökulhlaup úr Sólheimajökuli 18 Júlí 1999. *Jökull, 49*, 75–80.

Snorrason, Á., Jónsson, P., Pálsson, S., Árnason, S., Sigurðsson, O., Víkingsson, S., Sigurðsson, Á., and Zóphóniasson, S. (1997). Hlaupið á Skeiðarársandi haustið 1996 – útbreiðsla, rennsli og aurburður. In H. Haraldsson (Ed.), *Vatnajökull – Gos og hlaup 1996 (Vatnajökull – Eruption and Jökulhlaup 1996)* (pp. 79–137). Reykjavík: The Icelandic Public Road Administration.

Stevenson, J. A., McGarvie, D. W., Smellie, J. L., & Gilbert, J. S. (2006). Subglacial and ice-contact volcanism at the Öræfajökull stratovolcano, Iceland. *Bulletin of Volcanology, 68*, 737–752.

Sturm, M., Benson, C., & MacKeith, P. (1986). Effects of the 1966–68 eruptions of Mount Redoubt on the flow of Drift Glacier, Alaska, USA. *Journal of Glaciology, 32*, 355–362.

Sæmundsson, K. (1979). Outline of the geology of Iceland. *Jökull, 29*, 7–28.

Thompson, A., & Jones, A. (1986). Rates and causes of proglacial river terrace formation in southeast Iceland: An application of lichenometric dating techniques. *Boreas, 15*, 231–246.

Thorarinsson, S. (1956). On the variations of Svínafellsjökull, Skaftafellsjökull and Kviárjökull in Öræfi. *Jökull, 6*, 1–15.

Thorarinsson, S. (1958). The Öræfajökull eruption of 1362. *Acta Naturalia Islandica, 2*(4), 100.

Thorarinsson, S. (1959). Der Öræfajökull und die Landschaft Öræfi: Die Entwicklung einer isländischen Siedlung im Kampf gegen die Naturgewalten. *Erdkunde, 13*, 124–138.

Tilling, R. I. (1989). Volcanic hazards and their mitigation: progress and problems. *Reviews of Geophysics, 27*, 237–269.

Torfason, H. (1985). Geological map of Iceland, sheet 9, scale 1:250,000. SE-Iceland. Reykjavík, Iceland: Icelandic Museum of Natural History and Iceland Geodetic Survey.

Tómasson, H. (1996). The Jökulhlaup from Katla in 1918. *Annals of Glaciology, 22*, 249–254.

Trabant, D., Waitt, R. B., & Major, J. J. (1994). Disruption of Drift glacier and origin of floods during the 1989–1990 eruptions of Redoubt Volcano, Alaska. *Journal of Volcanology and Geothermal Research, 62*, 369–385.

Waitt, R. B., Gardner, C. A., Pierson, T. C., Major, J. J., & Neal, C. A. (1994). Unusual ice diamicts emplaced during the December 15, 1989, eruption of Redoubt Volcano, Alaska. *Journal of Volcanology and Geothermal Research, 62*, 409–428.

Waythomas, C. F. (2015). Geomorphic consequences of volcanic eruptions in Alaska: A review. *Geomorphology, 246*, 123–145.

Waythomas, C. F., Pierson, T. C., Major, J. J., & Scott, W. E. (2013). Voluminous ice-rich and water rich lahars generated during the 2009 eruption of Redoubt Volcano, Alaska. *Journal Volc. Geoth. Res., 259*, 389–413.

Þórarinsson, S. (1974). *Vötnin Stríð: Saga Skeiðarárhlaupa og Grímsvatnagosa.* Reykjavík, Iceland: Menningarsjóður.

III. ÖRÆFAJÖKULL VOLCANO: ERUPTION MELTING SCENARIOS

Magnús T. Gudmundsson *, Þórdís Högnadóttir *, Eyjólfur Magnússon *

* *Nordic Volcanological Centre, Institute of Earth Sciences, University of Iceland*

1. Introduction

Observations of recent volcanic unrest demonstrate that melting of ice in eruptions within glaciers can be extremely fast. The best documented cases have occurred in the last quarter of a century in Grímsvötn, Gjálp, Eyjafjallajökull and Redoubt in Alaska (e.g. Gudmundsson *et al.*, 1997, 2004; Gudmundsson, 2005; Magnússon *et al.*, 2012a; Waythomas *et al.*, 2013) and some earlier events such as the Katla 1918 eruption (Tómasson, 1996; Björnsson, 2003) and the eruptions of Mount St. Helens in 1980–1983 (Pierson, 1999), Nevado del Ruiz in 1985 (Pierson *et al.*, 1990) and Redoubt in 1989–90 (Dorava and Meyer, 1994; Trabant *et al.*, 1994). For eruptions observed in Iceland, the highest rates of heat transfer and melting occur in the early, fully subglacial phases of explosive eruptions where the magma is fragmented into glass particles, typically in the size range 0.01–1 mm (e.g. Gudmundsson, 2003). More gradual melting is expected to occur when heat transfer takes place largely by free convection of water above rapidly cooled lava under ice (e.g. Höskuldsson and Sparks, 1997; Gudmundsson, 2003; Woodcock *et al.*, 2012, 2014). Thus, because of their greater potential to melt large amounts of ice in a short period of time, eruptions where fragmentation is dominant are more dangerous. The analysis presented here is therefore mostly concentrated on eruptions dominated by fragmentation and their consequences.

The purpose of the present work is to estimate the potential hazard due to jökulhlaups associated with volcanic activity in Öræfajökull. The approach is therefore to consider what can be defined as realistic worst case scenarios. This needs to be kept in mind when considering the results. The scenarios with the highest probability are less extreme. Three types of eruptions/events are considered. (1) Eruptions within the caldera of Öræfajökull (thick ice), (2) eruptions on the flanks (thin ice), and (3) pyroclastic density currents (PDCs). The values of various parameters used in calculations and definitions of terms are listed in Table III-1. In this chapter a short overview of the area being considered is given in Section 2 while the magnitudes of eruptions that occur in Iceland are reviewed briefly in Section 3. In Section 4, calorimetric considerations on the various types of volcanic events are presented and empirical data used to constrain efficiencies of processes. The jökulhlaups, their entrainment of volcanic material and the onset times are considered in Section 5. It is assumed that a flood breaks through the ice and starts to cascade downslope mostly on the surface and along the margins of outlet glaciers where ice on the slopes is shallow as on Öræfajökull. This behaviour was for example observed in Eyjafjallajökull in 2010 (Magnússon *et al.*, 2012a). The propagation of the flood once it has reached the upper parts of the outlets is not considered further here since it is dealt with in Chapter IV (Helgadóttir *et al.*, 2015). The results for the various catchments and outlet glaciers for the three types of events considered are presented in Section 6.

Table III-1: List of symbols, abbreviations and numerical values of parameters.

Symbol	definition	Unit
PDC	Pyroclastic density current	-
MER	Mass eruption rate	kg/s
EOT	Eruption onset time	min
STT	Subglacial transport time	min
FTT	Flank transit time	min
$\frac{dE}{dt}$	Rate of heat transfer / energy flux	W
E_p	Energy available to melt snow and ice in a PDC	J
f	Efficiency of heat transfer (0–100%, in reality f_{max}~80–90%)	Dimensionless
χ	Fraction of tephra entrained in phoenix cloud during PDC formation	Dimensionless
ξ	Fraction of PDC flowing over a particular catchment	Dimensionless
Q_m	Volumetric flow rate of magma	m^3/s
$\dot{M}_m$	Mass eruption rate	kg/s
$\dot{m}$	Mass eruption rate per unit length of volcanic fissure	(kg/s)/m
$\dot{M}_p$	Mass generation rate of pyroclastic material at eruption site (usually equal to mass eruption rate)	kg/s
$\dot{M}_w$	Mass generation rate of meltwater at eruption site	kg/s
Q_1, Q_2, Q_w	Rate of liquid water generation by ice melting	m^3/s
Q_T	Discharge of jökulhlaup (liquid water + entrained ice and pyroclasts)	m^3/s
ρ_m	Magma density	kg/m^3
ρ_g	Tephra	kg/m^3
ρ_i	Density of ice	kg/m^3
ρ_w	Density of liquid water	kg/m^3
T_i, T_f, ΔT	Temperature, i: initial, f: final, ΔT: temperature difference	°C
T_e	Emplacement temperature of pyroclastic density current	°C
T_0	Ambient air/snow temperature (~0°C)	°C
L_i	Latent heat of solidification of ice, $L_i = 3.34 \times 10^5$ J/kg	J/kg
C_g	Specific heat capacity of fresh volcanic glass	J/(kg °C)
C_p	Specific heat capacity of pyroclastic material in collapse	J/(kg °C)
l	Length – used here for volcanic fissure at base of glacier	m
x	Length	m
q	Rate of meltwater production per unit length of fissure	m^2/s
ΔV_i	Volume of ice	m^3
M_p	Massi of pyroclastic material	kg
M_g	Mass of pyroclasts interacting with glacier/snow in pyroclastic density current	kg

Symbol	definition	Unit
τ	Duration of plume collapse forming pyroclastic density current.	s
t_{run}	Period it takes a ground hugging PDC to flow over snow/ice and release heat	s
φ	Static fluid potential of water flow under ice	Pa
g	Acceleration due to gravity g = 9.82 m/s^2	m/s^2
z_b	Height of glacier bed (usually above sea level)	m
z_s	Height of glacier surface (usually above sea level)	m

2. Öræfajökull and its potential to generate jökulhlaups

The height and overall morphology of Öræfajökull with an ice-filled caldera and ice covered upper slopes makes jökulhlaups an almost inevitable consequence of eruptions on the upper parts of the volcano. The two historical examples of 1362 and 1727 demonstrate this, as shown by Thorarinsson (1958) and Roberts and Gudmundsson (2015; this volume, chapter II). The part of the mountain massif considered here is the presently active volcano south of Svínafellsjökull and Hermannaskarð (Figures III-1 and III-2). The ice-covered part of the volcano has recently been mapped with radio-echo soundings (Magnússon *et al.*, 2012b). For the jökulhlaup hazard, the following water catchment basins were considered:

i) The southern catchment of Svínafellsjökull: Only considered here as a potential source of jökulhlaups caused by pyroclastic density currents.

ii) Virkisjökull-Falljökull: This includes a section of the caldera and the flanks north of Sandfell. Can be affected by caldera eruptions, flank eruptions and pyroclastic density currents. This also includes Grænafjallsgljúfur, to the south of Falljökull.

iii) Kotárjökull: This catchment reaches the caldera rim but is mainly confined to the slopes. Flank eruptions can occur here and the flanks of the catchment can be affected by pyroclastic density currents.

iv) Rótarfjallshnjúkur-Hnappur and glaciers to the south of these nunataks: The upper boundary of this segment is the southern caldera rim. Can be affected by flank eruptions and pyroclastic density currents.

v) Kvíárjökull: This includes a large part of the caldera, the slopes of Kvíárjökull and its lower part. Can be affected by caldera eruptions, flank eruptions and pyroclastic density currents.

vi) Eastern flank of Öræfajökull north of Kvíárjökull: The upper slopes are similar to those on the west side and can be affected by flank eruptions and possibly pyroclastic density currents. However, since the inundation area of jökulhlaups is not inhabited, this segment is not considered in the same way as those on the west and south side.

3. Magma discharge in eruptions

Models exist that relate magma flow rate in an explosive eruption with eruption plume height (Sparks *et al.*, 1997; Mastin *et al.*, 2009; Woodhouse *et al.*, 2013; Degruyter and Bonadonna, 2012). These equations, however, are very sensitive to the plume height, the plume height is related to both magma flow rate and wind speed and discrepancies between predicted and observed flow rate may be as much as a factor of 3–4 (Oddsson *et al.*, 2012). These equations are not used here.

In Table III-2 the estimated magma flow rate of several Icelandic eruptions are given

together with known fissure lengths. In most cases the numbers in the table are mean values over some interval during the most powerful phase of the eruption.

However, the peak values may well have been 2–3 times higher in some cases and for the largest ones $\dot{M}$ may have reached or exceeded 10^8 kg/s.

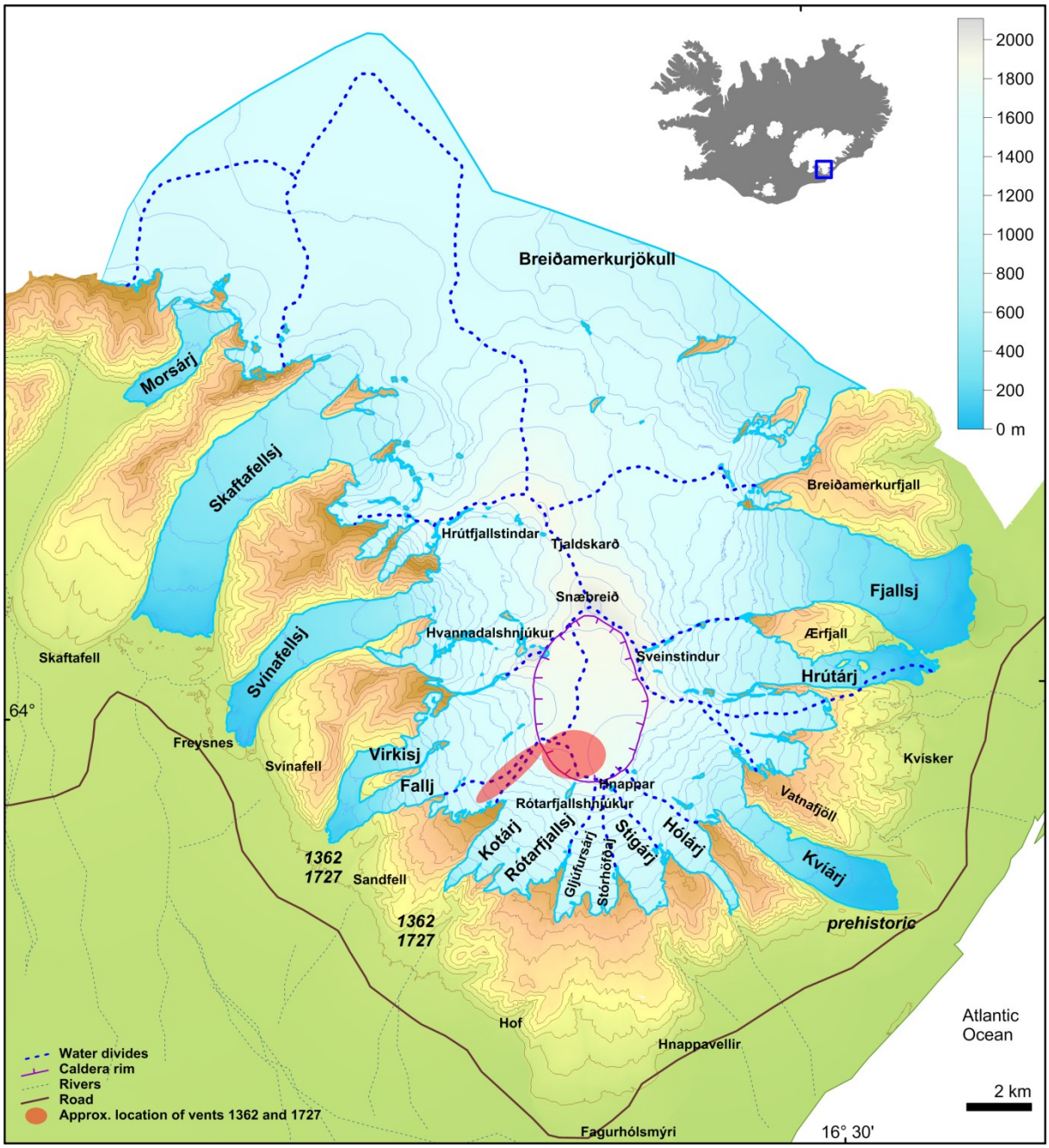

Figure III-1: Öræfajökull and surroundings, Surface topography and ice catchment basins. The main pathways of the jökulhlaups of 1362 and 1727 were down Falljökull and Kotárjökull.

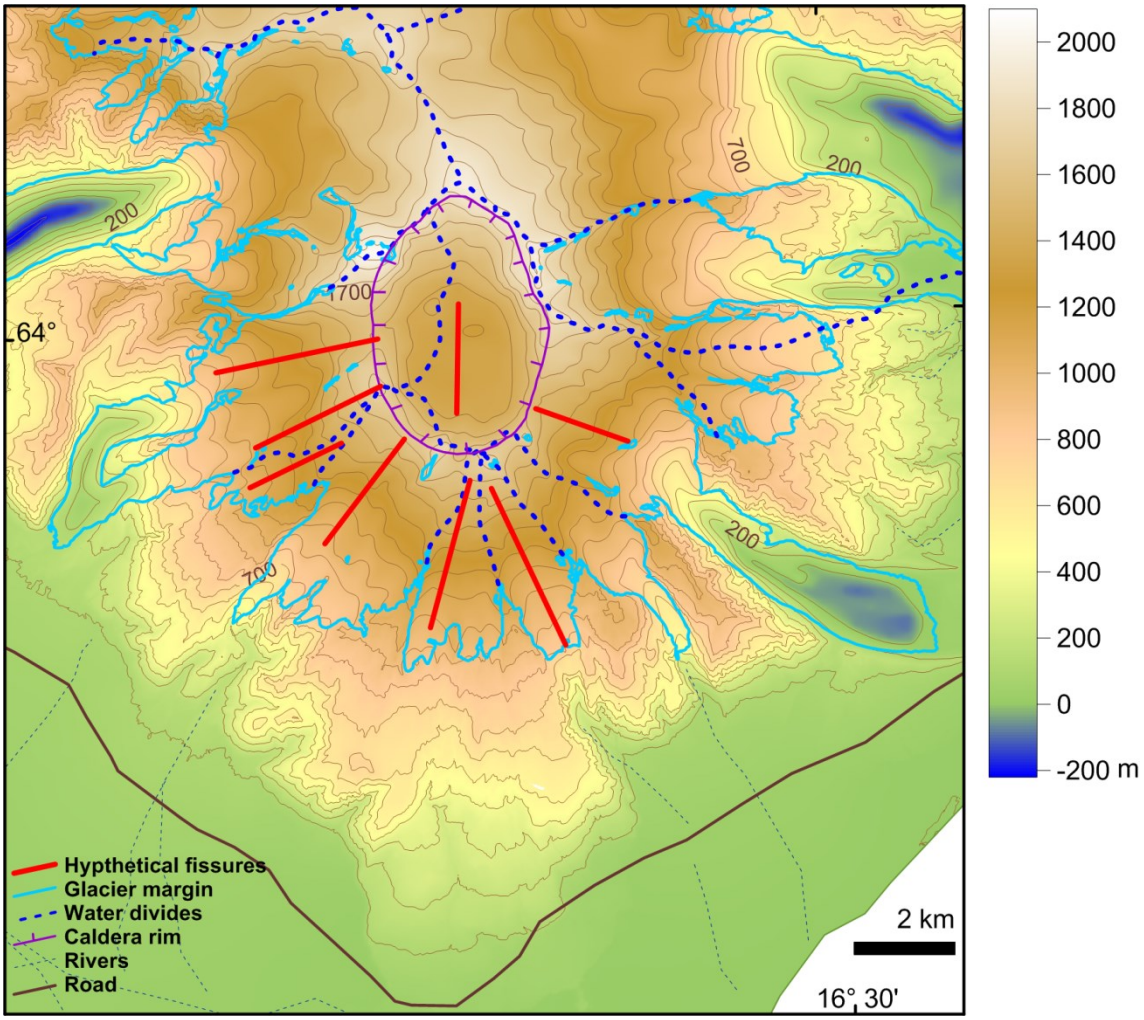

Figure III-2: Bedrock topography of Öræfajökull (after Magnússon et al. 2012b). The bottom of the caldera is an enclosed depression that would collect water if it were not ice-filled.

4. Models of ice melting in eruptions

The conceptual models of magma melting considered here concur with the highest melting rates observed at certain ice thicknesses and eruption rates (Figure III-3):

- *Magma fragmentation under thick ice (>200 m),* initially within a mostly water-filled cavity under a glacier, leading to highly efficient heat transfer from magma. An ice cauldron bounded by concentric crevasses may form on the surface as meltwater drains away subglacially. This type of event can be expected within the caldera of Öræfajökull.

- *Magma fragmentation within a fissure through ice*, with rapid initial widening of the fissure through melting. This model applies where rapid opening to the ice surface takes place and ice deformation is small in relation to vertical ice melting rates. This applies to relatively thin ice, but the thickness at which this occurs is expected to depend on the intensity of the eruption. In most cases this behaviour, as opposed to a subglacial water-filled cavity, is expected to occur in ice <200 m thick.

- *Snow and ice melting where pyroclastic density currents*, caused by plume collapse, flow over glaciers.

In Section 4.1 general considerations of heat content and calorimetric equations presented for heat transfer. In 4.2 the effect of an elongated vent (volcanic fissure) are considered, in 4.3 equations for thin ice (~<200 m) are presented and the thick ice in Section 4.4. In 4.5 estimates for the melting potential of pyroclastic density currents are given.

Table III-2: Maximum discharge (Q_m, in m^3/s), mass eruption rate ($\dot{M}$ in kg/s), fissure length (l) and mass eruption rate per unit length of fissure ($\dot{m} = \dot{M}/l$) where known, for some Icelandic eruptions.

Eruption	*Ref.*	*Magma type*	Q_m m^3/s	ρ_m kg/m^3	$\dot{M}$ kg/s	l m	m' kg/m/s
Hekla 1947	1	dacite	75,000	620	$4{,}7 \cdot 10^7$	4000	11600
Hekla 1991	2,3	andesite			$\sim 6 \cdot 10^6$	~4000	~1500
Gjálp 1996	4	Icelandite			$4 \cdot 10^6$	~4000	~1000
Grímsvötn 2004	5	basalt			$6 \cdot 10^5$	600	1000
Grímsvötn 2011	6	basalt			$1 \cdot 10^7$	1500	6700
Eyjafjallajökull 2010	7	trachyandesite			$1 \cdot 10^6$	1000	1000
Skaftáreldar* 1783	8	basalt	8,500	1450	$1{,}2 \cdot 10^7$	2200	5600
Askja 1875	9	rhyolite	125,000	-	$6.8 \cdot 10^7$	-	-

(1) Thorarinsson (1967); (2) Gudmundsson *et al.* (1992); (3) Larsen *et al.* (1992); (4) Gudmundsson *et al.* (2004); (5) Jude-Eton *et al.* (2012); (6) Hreinsdóttir *et al.* (2014); (7) Gudmundsson *et al.* (2012); (8) Thordarson and Self (1993), Carey *et al.* (2010). * For Laki (Skaftáreldar 1783) the values of Q_m and l given applies to the segment active at any given time (for details see Thordarson and Self (1993).

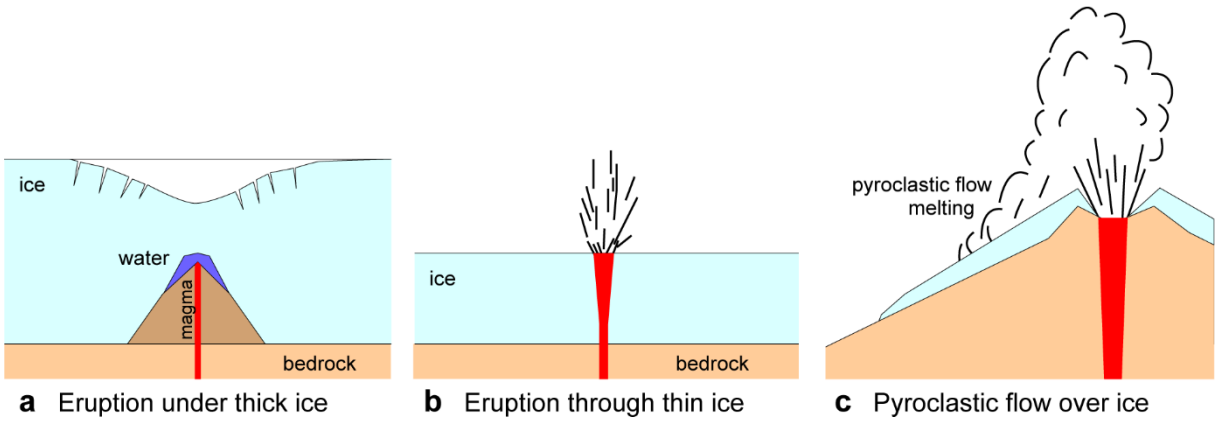

Figure III-3: The main scenarios for ice melting in eruptions at ice covered volcanoes. (a) Eruption under thick ice, (b) eruption through thin ice, and (c) pyroclastic density currents flowing over ice covered slopes (modified from Edwards et al., 2015).

4.1. Heat transfer and efficiency

In the end-member case when all the magma erupted is fragmented into glass particles, no crystallisation occurs (Carmichael *et al.*, 1974; Wohletz *et al.*, 2013). The products of several recent subglacial eruptions suggest that this is a good approximation to the actual process (Gudmundsson, 2003; Jarosch *et al.*, 2008; Jude-Eton, 2012). Thus, it can be assumed that the latent heat of crystallization is insignificant. The processes that occur

when magma encounters ice are complicated, involving rapid cooling and breakup of the magma into mostly angular and blocky glass particles of dimensions <1 mm (Zimanowski, 1998; Zimanowski and Büttner, 2003). The cooling rates of these particles are characteristically in the range 10^3–10^5 °C/s. As a result, rapid heating of water with a varying degree of boiling occurs (Figure III-4). This is expected to result in fast, partially forced convection that transfers magmatic heat to overlying ice with meltwater as the working fluid, probably with two phases present, liquid and steam (Gudmundsson, 2003; Woodcock *et al.*, 2012; Woodcock *et al.*, 2014). The details of these processes are beyond the scope of this report. Instead the heat transfer is approached through calorimetric considerations using extensively the concept of efficiency of heat transfer from the magma (Höskuldsson and Sparks, 1997; Gudmundsson, 2003).

The rate of heat transfer (dE/dt) in a subglacial eruption from magma to the surroundings is given through:

$$\frac{dE}{dt} = f\rho_m Q_m C_g \Delta T = f\dot{M}_m C_g \Delta T \qquad (1)$$

Here ρ_m is magma density, Q_m is the flow of magma (m^3/s) with $\rho_m Q_m$ being equivalent to the magma mass flux $\dot{M}_m$ (in kg/s), C_g is the specific heat capacity of the glass (J/(kg K)), $\Delta T = (T_i - T_f)$ is the change in temperature with T_i being magma temperature, T_f the temperature of the glass after cooling to ambient temperature, and f is efficiency of the heat transfer process (Gudmundsson, 2003) — see also Table III-1 for nomenclature. The simplifying assumption is made that C_g is a constant when in reality it is a moderately varying function of temperature. However, the error introduced by assuming constant specific heat capacity is small (Gudmundsson, 2003). Another factor not considered here is the energy required to fragment the magma (Schmid *et al.*, 2010). This may amount to 5–10% of the original thermal energy. However, this factor is only indirectly accounted for in the equations as an upper limit on the thermal efficiency.

The efficiency f is difficult to estimate directly. It was, however, done for the Gjálp 1996 eruption, defined as the ratio of the energy required to melt the ice during the eruption (30 September – 13 October 1996) and the total thermal energy of the erupted magma. Two definitions of thermal efficiency have been used: The efficiency of heat transfer from magma to ice, and the efficiency of heat transfer from magma to meltwater. These two definitions give different results when applied at the eruption site itself, where the meltwater usually has a temperature substantially above zero.

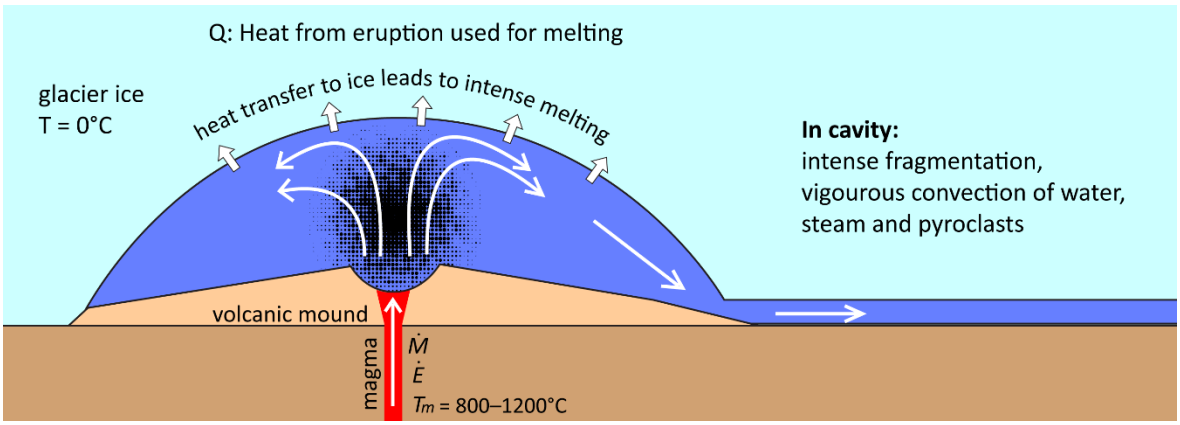

Figure III-4: Conceptual model of heat transfer and melting in an eruption under thick ice (>200 m).

If a jökulhlaup has a long subglacial path, this heat, initially stored in the meltwater, is released through ice melting along the flow path.

For Gjálp the efficiency of heat transfer to ice was 0.50-0.61 (50–61%) and to water 0.63–0.77 (63–77%) (Gudmundsson *et al.*, 2004). In most cases relating to jökulhlaup hazard, the efficiency of heat transfer to water is relevant because the melting along the path contributes to the meltwater generation. During some eruptions the efficiency of heat transfer to water may have been even higher than for the Gjálp event. This may have been the case during the Katla eruption of 1918, where the majority of the initially erupted material was volcanic glass transported with the meltwater (Tómasson, 1996; Larsen, 2000) — hereafter referred to as water-transported tephra. The temperature of these pyroclasts as they emerged with the floodwaters in 1918 was probably close to zero, way below the 200–300°C obtained as residual heat in the volcanic edifice built during the Gjálp eruption; a value obtained by considering heat released during post-eruption melting (Jarosch *et al.*, 2008).

Under a glacier, the heat transferred rate from magma is largely dissipated through ice melting. If it is assumed that the ice is temperate (at pressure melting point for ice – close to 0°C) as applies to Icelandic glaciers (e.g. Björnsson and Pálsson, 2008), ρ_i and ρ_w are the densities of ice and water respectively and L_i latent heat of solidification of ice, the melting rate Q_w (in water equivalent m^3/s) is:

$$Q_w = \frac{\rho_i}{\rho_w}\frac{1}{\rho_i L_i}\frac{dE}{dt} = \frac{f\dot{M}_m C_g \Delta T}{\rho_w L_i} \qquad (2)$$

This equation can be applied to all cases where an estimate of efficiency and mass flux can be made. The magnitude of some of the parameters is dependent on magma type, where ΔT ranges from up to 1200°C for primitive basalts to ~800°C for rhyolites. Likewise, C_g is higher for basalts (1000–1200 J/kg K) than for rhyolites (~900 J/kg K) (e.g. Höskuldsson and Sparks, 1997; Bacon, 1977).

4.2. Fissure eruptions

For a fissure eruption with length l and magma flux $\dot{m} = \dot{M}/l$ per unit length of fissure (in kg/s m) equation (2) becomes:

$$Q_w = \frac{f l \dot{m} C_g \Delta T}{\rho_w L_i} \qquad (3)$$

This equation could be used to calculate the mass flux in an eruption if both fissure length l and meltwater discharge Q_w are known. However, in practice this is difficult since independent estimates of the meltwater flow rate are often hard to obtain in real cases. The equation is nevertheless useful since it provides a way to estimate possible ranges of melting rates and hence jökulhlaup sizes in eruptions on ice covered volcanoes (Gudmundsson and Högnadóttir, 2005, 2006). Although the magma flow rates have only been estimated for a handful of subglacial eruptions, a considerable body of data exists on magma flow rates in e.g. effusive eruptions in Iceland and elsewhere (Table III-2).

4.3. Thin ice (less than ~200 m)

Experience from eruptions in Iceland and elsewhere suggests for basaltic and intermediate compositions, that all eruptions except the smallest ones starting under ice thicknesses <200 m melt their way through the overlying ice by forming cauldrons with vertical ice walls (Smellie, 2002; Gudmundsson, 2005; Magnússon *et al.*, 2012a). Observations are lacking for dacitic and rhyolitic eruptions within glaciers but it is expected that they would behave in a similar way. Within the walls, ice is completely melted away, but ice deformation and flow into the depression is relatively minor, except on steep ground where gravity pulls ice downwards into the crater from the uphill side. Thus a cauldron with very steep to vertical ice walls is typically formed around the eruption site.

In the case of a fissure eruption, the cauldron is elongated, forming an ice canyon reaching from the base of the glacier to the surface. Observations of the rate at which cauldrons widen can provide constraints on the melting rate. Table 3 shows the available data on the widening of ice cauldrons, based on observations of eruptions at Grímsvötn, Eyjafjallajökull and Deception Island.

4.3.1. Widening of ice cauldrons

The widening rate of an ice cauldron (Figure III-5) can be used to estimate the approximate melting rate in an eruption within a glacier characterized by thin ice (~200 m or less). If ρ_i and ρ_w are defined as before, h is ice thickness and l is the length of the eruptive fissure, an elongated ice cauldron is formed that acquires a width Δb during time Δt. The rate of melting is then given with:

$$Q_1 = \frac{\rho_i}{\rho_w} hl \frac{\Delta b}{\Delta t} \quad (4)$$

The most critical parameter here is Δb.

Table III-3: Dimensions and widening rates of ice cauldrons/canyons formed around volcanic fissures in eruptions under shallow ice. Estimates of parameters for equation (4) and (5).

Eruption	Width of cauldron: Δb (m)	Time since start or eruption: Δt (s)	$\frac{\Delta b}{\Delta t}$ (m/s)
Grímsvötn 1998	~100	~7200	$1.4 \cdot 10^{-2}$
Deception Island 1969	~100	~7200	$1.4 \cdot 10^{-2}$
Grímsvötn 2004	~400	~45000	$0.9 \cdot 10^{-2}$
Eyjafjallajökull 2010	~250	~25000	$1.0 \cdot 10^{-2}$

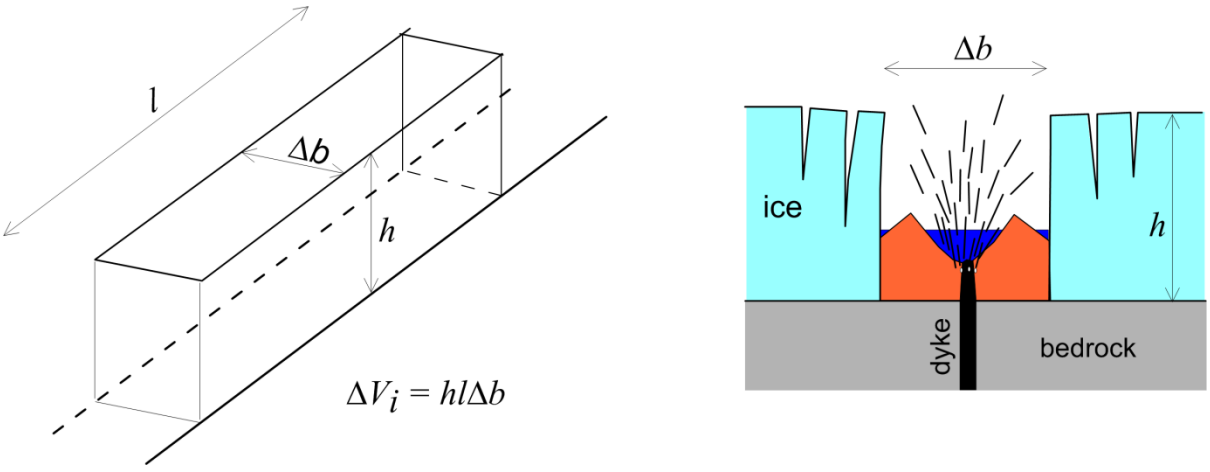

Figure III-5: Schematic setting for a volume model for melting rates in a fissure eruption on a flank where ice is thin (<200 m). From Gudmundsson and Högnadóttir (2005).

4.3.2. Melting rate per unit length of fissure

An alternative approach is to use a purely empirical equation, where the average melting rate per unit length of the volcanic fissure is obtained as the mean of the available data. The total melting rate is then a simple scaling with respect to the fissure length. The difference between this approach and equation (4) is that thickness of ice is not used as a variable. The melting rate factor q is obtained for each test case from:

$$q = \frac{\rho_i}{\rho_w}\frac{\Delta V_i}{l\Delta t} \quad (5)$$

Here ΔV_i is the volume of ice melted over time Δt and length of volcanic fissure is l as in eq. (4). The range of values obtained for the eruptions used in Table III-3 is 0.9–1.4 m^2/s. The highest values are considered to be the most representative for the initial 1–2 hours and they are therefore used in our calculations.

The total melting rate in a fissure eruption using this approach is given by:

$$Q_2 = ql \quad (6)$$

Equations (4) and (6) are applied to estimate the melting rate in hypothetical fissure eruptions on the flanks of Öræfajökull. It should be noted that the equations provide estimates that only apply to the first few hours of an eruption starting under thin (<200 m) ice. After the initial phase, when the cauldron/canyon has reached a width of 200–300 m, the increased distance between volcanic fissure and the ice wall will lead to reduced melting as an increased fraction of the heat associated with the eruption is transferred to the atmosphere with the eruption plume.

4.4. Thick ice (>200 m)

When the ice thickness exceeds 200 meters, in all but the most powerful eruptions, the effects of ice flow are expected to begin to play a role, with meltwater draining away from the eruption site in most cases, leading to the formation of an initial ice depression (ice cauldron) over the subglacial vents (Figures III-3a and III-4). The time it takes to melt through the ice and establish a connection to the atmosphere will be significant, and an interval will exist where the eruption is fully subglacial and meltwater drains away at a rate comparable to the rate at which meltwater is generated. During this subglacial period the melting rate will be governed by the magma flow rate (eq. 2).

Effusive, fully subglacial eruptions may occur at Öræfajökull. Equation (2) still holds but the efficiency is expected to be much less than the 0.6–0.8 used for fragmentation; values in the range 0.10–0.45, with the lower values applying to eruptions with high magma discharge (Gudmundsson, 2003).

Mass eruption rates (MER), observed during large eruptions in Iceland are in the range 10^7–10^8 kg/s (Table III-2). The efficiencies used for magma fragmentation (0.6–0.8) translate to meltwater generation rates of 30,000–300,000 m^3/s. These values are of the right order of magnitude compared to large historically documented jökulhlaups from Katla and Öræfajökull.

4.5. Pyroclastic density currents

Melting of snow and ice by PDC's is well documented for the eruptions of Redoubt in 1989–90 and 2009. Column collapses in vulcanian explosions lead to the flow of hot pyroclasts down the steep slopes of Drift Glacier, entrainment of snow and rapid melting. Debris flows caused by dome collapses had a similar effect. These melting events lead to lahars (hyperconcentrated floods) down the Drift River Valley. The peak discharges high in the valley have been estimated as 10^4–10^5 m^3/s (Waythomas *et al.*, 2013). The events were, however, of short duration and the peak discharges observed at the mouth of the valley were much reduced. Similar events were observed at Mount St. Helens in 1980–83 (Waitt *et al.*, 1983).

At Nevado del Ruiz on 13 November 1985 a series of PDCs were formed over a period of a few minutes at the start of the main eruptive pulse of a VEI 3 eruption (Pierson *et al.*, 1990). These PDC's were initiated at the summit vent at an elevation over 5000 m. They swept across the 10 km^2 summit ice cap and within minutes of their start, dilute flows of water and tephra cascaded down the steep slopes into narrow canyons radiating outwards from the volcano. Within the canyons, the lahars accumulated more solid material, including loose sediments at the bottom of the canyons and tephra from the ongoing eruption. These lahars flowed along these canyons for tens of kilometres. One of them inundated the town of Armero, located at the mouth of a canyon, 74 km from the summit, killing 23 thousand people over the course of several minutes. From the perspective of lahar initiation, an important lesson from Nevado el Ruiz is that the ice and snow melting occurred over a period of only a few minutes.

The events observed in the eruptions mentioned above where of short duration and high discharge, but usually at short runout distances (<50 km). The pyroclastic density currents/debris flows causing them were moderate in size compared to what is to be expected in a major Plinian eruption such as occurred in Öræfajökull in 1362.

Walder (1999) studied melting of pyroclastic deposits on Mount St. Helens and came to the conclusion that pumice deposits melted a layer that was about the same thickness as the pyroclastic deposit. However, no models, comparable to those already presented for subglacial eruptions, have been published to estimate the melting rates and melted volumes generated by hot PDCs flowing over snow and ice. Observations and experimental results indicate that PDCs scour the underlying snow and ice surface, not only mechanically but also thermally (Walder, 2000a, b). The mechanical scouring occurs as the PDC erodes and excavates the underlying snow and ice. The thermal scouring follows from heating of the ice and snow resulting in thermal convection that can promote fluidization of the pyroclast-snow-meltwater mixture (Walder, 2000a, b).

PDCs are characteristically dense, hot, ground hugging granular avalanches (Branney and Kokelaar, 2002; Roche *et al.*, 2013). The dilute end-member of a PDC, is the pyroclastic surge which is principally made of hot gas with pyroclastic particles suspended in the flow (e.g. Roche *et al.* 2013). For the case of ice surface melting, it is the dense types of PDCs that are relevant. It is not the intention here to go deeply into the physics of PDCs. Instead the following treatment will consider the thermal energy of PDCs and to what extent they can melt snow and ice.

In what follows, an attempt is made to quantify melting rates resulting from pyroclastic density currents flowing over snow and ice (Figure III-6). The key parameters are the mass eruption rate (MER), the mass of pyroclastic material in a collapsing plume event, the duration of collapse and the emplacement temperature T_e of the currents (the temperature of current when it first makes contact with snow/ice). We consider the case where, during an explosive eruption with a MER $\dot{M}$, the column collapses. The collapse occurs over time τ. The total mass of pyroclastic material that collapses is:

$$M_p = \dot{M}\tau \qquad (7)$$

A fraction χ of this material entrains sufficient air to become buoyant and forms a secondary eruption cloud (phoenix cloud). This material does not contribute energy towards snow melting. The mass of pyroclastic material in contact with ice and snow is:

$$M_g = (1-\chi)M_p = (1-\chi)\dot{M}\tau \qquad (8)$$

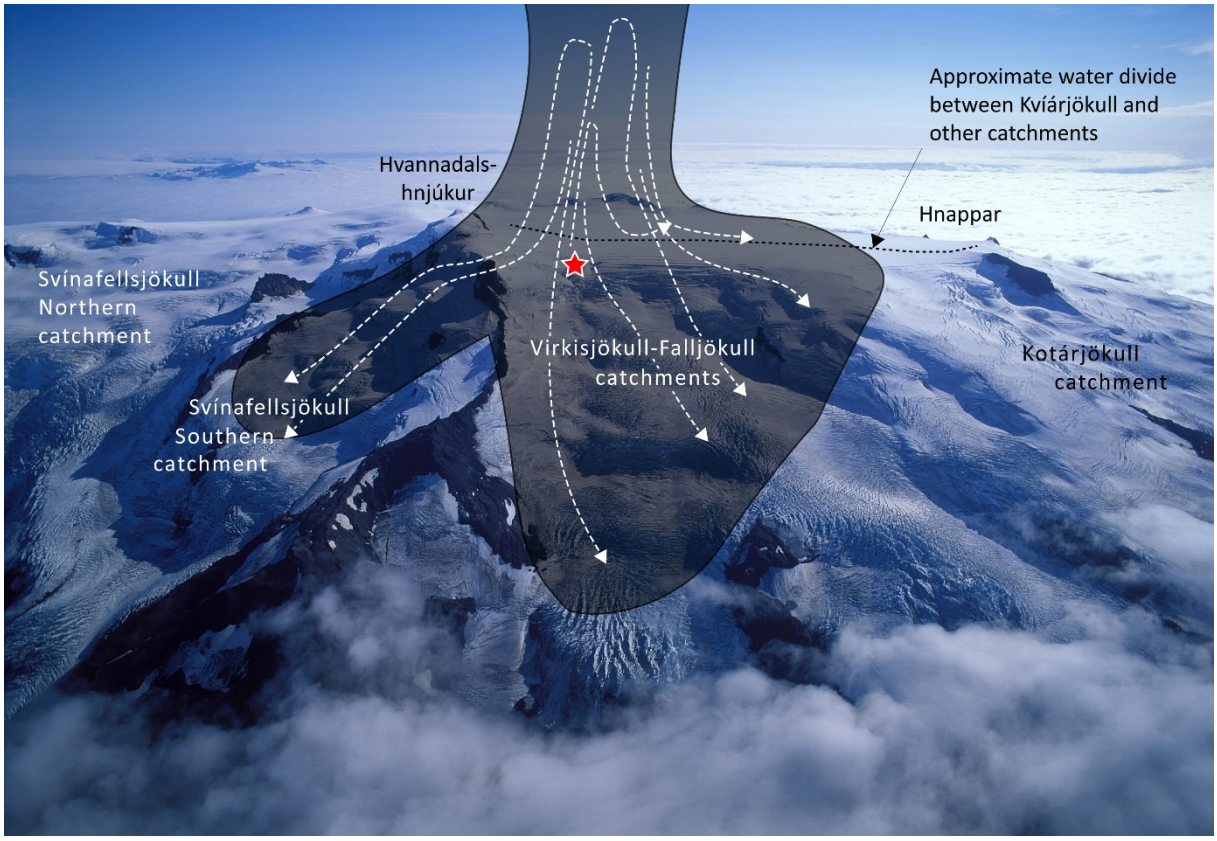

Figure III-6: Hypothetical setting for pyroclastic density current (PDC) generation in a Plinian eruption in the northwest part of the Öræfajökull caldera. The dark areas indicate the plume and the PDC. It is expected that a large PDC will cover a much greater area, reaching the lowlands beyond the volcanic edifice. Photo: Snævar Guðmundsson.

The energy that is available to melt snow and ice is therefore:

$$E_p = f(1-\chi)\dot{M}\tau C_p(T_e - T_0) \qquad (9)$$

Where f is the efficiency of the process, C_p is the specific heat capacity of the pyroclasts, T_e is emplacement temperature and T_0 ambient temperature (~0°C). It is to be expected that effective mixing of pyroclasts and snow will occur as the density current advances at high velocity along the surface, as it did at Nevado de Ruiz, Redoubt and Mount St Helens. The total amount of snow and ice melted from the surface of the glacier is:

$$V_w = \frac{E_p}{L_i\rho_w} = \frac{f(1-\chi)\dot{M}\tau C_p(T_e-T_0)}{L_i\rho_w} \qquad (10)$$

The average melting rate (meltwater generation rate) for a given catchment is then found from:

$$Q_w = \xi\frac{V_w}{t_{run}} = \frac{\xi f(1-\chi)\dot{M}\tau C_p(T_e-T_0)}{L_i\rho_w t_{run}} \qquad (11)$$

Where ξ is the fraction of the total pyroclastic density current generated that affects the catchment. For example, a large column collapse in a hypothetical major eruption with a vent in the western part of the caldera may lead to pyroclastic density currents that will partly overspill to the Svínafellsjökull catchment, partly flow down Virkisjökull-Falljökull and partly flow across the more southerly catchment of Kotárjökull and possibly further to the south.

Jökulhlaups could occur from all these catchments simultaneously as a result. The time t_{run} is the time it takes for a PDC to flow over the glacier and release its heat to the underlying snow and ice. The variable t_{run} is not well constrained, but it is here set as 10 minutes.

Mass eruption rate (MER): During major Plinian eruptions, usually erupting dacite or rhyolite (Table III-2), MERs of 10^8 kg/s occur in Iceland. The recent example is considered to be Askja 1875, since although the mean eruption rate did not quite reach this value (Table III-2), Carey *et al.* (2010) suggest that during the peak of the eruption the mass eruption rate was ~10^8 kg/s. Other eruptions of this magnitude include Öræfajökull 1362, Hekla 1104, Hekla 3, Hekla 4 and Katla ~10–11 kyr BP (Vedde ash eruption). We therefore use 10^8 kg/s for estimating the possible effects at a major eruption in Öræfajökull.

Heat transfer efficiency: The efficiency of melting by PDCs is highly uncertain and depends on the thermal effects of pyroclast interaction with snow and ice, the degree of scouring and entrainment of the snow and ice and the interplay among these processes. As in the other cases considered, it is the fast or semi-instantaneous rate of heat loss that is relevant. In the light of the observed melting at e.g. Redoubt and Nevado de Ruiz, it is likely that the efficiency can be comparable to that of a subglacial eruption with fragmentation, requiring very effective mixing of the pyroclasts with ice and snow. The converse is also possible, that very little melting occurs if the glacier surface is smooth, without crevasses and covered by a tephra layer that would act as an insulation. Considering that plausible worst case scenarios are being studied, a rather high value of $f = 0.5$ (50%) is adopted.

Partitioning between PDC and phoenix cloud: The partition between the ground-hugging component of the PDC and a phoenix cloud can only be approximated crudely; we will use a value of 0.5 here.

Emplacement temperature: Finally, for pyroclastic density currents not associated with fragmentation by external water, emplacement temperatures have been estimated as ranging from ~300°C to at 550°C (e.g. Mandeville *et al.*, 1994; Scott and Glasspool, 2004). As seen from the above discussion, the estimates obtained are very crude, but are expected to give the approximate order of magnitude. For wet (phreatomagmatic) eruptions base surges are common but the temperature of these is low (<100°C). In recent eruptions in Iceland (Grímsvötn, Eyjafjallajökull) base surges have been frequently observed but have not resulted in significant ice melting. Thus, we only consider the case where the vent has melted a large enough opening in the glacier that external water flows away from the vent and is not a factor in influencing eruption dynamics. This exclusion of external water allows hot pyroclastic flows to occur, provided eruption rates are high enough. In our estimates for Öræfajökull, we therefore use $T_e = 550$°C.

In Figure III-7, the melting rate resulting from a pyroclastic density current obtained for the parameters specified above is shown as a function of ξ. Considering the magnitude of the event analysed (MER 10^8 kg/s), it would be unlikely that all the melting would occur in a single catchment ($\xi = 1.0$); a more likely scenario would be $0.2 < \xi < 0.5$ with melting spread over two or more catchments.

5. Jökulhlaups resulting from subglacial eruptions

The analysis presented in Section 4 gives plausible maximum melting rates for various eruptive scenarios. In this section, the transport of meltwater from the eruption site to the edge of glacier and the effects of entrainment of pyroclasts as water-transported tephra and ice is considered, in particular the effect of these processes on maximum discharge and transport properties of the jökulhlaups.

5.1. Subglacial hydrology

For a glacier that is a few hundred meters thick, any water at the base of the glacier is pressurised. This implies that that the water pressure is similar to the lithostatic pressure exerted by the load of the overlying ice (e.g. Björnsson, 1988, 2003). Thus, flow paths of water at the base are controlled by a static fluid potential:

$$\varphi = (\rho_w - \rho_i) g z_b + \rho_i g z_s \qquad (12)$$

Where g is acceleration due to gravity and z_b and z_s are the height of respectively the glacier base and the ice surface (Björnsson, 1976).

Flow paths of meltwater at the glacier base will be down the gradient of this potential. The potential (eq. 12) highlights the importance of the slope of the ice surface as it is 10 times more influential in driving water flow than is the bedrock slope. This implies that water can flow uphill provided the slope of the ice surface is opposite to that of the bedrock and the bedrock slope is less than 10 times greater than the surface slope. This is highly relevant to Öræfajökull, where the caldera bottom is an enclosed bedrock depression (Magnússon *et al.*, 2012b).

In a glacier the slope of the ice surface is generally away from the centre towards the edge of a glacier. This drives water from the interior towards the glacier margins. Moreover, conditions for water accumulation are seldom met, except in places where sustained geothermal activity has created deep depressions in the glacier surface. This is the case at Grímsvötn and Skaftárkatlar (e.g. Björnsson, 2003) and in isolated smaller cauldrons in such as Mýrdalsjökull (Gudmundsson *et al.*, 2007).

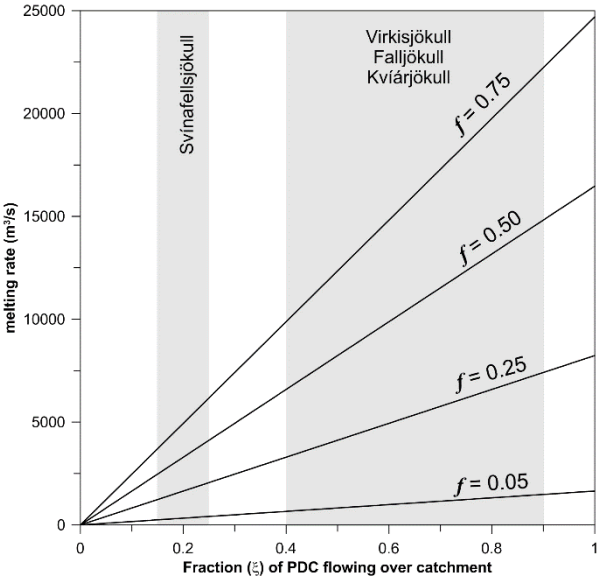

Figure III-7: Estimates of the rate of melting within an ice catchment area due to flow of a pyroclastic density current over snow and ice derived using equation (11). The mass eruption rate is assumed to be $\dot{M} = 10^8$ kg/s and the duration of collapse τ = 120 s. Values for different values of efficiency of heat transfer (f) are shown, with c = 0.5, T_e = 550°C, T_0 = 0°C and C_p = 1000 J/(kg °C). Likely maximum values of ξ for the main catchments are indicated.

In regions where ice thickness is substantial (>200 m) the static fluid potential is expected to dictate flow paths of meltwater.

For most regions within glaciers in Iceland and elsewhere, conditions are such that water will have a tendency to flow away from the eruption site. As a consequence, a depression will form in the ice surface above the subglacial eruption site. The resulting slope in the ice surface into the depression will cause ice flow into it, partly counteracting the subsidence. It is during this, initially fully subglacial stage, that ice melting in a subglacial eruption is expected to be highest.

5.2. Transport of solids with meltwater, bulking of jökulhlaups and lahars

Jökulhlaups caused by volcanic eruptions under glaciers are usually a mixture of water, sediments and ice. The sediments are usually pyroclasts from the eruption. Jökulhlaups can be water floods (often defined as having <40% of the mass as solids) or lahars, that is hyperconcentrated (40–80% solid) or debris flows (>80% solid material) (Beverage and Culbertson, 1964).

In jökulhlaups, the solid concentration is expected to depend on several factors and there is no straightforward way to constrain the expected ratio of liquid and solid in the flow. The type of eruption (effusive on one hand and fragmentation on the other) is of major importance since fragmentation leads to a high supply of fine-grained pyroclastic material that can easily be transported with meltwater. The steepness of the flow path of the meltwater down the slopes of a volcano is another factor that should lead to increased sedimentation. Detailed analysis of possible scenarios is beyond the scope of this chapter but it is important to consider the possible effect of the solid fraction originating as pyroclastic material at the source. This material can in some cases mostly be transported with the meltwater with minor amounts being left at the eruption site. In other cases most of it may be stored at or near the vents forming a volcanic edifice. In the former case the solids make up a substantial part of the flow, resulting primarily in hyperconcentrated flows.

The meltwater generated by subglacial eruptive activity is defined by eq. (2). The ratios of the mass generation rate of meltwater $\dot{M}_w$ and pyroclasts $\dot{M}_p$ (assumed to equal the MER $\dot{M}_m$ during full fragmentation) can be derived from equation (2) resulting in equation (13):

$$\frac{\dot{M}_p}{\dot{M}_w+\dot{M}_p} = \frac{1}{1+\frac{fC_g\Delta T}{L_i}} \quad (13)$$

Here ΔT is the difference in temperature of the water as it is released from the glacier and the temperature of the magma. Other parameters are defined as before. The volume ratios can also be determined using the densities of water (ρ_w) and pyroclasts (ρ_p) with Q_p being the volume flux of pyroclasts and Q_w the flux (volumetric flow rate) obtained from equations (2), (4) or (6):

$$\frac{Q_p}{Q_w+Q_p} = \frac{1}{1+\frac{\rho_p fC_g\Delta T}{\rho_w \quad L_i}} \quad (14)$$

Equations (13) and (14) can be used to evaluate the potential concentration of water-transported tephra in jökulhlaups. In Figure III-8 the variations in solid mass and volume fractions (eq. 13 and 14) are shown as a function of efficiency. If all the solid material is transported with the meltwater, the resulting jökulhlaup will have properties as shown by the solid curve.

If a fraction of the erupted material stays at the eruption site the concentrations of solids will be lower, within the shaded region.

The difference between a subglacial eruption and the melting by a PDC lies in the different temperature differences, 1100°C for the eruption and 550°C for the pyroclastic flow, resulting in about 50% less melting per unit mass of a pyroclastic density current. This suggests that PDCs may be more likely to produce hyperconcentrated-flow lahars than are the subglacial eruptions, in agreement with the observations from Redoubt, Mount St. Helens and Nevado de Ruiz mentioned previously.

5.3. Discharge of jökulhlaups and lahars

5.3.1. Flow rates with bulking, flank eruptions

From the discussion in 5.2 it is clear that in steep terrain the volume of water-transported tephra should be taken into account when evaluating the potential discharge of jökulhlaups. If Q_w is either Q_1 as obtained from eq. (4) or Q_2 from eq. (6), the effect of bulking is accounted for by combining these equations with (14) as:

$$Q_T = \left(1 + \frac{\rho_w}{\rho_p}\frac{L_i}{fC_g\Delta T}\right) Q_w \qquad (15)$$

This equation is used to calculate the maximum discharge for fissure eruptions on the ice-covered slopes of Öræfajökull. It is assumed that that the efficiency is 0.35–0.40, implying a solid mass fraction in the range 40–45%, reaching hyperconcentrated values and the generation of a lahar with Q_T = 1.25Q_w. During the 2010 Eyjafjallajökull eruption, jökulhlaups that formed during in the first two days of the eruption had a solid volume fraction of 26±10% (Magnússon *et al.*, 2012a), thus these estimates appear reasonable.

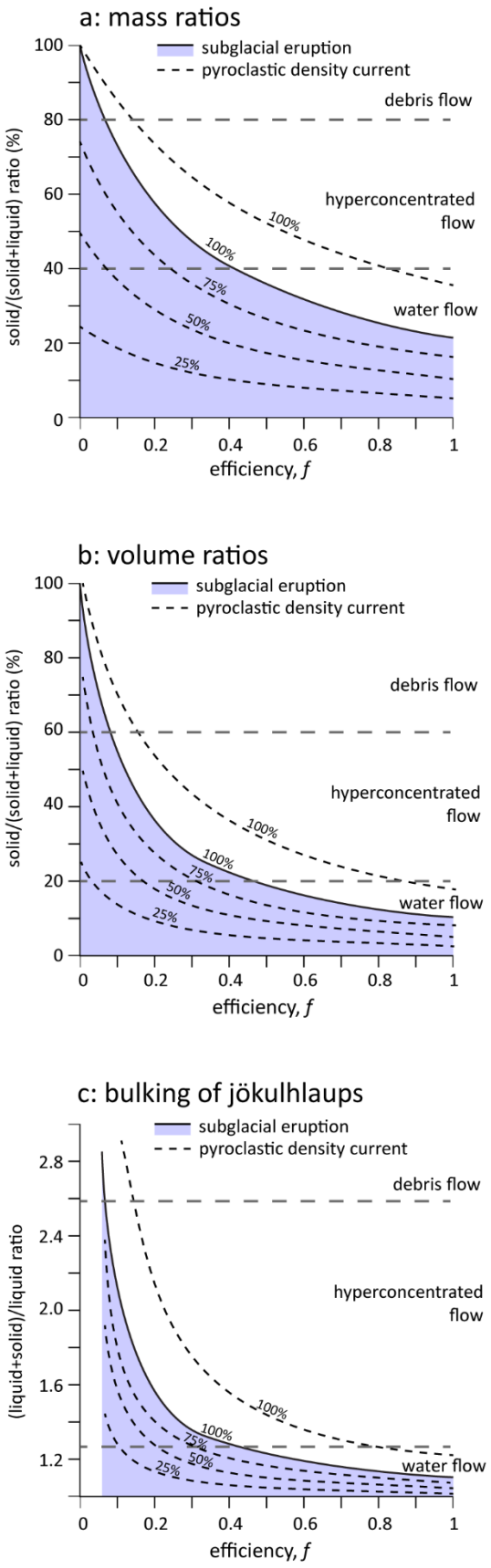

Figure III-8: Effects of pyroclast entrainment at the eruption site. a) Mass ratio of solids relative to the sum of solid and meltwater generated as a function of efficiency of heat transfer. The solid line shows 100% entrainment (all erupted material entrained in jökulhlaup). The broken lines show 75%, 50% and 25% entrainment. Possible bulking due to entrainment of material on slopes below eruption site is not considered. The dotted line shows mass ratios for 100% entrainment by pyroclastic density currents. b) Volume ratios of solid relative to the sum of solid and meltwater generated. c) Increase in volumetric flow rate due to entrainment of pyroclasts.

5.3.2. Discharge for eruptions under thick ice in caldera

For eruptions within the caldera, it is unclear how much water-transported tephra would be entrained by meltwater. The water would have to flow over a bedrock ledge for both outlets of Kvíarjökull and Virkisjökull-Falljökull. This means that the fluid potential gradient out of the caldera is smaller than on the slopes or would occur if no bedrock ledge was present. This could result in less sediment transport in a caldera eruption, but no model or theory exists on which to base an estimate. It will therefore not be attempted here to make such an estimate, apart from stating that 100% removal is highly unlikely because of the bedrock dam, with 50–75% removal being plausible worst cases. Using Figure III-8b, and efficiency of 0.6–0.8 for fragmentation as before, leads to a volume fraction of solids generated in the range 14–19%. Assuming 50–75% entrainment, this translates to 7–14% volume fraction in a jökulhlaup.

In the largest jökulhlaups with discharges of several tens of thousands of cubic meters per second, glacier termini can be extensively broken up by hydraulic fracturing and other mechanical disturbances. Tómasson (1996) estimated that the ice blocks amounted to 10–15% of the volume of the 1918 jökulhlaup of Katla. If a large jökulhlaup is generated through magma fragmentation under ice and the erupted material is mostly transported downslope with the meltwater as water-transported tephra, the combined bulking effect of the tephra entrainment (of 7–14%) and the ice blocks (10–15%) is 17–29%. The mean of this is 23%, not significantly different from the 25% bulking used for a flank eruption (see 5.3.1 above). We therefore apply the same multiplication factor of 1.25 to values calculated using eq. (2) or $Q_T = 1.25Q_w$. Thus, equation (16) is applied to both caldera and flank eruptions and accounts for the solid and liquid components of the flow where:

$$Q_T = 1.25Q_w \qquad (16)$$

5.3.3. Discharge of lahars resulting from pyroclastic density currents

Equation (11) is used to estimate the mean flow rates of meltwater from a pyroclastic density current. The values of ξ (the proportion of current affecting a single catchment) is approximated by considering that collapse of a large eruption plume will direct pyroclastic debris over a relatively large sector of the flanks. The results of applying equation (11) are shown in Figure III-7. As indicated in 5.3.2, jökulhlaups resulting from pyroclastic density currents are expected to have higher proportion of solid material mixed with the meltwater, due to the lower emplacement temperature.

5.4. Propagation times of jökulhlaups and lahars

From the viewpoint of melting rates and delivery of meltwater to outlet glaciers on Öræfajökull eruptions, three different settings have been defined:

1. Eruptions within the Öræfajökull caldera.

2. Fissure eruptions on the flanks of the volcano, outside the caldera.

3. Melting during an explosive eruption by pyroclastic density currents flowing over the glacier surface.

For analysing these different settings, we define the following time intervals (Figure III-9):

a) Eruption Onset Time (EOT): The time it takes for an eruption to start and establish a circular or elongated vent.

b) Subglacial Transport Time (STT): The time it takes for meltwater to reach the surface of the glacier on the volcano flanks or its outlet glaciers. This concept is useful for eruptions on volcanoes with considerable ice surface and bedrock relief, e.g. Katla, Eyjafjallajökull and Öræfajökull where most or all of the meltwater flows on the surface down the steep slopes after flowing along a subglacial path near the source. For an eruption and jökulhlaup at volcanoes covered

by large glaciers, such as Grímsvötn, supraglacial flow rarely occurs except as overspill near the terminus. For these events the STT should be taken as the total time of transport from the source to the point of outflow at the surface.

c) Flank Transport Time (FTT): The time it takes the flood to traverse the flanks of the volcano, from the point it emerges from base of the ice or, where flow becomes established on the surface of the glacier (e.g. as a lahar after initial melting by a pyroclastic density current). This is the time estimated in Chapter IV (Helgadóttir *et al.*, 2015).

Data on subglacial eruptions and meltwater travel time are given in Table 4. Data on Katla prior to 1918 is limited since eruption rate cannot be estimated in any meaningful way, given that the information is on timing of earthquakes, sighting of eruption plumes and times of jökulhlaups.

For eruptions within the Öræfajökull caldera, onset time, subglacial transport time and flank transport time need to be added to obtain an estimate of the time between the start of an eruption and the arrival of a jökulhlaup in the lowlands beyond the volcano. The effects of these eruptions is expected to be similar to Katla eruptions. The ice thickness is comparable, 400–500 m as opposed to 400–700 m at Katla. However, the distance from the vent to the glacier terminus is smaller for Öræfajökull than it is for Katla, or 7–11 km as opposed to about 17–20 km for Kötlujökull.

5.4.1. Eruption Onset Time (EOT)

For a large eruption (MER $>10^7$ kg/s) the timing of the initial arrival of magma at the surface (in this case the base of the glacier) and the formation of a fully established vent or fissure and the maximum MER, can be as low as 15–30 minutes. The 1947 Hekla eruption provides a similar example (Thorarinsson, 1954). Many basaltic eruptions also grow rapidly to a peak MER (e.g., the Krafla eruptions of 1975–1984; Einarsson, 1991). For most andesitic stratovolcanoes, a vent clearing phase on the order of 24 hours is common, often preceding the maximum MER during a vulcanian to Plinian phase (e.g. Bull and Buurman, 2013; Siebert *et al.*, 2015). For Öræfajökull hazard estimates, we adopt the lower value, of **15 minutes for EOT**. This time applies to both caldera and flank eruptions.

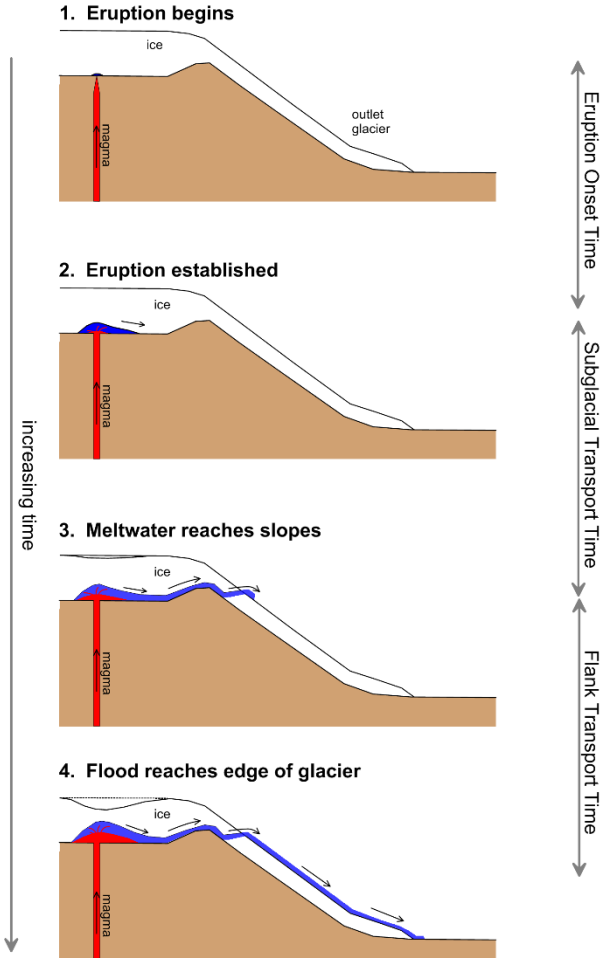

Figure III-9: Schematic setting for an eruption within Öræfajökull caldera and the eruption onset time (EOT), subglacial transport time (STT) and flank transport time (FTT).

Table III-4: Observed subglacial eruptions and travel times of meltwater.

	Initial ice thickness (m)	Initial Mass Eruption Rate (MER) (10^6 kg/s)	Melting time (hours)	Heat transfer rate (MW m^{-2})	Glacier path (km)	Av. glacier path gradient	Glacier travel time (hours)	Av. advance velocity (m/s)
Gjálp 1996	600	2-4	30	1.6	15	-	-	?
Gjálp 1996 - jökulhlaup	-	-	-	-	50	0.0003	10	1.4
Eyjafjalla-jökull 2010	200	0.5-1	4	4.3	5	0.27	5.5	0.25
Katla 1918	400	50-100	1-2	30	17	0.07	1-2	2.4-4.8
Katla 1660	(500)	?	(1)	-	(17)	(0.07)	(2-4)	-
Katla 1721	(500)	?	(<4)	-	(17)	(0.07)	(<4)	-
Katla 1755	(500)	?	(<6)	-	(22)	(0.06)	(<3)	-
Katla 1823	(500)	?	(<2)	-	(17)	(0.07)	(<3)	-
Katla 1860	(500)	(1-10?)	(<10)	-	(17)	(0.07)	(<10)	-

Sources: Gudmundsson *et al.* (2004), Magnússon *et al.* (2012), data in Larsen *et al.* (2013)

5.4.2. Subglacial Transport Time (STT)

The time it takes meltwater after the start of an eruption to propagate under ice from the eruption site until it reaches the slopes and may partly flow subaerially is highly uncertain. No theory backed up by empirical data exists as yet to calculate such times. Inferences can be made from empirical data in Icelandic eruptions, notably the Eyjafjallajökull eruption in 2010, Katla eruption in 1918 and indirect evidence from some earlier Katla eruptions. During the 2010 Eyjafjallajökull eruption, the STT was 3–4 hours (Magnússon *et al.*, 2012a), even though the transport length under ice was only 1.5–2 km. Beyond that distance, the flood was mostly supraglacial. For **flank eruptions** this time merges with the flank transit time and should be taken as equal to zero. For **caldera eruptions** in Öræfajökull the meltwater will travel 1–1.5 km (Virkisjökull) and 1–3 km (Kvíarjökull) before it can be expected to breach the surface and propagate subaerially from then on as observed at Eyjafjallajökull in 2010 (Magnússon *et al.*, 2012a). Using the minimum distance of 1 km for both cases to obtain the likely minimum subglacial transport time, and the advance velocities from Table III-4 we obtain a maximum STT of 60–80 minutes (similar to Eyjafjallajökull 2010) — a plausible value for a small to moderate eruption within the caldera. Minimum STT is 3–7 minutes (right order of magnitude for Katla 1918). The fact that there is a high bedrock step that the meltwater from a caldera eruption in Öræfajökull has to overflow is not taken into account. In the absence of a tested model for the propagation of such a flood under the glacier, no reliable estimates can be obtained on the likely delay that this may cause. To be conservative, this possible delay is ignored here, and the minimum values are adopted. Thus we use a STT of 30 minutes for small to moderate eruptions in the caldera and a value of 5 minutes for large eruptions.

Caldera eruptions: The combined minimum onset and subglacial transport times are defined as 15 + 30 minutes = **45 minutes for a small to moderate eruption**. For **a large eruption** this combined time is 15 + 5 minutes = **20 minutes**.

Flank eruptions: Here only the onset time is relevant, taken as **15 minutes**.

5.4.3. Flank Transit Time (FTT)

The Flank Transit Time can be approximated for some past eruptions on the basis of observations and it can be estimated using flood routing. Here the Samos code, initially written to simulate flow of snow avalanches is used (Hákonardóttir *et al*., 2005). The flank transit times, flow velocities, inundation zones and water depths are not the topic of this chapter. They are considered in detail in Chapter IV (Helgadóttir *et al.*, 2015) and therefore not estimated here.

5.4.4. Onset times and occurrence of pyroclastic density currents

Pyroclastic density currents should **not happen** at the very beginning of an eruption, since an ice cauldron or a wide fissure would have to be melted out before conditions for pyroclastic density currents are established. If we define the onset time of PDCs as the time from start of collapse until a flood is established on the upper slopes, this time is very short, **of order 5 minutes**.

PDCs and associated jökulhlaups can take place at any time after an eruption has established a vent open to the atmosphere, provided the eruption rate is high enough (>5 x 10^7 kg/s). This eruption rate need not be sustained, as discrete explosions can generate substantial PDCs.

5.4.5. Hydrographs of jökulhlaups

The hydrographs of jökulhlaups from all types of events considered can vary depending on conditions at the eruption site and the characteristics of the jökulhlaup path. Data on hydrograph shape for jökulhlaups caused directly by eruptions are limited, but rapid approximately linear increase in discharge is observed in many cases (e.g. the jökulhlaups from Eyjafjallajökull in 2010; Gudmundsson and Larsen, 2013). Observations of lahars from Redoubt in 2013 and Nevado del Ruiz 1985 also show the initial advance of a flow front, possibly followed by repeated waves of high discharge (Waythomas *et al.*, 2013; Pierson *et al.*, 1990). Hydraulic simulations of Katla jökulhlaups (Hólm and Kjaran, 2005) were conducted using a simple triangular-shaped hydrograph with a linearly rising discharge, followed by a period of maximum discharge and a period of linear decline. This approach is applied in this study. For hazard purposes at Öræfajökull, where the effects of the jökulhlaups in the few-kilometres wide strip of lowland below the slopes are of primary interest, the most important parameters are the rate of increase of discharge and the peak discharge. The selected initial hydrographs are shown in Figure III-10.

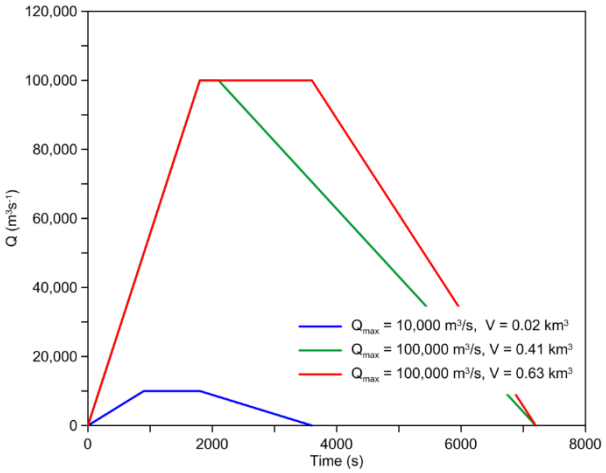

Figure III-10: Plausible hydrographs for jökulhlaups caused by eruptions at Öræfajökull. A discharge of 10,000 m^3/s applies to a moderate flank eruption, while the other two cases (Q_{max} = 100,000 m^3/s).

These hydrographs are applicable to situations where the meltwater emerges high on the flanks. The slope of the rising limb and time to peak discharge should reflect the fast but yet not instantaneous increase in melting during the eruption onset time.

It is possible that the time to peak discharge is considerably faster than estimated. However, the most likely scenario where this could happen is when meltwater is initially retained at the eruption site or the subglacial transport time is slow, possibly due to low potential gradient between the eruption site and the caldera rim.

6. Results

The melting potential and likely initial maximum discharges of jökulhlaups resulting from eruptions on Öræfajökull are presented in Tables III-5, III-6 and III-7, with the three main scenarios in each table: Flank eruptions, caldera eruptions, and pyroclastic density currents during an ongoing eruption.

6.1. Maximum discharge for fissure eruptions on ice covered flanks

The hypothetical fissures considered are shown in Figures III-11 and III-12. The results for Q_w calculated from both eq. (4) and (6) are given in Table III-5 and the higher of the two values is used to estimate Q_T for a plausible scenario using equation (16).

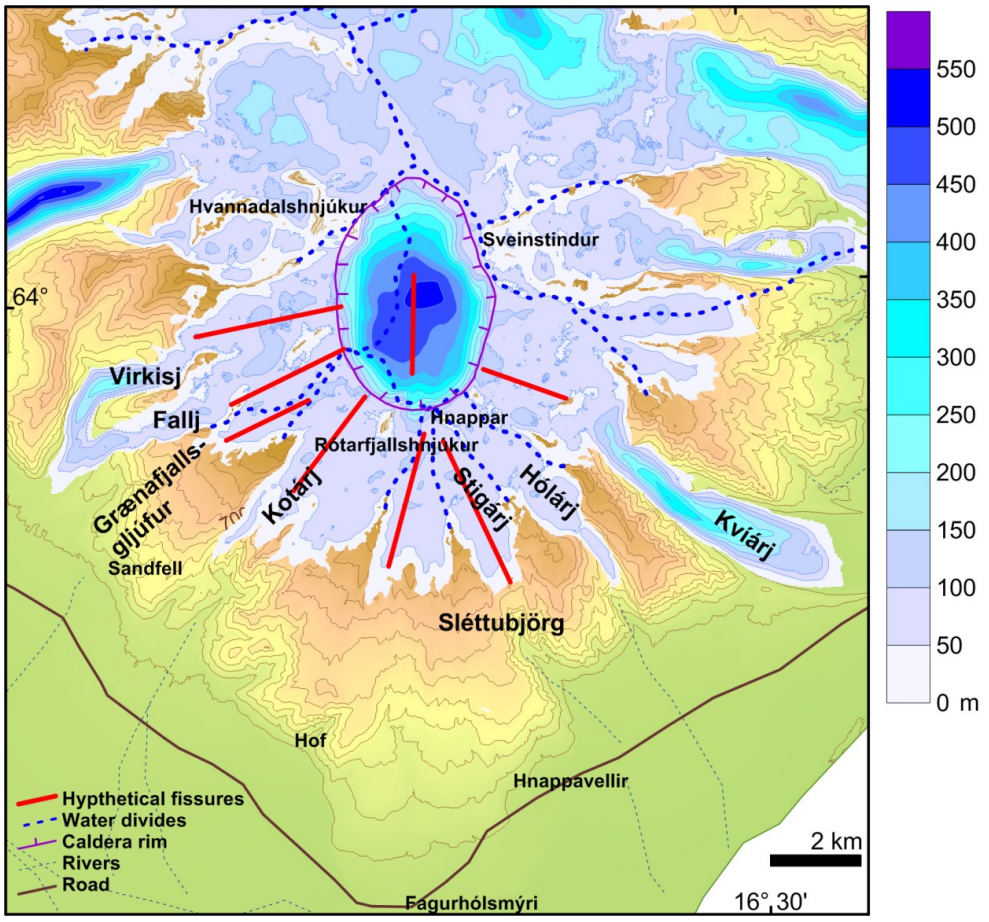

Figure III-11: Ice thickness map of Öræfajökull (after Magnússon et al., 2012b). Hypothetical volcanic fissures on the flanks and within the caldera of Öræfajökull, used to calculate possible discharge of jökulhlaups based on ice thickness and fissure length (Table III-5).

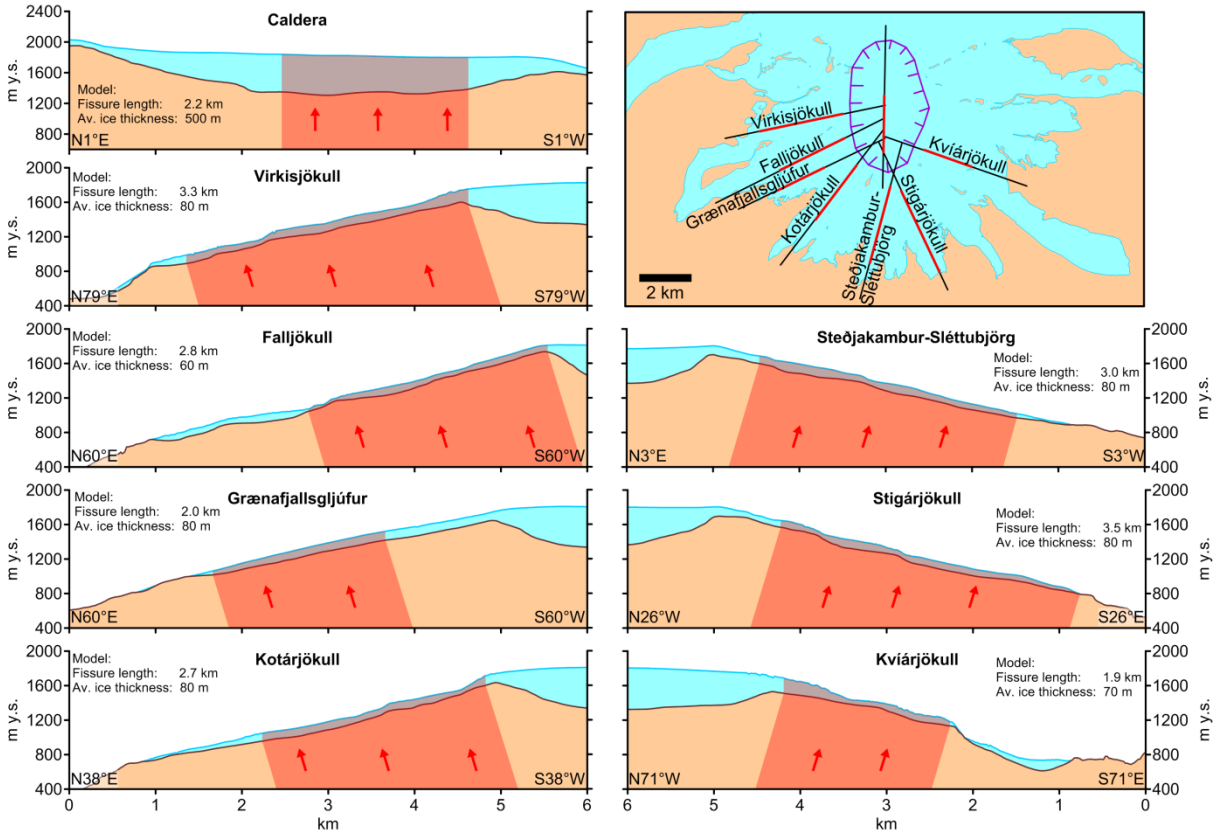

Figure III-12: Cross sections of bedrock and ice cover at locations of hypothetical fissure eruptions on the flanks of Öræfajökull and a fissure within the caldera apply to the maximum expected discharge on a single flank of the volcano in a major eruption.

Table III-5: Melting rates (Q_1 from eq. 4 and Q_2 from eq. 6) and estimated discharge of jökulhlaups (eq. 16) from basaltic fissure eruptions on flanks and fissure eruptions within the caldera.

	Fissure length (m)	**ice thickness (m)**	**Q1 (m^3/s)**	**Q2 (m^3/s)**	**QT (m^3/s)**	**Jökulhlaup class**
Virkisjökull	3300	80	3,326	4,620	5,775	2
Falljökull	2800	60	2,117	3,920	4,900	2
Grænafjallsgljúfur	2000	80	2,016	2,800	3,500	2
Kotárjökull	2700	80	2,722	3,780	4,725	2
Stígárjökull	3500	80	3,528	4,900	6,125	2
Kvíárjökull	1900	70	1,676	2,660	3,325	2
Steðjakambur-Sléttubjörg	3000	80	3,024	4,200	5,250	2
Caldera - N-S fissure	2200	500	13,860	3,080	17,325	3

Table III-6: Large caldera eruptions, melting rates (eq. 1) and estimated discharge of jökulhlaups (eq. 16) resulting from a rhyolitic, fully subglacial eruption with magma fragmentation.

M' (kg/s)	E' (W)	Q (m^3/s)	Q_T (m^3/s)
1.00E+06	5.6.E+11	1,677	2,300
1.00E+07	5.6.E+12	16,766	23,000
1.00E+08	5.6.E+13	167,665	230,000

$f = 0.7$, $C_g = 1000$ J/(kg °C), $\Delta T = 800$°C

Hypothetical volcanic fissures are oriented radially and the length is dictated by the space available for such a fissure on the ice covered flank. A fissure is not extended onto the lower flanks below ~1000 m elevation, as no geological evidence exists for the presence of such long fissures. The results indicate that jökulhlaups of 3,000–6,000 m^3/s are possible for flank eruptions during the initial stages as they melt openings in the predominately 60–80 m thick glacier ice on the flanks of Öræfajökull. The size of jökulhlaup does not depend on the size of the outlet glacier, it depends on the length of the volcanic fissure and the ice thickness.

6.2. Discharge for eruptions under thick ice in caldera

Three eruption sizes are considered (Table III-6) for the general setting shown in Figure III-10. The smallest eruption magnitude is comparable to the 2010 Eyjafjallajökull eruption (MER = $1 \cdot 10^6$ kg/s) resulting in melting rates of about 1,700 m^3/s and a jökulhlaup peak discharge of 2,300 m^3/s. The second class would correspond to a medium sized sub-Plinian eruption (MER = $1 \cdot 10^7$ kg/s) and melting rate of about 17,000 m^3/s and jökulhlaup peak discharge of 23,000 m^3/s. The largest size considered corresponds to a major Plinian eruption, melting rate of 170,000 m^3/s and a peak discharge of 230,000 m^3/s. All of the above scenarios should be regarded as plausible, although the largest event is the most unlikely. An eruption of this magnitude may happen only after a connection has been established to the surface by melting associated with more modest activity preceding a climactic major Plinian phase. Thus, it may be regarded probable that in a real eruption (such as occurred in 1362), the melting rates never reach the calculated value even though the MER most likely has at some point reached or even exceeded 10^8 kg/s. Moreover, such extremely high melting rates would also be expected to result in meltwater seeking pathways out of the caldera through two or more outlets simultaneously (e.g. Falljökull-Virkisjökull, Kotárjökull and Kvíárjökull). The resulting jökulhlaup through each channel would then represent only a part of the total melting. Therefore, the maximum discharge for a jökulhlaup down a particular channel used in modelling is 100,000 m^3/s.

It should also be clear that the methods applied here do not consider details of hydrograph shape. It is possible that a short lived peak in discharge occurs, that is considerably higher than the calculated melting rates.

6.3. Jökulhlaups/lahars resulting from pyroclastic density currents

The results obtained using eq. (11) are presented in Table III-7. The final estimates of $Q_{T,min}$ and $Q_{T,max}$ are obtained by adding the volume of pyroclastic material to the meltwater volume, assuming that it is a plausible end-member case that most of the material is transported by the meltwater. The fraction of a large PDC assumed to lead to melting varies between catchments. For the largest catchments draining the caldera, Virkisjökull-Falljökull and Kvíárjökull, it is assumed that up to 80% of a PDC can flow over these catchments. For Svínafellsjökull it is assumed that an overspill from a PDC principally flowing down Virkisjökull-Falljökull can occur (20% of the PDC) while up to 40% of a large PDC can enter other catchments. Hrútárjökull to the east of Sveinstindur is also included, with a possible 20% of the PDC affecting the catchment. This is an area not considered for flood routing,

but in the event of a large Plinian eruption this sort of event cannot be ruled out.

The results are approximate, and provide only order-of-magnitude estimates, but indicate that lahars of 10,000–20,000 m^3/s can occur as a result of PDCs. It should also be kept in mind that the values given are averages over 5–10 minutes and the maximum discharge could be higher by a factor of two or so.

Finally, the entrainment of pyroclastic material by meltwater results in high concentrations of solids, putting the resulting events firmly in the class of hyper-concentrated flows. The assumption of full entrainment yields a solid mass fraction of about 55%. In reality this value is expected to be somewhat lower. However, entrainment of sediment along the flow path may lead to additional bulking and at least locally, sediment concentrations may be high enough for the flows to behave as debris-flow lahars.

Table III-7: Melting rates and estimated discharge of lahars caused by pyroclastic density currents (eqs. 11 and 16) resulting from collapse of a plume with mass eruption rate $\dot{M} = 10^8$ kg/s for τ = 120 s. Parameters in eq. (11) – min: f=0.25, χ=0.25, t_{run} = 10 minutes. – max: f=0.7, χ=0.5m, t_{run} = 5 minutes. V_w is total volume of meltwater, $V_p = \zeta \dot{M} \rho_p \tau$ is volume of pyroclastic material deposited on glacier. V_T is the combined volume of meltwater and pyroclasts.

	Svínafellsjökull	**Virkisjökull, Falljökull**	**Kotárjökull**	**Steðjaklettur-Sléttubjörg**	**Hólár-Stigárjöklar**	**Kvíárjökull**	**Hrútárjökull**
ξ	0.2	0.8	0.4	0.4	0.4	0.8	0.2
$V_{w,min}$ (m^3)	2.5×10^5	9.9×10^5	4.9×10^5	4.9×10^5	4.9×10^5	9.9×10^5	2.5×10^5
$V_{w,max}$ (m^3)	9.9×10^5	4.0×10^6	2.0×10^6	2.0×10^6	2.0×10^6	4.0×10^6	9.9×10^5
Q_{min} (m^3/s)	412	1,647	823	823	823	1,647	412
Q_{max} (m^3/s)	3,293	13,174	6,587	6,587	6,587	13,174	3,293
$V_{p,min}$ (m^3)	1.2×10^5	4.8×10^5	2.4×10^5	2.4×10^5	2.4×10^5	4.8×10^5	1.2×10^5
$V_{p,max}$ (m^3)	2.4×10^5	9.6×10^5	4.8×10^5	4.8×10^5	4.8×10^5	9.6×10^5	2.4×10^5
$V_{T,min}$ (m^3)	3.7×10^5	1.5×10^6	7.3×10^5	7.3×10^5	7.3×10^5	1.5×10^6	3.7×10^5
$V_{T,max}$ (m^3)	1.2×10^6	5.0×10^6	2.5×10^6	2.5×10^6	2.5×10^6	5.0×10^6	1.2×10^6
$Q_{T,min}$ (m^3/s)	600	2,500	1,200	1,200	1,200	2,500	600
$Q_{T,max}$ (m^3/s)	4,000	16,700	8,300	8,300	8,300	16,700	4,000

7. Conclusions

Models of melting in the cases of caldera eruptions, flank eruptions and pyroclastic density currents during major eruptions have been presented and applied to the catchment areas of Öræfajökull between Svínafellsjökull in the west to Kviárjökull in the east. The models are simplified semi-empirical approximations constrained by data from known past eruptions. In particular for the PDCs the results can only be regarded as order-of-magnitude estimates.

The results indicate that:

- Eruptions on radial fissures through the shallow ice covering the upper flanks of the volcano should give rise jökulhlaups in the size class 3,000–10,000 m^3/s.
- The largest caldera eruptions with MERs up to 10^8 kg/s may cause melting rates as high as 200,000 m^3/s and initiate jökulhlaups with peak discharges up to 260,000 m^3/s. It is unclear whether a major silicic Plinian eruption would reach such high eruption rates prior to penetration of the glacier. However, jökulhlaups with peak discharges of about 100,000 m^3/s are considered plausible under present conditions.
- Pyroclastic density currents could generate jökulhlaups with discharges in the range of 10,000–20,000 m^3/s, which would most likely be hyperconcentrated-flow lahars.

8. Acknowledgements

We are grateful to Chris Waythomas for reviewing the chapter. Trausti Jónsson and Tómas Jóhannesson are thanked for proof-reading.

This study was funded by the Icelandic Avalanche Mitigation Fund, the National Power Company, and the Icelandic Road and Coastal Administration.

9. References

Bacon, C. R. (1977). High temperature heat content and heat capacity of silicate glasses: Experimental determination and a model for calculation. *Am. J. Sci., 277*, 109–135.

Beverage, J. P., & Culbertson, J. K. (1964). Hyperconcentrations of suspended sediment. *J. Hydraul. Div., Am. Soc. Civ. Eng., 90*, 117–128.

Björnsson, H. (1976). Subglacial water reservoirs, jökulhlaups and volcanic eruptions. *Jökull, 25*, 1–15.

Björnsson, H. (1988). Hydrology of ice caps in volcanic regions. *Soc. Sci. Isl., 45*, 139, 21 maps.

Björnsson, H. (2003). Subglacial lakes and jökulhlaups in Iceland. *Global and Planetary Change, 35*, 255–271.

Björnsson, H., & Pálsson, F. (2008). Icelandic glaciers. *Jökull, 58*, 365–386.

Branney, M. J., & Kokelaar, P. (2002). *Pyroclastic density currents and the sedimentation of ignimbrites* (Vol. 27). London: Geological Society.

Bull, K. F., & Buurman, H. (2013). An overview of the eruption of Redoubt Volcano, Alaska. *Journal of Volcanology and Geothermal Research, 259*, 2–15.

Carey, R. J., Houghton, B. F., & Thordarson, T. (2010). Tephra dispersal and eruption dynamics of wet and dry phases of the 1875 eruption of Askja Volcano, Iceland. *Bull. Volc., 72*, 259–278.

Carmichael, I. S., Turner, F. J., & Verhogen, J. (1974). *Igneous Petrology.* New York: McGraw-Hill.

Degruyter, W., & Bonadonna, C. (2012). Improving on mass flow rate estimates of volcanic eruptions. *Geophys. Res. Lett., 39*(L16308).

Dorava, J. M., & Meyer, D. F. (1994). Hydrologic hazards in the lower Drift River basin associated with the 1989–90 eruptions of Redoubt Volcano, Alaska. *Journal of Volcanology and Geothermal Research, 62*, 387–407.

Edwards, B. R., Gudmundsson, M. T., & Russell, J. K. (2015). Glaciovolcanism. In H. Sigurdsson, B. Houghton, S. R. McNutt, H. Rymer, & J. Stix (Eds.), *Encyclopedia of Volcanoes* (2nd ed., pp. 377–393). Elsevier.

Einarsson, P. (1991). Umbrotin við Kröflu 1975-1989 (the Krafla episode 1975-1989). In A. Garðarsson, & Á. Einarsson (Eds.), *Náttúra Mývatns* (pp. 321–336). Reykjavík: Hið Íslenska Náttúrufræðifélag.

Gudmundsson, Á., Óskarsson, N., Grönvold, K., Saemundsson, K., Sigurdsson, O., Stefánsson, R., Gíslason, S. R., Einarsson, P., Brandsdóttir, B., Larsen, G., Jóhannesson, H., and Thordarson, T. (1992). The 1991 eruption of Hekla, Iceland. *Bull. Volc., 54*, 238–246.

Gudmundsson, M. T. (2003). Melting of ice by magma-ice-water interactions during subglacial eruptions as an indicator of heat transfer in subaqueous eruptions. In J. D. White, J. L. Smellie, & D. Clague (Eds.), *Explosive Subaqueous Volcanism* (pp. 61–72). Washington D.C.: American Geophysical Union.

Gudmundsson, M. T. (2005). Subglacial volcanic activity in Iceland. In C. Caseldine, A. Russell, J. Hardardóttir, & Ó. Knudsen (Eds.), *Iceland: Modern processes, Past Environments* (pp. 127–151). Amsterdam: Elsevier.

Gudmundsson, M. T., & Högnadóttir, Þ. (2005). Ísbráðnun og upptakarennsli jökulhlaupa vegna eldgosa í Eyjafjallajökli og vestanverðum Mýrdalsjökli. (Ice melting and discharge of jökulhlaups due to eruptions in Eyjafjallajökull and the western part of Mýrdalsjökull). In M. T. Guðmundsson, & Á. G. Gylfason (Eds.), *Hættumat vegna eldgosa og hlaupa frá vestanverðum Mýrdalsjökli og Eyjafjallajökli* (pp. 159–180). Reykjavík: Ríkislögreglustjórinn, Háskólaútgáfan.

Gudmundsson, M. T., & Högnadóttir, Þ. (2006). *Ísbráðnun og upptakarennsli jökulhlaupa vegna eldgosa í Kötluöskju og austanverðum Mýrdalsjökli.* Reykjavík: Jarðvísindastofnun Há-skólans.

Gudmundsson, M. T., Högnadóttir, Þ., Kristinsson, A. B., & Gudbjörnsson, S. (2007). Geothermal activity in the subglacial Katla caldera, Iceland, 1999-2005, studied with radar altimetry. *Annals of Glaciology, 45*, 66–72.

Gudmundsson, M. T., Sigmundsson, F., & Björnsson, H. (1997). Ice-volcano interaction of the 1996 Gjálp subglacial eruption, Vatnajökull, Iceland. *Nature, 389*, 954–957.

Gudmundsson, M. T., Sigmundsson, F., Björnsson, H., & Högnadóttir, Þ. (2004). The 1996 eruption at Gjálp, Vatnajökull ice cap, Iceland: efficiency of heat transfer, ice deformation and subglacial water pressure. *Bulletin of Volcanology, 66*, 46–65.

Gudmundsson, M. T., Thordarson, T., Höskuldsson, Á., Larsen, G., Björnsson, H., Prata, F. J., Oddsson, B., Magnússon E., Högnadóttir, T., Petersen, G. N., Hayward, C. L., Stevenson, J. A., and Jónsdóttir, I. (2012). Ash generation and distribution from the April-May 2010 eruption of Eyjafjallajökull, Iceland. *Scientific Reports, 2*(572).

Gudmundsson, M., & Larsen, G. (2013). Jökulhlaup. In J. Sólnes, F. Sigmundsson, & B. Bessason (Eds.), *Náttúruvá á Íslandi. Eldgos og Jarðskjálftar* (pp. 156–170). Reykjavík: Viðlaga-trygging Íslands, Háskólaútgáfan.

Hákonardóttir, K. M., Jóhannesson, T., & Sampl, P. (2005). Líkanreikningar á jökulhlaupum niður suðurhliðar Eyjafjallajökuls (Hydraulic simulations of glacial outbursts on the southern slopes of Eyjafjallajökull). In M. T. Guðmundsson, & Á. G. Gylfason (Eds.), *Hættumat vegna eldgosa og hlaupa frá vestanverðum Mýrdalsjökli og Eyjafjallajökli (Hazard assessment of volcanic eruptions and glacial outbursts for Eyja-fjallajökull and the western outwash plain of Mýrdalsjökull)* (pp. 181–196). Reykjavík: Ríkislögreglustjórinn, Háskólaútgáfan.

Helgadóttir, Á., Pagneux, E., Roberts, M. J., Jensen, E. H., & Gíslason, E. (2015). Öræfajökull Volcano: Numerical simulations of eruption-induced jökulhlaups using the SAMOS flow model. In E. Pagneux, M. T. Gudmundsson, S. Karlsdóttir, & M. J. Roberts (Eds.), *Volcanogenic floods in Iceland: An assessment of hazards and risks at Öræfajökull and on the Markarfljót outwash plain* (pp. 73–100). Reykjavík: IMO, IES-UI, NCIP-DCPEM.

Hólm, S. L., & Kjaran, S. P. (2005). Reiknilíkan fyrir útbreiðslu hlaupa úr Entujökli (Hydraulic model of floods from Entujökull). In M. T. Guðmundsson, & Á. G. Gylfason (Eds.), *Hættumat vegna eldgosa og hlaupa frá vestanverðum Mýrdalsjökli og Eyjafjallajökli (Hazard assessment of volcanic eruptions and glacial outbursts for Eyjafjallajökull and the western outwash plain of Mýrdalsjökull)* (pp. 197–210). Reykjavík: National Commissioner of Police.

Hreinsdóttir, S., Sigmundsson, F., Roberts, M. J., Björnsson, H., Grapenthin, R., Arason, P., Árnadóttir, T., Hólmjárn, J., Geirsson, H., Bennett, R. A., Gudmundsson, M. T., Oddsson, B., Ófeigsson, B. G., Villemin, T., Jónsson, T., Sturkell, E., Höskuldsson, Á., Thordarson, T., and Óladóttir, B. A. (2014). Volcanic plume height correlated with magma pressure change at Grímsvötn Volcano, Iceland. *Nature Geoscience, 7*, 214–218.

Höskuldsson, Á., & Sparks, R. S. (1997). Thermo-dynamics and fluid dynamics of effusive subglacial eruptions. *Bull. Volcanol., 59*, 219–230.

Jarosch, A. H., Gudmundsson, M. T., Högnadóttir, T., & Axelsson, G. (2008). The progressive cooling of the hyaloclastite ridge at Gjálp, Iceland, 1996-2005. *Journal of Volcanology and Geothermal Research, 170*, 218–219.

Jude-Eton, T. C., Thordarson, T., Gudmundsson, M. T., & Oddsson, B. (2012). Dynamics, stratigraphy and proximal dispersal of supraglacial tephra during the ice-confined 2004 eruption at Grímsvötn volcano, Iceland. *Bull. Volc., 74*, 1057–1082.

Larsen, G. (2000). Holocene eruptions within the Katla volcanic system, south Iceland: Characteristics and environmental impact. *Jökull, 49*, 1–28.

Larsen, G., Guðmundsson, M. T., & Sigmarsson, O. (2013). Katla. In J. Sólnes, F. Sigmundsson, & B. Bessason (Eds.), *Náttúruvá á Íslandi. Eldgos og Jarðskjálftar* (pp. 211–233). Reykjavík: Viðlagatrygging Íslands/Háskólaútgáfan.

Larsen, G., Vilmundardóttir, E., & Þorkelsson, B. (1992). Heklugosið 1991: Gjóskufallið og gjóskulagið frá fyrsta degi gossins. (Hekla eruption of 1991: Fallout of tephra on first day of eruption). *Náttúrufræðingurinn, 61*, 159–176.

Magnússon, E., Gudmundsson, M. T., Sigurdsson, G., Roberts, M. J., Höskuldsson, F., & Oddsson, B. (2012a). Ice-volcano interactions during the 2010 Eyjafjallajökull eruption, as revealed by airborne radar. *J. Geophys. Res., 117, B07405*.

Magnússon, E., Pálsson, F., Björnsson, H., & Gudmundsson, S. (2012b). Removing the ice cap of Oraefajokull central volcano, SE-Iceland: Mapping and interpretation of bedrock topography, ice volumes, subglacial troughs and implications for hazards assessments. *Jökull, 62*, 131–150.

Mandeville, C. W., Carey, S., Sigurdsson, H., & King, J. (1994). Areomagnetic evidence for high-temperature emplacement of the 1883 subaqueous pyroclastic flows from Krakatau Volcano, Indonesia. *Journal of Geophysical Research, 99*(B5), 9487–9504.

Mastin, L. G., Guffanti, M., Servranckx, R., Webley, P., Barsotti, S., Dean, K., . . . Waythomas, C. F. (2009). A multidisciplinary effort to assign realistic source parameters to models of volcanic ash-cloud transport and dispersion during eruptions. *Journal of Volcanology and Geothermal Research, 186*(1–2), 10–21.

Oddsson, B., Gudmundsson, M. T., Larsen, G., & Karlsdóttir, S. (2012). Monitoring the plume from the basaltic phreatomagmatic 2004 Grímsvötn eruption — application of weather radar and comparison with plume models. *Bull. Volc., 74*, 1395–1407.

Pierson, T. C., editor. (1999). *Hydrologic consequences of hot-rock/snowpack interactions at Mount St. Helens Volcano, Washington 1982–84.* Denver: U.S. Dept. of the Interior, U.S. Geological Survey Information Services.

Pierson, T. C., Janda, R. J., Thouret, J. C., & Borrero, C. A. (1990). Perturbation and melting of snow and ice by the 13 November 1985 eruption of Nevado del Ruiz, Columbia, and consequent mobilization, flow and deposition of lahars. *Journal of Volcanology and Geothermal Research, 41*, 17–66.

Roberts, M. J., & Gudmundsson, M. T. (2015). Öræfajökull Volcano: Geology and historical floods. In E. Pagneux, M. T. Gudmundsson, S. Karlsdóttir, & M. J. Roberts (Eds.), *Volcanogenic floods in Iceland: An assessment of hazards and risks at Öræfajökull and on the Markarfljót outwash plain* (pp. 17–44). Reykjavík: IMO, IES-UI, NCIP-DCPEM.

Roche, O., Phillips, J., & Kelfoun, K. (2013). Pyroclastic density currents. In S. A. Fagents, T. K. Gregg, & R. M. Lopes (Eds.), *Modeling volcanic processes* (pp. 203–229). Cambridge University Press.

Schmid, A., Sonder, I., Seegelken, R., Zimanowski, B., Büttner, R., Gudmundsson, M. T., & Oddsson, B. (2010). Experiments on the heat discharge at the dynamic magma-water-interface. *Geophys. Res. Lett., 37*, L20311.

Scott, A. C., & Glasspool, I. (2004). Charcoal reflectance as a proxy for the emplacement temperature of pyroclastic flow deposits. *Geology, 33*, 589–592.

Siebert, L., Cottrell, E., Venske, E., & Andrews, B. (2015). Earth's volcanoes and their eruptions: An overview. In H. Sigurdsson, B. Houghton, S. R. McNutt, H. Rymer, & J. Stix (Eds.), *Encyclopedia of Volcanoes* (2nd ed., pp. 239–255). Elsevier.

Smellie, J. L. (2002). The 1969 subglacial eruption on Deception Island (Antarctica): events and processes during an eruption beneath a thin glacier and implications for volcanic hazards. In J. L. Smellie, & M. Chapman (Eds.), *Ice-volcano interaction on Earth and Mars* (pp. 59–80). London: Geological Society.

Sparks, R., Bursik, M., Carey, S., Gilbert, J., Glaze, L., Sigurðsson, H., & Woods, A. (1997). *Volcanic Plumes.* Chichester: John Wiley and Sons.

Thorarinsson, S. (1958). The Öræfajökull eruption of 1362. *Acta Naturalia Islandica, 2*(4), 100.

Thorarinsson, S. (1967). The eruption of Hekla in historic times. A tephrocronological study. In *The eruption of Hekla 1947–48.* Reykjavík: Societas Scientiarum Islandica.

Thordarson, T., & Self, S. (1993). The Laki (Skaftár Fires) and Grímsvötn eruptions in 1783–1785. *Bull. Volc., 55*, 233–263.

Tómasson, H. (1996). The Jökulhlaup from Katla in 1918. *Annals of Glaciology, 22*, 249-254.

Trabant, D., Waitt, R. B., & Major, J. J. (1994). Disruption of Drift glacier and origin of floods during the 1989–1990 eruptions of Redoubt Volcano, Alaska. *Journal of Volcanology and Geothermal Research, 62*, 369–385.

Waitt, R., Pierson, T. C., Macleod, N. S., Janda, R. J., Voight, B., & Holcomb, R. T. (1983). Eruption-triggered avalanche, flood and lahar at Mount St. Helens – effects of winter snowpack. *Science, 221*, 1394–1397.

Walder, J. S. (1999). Nature of depositional contacts between pyroclastic deposits and snow and ice. In T. Pierson (Ed.), *Hydrologic consequences of hot-rock/snowpack interactions at Mount St. Helens Volcano, Washington 1982–1984* (pp. 9–18). Denver: U.S. Dept. of the Interior, U.S. Geological Survey Information Services.

Walder, J. S. (2000). Pyroclast/snow interactions and thermally driven slurry formation. Part 1: theory for monodisperse grain beds. *Bulletin of Volcanology, 62*, 105–118.

Walder, J. S. (2000). Pyroclast/snow interactions and thermally driven slurry formation. Part 2: experiments and theoretical extension to polydisperse tephra. *Bulletin of Volcanology, 62*, 119–129.

Waythomas, C. F., Pierson, T. C., Major, J. J., & Scott, W. E. (2013). Voluminous ice-rich and water rich lahars generated during the 2009 eruption of Redoubt Volcano, Alaska. *Journal Volc. Geoth. Res., 259*, 389–413.

Wohletz, K., Zimanowski, B., & Büttner, R. (2013). Magma-water interactions. In S. A. Fagents, T. K. Gregg, & R. M. Lopes (Eds.), *Modeling Volcanic Processes* (pp. 230–254). Cambridge University Press.

Woodcock, D. C., Lane, S. J., & Gilbert, J. S. (2012). Particle-water heat transfer during explosive eruptions. *J. Geop.. Res. Solid Earth, 117*, B10205. doi:10.1029/2012JB009240

Woodcock, D. C., Lane, S. J., & Gilbert, J. S. (2014). Ice-melt rates in liquid-filled cavities during explosive subglacial eruptions. *J. Geop. Res. Solid Earth, 119*, 1803–1817.

Woodhouse, M. J., Hogg, A. J., Phillips, J. C., & Sparks, R. S. (2013). Interaction between volcanic plumes and wind during the 2010 Eyjafjallajökull eruption, Iceland. *J. Geophys. Res., 118*, 92–109.

Zimanowski, B. (1998). Phreatomagmatic explosions. In A. Freundt, & M. Rosi (Eds.), *From Magma to Tephra: Modelling Physical Processes of Explosive Volcanic Eruptions* (pp. 25–54). Elsevier.

Zimanowski, B., & Büttner, R. (2003). Phreato-magmatic explosions in subaqueous eruptions, in Explosive Subaqueous Volcanism. In J. D. White, J. L. Smellie, & Clague, D. A. (Eds.), *Explosive Subaqueous Volcanism* (pp. 51-60). Washington D.C.: American Geophysical Union.

IV. ÖRÆFAJÖKULL VOLCANO: NUMERICAL SIMULATIONS OF ERUPTION-INDUCED JÖKULHLAUPS USING THE SAMOS FLOW MODEL

Ásdís Helgadóttir *, Emmanuel Pagneux *, Matthew J. Roberts *, Esther H. Jensen *, Eiríkur Gíslason *

* *Icelandic Meteorological Office*

1. Introduction

This study identifies regions around Öræfajökull Volcano that would be liable to flooding in the event of a subglacial eruption. Melting scenarios (Gudmundsson *et al.*, 2015) are used to simulate the routing of glacial outburst floods (jökulhlaup) over the ice surface and the propagation of floodwater from the base of the glacier on the western and southern flanks of the volcano. Jökulhlaups are simulated as fluids using the SAMOS numerical model, developed for shallow and fast moving granular gravity currents (Zwinger *et al.*, 2003). The uncertainty in rheology of the floods is dealt with by using predefined Manning's *n* coefficients ranging 0.05–0.15. Simulations are made for outburst floods caused by: (i) a caldera eruption, (ii) flank eruptions, and (iii) pyroclastic density currents.

The main objective of the study is to provide information on inundation extent, maximum depths of flooding, maximum flow speeds, and minimum surface transport times, computed for several scenarios and aggregated into thematic datasets. Aggregated results on inundation extent are used in an assessment of the populations exposed to floods (Pagneux, 2015a) while information on maximum flood depths and maximum flow speeds serve as input for rating flood hazards (Pagneux and Roberts, 2015).

Results on minimum surface transport time found in this study are used, along with estimates of eruption onset time, subglacial retention time and subglacial transport time (Gudmundsson *et al.*, 2015), in an assessment of the time available for evacuating the areas at risk of flooding (Pagneux, 2015b).

1.1. Past volcanogenic floods

Since Iceland was first populated in 874 CE, two eruptions have occurred beneath the Öræfajökull ice-capped stratovolcano (Figure IV-1). The first observed historical eruption occurred in mid-June 1362, and the second eruption began on 7 August 1727 (Thorarinsson, 1958). Both eruptions were accompanied by a massive, short-lived jökulhlaup that inundated several areas simultaneously. Accounts of the 1727 eruption reveal that it rose rapidly, within hours, to a maximum discharge that was exceptionally large compared to the volume of floodwater drained. For the 1362 jökulhlaup, Thorarinsson (1958) estimated a maximum discharge of ~100,000 m^3/s, attained within a matter of hours. Debris transport was also a significant factor during both jökulhlaups. Debris-laden flows would have comprised juvenile eruptive material, glacial ice, and glaciofluvial sediments, as described in chapter III (Roberts and Gudmundsson, 2015).

The 1362 jökulhlaup is thought to have burst primarily from the glaciers Virkisjökull, Falljökull, and Kotárjökull (Thorarinsson, 1958). Apparently, the 1727 jökulhlaup from Kotárjökull was comparable in size to the 1362 jökulhlaup from the same glacier (Thorarinsson, 1958). However, the 1362 jökulhlaup from Falljökull was much larger than the 1727 jökulhlaup there. Similar to modern-day volcanogenic floods from steep, ice-capped volcanoes (Tómasson, 1996; Magnússon *et al.*, 2012a; Waythomas *et al.*, 2013), it is probable that the 1362 and 1727 jökulhlaups burst initially through the surface of the ice cap at high elevation. Flood sediments from the 1362 jökulhlaup extend over a much greater area than those from the 1727 jökulhlaups, especially towards the northwest and west of Falljökull (Thorarinsson, 1958). Pyroclastic flows would have been prevalent during eruptions of Öræfajökull. These flows would have scoured large zones of the ice cap, causing significant and pervasive ice-melt.

For a full description of the 1362 and 1727 jökulhlaups, see chapter II (Roberts and Gudmundsson, 2015).

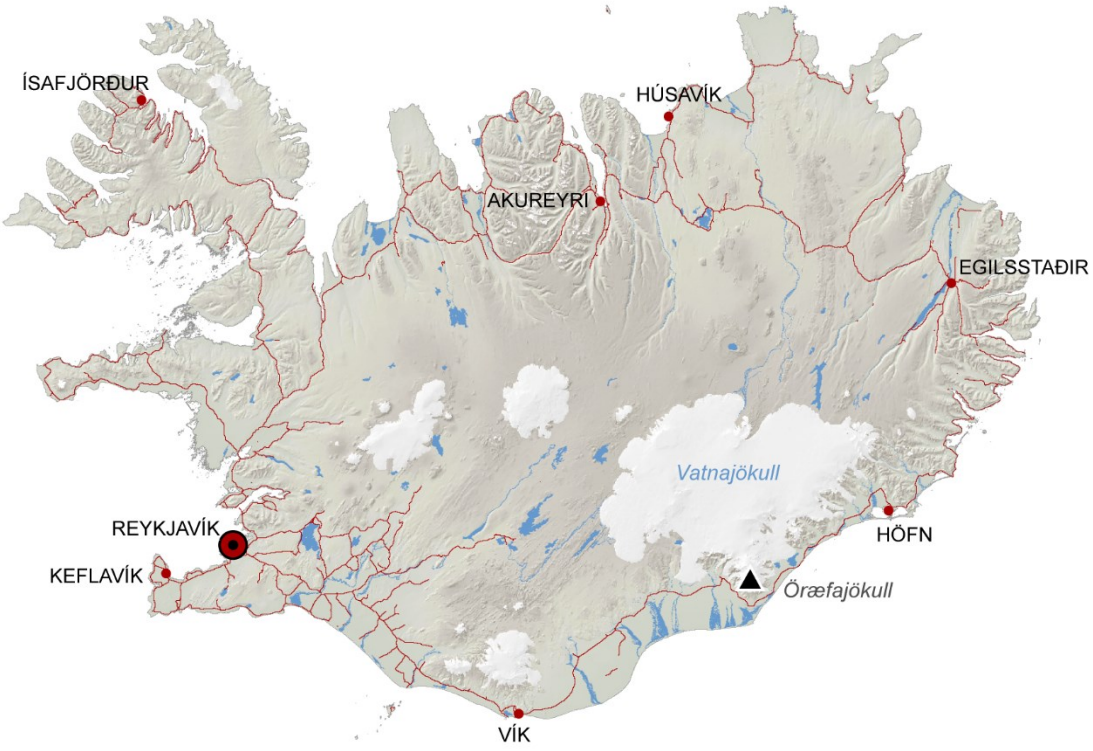

Figure IV-1: Öræfajökull ice-capped stratovolcano, shown by a black triangle, is a separate accumulation area of the Vatnajökull ice cap in south-east Iceland.

1.2. Melting scenarios

Ten melting scenarios relating to volcanic eruptions of various sizes, types, and locations were considered in the modelling of floods due to eruptions of Öræfajökull volcano. Full description of the scenarios is given in chapter III (Gudmundsson *et al.*, 2015).

Flow simulations were restricted to primary jökulhlaups, i.e. floods induced by the eruption itself. A distinction was made between floods due to a caldera eruption, floods due to a flank eruption, and floods due to pyroclastic density currents. Post-eruptive floods, as well as syn-eruptive floods due to precipitation, were not considered in the modelling. Meltwater volume and maximum peak discharge were determined for each scenario using an order-of-magnitude approach (Table IV-1, Figure IV-2). A comparison can be made with the explosive eruptions of Mount Redoubt in 2009, which produced lahars having volumes of 10^7–10^8 m^3 and peak discharges of 10^4–10^5 m^3/s (Waythomas *et al.*, 2013).

Table IV-1: Melting scenarios, with special reference to risk source, meltwater origin and peak discharge (Gudmundsson et al., 2015).

Scenario ID	Glacier catchment	Risk source	Meltwater origin	Peak discharge (m^3/s)
S01c	Virkisjökull – Falljökull (VIR)	Caldera eruption	Falljökull – Virkisjökull	10^4
S01f		Flank eruption	Falljökull – Virkisjökull	10^3
S02c	Suðurhlíðar (SUD)	Caldera eruption	Kotárjökull	10^4
S02f		Flank eruption	Kotárjökull	10^3
S03f		Flank eruption	Stigárjökull	10^3
S03p		Pyroclastic flow	East from Rótarfjallshnúkur*	$3 \cdot 10^3$
S04c	Kvíarjökull (KVI)	Caldera eruption	Kvíarjökull	10^4
S04f		Flank eruption	Kvíarjökull	10^3
S05p	Svínafellsjökull (SVI)	Pyroclastic flow	Svínafellsjökull, south from Svínafellshryggur Ridge	10^3
S06p		Pyroclastic flow	Svínafellsjökull, north from Svínafellshryggur Ridge	10^3

*Kotárjökull excluded

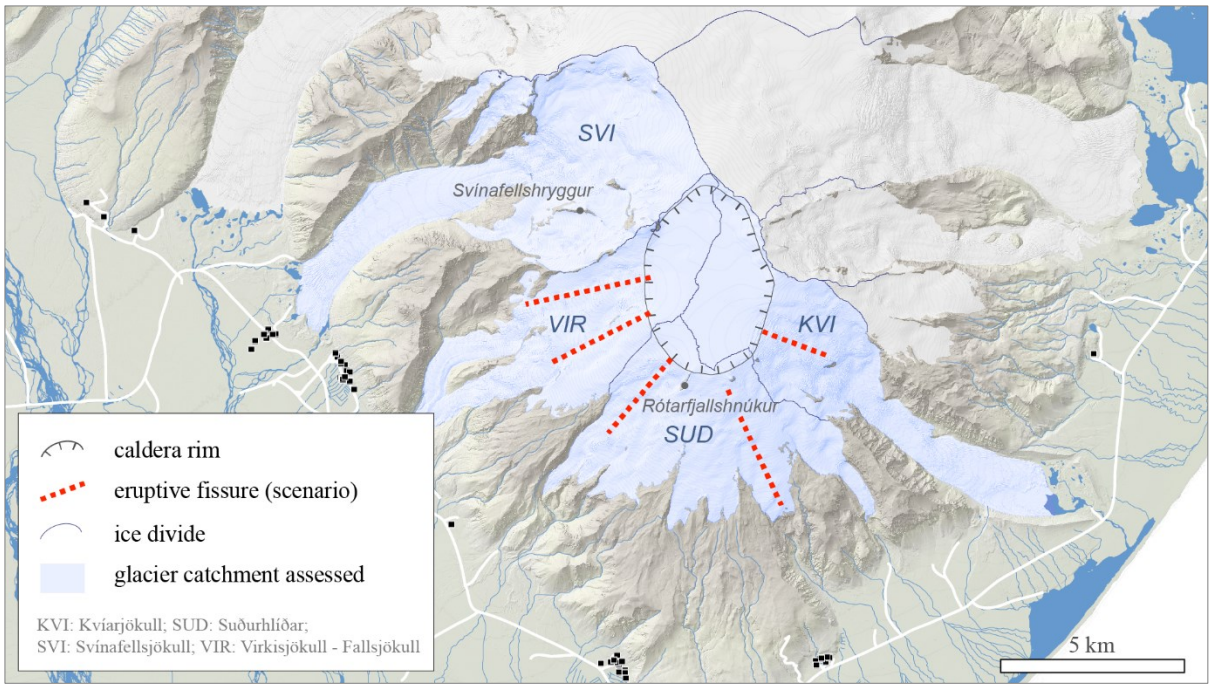

Figure IV-2: Hypothetical eruptive fissures proposed by Gudmundsson et al. (2015). Delineation of the caldera rim is based on ice thickness estimations by Magnússon et al. (2012b). Ice divide is based on airborne LiDAR survey performed in 2011 (see section 3.2.2).

2. Modelling assumptions

Recent observations of high-magnitude jökulhlaups due to volcanism have shown that floodwater often bursts through the surface of steeply sloping glaciers (Roberts, 2005; Magnússon *et al.*, 2012a). This was also the case for large jökulhlaups from the outlet glaciers Kötlujökull (Mýrdalsjökull) and Skeiðarárjökull (Vatnajökull) in 1918 and 1996, respectively (Roberts, 2002). Likewise, anecdotal accounts of the 1727 jökulhlaup from Öræfajökull describe water draining from the glacier. Given that ice thicknesses on the upper slopes of Öræfajökull, outside the volcano's caldera, are widely less than 100 m (Magnússon *et al.*, 2012b), it is likely that floodwater would emerge from crevasses at elevations exceeding 1,000 m AMSL. Hence, for the simulations in this study, floodwater descends initially from the surface of the ice cap at predetermined elevations. In reality a fraction of the flood would also propagate across the glacier bed, but such routing is not considered here. This is in agreement with recent observations of volcanogenic jökulhlaups in Iceland and Alaska (Magnússon *et al.*, 2012a; Waythomas *et al.*, 2013). Significant volumes of snow and ice would be incorporated into a surface-based (supra-glacial) flow. We make no attempt to incorporate the dynamic effects of ice-block transport and floodwater bulking. However, the increased friction resulting from this is taken into account indirectly by using a higher Manning's roughness coefficient (n). The geomorphic consequences of ice-block deposition are addressed by Roberts and Gudmundsson (2015).

3. SAMOS modelling

Several numerical flow models have been used in recent years in the modelling of volcanogenic floods, including LaharZ (e.g. Hubbard *et al.*, 2007; Capra *et al.*, 2008; Muños-Salinas *et al.*, 2009; Magirl *et al.*, 2010; Muños-Salinas *et al.*, 2010), Titan2D (e.g. Charbonnier and Gertisser, 2009; Charbonnier *et al.*, 2013), and VolcFlow (e.g. Charbonnier *et al.*, 2013).

In this study, the SAMOS numerical model is used for the simulation of jökulhlaups. SAMOS is a two dimensional depth-averaged numerical avalanche model initially developed for the Austrian Avalanche and Torrent Research Institute in Innsbruck to model dry-snow avalanches (Sampl *et al.*, 2004; Sampl and Granig, 2009; Zwinger *et al.*, 2003). The model has been used intensively in Iceland in the assessment of run-out zones of snow avalanche (Gíslason and Jóhannesson, 2007), and occasionally in the assessment of floods caused by volcanic eruptions (Hákonardóttir *et al.*, 2005).

3.1. Benefits and constraints

3.1.1. Benefits

Initially developed to model dry-snow avalanches, SAMOS allows the physical properties of the gravity current to be adjusted and fit liquid flow and, therefore, the model is suitable for the modelling of bursts of water on steep slopes. Additionally, SAMOS offers a broad range of model outputs (Table IV-2) that fit with the aim of this study, whose main objective is to provide critical information on flood depths, flow speeds, and flood transport times.

Table IV-2: Comparison of model outputs in LaharZ and SAMOS numerical models.

	LaharZ	SAMOS
Inundation extent	✓	✓
Depths of flooding		✓
Flow speeds		✓
Peak pressure		✓
Transport times		✓

3.1.2. Constraints and limitations

Several constraints or limitations inherent in using SAMOS should be named. First, supraglacial floods are simulated as instant release waves and the effects of sediment bulking and de-bulking (erosion and entrainment) are not taken into account. Hydraulic equations at each location are solved using a digital surface model that remains unchanged during simulations. During such sediment-loaded floods, pronounced landscape change is likely to occur (Roberts and Gudmundsson, 2015), thus affecting the evolution of the floodplain during the jökulhlaup, as well as influencing the characteristics of future floods in the region. SAMOS is unable to take such dynamic geomorphic changes into account.

Secondly, floods are simulated in SAMOS as viscous fluids, i.e. as water, and not as hyperconcentrated flows or flows with significant amounts of debris (see Figure IV-3).

Two main courses are generally taken to simulate flows with large amounts of debris (i.e. Non-Newtonian fluids). One is to consider debris flows as a viscous flow with force-free particles (Bagnold, 1954; Takahashi, 1978; Lun *et al.*, 1984; Savage, 1984), which is mathematically simple but leads to unrealistic solutions for water-debris mixtures (Coussot *et al.*, 1996). The other method is to use various viscoplastic flow models like the Bingham (Bingham, 1916; Bingham *et al.*, 1919) or Herschel-Bulkley model (Herschel and Bulkley, 1926). Those viscoplastic flow models are chosen since the particles in debris flow yield stress and the combined fluid shows non-Newtonian characteristics (i.e. viscous stress is not proportional to shear stresses) (Leyrit *et al.*, 2000).

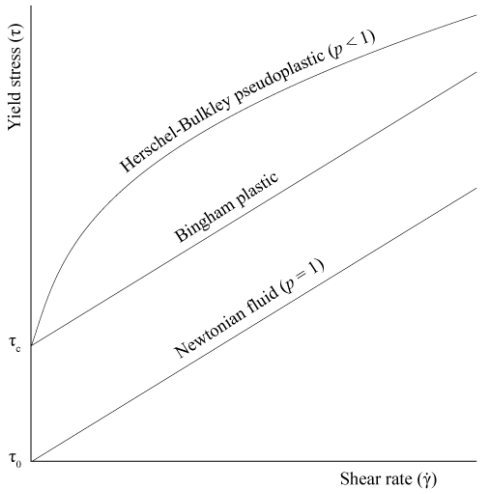

Figure IV-3: Yield stress ($\tau = \tau_c + \dot{\gamma}^p$, where τ_c is the shear stress at zero shear rate and p a positive parameter (Coussot et Meunier, 1996) as a function of share rate ($\dot{\gamma}$) for various fluid models. For Newtonian fluids, yield stress and shear rate are linearly dependent and at zero shear rate the yield stress is zero. Viscoplastic fluids can be modelled with the Bingham model or the Herschel-Bulkley model. For both viscoplastic models at zero shear rate yield stress is not zero. For the Bingham plastic model yield stress and shear rate are linearly dependent but the Herschel-Bulkley model takes shear thinning into account.

In the Bingham model, yield strain and rate of shear strain are linearly dependent but at zero rate of shear strain the yield stress is not zero (see Figure IV-3). In the Herschel-Bulkley model the shear thinning behaviour of water-clay-grain mixtures is taken into account and the magnitude of the shear stress, τ, is given by $\tau = \tau_c + \dot{\gamma}^p$ where τ_c is the shear stress at zero shear rate, $\dot{\gamma}$ is the shear rate and p is a positive parameter (Coussot and Meunier, 1996). The Bingham model has been used for debris flow modelling by Johnson (1970) and Daido (1971) to name a few and the Herschel-Bulkley model has as well been used by multiple researches (Michaels and Bolger, 1962; Nguyen and Boger, 1983; Locat and Demers, 1988; Major and Pierson, 1992; Coussot and Piau, 1994; Wang *et al.*, 1994, Atapattu *et al.*, 1995). For more methods and details on viscoplastic fluids see, for example, the review paper by Coussot and Meunier (1996) and references therein. However, it should be noted that Coussot (1994) has shown that gradually varying mudflows experience the same flow characteristics (hydraulic jump, subcritical and supercritical regimes, instability and more) as water flow and when viscosity parameters are adequately chosen, St.Venant derived equations (as SAMOS is based on) can be used for studying natural flows within small spatial and temporal scales (Coussot and Meunier, 1996).

3.2. Input data and modelling parameters

In this study, the input data required for flood simulation using SAMOS are: (i) physical properties (including roughness parameters); (ii) topographic envelope; (iii) predefined release areas; and (iv) the height of the water column in the release area (i.e. initial flow depth), which in the SAMOS formulation determines the peak discharge.

3.2.1. Rheology

In order to define the rheology for glacial outbursts in SAMOS, the bed friction angle is set to zero and the turbulent friction coefficient is adapted to fit a predefined average Manning's *n* coefficient value. The Manning's *n* coefficient is an empirical coefficient with dimensions $s/m^{1/3}$. It represents flow roughness and ranges from 0.035 to 0.15 (Chow, 1959; Gerhart *et al.*, 1993). The Manning's *n* values used in this study were derived from previous glacial outbursts and roughness estimates for river-beds.

Several factors influence the Manning's *n* value, including surface roughness and sinuosity of channels (Table IV-3). Land-scapes in Iceland are typically devoid of mature trees and other vegetation that would lead to high frictional effects. Although the outwash plains (*sandar*) around Öræfajökull are low-angled and relatively smooth, a volcanogenic jökulhlaup would be laden with friction-adding debris. In addition to coarse-

grained eruptive products, masses of glacial ice would be mobilised by deep, fast-flowing water. Similarly, erosion of unconfined deposits such as glaciofluvial sediments would lead to hyperconcentrated flows, which cannot be modelled adequately using SAMOS.

Table IV-3: Examples of the empirical Manning's n for channels (After Chow, 1959).

Surface	Manning's *n*
Asphalt, smooth	0.013
Excavated channel	0.028
Clean, straight channel full of water	0.03
Streams containing cobbles and large boulders	0.05
Forested area	0.12

Based on accounts of the 1918 eruption of the Katla subglacial volcano, Tómasson (1996) estimated floodplain Manning's *n* coefficients of 0.08 to 0.1. Nye (1976) calculated the Manning's *n* coefficients of the Grímsvötn 1972 jökulhlaup and got 0.12 and when Björnsson (1992) repeated the Manning's *n* coefficient calculations, resulting in an estimate of 0.08. It should be noted that estimations in Nye (1976) and Björnsson (1992) are inferences about the roughness of the subglacial flood-path, not the sub-aerial route.

Russell *et al.* (2010) estimated the Manning's *n* coefficients of 13 cross sections following a jökulhlaup from Sólheimajökull in July 1999. Various methods were used, including measurements based on bulk sediment samples collected in the days after the jökulhlaup. The estimated Manning's *n* coefficients of the cross sections ranged from 0.03 to 0.08. Gíslason (2012) used HEC-RAS to reconstruct the supraglacial jökulhlaup in on the southern slope of Eyjafjallajökull in 2010. There, he concluded the Manning's *n* coefficient on the lower slopes to be 0.03–0.04 whereas in the steep slopes Manning's *n* values of 0.1–0.13 were more realistic. Hákonardóttir *et al.* (2005) used SAMOS to simulate supraglacial outbursts on the southern slopes of Eyjafjallajökull volcano. The uncertainty in rheology of the supraglacial floods was dealt with by choosing three Manning's values $n = 0.05$, $n = 0.10$, $n = 0.15$. In relation to inundation area, the results of Hákonardóttir *et al.* (2005) are in good accordance with the observations made in the Svaðbælisá Valley after the 2010 jökulhlaup in Eyjafjallajökull (Snorrason *et al.,* 2012). Elíasson *et al.* (2007) numerically computed a translatory wave down the Markarfljót valley using equations derived from the two dimensional St. Venant's equations. Their conclusions were among other, that the Manning's *n* could change considerably with depth although Chézy's *C* (see § 3.3) would remain constant.

Roberts and Gudmundsson (2015) show that the initial composition of floodwater during the 1362 and 1727 jökulhlaups was hyperconcentrated, having a sediment-by-volume fraction as high as 60% at the beginning of the floods. From contemporary observations of volcanogenic jökulhlaups (Magnússon *et al.*, 2012a), such flow conditions would apply to the initial propagation of the flood. More fluidal flows would be expected following the initial wave front.

Given the large uncertainty about flow rheology, Manning's *n* values in this study have been split into three intervals, similar to the approach by Hákonardóttir *et al.* (2005):

- Low Manning's hypothesis: $n = 0.05$
- Medium Manning's hypothesis: $n = 0.10$
- High Manning's hypothesis: $n = 0.15$

3.2.2. Topographic envelope

A 5 m cell-size Digital Surface Model (DSM) covering the Öræfajökull ice-cap and a significant portion of the surrounding non-glaciated areas was used as the topographic envelope for the hydraulic simulations

(Figure IV-4). The DSM is derived from an airborne LiDAR survey performed by TopScan GmbH during the summers of 2011 and 2012. The vertical accuracy of the LiDAR measurements and the average density of the point cloud are estimated <0.5m and ~0.33point/m^2, respectively (Jóhannesson *et al.*, 2011; Jóhannesson *et al.*, 2013). Hydro-enforcement of the glacial part of the DSM was performed to ensure that water would not be trapped in crevasses. In turn, bridges and buildings in the non-glaciated area were not removed. In order to reduce the use of computational resources and optimize stability during simulations, spatial subsets of the LiDAR-derived DSM were used. Each subset extends from one release area or more, upstream, to portions of ocean or of active *sandar* downstream (Figure IV-4).

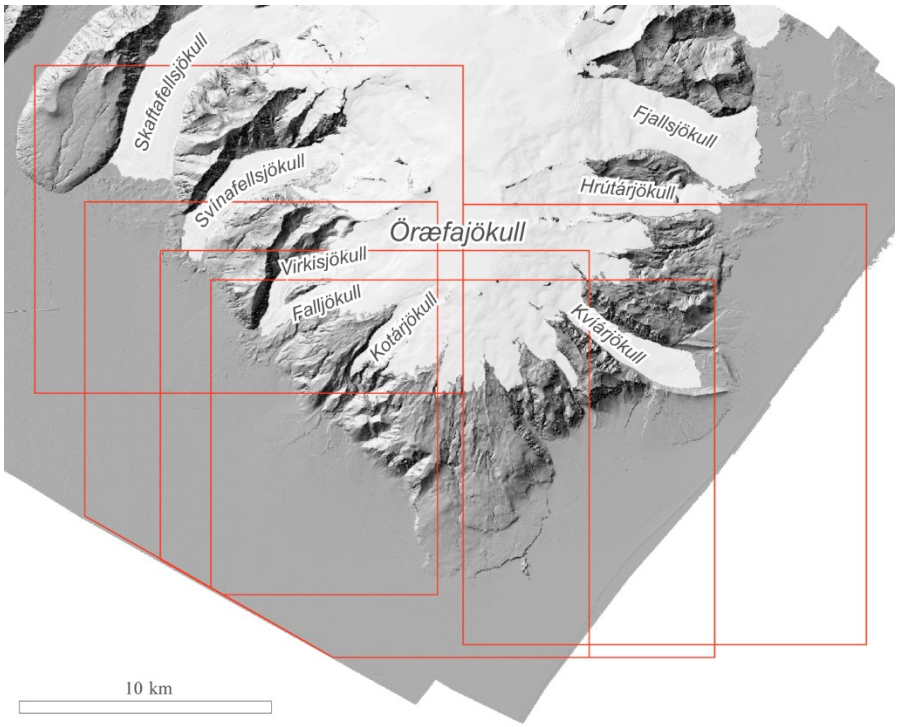

Figure IV-4: Extent of the LiDAR DSM (Öræfajökull and surrounding non-glaciated areas) used in the hydraulic simulations. The rectangles show spatial subsets of the DSM.

3.2.3. Release areas, maximum discharge, and initial flow depth

Ten areas were delineated, from which floods due to caldera eruptions, flank eruptions, and pyroclastic flows were released (Figure IV-5). The lower boundary of the release areas corresponding to a caldera eruption was placed at ~1,500 m AMSL. At this elevation, subglacial floodwater flowing down from the caldera is expected to burst onto the glacier surface, as ice thicknesses are only ~50 – 100 m, as estimated by Magnússon *et al.* (2012b). The lower boundary of the release areas for floods caused by the formation of pyroclastic density currents was placed at a distance of 1–2.8 km from the caldera rim. The release areas corresponding to floods caused by flank eruptions were delineated to enclose the hypothetical eruptive fissures (Figure IV-2) proposed by Gudmundsson *et al.* (2015).

The mean slope angle in the release areas varies between 14° and 24.5° (Figure IV-6). For each scenario, iterative runs were performed to determine the initial flow depth (Figure IV-6) in the release areas necessary to reach the predefined maximum discharge (Table IV-1) at the cross-sections near to the glacier margins.

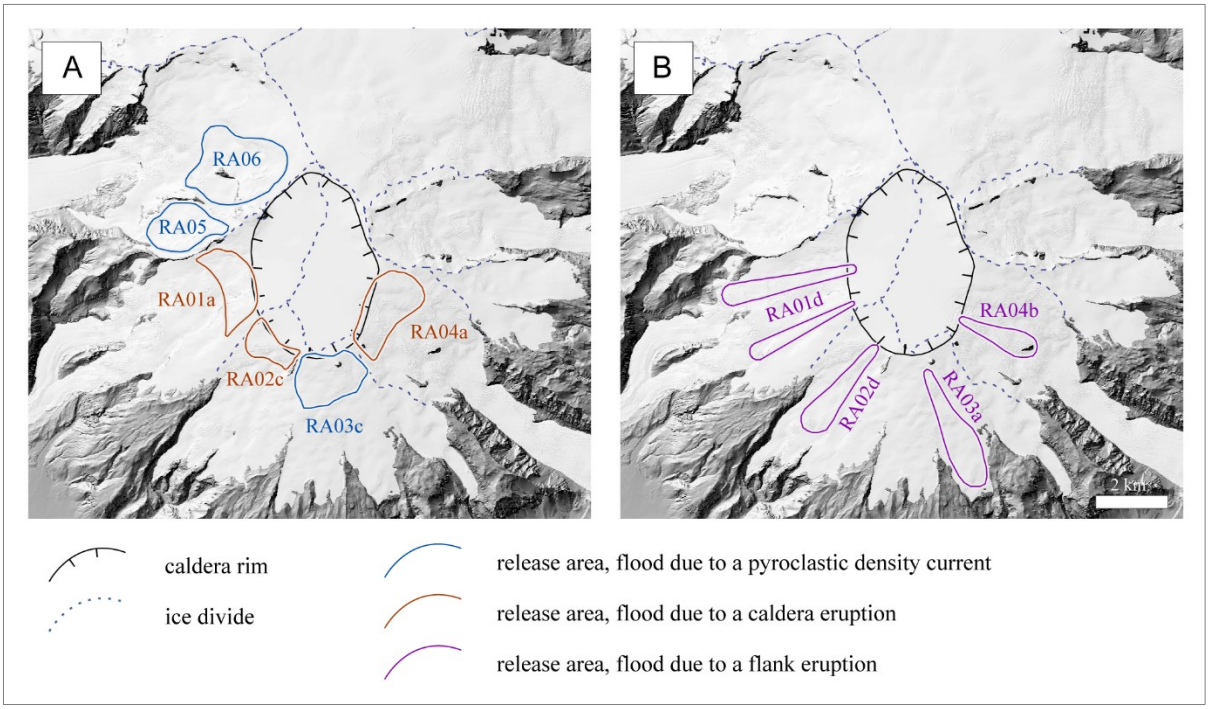

Figure IV-5: Flood release areas in the case of pyroclastic density currents (A), caldera eruption (A), and flank eruptions (B). Delineation of the caldera rim is derived from ice thickness estimations by Magnússon et al. (2012b). Flood release areas in the case of flank eruptions (B) enclose the hypothetical eruptive fissures (Figure IV-2) proposed by Gudmundsson et al. (2015).

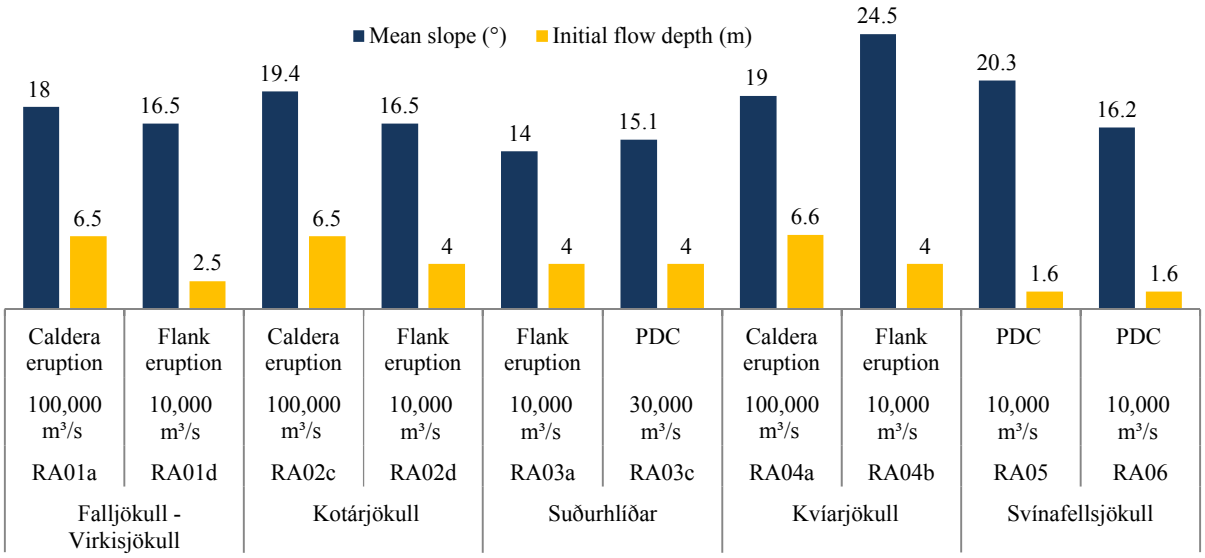

Figure IV-6: Mean slope (°) of the release areas and corresponding initial flow depth (m) necessary to match the required maximum discharge at the downstream cross-sections.

3.3. Equations of motion

The SAMOS model solves numerically the two dimensional depth averaged St. Venant's equations. One can choose between several different bed friction models but the Manning equation is not an option. Of the models available in SAMOS the Chézy's friction model is the most appropriate to simulate fluid flow in jökulhlaups. In the Chézy's model the shear stress, τ_b, is dependent on the mean speed of the fluid, *u,* according to

$$\tau_b = \rho C_{dyn} u^2,$$

where ρ is the density of the fluid, and C_{dyn} is a dynamic friction coefficient that needs to be determined. It should be noted that the SAMOS model finds the time dependent speed unlike the traditional Chézy's equation for a steady, open channel turbulent flow where the speed is described by

$$u = C\sqrt{RSg},$$

where *R* is the hydraulic radius of the channel, *S* is the slope of the energy grade line, *C* is a dimensionless friction parameter often called Chézy's *C* and *g* is gravitational acceleration.

3.3.1. Dynamic friction

We assume that friction is the same for the transient case as for the steady state case so exploring the friction of the steady state case is sufficient. Consider a cross section of a hill that is tilted θ degrees from horizontal (Figure IV-7). When steady state is reached the force balance on a small unit is:

$$\rho g \sin(\theta) = \frac{\tau_b}{h},$$

where ρ is the density of the fluid, *g* is gravity, τ_b is the shear stress and *h* is the height of the unit (flow depth in our case). The shear stress using the Chézy's friction model was given above as

$$\tau_b = \rho C_{dyn} u^2,$$

where *u* is the mean speed of the fluid and C_{dyn} is the dynamic friction coefficient that needs to be determined. If the Chézy's friction model is written in terms of this dynamic frictional coefficient the speed becomes

$$u = \sqrt{\frac{hgsin(\theta)}{C_{dyn}}},$$

or the frictional coefficient is

$$C_{dyn} = \frac{g \sin(\theta) h}{u^2}.$$

If we chose to use the Chézy's equation for the steady state speed (as given above) and note that the flow is thin (i.e. $h \ll b$ where *h* is the flow depth and *b* is the width of the flow) so the hydraulic radius is

$$R = \frac{hb}{b+2h} \to h,$$

and the flow is uniform so $S = sin(\theta)$, where θ is the slope of the channel (see Figure IV-7), the relationship between the dynamic friction coefficient, C_{dyn}, and Chézy's, *C,* is

$$C_{dyn} = \frac{1}{C^2}.$$

Therefore, with a given Chézy's, *C,* the dynamic friction coefficient, C_{dyn}, (as needed by SAMOS) could be found.

The use of Manning's equation is more common when describing uniform, steady open channel flow. In Manning's equation the mean speed is given by

$$u = \frac{1}{n} R^{2/3} S^{1/2},$$

where *n* is an empirical Manning coefficient, *R* is the hydraulic radius of the channel (again for thin flow $R \approx h$) and *S* is again the slope of the energy grade line (for uniform flow $S = sin(\theta)$). The dynamic friction coefficient, C_{dyn}, may then be written in terms of Manning's resistance coefficient, *n*, by

$$C_{dyn} = \frac{n^2 g}{h^{1/3}}.$$

Therefore, with a given Manning's *n* coefficient and given initial flow depth the dynamic friction coefficient, C_{dyn}, (as needed by SAMOS) can be found.

In SAMOS the dynamic friction coefficient, C_{dyn}, is set to the same value in the whole domain. This is, therefore, equivalent to setting the Chézy's *C* to the same value in the whole domain but the Manning's *n* will vary with depth (the values given are averaged Manning values). Choosing a constant Chézy's *C* within the whole domain has been shown to be more realistic in jökulhlaups than choosing a constant Manning's *n* in the whole domain (Elíasson *et al.*, 2007). Since the literature on Manning's *n* in jökulhlaups is greater than on Chézy's *C,* Manning's *n* values will be referred to in all scenarios listed below instead of the Chézy's *C*. The interested reader can refer to the equations above if the values of Chézy's *C* are preferred.

3.3.2. Initial flow depth

An estimate of the discharge of the flow is given by $Q = uhb = \frac{1}{n}R^{5/3}S^{1/2}b$ so the flow depth is

$$h = \left(\frac{nQ}{S^{1/2}b}\right)^{3/5}.$$

When determining the initial flow depth in the release area, the desired Manning's *n* coefficients and the desired maximum discharge at predefined cross-sections need to be specified. The mean angle of the slope can be found from the DSM and an estimate of the length of the cross-section can also be made. The actual initial flow depth in the release area can only be found with an iterative process where one initial flow depth is tested and the maximum discharge at the glacier edge is calculated. If the maximum discharge is not as desired, the initial flow depth is increased if the discharge is too low and decreased if the discharge is too high. This process is repeated until the maximum discharge reaches the desired value.

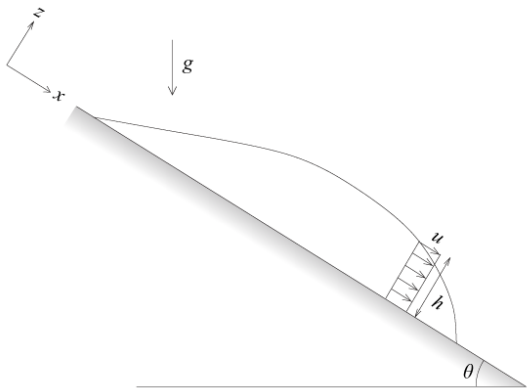

Figure IV-7: The slope and the coordinates in SAMOS.

3.4. Computations and visualisation

Inundation extent, flood depths, and flow speeds were computed for every scenario along with minimum surface transport times and exported to 10 m cell-size grids.

3.4.1. GIS post-processing

The output grids were finally post-processed in a Geographic Information System (GIS). Four thematic mosaics were produced, i.e. one mosaic per model output (inundation extent, depths, flow speeds, and travel times), such as to provide an overall picture of the flood area. For each model output, modelling results for Manning's *n* 0.05 and 0.10 were combined. For the depths of flooding and flow speeds, the output rasters were merged to extract the maximum values found for every cell within the modelling domain. For the surface transport times, in turn, the output grids were merged such as to determine the minimum values at peak discharge.

3.4.2. Planned use

Maximum flood depths and maximum flow speeds were extracted to serve as input for rating flood hazards (Pagneux and Roberts, 2015), and in an assessment of the populations exposed to floods (Pagneux, 2015a) along with results on inundation extent.

Minimum surface transport times were processed to be used along with estimates of

eruption onset time, subglacial retention time, and subglacial transport time (Gudmundsson *et al.*, 2015) in an assessment of the time available for evacuating the areas at risk of flooding (Pagneux, 2015b).

4. Results

4.1. Inundation extent

4.1.1. Individual simulations

Figures IV-8 to IV-17 show the results of the individual simulations. The principal findings regarding the inundation extent, as estimated from the simulations, are:

- The use of an average Manning's *n* 0.15 led to an underestimation of the inundation extent in the areas flooded in 1362 and 1727 as estimated by Roberts and Gudmundsson (2015). Simulation results using Manning's *n* 0.15 were, therefore, not used.
- On the alluvial fans, little difference in extent was found between Manning's *n* 0.05 and Manning's *n* 0.10 scenarios (e.g. Figure IV-10). Since the simulations were stopped after a time interval ranging 15,000 – 50,000 seconds, it can be considered that Manning's *n* 0.05 scenarios portray, "in advance", the inundation extent that the 0.10 scenarios reach at a later point in time.
- The simulated floods were individually large enough to inundate the entire alluvial fan at the base of the glaciers from which floodwater originate. Flood extent was eventually constrained by adjacent, overlapping fans. Where floodwater interacted with an adjacent fan, the extent of floodwater run-up was often considerable, ranging 500 – 800 m at some locations with Manning's *n* set to 0.05 (Figure IV-18).

4.1.2. Overall area at risk of flooding

Superimposition of the individual simulations results indicate that 237 km^2 are at risk of flooding (Figure IV-19). From an analysis of LiDAR-derived hillshades and aerial imagery, one can add to the flood area identified in the simulations about 110 km^2 of *sandar*, to the south (Skeiðarársandur) and to the east (Breiðamerkursandur). The Skaftafellsá river marks, to a significant degree, the limit of the flood area to the west as little water is shown to flow over the highway to Skaftafell, near the junction with the National road. The estuary of the Breiðá and Fjallsá rivers is the likely limit of the flood area to the east.

4.1.3. Inundation extent after risk source

Of the 347 km^2 of land identified at risk of flooding (simulations and photointerpretation), 284 km^2 (82%) were found exposed to floods caused by a caldera eruption, flank eruptions, or pyroclastic density currents, 42 km^2 (12%) to floods caused by flank eruptions or pyroclastic density currents, and 21 km^2 (6%) to floods caused by pyroclastic density currents only (Figure IV-19).

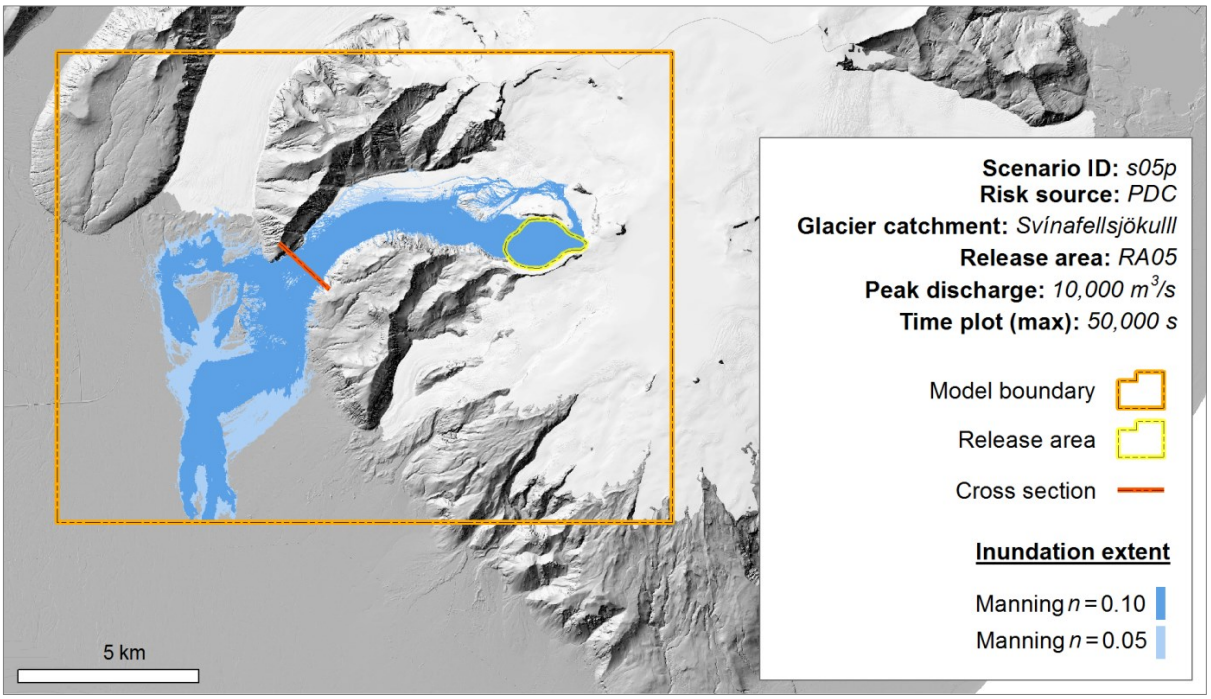

Figure IV-8: Inundation extent of a 10,000 m^3/s peak discharge flood caused by a pyroclastic density current in the Svínafellsjökull glacier catchment, south from the Svínafellshryggur ridge. Extent of inundation is shown for Manning's n 0.05 and 0.10 after 50,000 s.

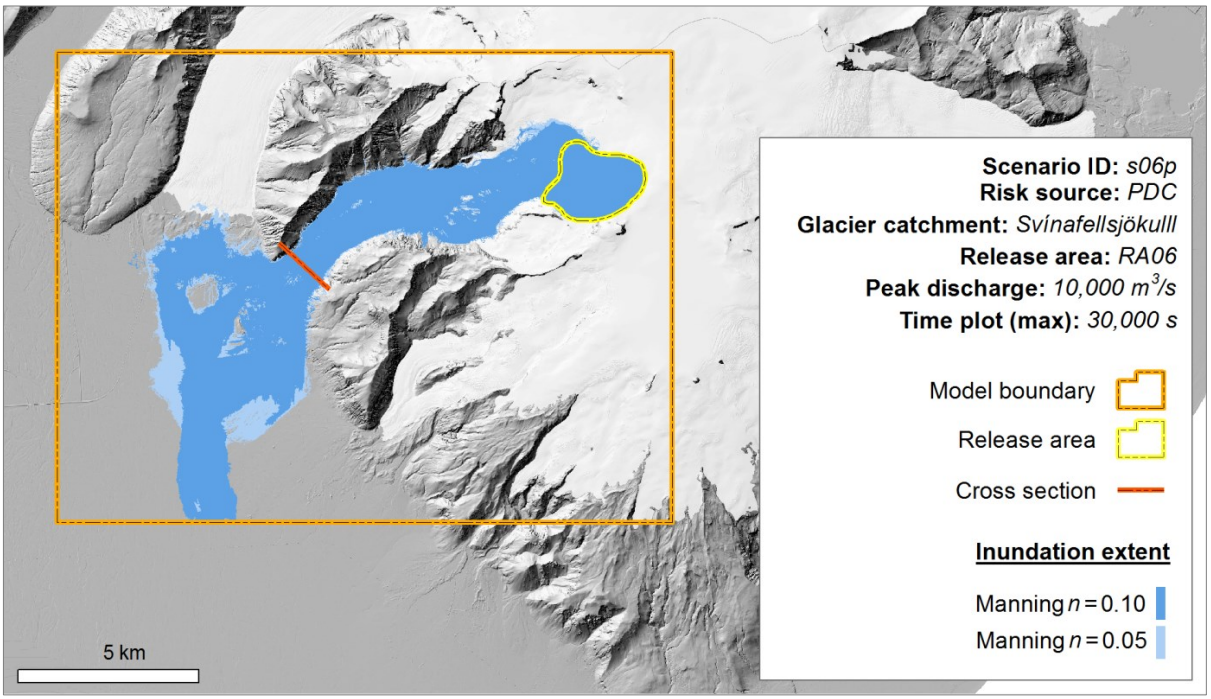

Figure IV-9: Inundation extent of a 10,000 m^3/s peak discharge flood caused by a pyroclastic density current in the Svínafellsjökull glacier catchment, north from the Svínafellshryggur ridge. Extent of inundation is shown for Manning's n 0.05 and 0.10 after 30,000 s.

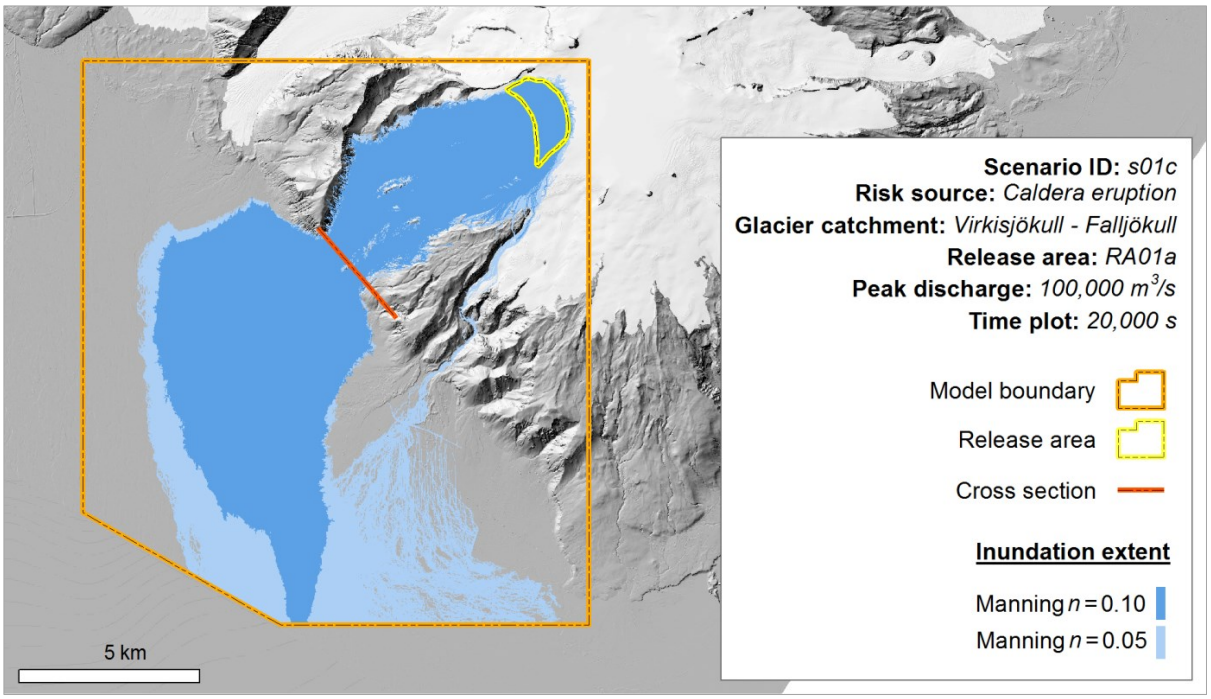

Figure IV-10: Inundation extent of a 100,000 m^3/s peak discharge flood in the Virkisjökull – Falljökull glacier catchment, caused by a caldera eruption. Extent of inundation is shown for Manning's n 0.05 and 0.10 after 20,000 s.

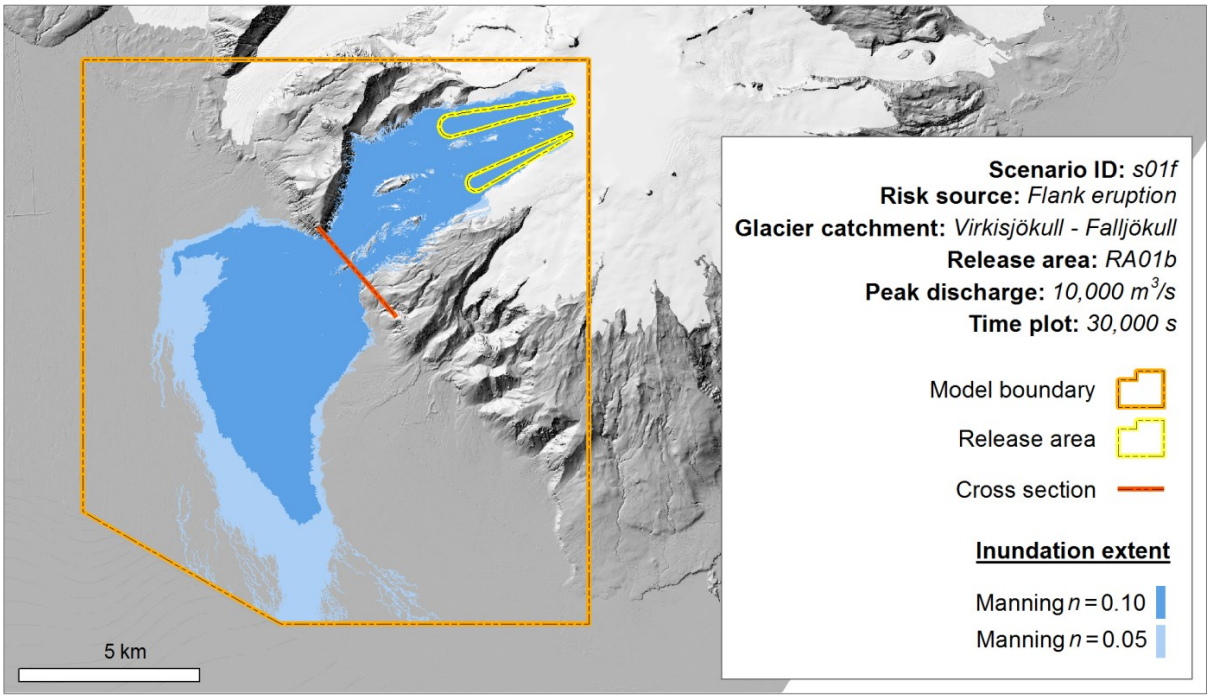

Figure IV-11: Inundation extent of a 10,000 m^3/s peak discharge flood in the Virkisjökull – Falljökull glacier catchment, caused by a flank eruption. Extent of inundation is shown for Manning's n 0.05 and 0.10 after 30,000 s.

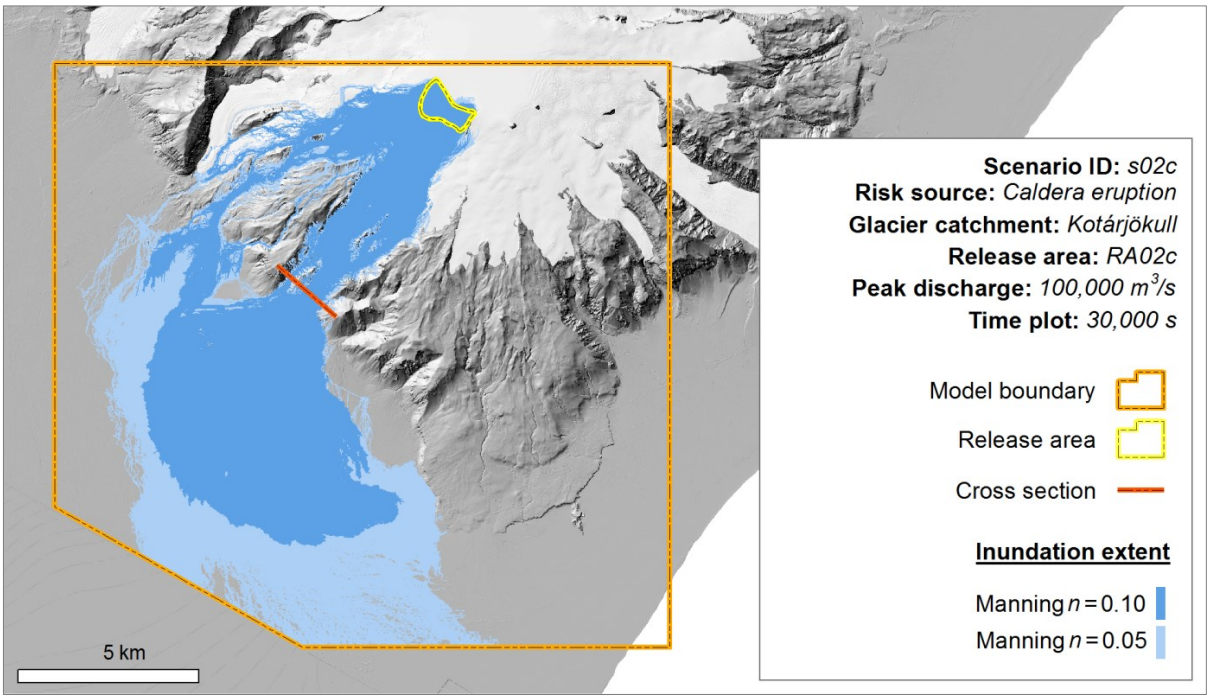

Figure IV-12: Inundation extent of a 100,000 m^3/s peak discharge flood caused by an eruption in the caldera that affects the Kotárjökull glacier catchment. Extent of inundation is shown for Manning's n 0.05 and 0.10 after 30,000 s.

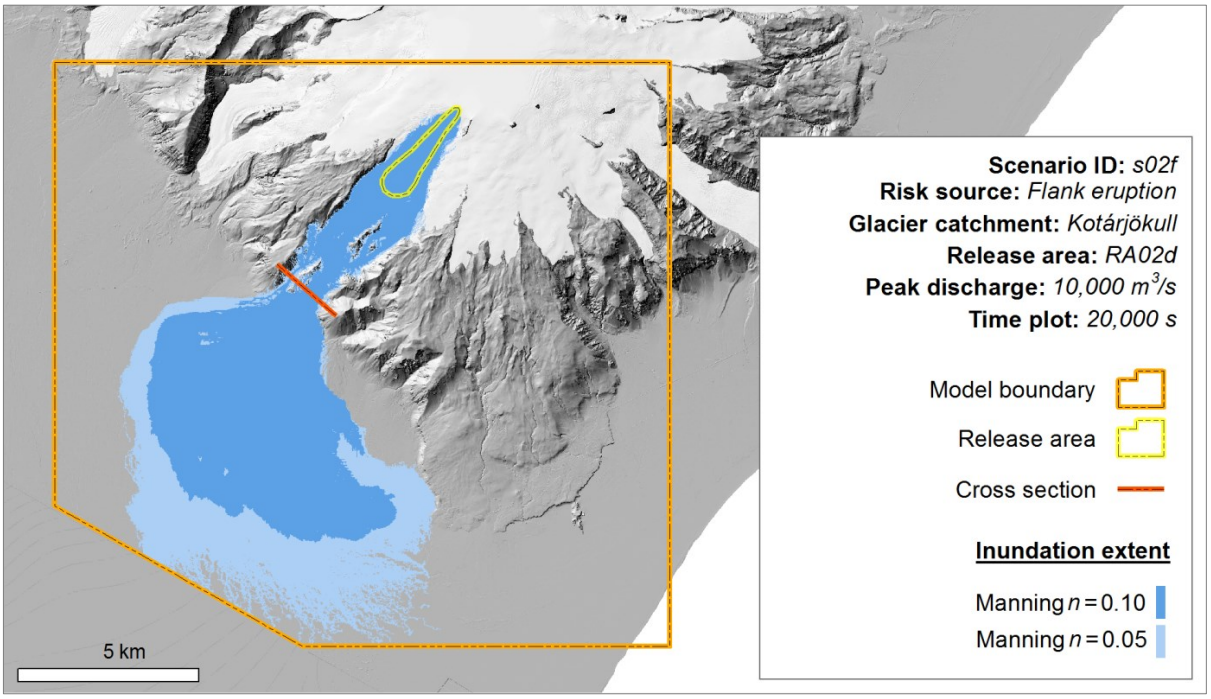

Figure IV-13: Inundation extent of a 10,000 m^3/s peak discharge flood caused by a flank eruption that affects the Kotárjökull glacier catchment. Extent of inundation is shown for Manning's n 0.05 and 0.10 after 30,000 s.

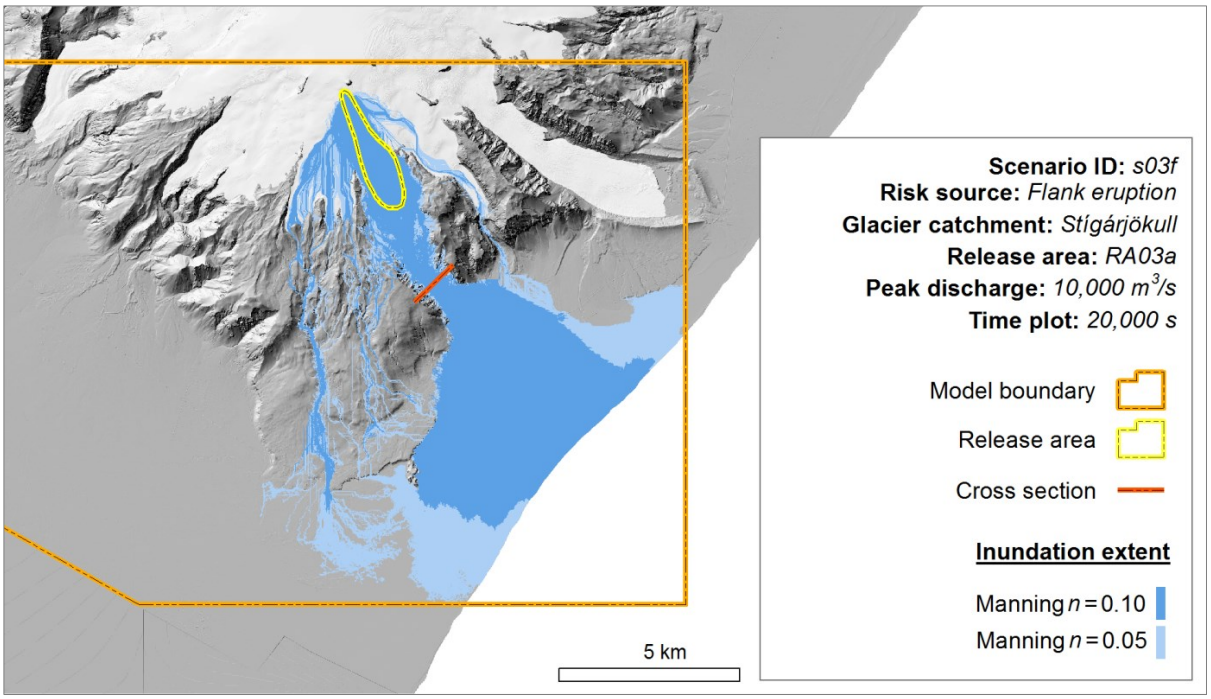

Figure IV-14: Inundation extent of a 10,000 m^3/s peak discharge flood caused by a flank eruption that affects the Stigárjökull glacier catchment. Extent of inundation is shown for Manning's n 0.05 and 0.10 after 20,000 s.

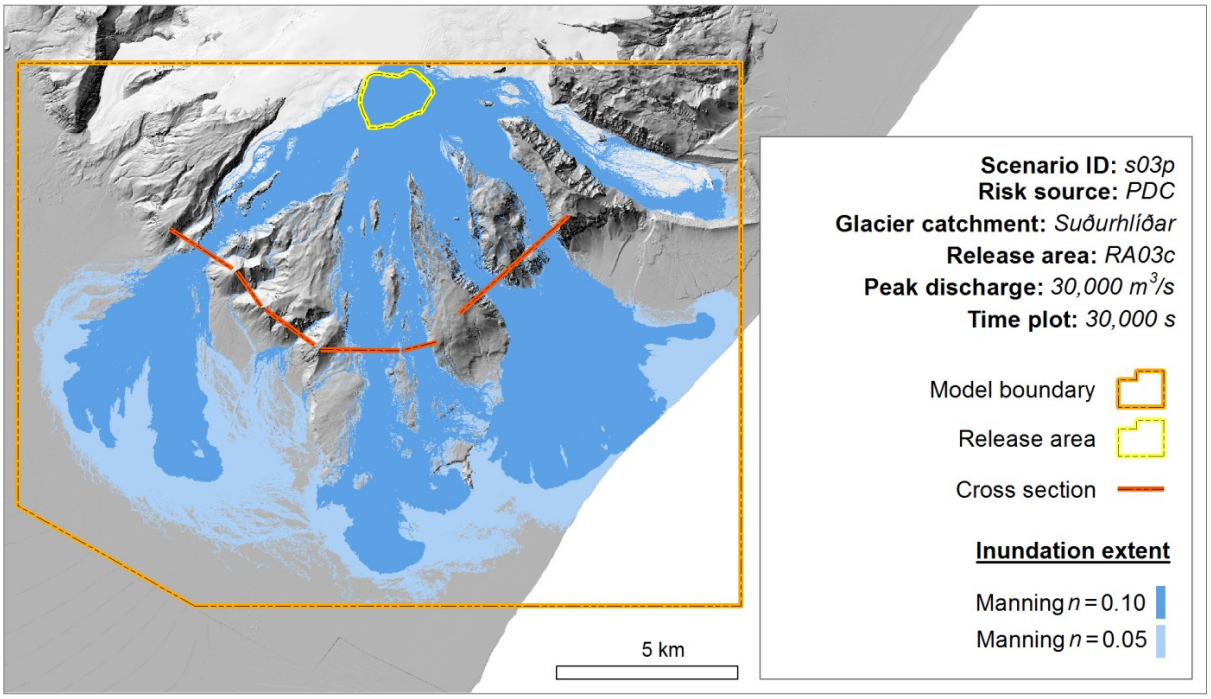

Figure IV-15: Inundation extent of a 30,000 m^3/s peak discharge flood caused by the formation of a pyroclastic density current in the Stigárjökull drainage area. Extent of inundation is shown for Manning's n 0.05 and 0.10 after 30,000 s.

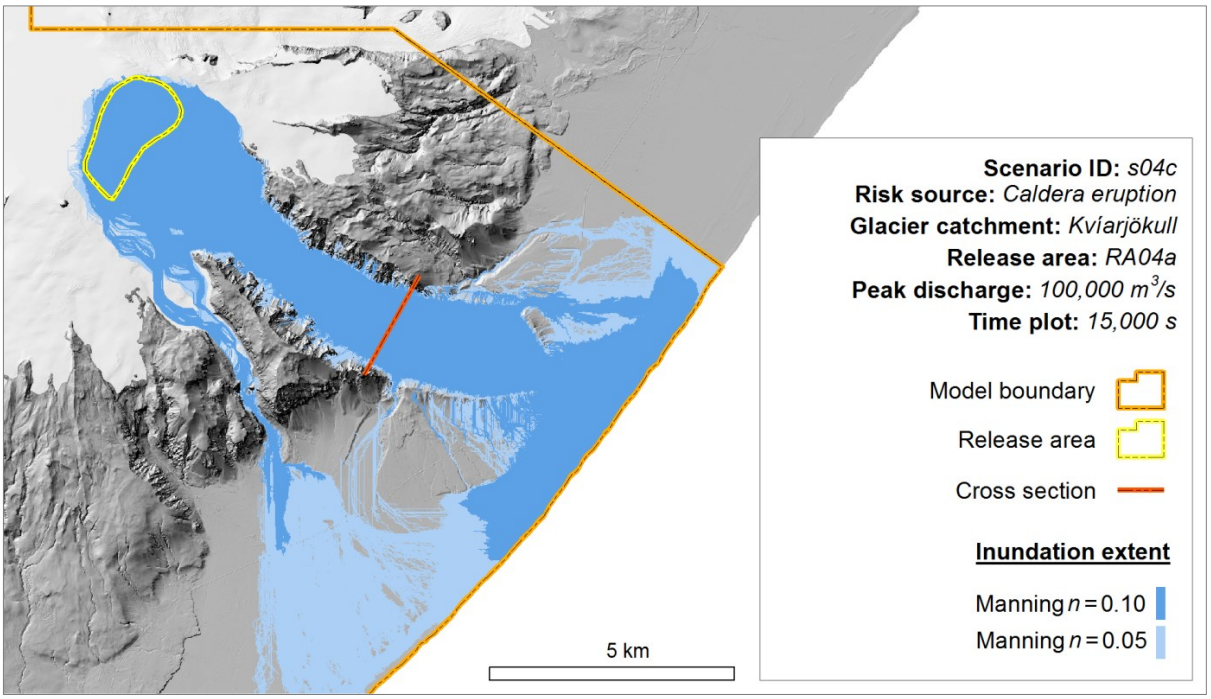

Figure IV-16: Inundation extent of a 100,000 m^3/s peak discharge flood caused by an eruption in the caldera that affects the Kviárjökull glacier catchment. Extent of inundation is shown for Manning's n 0.05 and 0.10 after 15,000 s.

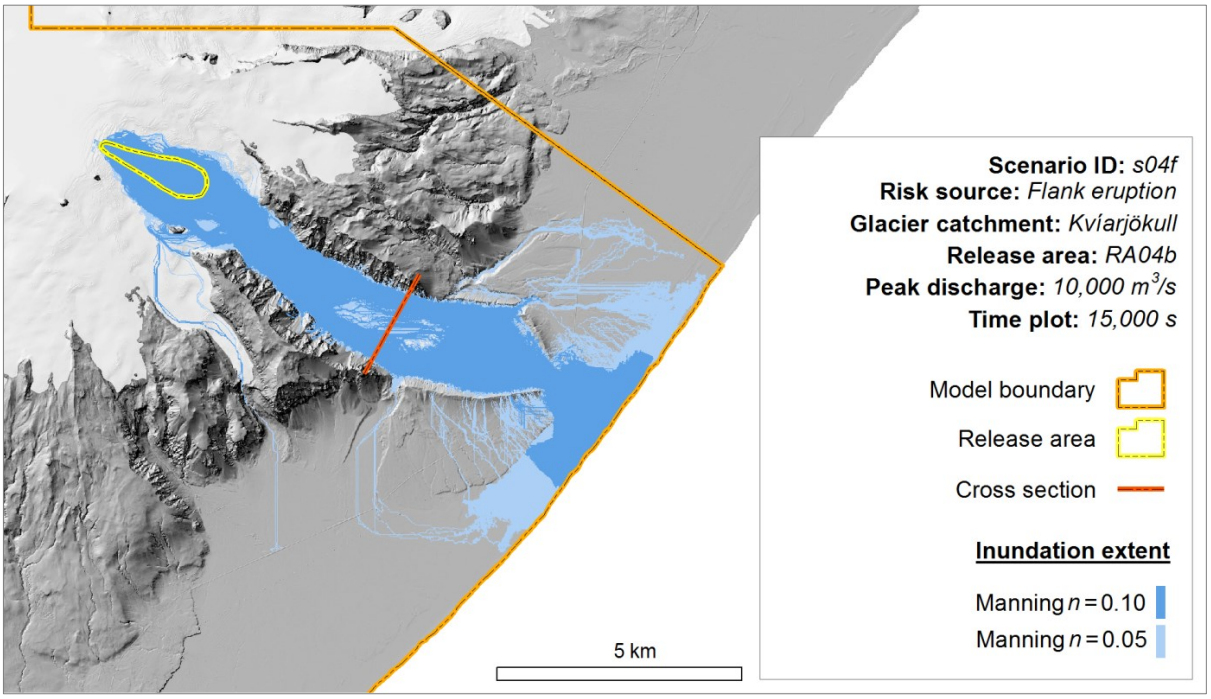

Figure IV-17: Inundation extent of a 10,000 m^3/s peak discharge flood caused by an eruption in the caldera that affects the Kviárjökull glacier catchment. Extent of inundation is shown for Manning's n 0.05 and 0.10 after 15,000 s.

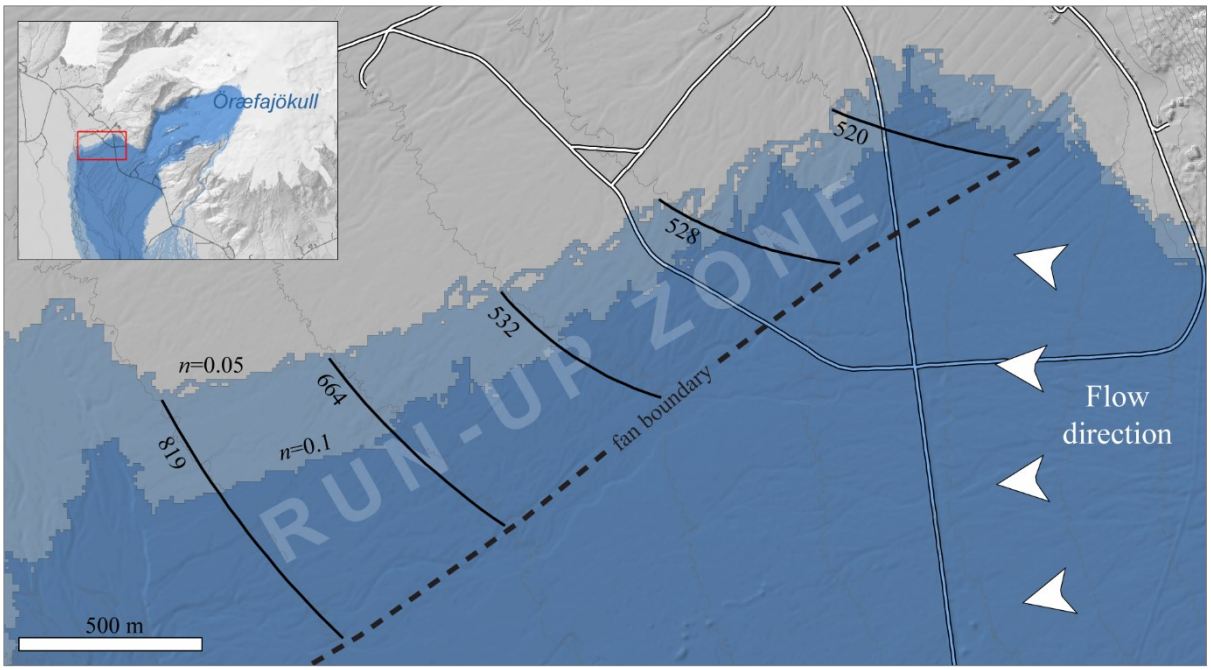

Figure IV-18: Run-up distances (m), onto adjacent alluvial fan to the north, of floodwater propagating on the Virkisá alluvial fan. The scenario is a 100,000 m^3/s flood initiated in the Virkisjökull-Falljökull glacier catchment, with Manning's n set to 0.05 and 0.10. Run-up distances (solid lines) are estimated from the boundary between fans (dashed line), based on constant elevations (contour lines in grey).

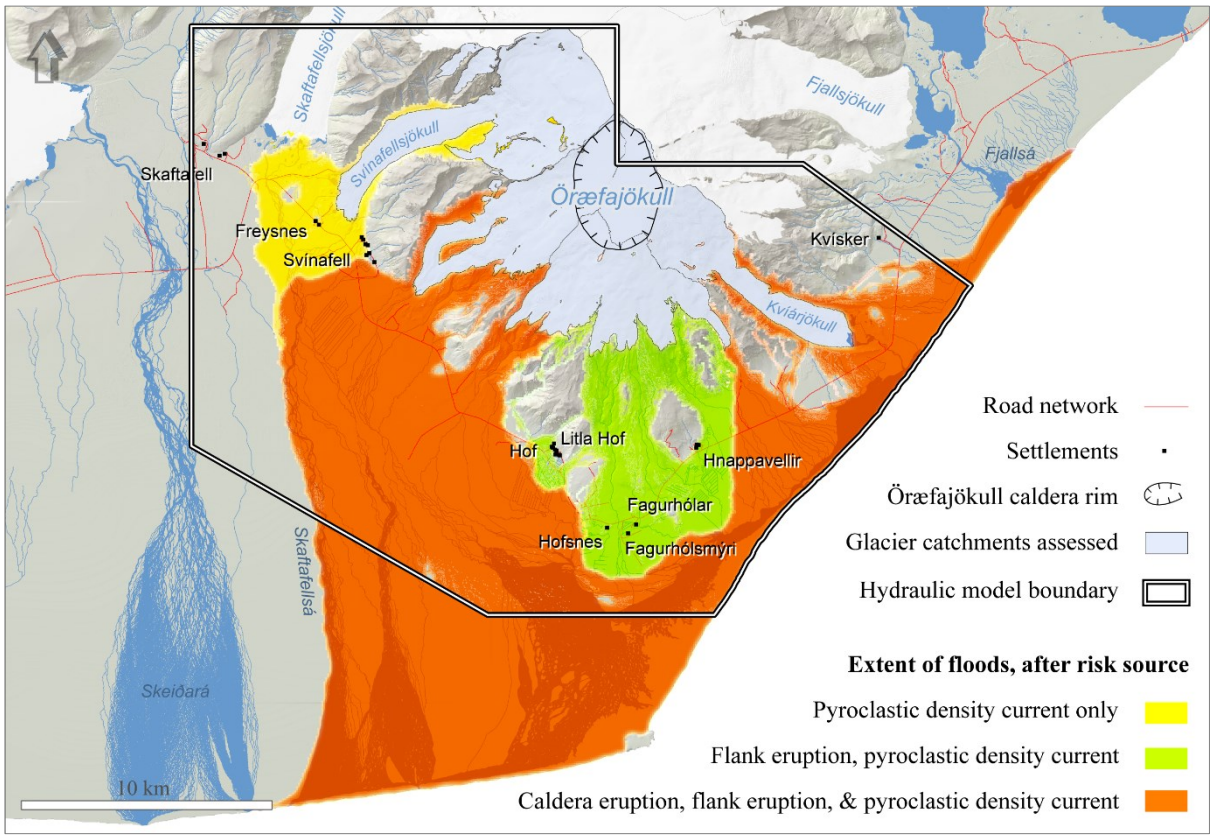

Figure IV-19: Areas at risk of flooding after superimposition of the individual simulations results and photointerpretation of the landscape beyond the spatial boundary of the numerical model.

4.2. Depths of flooding

On average, the maximum depths of flooding found in the proglacial area were ~4.5 m. Maximum flood depths in excess of 10 m were found in nearly 20% of the flooded area, mostly along the main axes of flow propagation (Table IV-4, Figure IV-20). Sectors where the maximum depths were below 0.50 m are much more limited in extent, representing only 12% of the area identified at risk of flooding.

Table IV-4: Extent of maximum flood depths in proglacial areas (Manning's n 0.05 and 0.10 combined).

Maximum depths (m)	Extent (km^2)	Extent (%)
< 0.5	28	12
0.5–1	23	10
1–2	29	12
2–5	84	35
5–10	45	19
> 10	28	12

4.3. Flow speeds

Maximum flow speeds in excess of 3 m/s were found on ~200 km^2 of non-glaciated terrains (Table IV-5, Figure IV-21).

On average, the maximum flow speeds found within the whole modelled domain ranged from 12 to 28 m/s (43 to 100 km/h). This range of values, which applies to the slopes of the volcano and to the lowland as one, should not be regarded as extravagant. If one considers the peak discharge of floods and the distance from the source of timing at which the average front speeds were estimated, the results on speeds are indeed in good accordance with empirical observations made for lahars triggered by the 1926 eruption of Mount Tokachi and the Mount St. Helens 1980 eruption (Pierson, 1998; Table IV-6). On the slopes of the volcano (above 100 m AMSL), which are characterised by a mean slope angle of 22.7° (~42%), the average flow speeds ranged 22 – 42 m/s.

Table IV-5: Extent of maximum flow speeds in proglacial areas (Manning's n 0.05 and 0.10 combined).

Maximum flow speeds (m/s)	Extent (km^2)	Extent (%)
< 3	35	15
3–5	12	5
5–10	72	31
10–20	54	23
> 20	64	27

4.4. Surface transport times

4.4.1. Transport time at maximum discharge

Minimum surface transport times from the lower boundaries of the release areas down to the National Road ranged between 4 minutes, downstream of Stigárjökull, and 51 minutes at the foot of Svínafellsjökull (Figure IV-22). Manning's *n* 0.05 scenarios yielded transport times half the transport times of Manning's *n* 0.10 scenarios; the lower the Manning's *n*, the shorter the transport times.

As the lower boundary of the release areas for floods due to a flank eruption are close to the glacier margins, the surface transport times of the corresponding floods were found to be identical or very similar in some glacier catchments (e.g. Kotárjökull, Virkisjökull-Falljökull) to the transport times of floods due to a caldera eruption. For floods due to a flank eruption, the proximity of the release areas to the lowland compensated, to a significant degree, for less discharge.

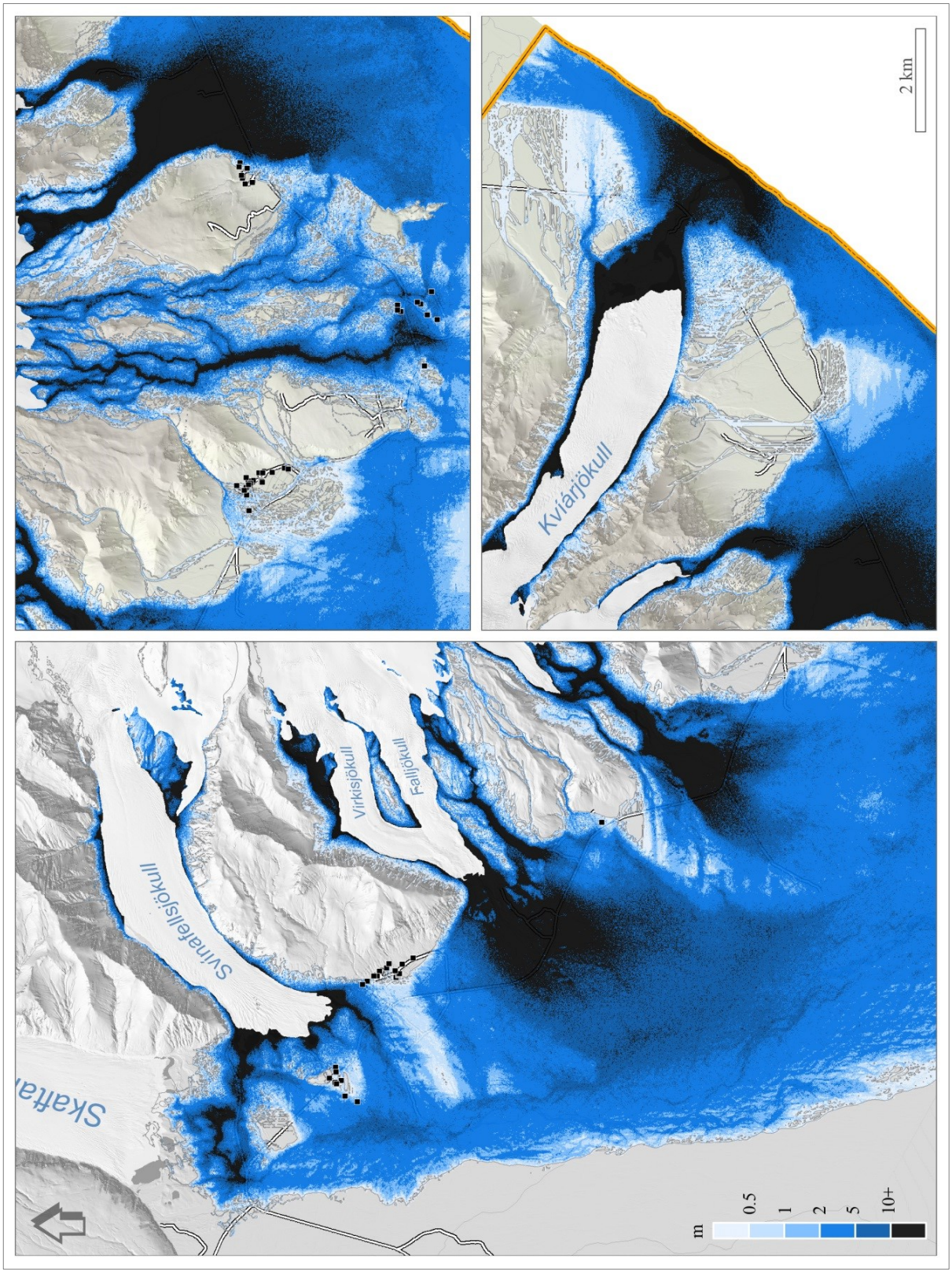

Figure IV-20: Aggregated maximum depths of flooding (Manning's n 0.05 and 0.10 combined). Depths in excess of 10 m cover nearly 20% of the flooded area, mostly along the main axes of flow propagation. Settlements are shown as black dots.

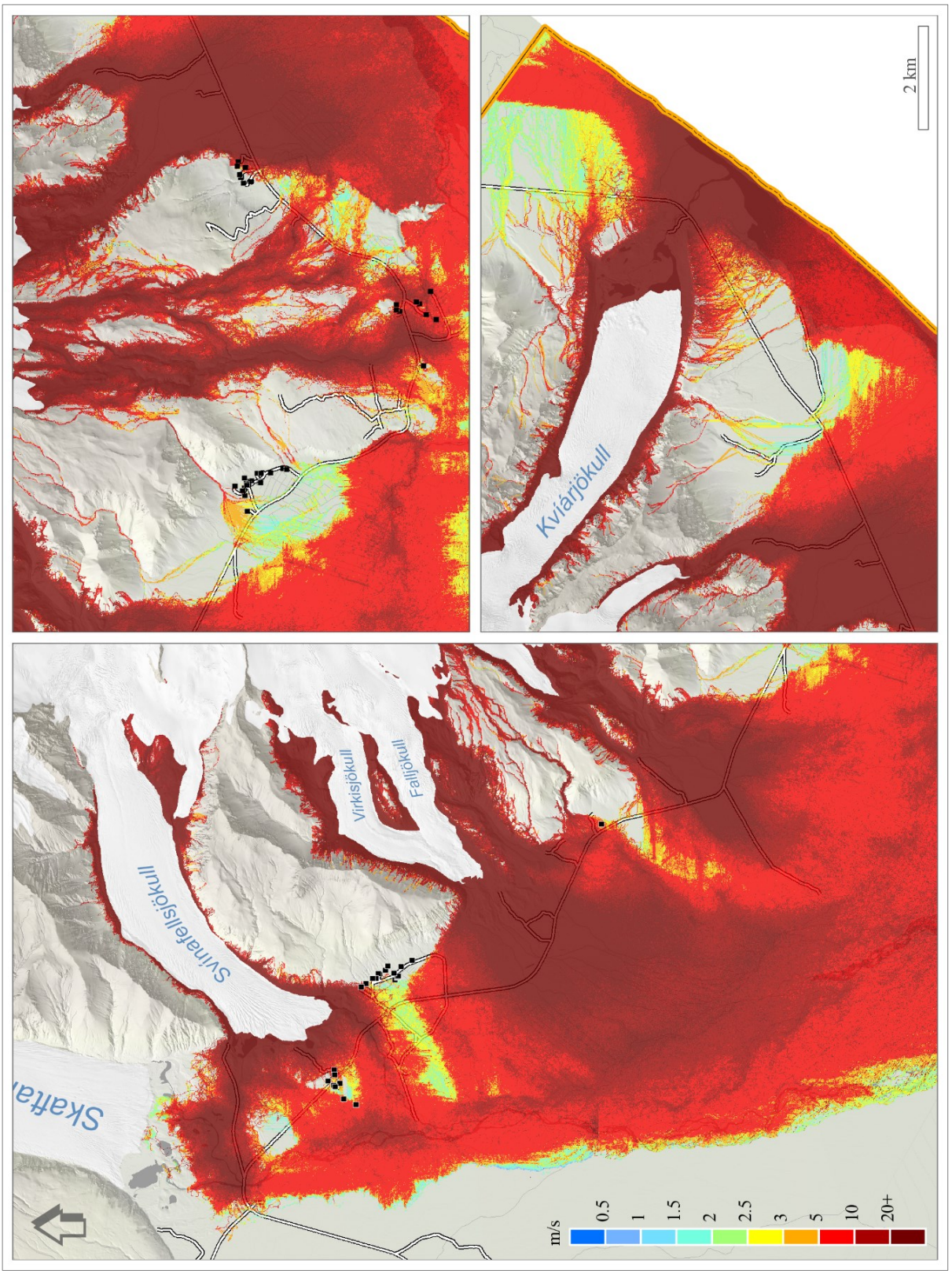

Figure IV-21: Aggregated maximum flow speeds (Manning's n 0.05 and 0.10 combined). Speeds in excess of 3m/s are found on 85% of the flood area. Settlements are shown as black dots.

Table IV-6: Average front speeds of floods caused by pyroclastic density currents during volcanic eruptions of Mount Tokachi (1926) and Mount St. Helens (1980). After Pierson (1998).

Event: location (year)	Distance from source of timing (km)	Average front speed from source of timing (m/s)	Peak discharge nearest source (m^3/s)	Risk source	Type of flood
Mount St. Helens: Pine Creek (1980)	4.4	35.7	50,000–100,000	Pyroclastic surge/flow	Debris flow
Mount St. Helens: South Fork Toutle River (1980)	4	38	68,000	Pyroclastic surge/flow	Debris flow, hyperconcentrated flow
Mount Tokachi: Huranogawa (1926)	2.4	42.1	14,800 at 8 km	Pyroclastic surge/flow	Debris flow

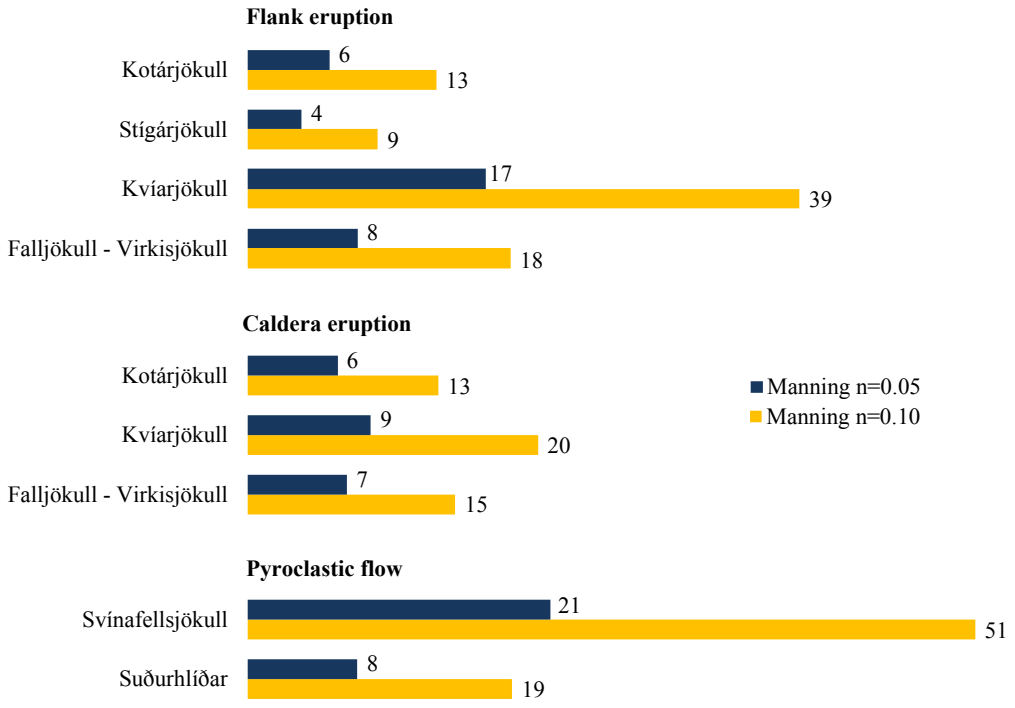

Figure IV-22: Floodwater surface transport times (min.) at peak discharge, from the lower boundaries of the release areas down to the national road.

4.4.2. Time available from the onset of supraglacial flow

The transport times at maximum discharge cannot be considered the equivalent of the time effectively available from the true onset of the floods without further investigation of the concentration phase. Gudmundsson *et al.* (2015) suggest for catastrophic floods caused by a caldera eruption of Öræfajökull Volcano an approximate rising rate in the form of $Q = At$, where Q is discharge, A = 55 m^3/s^2 and t the time from flood onset (Figure IV-23). At such a rate, it takes 30 minutes to reach a 100,000 m^3/s discharge but 3 minutes only to reach 10,000 m^3/s.

Simulation of a flood affecting the Virkisjökull-Falljökull glacier catchment indicates a 31-minute time down to the national road at input discharge 10,000 m^3/s and Manning's n set to 0.10, which is twice as long as at discharge 100,000 m^3/s (increase factor ~2). Using A = 55 m^3/s^2 as an assumption, floodwater at discharge 10,000 m^3/s is expected to reach the National road after 34 minutes following the flood onset while it does take 45 minutes for floodwater at 100,000 m^3/s (Table IV-7).

How surface transport times computed in SAMOS can be used in an estimation of the time effectively available from the onset of floods at the glacier surface is further addressed in chapter VII (Pagneux, 2015b).

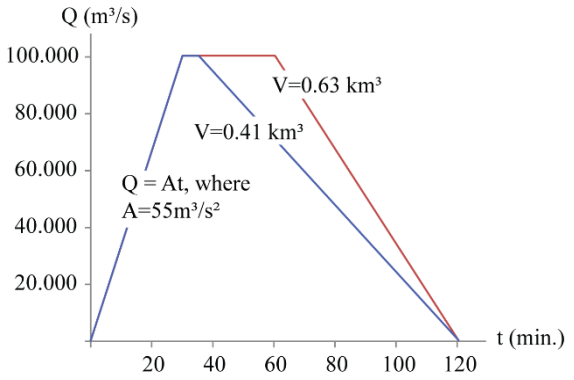

Figure IV-23: Hydrograph of possible catastrophic jökulhlaups (meltwater volumes of 0.41 km^3 and 0.63 km^3) caused by a caldera eruption of Öræfajökull Volcano (after Gudmundsson et al., 2015). Rising rate in the concentration phase is approximated as $Q = At$ (where Q is discharge, A = 55m^3/s^2 and t the time from flood onset).

Table IV-7: Minimum transport time at maximum discharge and time available from flood onset, using as assumptions a rising rate $Q = At$ where A = 55m^3/s^2 and an increase factor of ~2 in transport time between a 10,000 m^3/s discharge and a 100,000 m^3/s discharge.

Rising limb	Discharge (m^3/s)	Time elapsed from onset of supraglacial flow (min.)	Minimum transport time computed in SAMOS (min.)	Time available, from onset of supraglacial flow(min.)
Intermediate	10,000	3	31	34
Peak	100,000	30	15	45

5. Summary

Jökulhlaups resulting from subglacial volcanism at Öræfajökull have been modelled as viscous fluids using the SAMOS numerical model. Input data for the modelling were derived from ten estimates of maximum discharge for three eruptive processes (i.e. risk sources): caldera eruption, flank eruptions, and pyroclastic density currents. Because of the wide range of likely flow rheologies, three Manning's *n* values were assessed: 0.05, 0.1, and 0.15.

In each SAMOS simulation, predetermined volumes of water were released instantaneously from elevations where floodwater is expected to break through the surface of the ice-cap during a volcanogenic jökulhlaup (Gudmundsson *et al.*, 2015; Roberts and Gudmundsson, 2015). The resulting supraglacial cascade of floodwater was then modelled and a series of temporal snapshots of model output created, allowing inferences about inundation extent, maximum depths of flooding, maximum flow speeds, and minimum surface transport times. The main findings of the study can be summed up in the following points:

- A total of 237 km^2 of non-glaciated terrains, limited to the west by the Skaftafellsá river and to the east by the Breiðá river, was identified at risk of flooding within the spatial boundaries of the hydraulic model (Figure IV-8 to Figure IV-19). From an analysis of LiDAR-derived hillshades and aerial imagery, one can add to the flood area identified in the simulations about 110 km^2 of sandur, to the south (Skeiðarársandur) and to the east (Breiðamerkursandur).

- Shallow waters (< 0.5 m) were found in only one-tenth of the flooded area (Figure IV-20). Maximum flood depths in excess of 10 m were found along the main axes of flow propagation (20% of the flood area).

- The proglacial area is mainly affected by maximum flow speeds in excess of 3 m/s (Figure IV-21). On average, the maximum flow speeds found within the whole modelled domain ranged from 12 to 28 m/s (22 to 42 m/s on the slopes of the volcano).

- At maximum discharge, the minimum surface transport times to the National Road ranged between 4 minutes, downstream Stigárjökull, and 51 minutes, at the foot of Svínafellsjökull (Figure IV-22). These transport times are not an equivalent of the time effectively available from the onset of floods at the glacier surface. They can be used, however, in an estimation of the time available for evacuation, as addressed in chapter VII (Pagneux, 2015b).

Entrainment of ice during a high-magnitude jökulhlaup remains arguably one of the greatest unknown factors. Historical accounts of the 1727 jökulhlaup (Thorarinsson, 1958) imply that vast quantities of glacier ice were transported as floodwater descended onto the *sandar* (Roberts and Gudmundsson, 2015); this also implies that ice release was prevalent during the 1362 jökulhlaup. A high concentration of fragmented ice would cause floodwater bulking, which would affect the rheology of the flow and even the routing of floodwater, especially where temporary ice-jams formed. Such factors could not be addressed computationally in this study, but they should be kept in mind when a use is made of the simulations results in a damage potential assessment (Chapter V) and the estimation of the time available for evacuation (Chapter VII).

6. Acknowledgements

The authors would like to thank Magnús Tumi Gudmundsson, Kristín Martha Hákonardóttir, Tómas Jóhannesson, and Trausti Jónsson for their review and proof-reading of the chapter.

The present work was funded by the Icelandic Avalanche Mitigation Fund, the National Power Company, and the Icelandic Road and Coastal Administration.

7. References

Atapattu, D. D., Chhabra, R. P., & Uhlherr, P. H. (1995). Creeping sphere motion in Herschel-Bulkley fluids: Flow field and drag. *J. Non-Newt. Fluid Mech., 59*, 245–265.

Bagnold, R. A. (1954). Experiments on a gravity free dispersion of large solid spheres in a Newtonian fluid under shear. *Proc. R. Soc. London, A 225*, 49–63.

Bingham, E. C. (1916). An Investigation of the Laws of Plastic Flow. *U.S. Bureau of Standards Bulletin, 13*, 309–353.

Bingham, E. C., & Green, H. (1919). Paint, a plastic material and not a viscous fluid; the measurement of its mobility and yield value. *Proc. Am. Soc. Test. Mater., 19*, 640–664.

Björnsson, H. (1992). Jökulhlaups in Iceland: prediction, characteristics, and simulation. *Annals of Glaciology, 16*, 96–106.

Brunner, G. W. (2010). *HEC-RAS River Analysis System, User's Manual Version 4.1.* US Army Corps of Engineers, Hydrologic Engineering Center.

Capra, L., Norini, G., Groppelli, G., Macias, J. L., & Arce, J. L. (2008). Volcanic hazard zonation of the Nevado de Toluca volcano, Mexico. *Journal of Volcanology and Geothermal Research, 176*(4), 469–484.

Charbonnier, S. J., Germa, A., Connor, C., Gertisser, R., Preece, K., Komorowski, J. C., Lavigne, F., Dixon, T., and Connor, L. (2013). Evaluation of the impact of the 2010 pyroclastic density currents at Merapi volcano from high-resolution satellite imagery, field investigations and numerical simulations. *Journal of Volcanology and Geothermal Research, 261*, 295–315.

Charbonnier, S., & Gertisser, R. (2009). Numerical simulations of block-and-ashflows using the Titan2D flow model: examples from the 2006 eruption of Merapi Volcano, Java, Indonesia. *Bulletin of Volcanology, 71*, 953–959.

Chow, V. T. (1959). *Open – channel hydraulics.* McGill Hill.

Coussot, P. (1994). Steady, laminar, flow of concentrated mud suspension in open channel. *J. Hydraul. Res., 32*, 535–559.

Coussot, P., & Meunier, M. (1996). Recognition, classification and mechanical description of debris flows. *Earth – Sciences Reviews, 40*(3–4), 209–227.

Coussot, P., & Piau, J. M. (1994). Rheology of highly concentrated suspensions of coarse particles. *Cah. Rhéol. (J. French Rheol. Group), XIII*, 266–277.

Daido, A. (1971). On the occurrence of mud-debris flow. *Disaster Prevention Res. Inst. Bull., 21*, 126–169.

DHI. (2009). *MIKE11: A modelling system for Rivers and Channels, Users Guide.* DHI.

Dunning, S., Large, A. R., Russell, A. J., Roberts, M. J., Duller, R., Woodward, J., Mériaux, A. S., Tweed, F. S., and Lim, M. (2013). The role of multiple glacier outburst floods in proglacial landscape evolution: the 2010 Eyjafjallajökull eruption Iceland. *Geology, 41*(10), 1123–1126.

Elíasson, J., Kjaran, S. P., Holm, S., Gudmundsson, M. T., & Larsen, G. (2007). Large hazardous floods as translatory waves. *Environmental Modelling & Software, 22*, 1392–1399.

Gerhart, P. M., Gross, R. J., & Hochstein, J. I. (1993). *Fundamentals of Fluid Mechanics* (2nd ed.). Addison-Wesley.

Gíslason, E., & Jóhannesson, T. (2007). *Calibration of the samos AT 2D avalanche model for large Icelandic dry-snow avalanches.* Reykjavík: Icelandic Meteorological Office.

Gíslason, M. B. (2012). *Straumfræðileg hermun jökulhlaups niður suðurhlíðar Eyjafjallajökuls í apríl 2010: ákvörðun Manningsstuðla (Hydraulic modelling of April 2010 glacial outburst on the southern slopes of Eyja-fjallajökull: choice of Manning coefficient).* Reykjavík: University of Iceland.

Gudmundsson, M. T., Högnadóttir, Þ., & Magnússon, E. (2015). Öræfajökull: Eruption melting scenarios. In E. Pagneux, M. T. Gudmundsson, S. Karlsdóttir, & M. J. Roberts (Eds.), *Volcanogenic floods in Iceland: An assessment of hazards and risks at Öræfajökull and on the Markarfljót outwash plain* (pp. 45–72). Reykjavík: IMO, IES-UI, NCIP-DCPEM.

Hákonardóttir, K. M., Jóhannesson, T., & Sampl, P. (2005). Líkanreikningar á jökulhlaupum niður suðurhliðar Eyjafjallajökuls (Hydraulic simulations of glacial outbursts on the southern slopes of Eyjafjallajökull). In M. T. Guðmundsson, & Á. G. Gylfason (Eds.), *Hættumat vegna eldgosa og hlaupa frá vestanverðum Mýrdalsjökli og Eyjafjallajökli (Hazard assessment of volcanic eruptions and glacial outbursts for Eyja-fjallajökull and the western outwash plain of Mýrdalsjökull)* (pp. 181–196). Reykjavík: Ríkislögreglustjórinn, Háskólaútgáfan.

Herschel, W. H., & Bulkley, R. (1926). Über die viskosität und Elastizität von Solen. *Am. Soc. Test. Mater., 26*, 621–633.

Hsü, K. (1975). Catastrophic debris streams (Sturzstroms) generated by Rockfalls. *GSA Bulletin, 86*(1), 129–140. doi:10.1130/0016-7606

Hubbard, B. E., Sheridan, M. F., Carrasco-Núñez, G., Díaz-Castellón, R., & Rodríguez, S. R. (2007). Comparative lahar hazard mapping at Volcan Citlaltépetl, Mexico using SRTM, ASTER and DTED-1 digital topographic data. *Journal of Volcanology and Geothermal Research, 160*, 99–124.

Iverson, R. M., Schilling, S. P., & Vallance, J. W. (1998). Objective delineation of lahar-inundation hazard zones. *Geological Society of America Bulletin, 110*, 972–984.

Johnson, A. M. (1970). *Physical Processes in Geology.* San Francisco: Freeman, Cooper.

Jóhannesson, T., Björnsson, H., Magnússon, E., Guðmundsson, S., Pálsson, F., Sigurðsson, O., Thorsteinsson, T., and Berthier, E. (2013). Ice-volumes changes, bias estimation of mass-balance measurements and changes in subglacial lakes derived by lidar mapping of the surface of Icelandic glaciers. *Annals of Glaciology, 54*(63), 63–74.

Jóhannesson, T., Björnsson, H., Pálsson, F., Sigurðsson, O., & Thorsteinsson, T. (2011). LiDAR mapping of the Snæfellsjökull ice cap, western Iceland. *Jökull, 61*, 19–32.

Leyrit, H., & Montenat, C. (2000). *Volcaniclastic Rocks from magmas to sediments.* Gordon and Breach Science Publishers.

Locat, J., & Demers, D. (1988). Viscosity, yield stress, remolded strength, and liquidity index relationships for sensitive clays. *Can. Geotech. J., 25*, 799–806.

Lun, C. K., Savage, S. B., Jeffrey, D. J., & Cherpurniy, N. (1984). Kinetic theories for granular flow: inelastic particles in Couette flow and slightly inelastic particles in a general flowfield. *J. Fluid Mech., 140*, 223–256.

Magirl, C. S., Griffiths, P. G., & Webb, R. H. (2010). Analyzing debris flows with the statistically calibrated empirical model LAHARZ in south–eastern Arizona, USA. *Geomorphology, 119*(1-2), 111–124.

Magnússon, E., Gudmundsson, M. T., Sigurdsson, G., Roberts, M. J., Höskuldsson, F., & Oddsson, B. (2012a). Ice-volcano interactions during the 2010 Eyjafjallajökull eruption, as revealed by airborne radar. *J. Geophys. Res., 117, B07405*. doi:10.1029/2012JB009250

Magnússon, E., Pálsson, F., Björnsson, H., & Gudmundsson, S. (2012b). Removing the ice cap of Oraefajokull central volcano, SE-Iceland: Mapping and interpretation of bedrock topography, ice volumes, subglacial troughs and implications for hazards assessments. *Jökull, 62*, 131–150.

Major, J. J., & Pierson, T. C. (1992). Debris flow rheology: Experimental analysis of fine-grained slurries. *Water Resour. Res., 28*, 841–857.

Malin, M., & Sheridan, M. (1982). Computer-Assisted Mapping of Pyroclastic Surges. *Science, 217*(4560), 637–640.

Michaels, A. S., & Bolger, J. C. (1962). The plastic flow behavior of floculated kaolin suspensions. *Ind. Eng. Chem. Fundam., 1*, 153–162.

Muñoz-Salinas, E., Castillo-Rodriguez, M., Manea, V., Manea, M., & Palacios, D. (2010). On the geochronological method versus flow simulation software application for Lahar risk mapping: A case study of Popocatepetl volcano. *Geografiska Annaler, Series a – Physical Geography, 92*(A), 311–328.

Muñoz-Salinas, E., Castillo-Rodríguez, M., Manea, V., Manea, M., & Palacios, D. (2009). Lahar flow simulations using LAHARZ program: Application for the Popocatépetl volcano, Mexico. *Journal of Volcanology and Geothermal Research, 182*(1-2), 13–22.

Nguyen, Q. D., & Boger, D. V. (1983). Yield stress measurement for concentrated suspensions. *J. Rheol., 27*, 321–349.

Nye, J. F. (1976). Water flow in glaciers: Jökulhlaups, tunnels and veins. *Journal of Glaciology, 17*(76), 181–207.

Pagneux, E. (2015a). Öræfi district and Markarfljót outwash plain: Spatio-temporal patterns in population exposure to volcanogenic floods. In E. Pagneux, M. T. Gudmundsson, S. Karlsdóttir, & M. J. Roberts (Eds.), *Volcanogenic floods in Iceland: An assessment of hazards and risks at Öræfajökull and on the Markarfljót outwash plain* (pp. 123–140). Reykjavík: IMO, IES-UI, NCIP-DCPEM.

Pagneux, E. (2015b). Öræfajökull: Evacuation time modelling of areas prone to volcanogenic floods. In E. Pagneux, M. T. Gudmundsson, S. Karlsdóttir, & M. J. Roberts (Eds.), *Volcanogenic floods in Iceland: An exploratory assessment for Öræfajökull and the Markarfljót outwash plain* (pp. 141–164). Reykjavík: IMO, IES-UI, NCIP-DCPEM.

Pagneux, E., & Roberts, M. J. (2015). Öræfi district and Markarfljót outwash plain: Rating of flood hazards. In E. Pagneux, M. T. Gudmundsson, S. Karlsdóttir, & M. J. Roberts (Eds.), *Volcanogenic floods in Iceland: An assessment of hazards and risks at Öræfajökull and on the Markarfljót outwash plain* (pp. 103–124). Reykjavík: IMO, IES-UI, NCIP-DCPEM.

Pierson, T. C. (1998). An empirical method for estimating travel times for wet volcanic mass flows. *Bull Volcanol, 60*, 98–109.

Roberts, M. J. (2002). *Controls on supraglacial outlet development during glacial outburst floods.* Unpublished PhD thesis.

Roberts, M. J. (2005). Jökulhlaups: a reassessment of floodwater flow through glaciers. *Reviews of Geophysics, 43*, 1–21.

Roberts, M. J., & Gudmundsson, M. T. (2015). Öræfajökull Volcano: Geology and historical floods. In E. Pagneux, M. T. Gudmundsson, S. Karlsdóttir, & M. J. Roberts (Eds.), *Volcanogenic floods in Iceland: An assessment of hazards and risks at Öræfajökull and on the Markarfljót outwash plain* (pp. 17–44). Reykjavík: IMO, IES-UI, NCIP-DCPEM.

Russell, A. J., Tweed, F., Roberts, M. J., Harris, T. D., Gudmundsson, M. T., Knudsen, O., & Marren, P. M. (2010). An unusual jökulhlaup resulting from subglacial volcanism, Sólheimajökull, Iceland. *Quaternary Science Review*, 1363–1381.

Sampl, P., & Granig, M. (2009). Avalanche simulation with SAMOS-AT. *International Snow Science Workshop Proceedings*, (pp. 519–523). Davos, GR, Switzerland.

Sampl, P., & Zwinger, T. (2004). Avalanche simulation with SAMOS. *Annals of Glaciology, 38*, 393–398.

Savage, S. B. (1984). The mechanics of rapid granular flows. *Adv. Appl. Mech., 24*, 289–366.

Schilling, S. P. (1998). *LAHARZ: GIS programs for automated mapping of Lahar – inundation hazard zones.* Vancouver: U.S. Geological Survey Information Services.

Snorrason, Á., Einarsson, B., Pagneux, E., Hardardóttir, J., Roberts, M., Sigurðsson, O., Thórarinsson, Ó., Crochet, P., Jóhannesson, T., and Thorsteinsson, T. (2012). Floods in Iceland. In Z. W. Kundzewicz (Ed.), *Changes in flood risk in Europe* (pp. 257–276). IAHS Special Publication 10.

Stevens, N. F., Manville, V., & Heron, D. W. (2003). The sensitivity of a volcanic flow model to digital elevation model accuracy: experiments with digitised map contours and interferometric SAR at Ruapehu and Taranaki volcanoes, New Zealand. *Journal of Volcanology and Geothermal Research, 119*(1–4), 89–105.

Takahashi, T. (1978). Mechanical characteristics of debris flow. *J. Hydraul. Div., 104*, 1153–1169.

Thorarinsson, S. (1958). The Öræfajökull eruption of 1362. *Acta Naturalia Islandica, 2*(4), 100.

Tómasson, H. (1996). The Jökulhlaup from Katla in 1918. *Annals of Glaciology, 22*, 249–254.

Wang, Z., Larsen, P., & Xiang, W. (1994). Rheological properties of sediment suspensions and their implications. *J. Hydraul. Res., 32*, 560–580.

Waythomas, C. F., Pierson, T. C., Major, J. J., & Scott, W. E. (2013). Voluminous ice-rich and water rich lahars generated during the 2009 eruption of Redoubt Volcano, Alaska. *Journal Volc. Geoth. Res., 259*, 389-413.

Zwinger, T., Kluwick, A., & Sampl, P. (2003). Simulation of Dry-Snow Avalanche Flow over Natural Terrain. In K. Hutter, & N. Kirchner (Eds.), *Dynamic Response of Granular and Porous Materials under Large and Catastrophic Deformations* (Vol. 11, pp. 161-194). Heidelberg: Springer.

V. ÖRÆFI DISTRICT AND MARKARFLJÓT OUTWASH PLAIN: RATING OF FLOOD HAZARDS

Emmanuel Pagneux * and Matthew J. Roberts *

* *Icelandic Meteorological Office*

1. Introduction

In this chapter, a provisional method for the rating of flood hazards is proposed followed by the designation of flood hazard zones in the Markarfljót outwash plain and the Öræfi district, two inhabited regions of Iceland (Figure V-1) that have been subjected during the last millennium to jökulhlaups caused by subglacial eruptions of Katla, Eyjafjalla-jökull (Gudmundsson *et al.*, 2008; Snorrason *et al.*, 2012), and Öræfajökull volcanoes (Thorarinsson, 1958).

The aim of the study is to provide the national and local authorities with spatial information on flood danger and flood damage potential in the two study areas. The presence of life-threatening debris and the temperature of floodwater are considered, along with depths of flooding and flow velocities; these factors take into account the unique nature of volcanogenic floods. Flood-hazard zones are designated using the results of scenario-based hydraulic simulations performed by Hólm and Kjaran (2005) and Helgadóttir *et al.* (2015) in the Markarfljót outwash plain and in the Öræfi district, respectively. The method presented builds upon selected research on vulnerability of the human environment to floodwaters, including people's vulnerability (e.g. Foster and Cox, 1973; Abt *et al.*, 1989; Keller and Mitsch, 1993; Karvonen *et al.*, 2000; Jonkman and Kelman, 2005; Penning Rowsell *et al.*, 2005; Jonkman and Penning-Rowsell, 2008; Russo *et al.*, 2012) and vulnerability of the built environment (e.g. USBR, 1988; Karvonen *et al.*, 2000; Leone *et al.*, 2010, Valencia *et al.*, 2011).

The scope of the study is limited to an assessment of damage potential within the areas identified at risk of flooding. Characterisation of the likelihood of volcanogenic floods is not addressed. In short, one can describe such floods as hazardous events whose likelihood remains rather uncertain. Indeed, the magnitude and routing of volcanogenic floods depend on several factors, including the nature of ice-volcano interactions and the exact location of eruptions. As a consequence, the long-term probability of a subglacial eruption at a particular location in space and time, and incidentally of the floods it may cause, cannot be specified with confidence. It is estimated for instance that Katla eruptions capable of causing outbursts on the Markarfljót outwash plain have a return period ranging 100 – 1,000 years should they happen in the north-western part (23 km^2) of the volcano caldera, and 1000–10,000 years should an eruption happen on the western slopes (87 km^2) of the Mýrdalsjökull ice-cap (Guðmundsson *et al.*, 2005). Concerning Öræfajökull volcano, only two eruptions are known in historical times — the 1362 and 1727 eruptions — that were different in size and location and caused floods in two different glacier catchments (Thorarinsson, 1958; Roberts and Gud-mundsson, 2015). For the whole of Iceland, it is estimated that VEI 5 eruptions occur once every 100 – 200 years and VEI 6 eruptions once every 500 – 1000 years (Gudmundsson *et al.*, 2008).

The flood hazard rates proposed here are used for characterising, in the two study areas, exposure of populations to jökulhlaup hazards (Pagneux, 2015a).

The present study is noteworthy for being the first attempt to explore and map flood damage potential in Iceland. Taking into account natural hazards in spatial planning is a legal requirement (Parliament of Iceland, 2010) that is not yet supported, for what concerns riverine floods and glacial outbursts, by a set of rules describing how hazards and risks should be assessed. The Planning regulation (Ministry for the Environment and Natural Resources, 2013) specifies that it is forbidden to build in areas prone to floods from lakes, rivers, and the sea, irrespective of considerations on a flood return period for which flood hazards and flood risks should be mapped nor on the level of human and material loss beyond which risk is no longer acceptable.

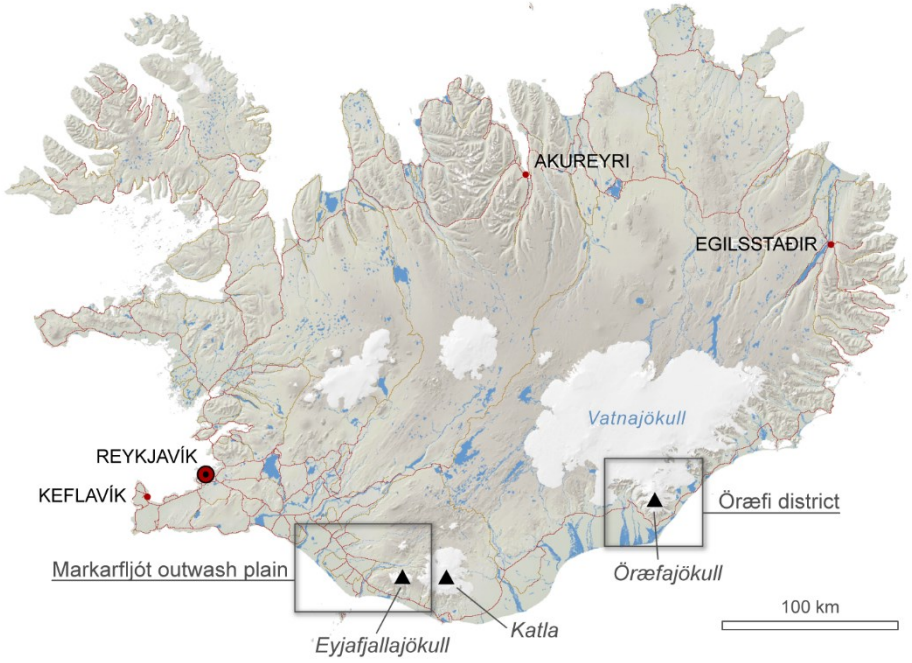

Figure V-1: General location of the Markarfljót outwash plain and Öræfi district.

1.1. Principle of flood hazard rating

Flood hazard "rating" can be thought of as marking off a reference flood into zones, using flood hazard characteristics in excess of which plausible and meaningful adverse consequences such as structural damage or loss of life are likely to occur (i.e. can be predicted at a significant confidence level) (DEFRA, 2006). In this approach, the possibility of events of credible magnitude and plausible outcomes is considered and an assessment of flood damage potential is performed (see §2.3 for examples of flood hazard rating abroad); flood hazard zones are differentiated primarily on the understanding that fatalities and significant economic damage due a given flood may vary spatially within areas flooded as a consequence of spatial variations in the magnitude of the flood (i.e. flood magnitude considered as a spatial variable), all other things being held equal (i.e. vulnerability purposively considered as a spatial constant). In that respect, rating of flood hazards differs from hazard zoning based on discharge exceedance probabilities (sometimes called "risk zoning"), where risk zones coincide with the spatial extent of flooding events having a known probability of occurrence or an established

return period (de Moel *et al.,* 2009; Figure V-2).

Indeed, the marking-off into zones of a reference flood does not require the flood considered to have a known probability of occurrence. The reference flood may be a historical event or simply hypothetical. In some cases, the marking-off may refer to an aggregated "worst-case" scenario (e.g. Tinti *et al.,* 2011), as a return period is not known or may appear of little relevance for risk management.

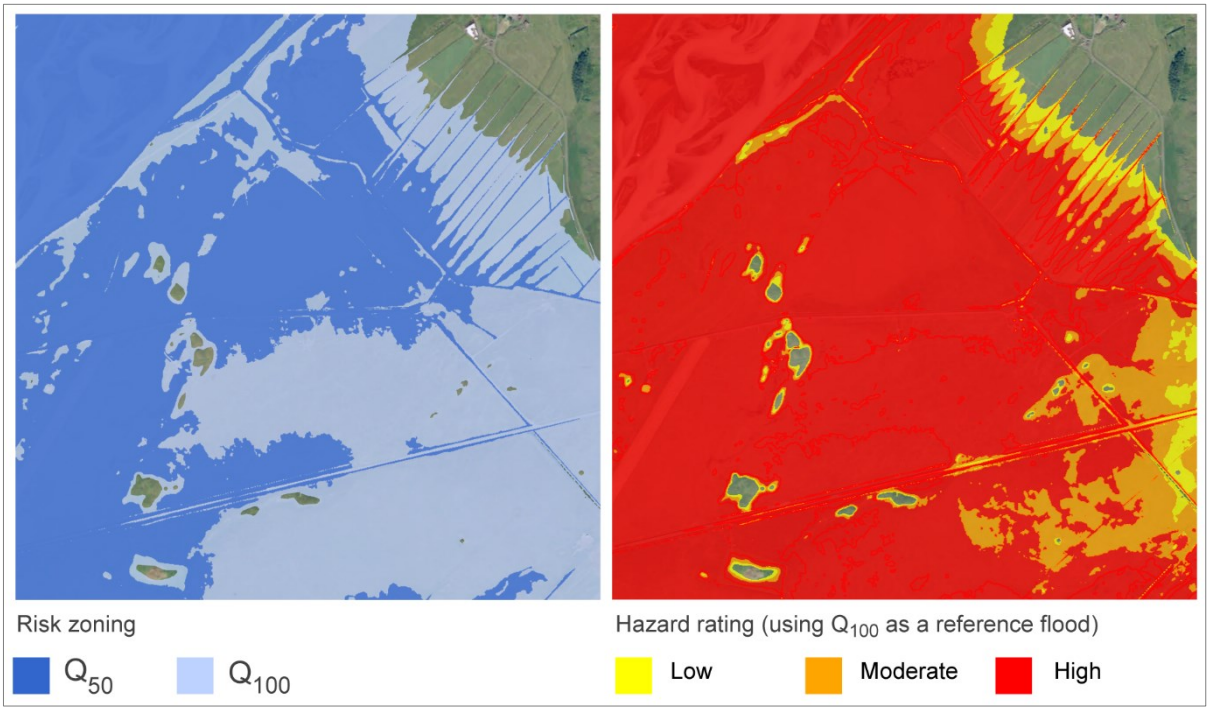

Figure V-2: Fictitious example showing the differences between hazard zoning based on discharge exceedance probabilities — sometimes called "risk zoning"— and hazard rating. In risk zoning (left), spatial extent of flooding events having known return periods, here Q50 (2% chance of occurring in any given year) and Q100 (1% chance) is shown. In hazard rating (right), a reference flood is used, here Q100, and distinction is made within its spatial extent between levels of danger or damage potential, based on flood hazard characteristics.

2. Vulnerability of humans and built environment

The main purpose of hazard rating is not to determine the likelihood of a hazardous event but to map in a sensible manner its potential consequences, including harm to people and damages to structures. It is a prerequisite to an estimation of injury and loss of life in floods, which requires in addition an assessment of the people characteristics (e.g. age, sickness and disabilities) and location within flood areas (Penning Rowsell *et al.*, 2005). It can also serve, coupled to an inventory of building and structure stocks, in an estimation of monetary losses due to direct damages to exposed physical assets (e.g. Schwarz and Maiwald, 2008; Van Vesten *et al.*, 2014).

Alongside water depths and flow velocities, sediment load and floodwater temperature are flood hazard characteristics that must be considered when tangible damages to buildings and short-term physical effects of floodwaters on humans, inside and outside buildings, are considered.

2.1. Damages to buildings

2.1.1. Effects of floodwater on buildings

The physical integrity of buildings is threatened by the hydrostatic and hydrodynamic actions of floodwater, scouring, and actions due to the presence of debris (impact loads). Detailed overviews of the physical effects of floods on buildings can be found in Kelman and Spence (2004) and Merz *et al.* (2010).

Hydrostatic actions, which are implied by the presence of water, consist of lateral and vertical pressures against buildings and capillarity rise inside building components. Lateral pressures may lead to the collapse of walls if not counteracted. Buoyancy, which is an uplift force exerted on submerged objects, can result in floating of buildings and may lead, in combination with lateral pressures, to displacement or destruction of buildings. It has been estimated, for example, that unanchored single-storey buildings can begin to float at flood depths of > 1.9 m (Black, 1975). Hydrostatic lateral pressures and capillarity rise can be considered the dominant cause of damage due to riverine floods implying slow rising (Kreibich *et al.*, 2009; Kreibich and Dimitrova, 2010) and long-lasting receding periods.

Hydrodynamic actions, which are due to the motion of water, relate to flow velocities and the formation of waves. Dynamic pressures due to flow velocities and breaking waves are much higher than static pressures due to stagnant waters, and are therefore more likely to cause structural damages to buildings.

Buildings may also be endangered by scouring. Black (1975) and Smith (1989) have estimated that due to severe erosion around foundations, the structural integrity of buildings comes into question at flow velocities higher than 1.5–2 m/s (1.1–2 kPa).

The presence of debris and sediments increases the dynamical forces exerted against buildings and thus the potential for structural damage, as exemplified by the March 11th 2011 tsunami in Great East Japan where concrete blocks removed from coastal defences by floodwater contributed, alongside other debris, to the destruction of thousands of light buildings and overturning of many reinforced concrete structures (Fraser *et al.*, 2013). Drawing a parallel between tsunamis and jökulhlaups is certainly worthwhile in that regard. The weight of boulders and ice blocks that can be mobilised by glacial floods due to volcanic eruptions, geothermal activity, or geological failure can effectively exceed hundreds of tons, as exemplified by recent jökulhlaups in Iceland. The 15 April jökulhlaup (peak discharge 10,000–15,000 m^3/s) caused by the Eyjafjallajökull 2010 eruption left thousands of clasts of glacier ice along the flood route, sizing each up to 5 t at nearly 5 km from the glacier margin (Figure V-3). During the 2010 Eyjafjallajökull eruption, an ice slurry flowing across the surface of Gígjökull and descending via a bedrock col adjacent to the main flood corridor managed to displace a 4,000 t boulder on a steep slope (Roberts *et al.*, 2011). Similarly, the 1999 jökulhlaup from Sólheimajökull (peak discharge ~4400 m^3/s) mobilised boulders up to 11 m in diameter (Russell *et al.*, 2010). During the 1996 glacial outburst on the Skeiðarársandur outwash plain (peak discharge 55,000 m^3/s), ice blocks 10–20 m in diameter were also filmed rolling down by the National road, 5–7 km away from the glacier margin (Figure V-4).

2.1.2. Damage functions and thresholds

Flood characteristics such as flood depths, flow velocities, impact pressures, and debris heights can be used, separately or in combination, in functions aimed at the prediction of damage to buildings (also known as vulnerability curves or fragility curves).

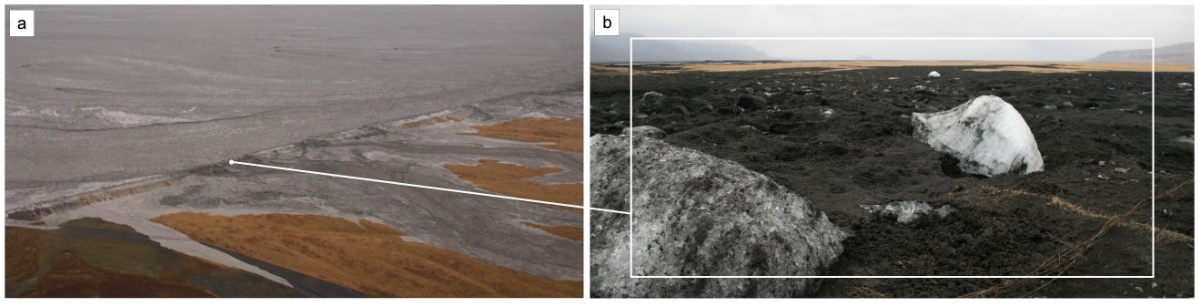

Figure V-3: (a) April 15 2010 jökulhlaup caused by eruption of Eyjafjallajökull volcano. Minutes after the flood begins, floodwater rapidly overtops a first levee, 5 km away from the glacier margin, which shows early signs of failure at several locations due to excessive flow velocities and impact of ice blocks (Credit: Matthew J. Roberts). In the end, 300 metres of levees were swept away. (b) Downstream view taken on April 30 2010 from the levee (failure location), showing hundreds of clasts of glacier ice, 1–5 t in size in a matrix of volcanic mud (Credit: Emmanuel Pagneux).

Figure V-4: Remnants of stranded ice blocks transported by floodwater during the November 1996 glacial outburst on the Skeiðarársandur outwash plain (peak discharge 55,000 m^3/s). Note the 1.70 m tall adult standing between the blocks. Credit: Oddur Sigurðsson, January 4 1997.

Depths of flooding and flow velocities can be combined for instance in a qualitative manner, using a matrix (e.g. MATE/METL, 2002), or as a quantitative aggregate, referred in the literature to as depth-velocity product, labelled *dv* or *hv* and expressed in m^2/s (e.g. Clausen and Clark, 1990; Karvonen *et al.*, 2000). Impact pressures (Wilhelm, 1998; Barbolini *et al.*, 2004) or debris heights (Fuchs *et al.*, 2007; Akbas *et al.*, 2009; Luna *et al.*, 2011) can be used alternatively in the definition of damage functions for gravity driven phenomena, such as hyperconcentrated flows, debris-flows, and avalanches.

As the actual level of damage is not only a consequence of flood characteristics but also of design, damage functions need to consider flood characteristics in relation to classes or types of buildings. A distinction is made in the literature between wooden and concrete structures (Karvonen *et al.*, 2000; Dutta *et al.*, 2003), anchored and unanchored structures (Karvonen *et al.*, 2000), and single storey and multiple-storey buildings (Black, 1975; Smith, 1991; Leone *et al.*, 2010) to name a few. An example of detailed classifications recently proposed is given in Schwarz and Maiwald (2008) who, in the aftermath of floods from the Elbe river that struck

Germany in 2002, 2005, and 2006, made an inventory of the building stock using the following six categories: clay, prefabricated, framework, masonry, reinforced concrete, and flood-proof.

Particular thresholds deserve attention when habitation buildings are considered, as they may mark, in the absence of better information, the lower boundary of zones of "total devastation":

- Total destruction of brick and masonry buildings can be expected at depth-velocity products $dv > 7$ m^2/s (Clausen and Clark, 1990; Karvonen *et al.*, 2000; Table V-1).

Valencia *et al.* (2011) estimated, after transposition to the European built environment of the empirical findings from Leone *et al.* (2010) on damages to buildings due to the 2004 tsunami in Banda-Aceh (Indonesia), that structural damage to reinforced concrete buildings that require demolition in the recovery phase should be expected where depths of flooding > 6 m (Table V-2).

- When gravitational flows are considered, total destruction of single to three-storey brick masonry and concrete structures can be expected at debris height ranging 2.5 m (Akbas *et al.*, 2009) to 3.6 metres (Luna *et al.*, 2011).

- Structures impacted by flows can be considered beyond repair in case of impact pressures > 34 kPa (Wilhelm, 1998; Barbolini, 2004).

Table V-1: Identified flow conditions causing partial or total structural damage of Finnish houses in the EU-project RESCDAM (After Karvonen et al., 2000). Flow velocities alone and/or the product of flow velocities and water depths, referred in the literature as depth-velocity product (dv) are used.

House type	**Partial damage**	**Total damage**
Wood-framed		
Unanchored	$dv \geq 2$ m^2/s	$dv \geq 3$ m^2/s
Anchored	$dv \geq 3$ m^2/s	$dv \geq 7$ m^2/s
Masonry, concrete & brick	$v \geq 2$ m/s and $3 > dv > 7$ m^2/s	$v \geq 2$ m/s and $dv \geq 7$ m^2/s

Table V-2: Depth-damage matrix adopted in the SCHEMA project (After Valencia et al., 2011).

Building classes		I. Light	II. Masonry, and not reinforced concrete	III. Reinforced concrete
Height and storeys		0 to 1 level, rarely 2	1 to 3 levels	0 to 3 levels
Damage levels	**Actions**	**Depths of flooding**		
D1, Light damage	Immediate occupancy / repairable	< 1.8	< 2	< 3
D2, important damage	Evacuation / repairable	1.8 < d < 2.2	2 < d < 4.5	3 < d < 6
D3, Heavy damage	Evacuation / demolition required	2.2 < d < 2.6	3 < d < 6.5	6 < d < 9.5
D4, Partial collapse	Evacuation / demolition required	2.6 < d < 3.8	4 < d < 9	9.5 < d < 12.5
D5, Total collapse		> 3.8	5 < d < 9	> 12.5

2.2. Human safety

Since the early 1970s, the short-term physical effects of floods on human life have been mainly analysed from the angle of human instability in floodwaters. Two hydrodynamic mechanisms, causing instability at depths of flooding not exceeding a person's height, have been identified (Jonkman and Penning-Rowsell, 2008):

- Toppling (moment instability), which relates to the depth-velocity product *dv;*
- Sliding (frictional instability), which relates to the dv^2 product.

Early experiments on pedestrians' safety suggest a critical depth-velocity product dv_c ranging 0.16–0.52 m^2/s for children aged 9–13 years (Foster and Cox, 1973). Keller and Mitsch (1993) estimated dv_c ranging 0.21–0.32 m^2/s for a 5-year old child 1.11 m tall and weighing 19 kg, i.e. a critical velocity of 0.5 m/s for a 0.6 m depth of flooding. Abt *et al.* (1989) suggest a dv_c ranging 0.71–2.13 m^2/s for adults. Experiments realised during the RESCDAM project (Karvonen *et al.,* 2000) suggest a lower critical dv_c, ranging 0.64–1.26 m^2/s. A recent study from Jonkman and Penning-Rowsell (2008) indicates that human instability due to toppling is dominant at depths > 0.8 metre and corresponds to a constant $dv_c = 1.32$ m^2/s for an individual 1.75 m tall and weighing 75 kg (Figure V-5). At depths of flooding < 0.8 metre, sliding becomes the dominating phenomenon and is likely the mechanism prevailing in urban floods where shallow waters are associated with excessive velocities. Russo *et al.* (2012) propose a critical velocity $v = 1.88$ m/s at flow depths 15–20 cm.

As for pedestrians, safety of car users and passengers has been analysed until now under the prism of thresholds in flow velocities and water depths. An early study on passengers' safety in the case of a dam break published by the US Bureau of Reclamation (1988) suggests that automobilists of "almost any size" are in danger in stagnant waters when depth of flooding is in excess of 1 m, the threshold in water depth being decreased to 0.7 m at flow velocity ~2 m/s. More recently, critical depth-velocity products dv_c 0.25 for children and 0.7 for adults have been proposed (Reiter, 2000).

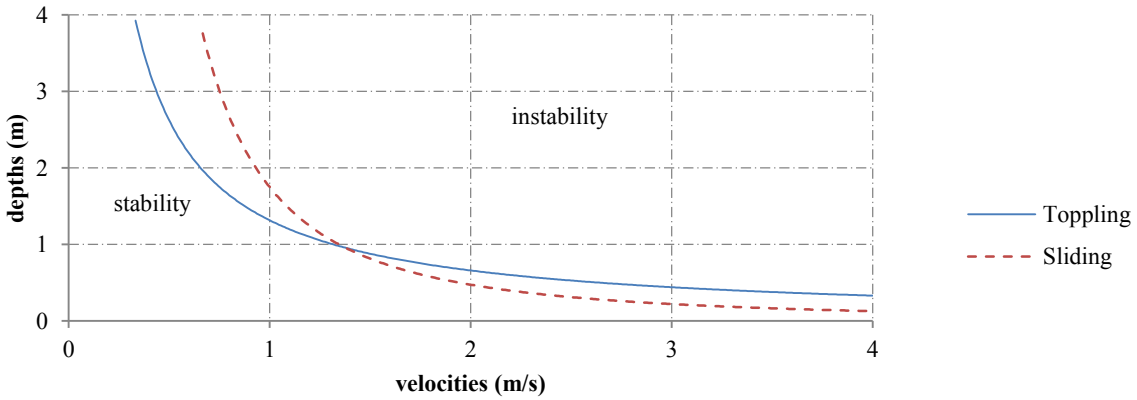

Figure V-5: Theoretical boundary between stability and instability in flood waters for an individual m = 75 kg and L = 1.75 m. Instability due to toppling is reached at depth-velocity product dv 1.3 m^2/s. Modified from Jonkman and Penning-Rowsell (2008).

The depth-velocity products *dv* and dv^2 are only an approximation of the ability of individuals to remain in control in floodwater in real conditions. Stress, poor lighting or darkness, disabilities, water temperature or injuries due in particular to transported

debris, all contribute to a significant attenuation of stability in floodwater and therefore increase the risk of drowning, which has been identified as the dominant mode of death when riverine floods and flash floods are considered (French *et al.*, 1983). It should be observed, in particular, that the question of instability in floodwater is of a limited relevance when hyper-concentrated flows and debris flows (sediment load > 60%) are considered. In such situations, injuries and short-term fatalities may relate directly to debris (see §2.1.1) and excessive sediment loads. Most of the fatalities due to lahars triggered by the 1985 eruption of Nevado Del Ruiz Volcano (~25,000 deaths) concerned people that became trapped in the mud and debris and were eventually buried by the flows of sediments (Voight, 1990; Mileti *et al.*, 1991). The Nevado Del Ruiz 1985 event exemplifies the potency of floods triggered by volcanic eruptions, emphasising the necessity of identifying areas that are at risk of volcanogenic floods.

Finally, jökulhlaups and lahar pulses generated by a volcanic eruption can be alternatively ice-cold or burning hot. For instance, a temperature of 92 °C was reported at a one-foot depth in a lahar deposit due to the 1919 eruption of Kelut volcano (East Java, Indonesia), a few days after it had formed (Kemmerling, 1921). The risk of severe burning should therefore be kept in mind, as well as the risk of drowning due to accidental hypothermia (Lloyd, 1996) and numbness-related loss of stability.

2.3. Rating methods

The choice of input parameters and thresholds is quite variable between countries and may look, for this reason, somewhat arbitrary. In reality, the methods in the selection and use of the parameters depend on their availability and on the adverse consequences considered: human safety, damages to building, emergency response, compensation schemes, etc.

In northern America, zoning is most often performed using the 100-year flood as a reference. A distinction is made there between the floodway, which includes the main channel and the adjacent overbank areas of greatest water depths and flow velocities, and the flood fringe, where depths and velocities are lower (Environment Canada, 1993; NARA, 2009). A one-foot depth is usually retained to differentiate between the flood way and the fringe. In France and in Austria, flood depths and flow velocities corresponding to a computed 100-year flood are combined and itemised into low, moderate, and high danger classes (MATE/METL, 1999; EXIMAP, 2007). In the UK, rating of hazards due to riverine floods relies on a 4-point classification of the 100-year and 1000-year floods (Table V-3), where harm potential of floating debris recruited is added to the depth-velocity product (DEFRA, 2006; DEFRA, 2008).

In the absence of hydraulic modelling, flow speeds may be deduced from the course of floating objects but at specific locations only. In reality, depths of flooding or debris heights are most often the only empirical data available and therefore the main characteristic considered when it comes to mark off a flooding event into danger zones (MATE/METL, 1999) and develop damage functions based on empirical evidence (e.g. Leone *et al.*, 2010; Valencia *et al.,* 2011).

3. Methodology

Thresholds in computed depths of flooding and flow velocities on the one hand, presence of life-threatening debris and temperature of floodwaters on the other, were used to perform a danger-oriented, semi-quantitative rating of flood hazard.

Table V-3: Safety-to-person classification of flood hazard adopted in the UK (DEFRA, 2006; DEFRA, 2008).

Rating formula	**Hazard rate = d (v + n) + DF** **d = depth of flooding (m);** **v = velocity of floodwaters (m/s);** **DF = debris factor (0, 0.5, 1 depending on probability that debris will lead to a hazard)** **n = a constant of 0.5**	
Flood hazard rates	**Colour scheme**	**Hazard to People Classification**
Less than 0.75	-	Very low hazard – Caution
0.75 to 1.25	Yellow	Danger for some – includes children, the elderly and the infirm
1.25 to 2.0	Orange	Danger for most – includes the general public
More than 2.0	Red	Danger for all – includes the emergency services

3.1. Rules of rating

A distinction is made between four flood hazard rates: low (1), moderate (2), high (3) and extreme (4), described below and summarized in Table V-5. An additional category (-99) is used when flood hazard cannot be rated.

Computed depth-velocity products *dv* should be used when depths of flooding and flow velocities are known. Water depths *d* can be used alone when information about flow velocities *v* is missing.

The peculiar rheologies of volcanogenic floods is addressed by taking into account the presence of life-threatening debris and sediments, decided on expert judgement: index l is set to 1 when debris are estimated life-threatening, otherwise l is set to 0; l should be set to NULL if not determined. Judging of the presence of life-threatening debris is particularly recommended when information on flow velocities and depths of flooding is missing.

The risk of severe injuries and fatalities due to temperature of floodwater, both stagnant and moving, can be taken into account when deemed relevant using expert judgement: index t is set to 1 when water temperature implies severe injuries or fatalities; otherwise t is set to 0; t should be set to NULL if not determined.

The time available for evacuating areas at risk of flooding (addressed in Pagneux, 2015b) is not formally taken into account in the methodology.

3.1.1. Level of hazard undetermined

Flood hazard should be rated as "undetermined" (-99) when depths of flooding d and flow velocities v are not known or cannot be inferred and the impact of debris and sediment load l and of water temperature t remains unevaluated; Value of d, v, l, and t is then set to NULL.

3.1.2. Low hazard

Hazard should be rated as *low* if $dv < 0.25$ m^2/s. When flow velocities v are not known, dv is replaced by $d < 0.5$ m (it is assumed that $v < 0.5$ m/s when $d < 0.5$ m).

Injuries or fatalities are unlikely. Damages are mostly limited to furniture inside buildings.

3.1.3. Moderate hazard

Hazard should be rated as *moderate* if sediment load index $l = 0$ and floodwater temperature index $t = 0$ and dv is between 0.25–.3 m^2/s. When flow velocities are not known, dv can be replaced by d ranging 0.5–1 m.

Danger is for some, including children, the elderly and the infirm, inside and outside buildings. Damages to buildings are expected but the structural integrity of buildings remains preserved.

3.1.4. High hazard

Hazard should be rated as *high* if $dv > 1.3$ m^2/s or sediment load index l=1 or floodwater temperature index $t = 1$. When flow velocities are not known, dv can be replaced by $d > 1$ m.

All lives are in jeopardy, outside and inside habitation buildings. The risk of drowning is significant as the wading limit for a normalised adult is reached; severe injuries or fatalities due to debris load and temperature of floodwaters may be expected.

Partial or total collapse of light buildings is expected due to scouring, buoyancy, and lateral pressures exerted against walls.

3.1.5. Extreme hazard

Hazard can be rated as *extreme* when $dv \geq 7$ m^2/s, irrespective of considerations on debris and temperature of floodwaters. When flow velocities are not known, dv can be replaced by $d > 6$ m.

Total destruction of non-reinforced buildings is expected. Structural damages to reinforced concrete dwellings are expected to a degree that would require demolition in the recovery phase.

3.2. Visualisation

Hazard rates are displayed as a layer of surficial tints showing on top of a basemap. Each rate is represented by a unique colour code, ranging from yellow to brown (Table V-5). Grey colour is used when the level of hazard is not determined.

4. Flood models and geomorphic evidence

4.1. Markarfljót outwash plain

Simulation of a glacial outburst flood originating from Entujökull glacier performed by Hólm and Kjaran (2005) was used for the rating of flood hazard. A maximum discharge of 300,000 m^3/s estimated by the National Road, and an average Manning roughness coefficient n 0.1 s/m$^{1/3}$ were used in the simulation, the output readily available being the maximum depths of flooding. It should be noted that the simulation made no account for sediment erosion and deposition. Results of the simulation indicate an inundation area of ~810 km^2, extending all the way from the glacier margin west to the Þjórsá river, 75 km away (Figure V-6).

The DEM used in the numerical simulation by Hólm and Kjaran (2005) was derived from elevation contours ranging 0.5–1 metre below 50 metres ASL, 2-metres contours between 50 and 70 metres ASL, 2.5-metres contours between 70 and 100 metres above ASL, and contours ranging 5–10 metres above 100 metres ASL. As changes in altitude, and not slope variations, were used therein to decide of the contour intervals, one cannot expect the results of the simulation to be particularly reliable in nearly-flat areas. Moreover, the flood area identified in the simulation is contiguous, south from Eyjafjallajökull volcano, to the spatial boundary of the hydraulic model. Considering the rheological settings of the simulation and the depths of flooding found at the boundary of the model, it is likely that floodwater would have propagated further to the east had a larger topographic envelope been used in the simulation. Based on an analysis of elevation contours beyond the model boundaries, it seems reasonable to make a 33 km^2 addition to the flood area, extending east to the Holtsós coastal lagoon (Figure V-6).

Table V-4: Provisional flood hazard rates proposed. Each hazard rate is verified if value of d, dv, l, or t is true. Depth-velocity product has precedence on other flood hazard characteristics.

Hazard rate	**Quantitative thresholds**		**Qualitative thresholds**		**Damages to buildings**	**Casualties**
	dv (m^2/s) *	**d (m) ****	**l *****	**t ******		
Low	< 0.25	< 0.5	n.a.	n.a.	Mostly limited to furniture inside buildings	Injuries or fatalities are unlikely
Moderate	0.25–1.3	0.5–1	n.a.	n.a.	Damages to buildings expected but structural integrity of buildings preserved	Danger for some (including children, the elderly and the infirm) inside and outside buildings
High	> 1.3	> 1	1	1	Partial or total collapse of light buildings expected	All lives in jeopardy, outside and inside habitation buildings
Extreme	≥ 7	> 6	n.a.	n.a.	Total destruction of non-reinforced buildings expected. Structural damages to reinforced concrete dwellings expected to a degree that would require demolition in the recovery phase	All lives in jeopardy, outside and inside habitation buildings

* Flood depth - flow velocity product ** Flood depth *** Debris and sediment load index **** Water temperature index

Table V-5: Flood hazard rates and corresponding colour codes. Screen colours values (RGB) are given in brackets.

Hazard rate	Code	Colour
Undetermined	-99	Grey (190, 190, 190)
Low	1	Yellow (255, 255, 0)
Moderate	2	Orange (255, 165, 0)
High	3	Red (255, 0, 0)
Extreme	4	Brown (128, 0, 0)

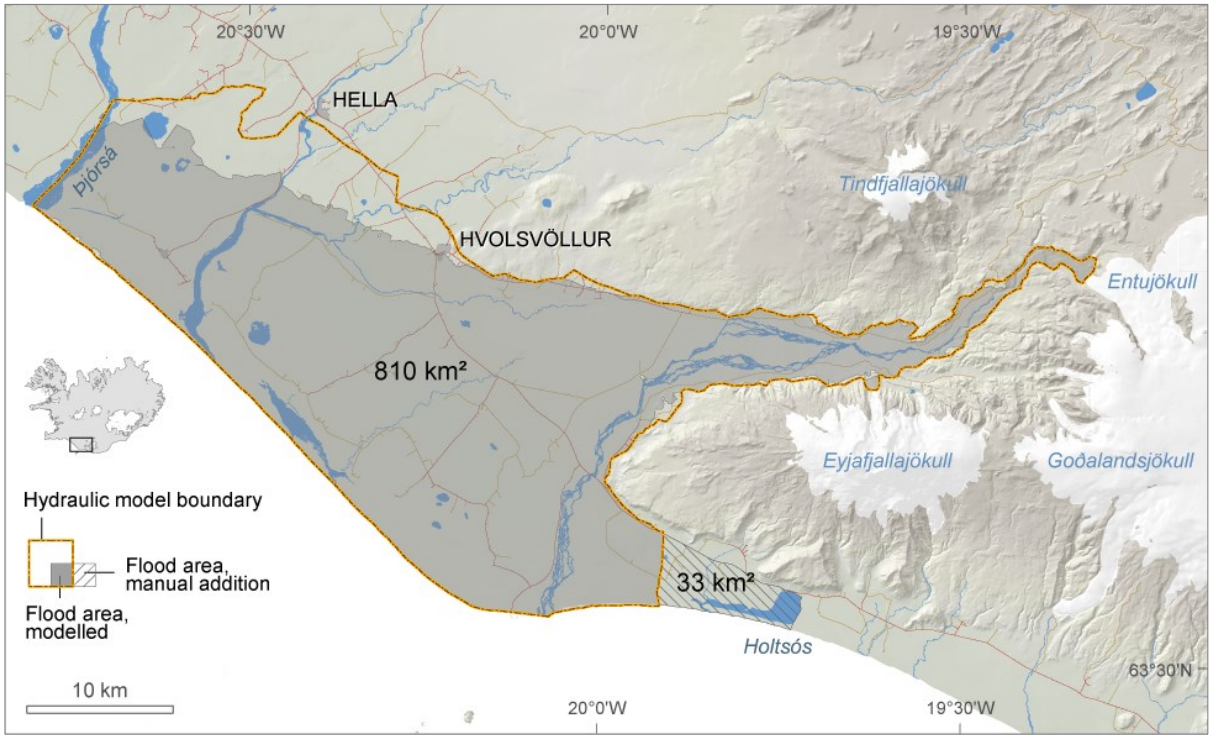

Figure V-6: Area identified at risk of flooding (greyish area) in the Markarfljót outwash plain due to volcanic activity under the Mýrdalsjökull ice-cap (Hólm and Kjaran, 2005). A maximum discharge of 300,000 m^3/s estimated by the National Road and an average Manning roughness coefficient n= 0.1 $s/m^{1/3}$ were used as inputs in the simulation. A manual extension of the flood area (striped pattern) beyond the boundaries of the hydraulic model is added, based on an analysis of elevations contours.

4.2. Öræfi district

For the Öræfi region, information on depths of flooding and flow velocities was extracted from numerical simulations performed by Helgadóttir *et al.* (2015) (Figure V-7). The simulations were performed within the spatial limits, here referred to as hydraulic model boundary, of a 5 m cell-size Digital Elevation Model (DEM) that covers the Öræfajökull ice-cap and its non-glaciated surrounds. The DEM originates from an airborne LiDAR survey performed during the summers of 2011 and 2012. The vertical accuracy of the LiDAR measurements and the average density of the point cloud are estimated < 0.5 m and ~0.33 point/m^2, respectively (Jóhannesson *et al.*, 2011; Jóhannesson *et al.*, 2013).

The simulations build upon melting scenarios in which melting of ice and snow is caused alternatively by (i) eruptions in the caldera and on the flanks of Öræfajökull ice-capped stratovolcano, and the (ii) formation of pyroclastic density currents (Gudmundsson *et al.*, 2015). The floods were simulated as

instant release waves of water flowing at the surface of the glacier, using predefinitions of peak discharge at the glacier margins ranging 10,000 - 100,000 m^3/s and average Manning roughness coefficients *n* ranging 0.05–0.15 $s/m^{1/3}$. It should be noted that the simulations made no account for sediment erosion and deposition. The results of the individual simulations were combined into one aggregated hazard scenario describing the maximum depths of flooding and maximum flow velocities that can be expected at every location within the 237 km^2 of land identified at risk of flooding within the spatial limits of the hydraulic model.

Helgadóttir *et al.* (2015) completed the cartography of the flood area beyond the boundaries of the hydraulic model by analysing sub-metre resolution aerial imagery taken by *Loftmyndir ehf.* in 2003 and 2007. An approximate 111 km^2 extension was found, delimited to the west by the Skaftafellsá river and to the east by the estuary of the Fjallsá river.

Information given by Thorarinsson (1958) and Roberts and Gudmundsson (2015) was used to estimate the threat posed by debris and water temperature.

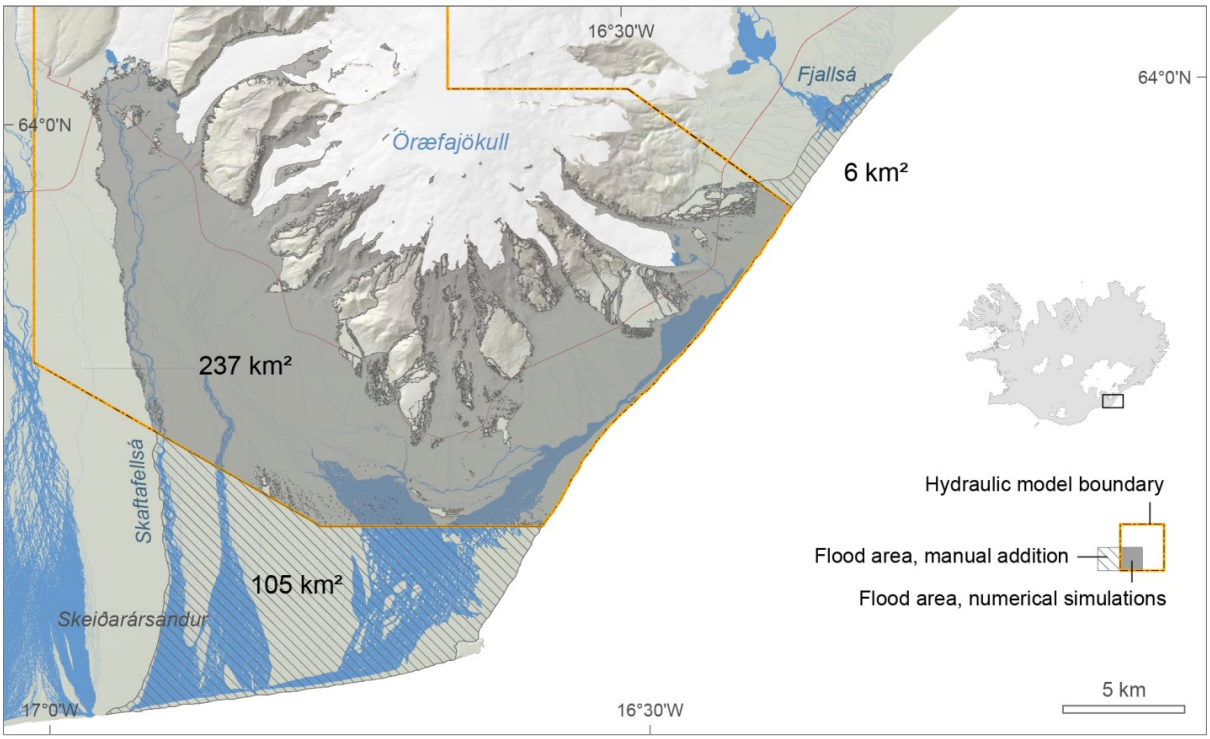

Figure V-7: Areas identified at risk of flooding in Helgadóttir et al. (2015). The flood area identified in the numerical simulations is shown in grey; extension of the flood area beyond the boundaries of the hydraulic model does show as a striped pattern.

5. Results

5.1. Markarfljót outwash plain

Flood-hazard rating was performed using the depths of flooding *d* only. Flow velocities, water temperature and debris load were not investigated thoroughly for this area and therefore not used in the rating.

Flood hazard was rated as *high* (depths ranging 1–6 m) or *extreme* (depths in excess of 6 m) on 384 and 332 km^2 of land, respectively, representing together 85% of the design flood area (Table V-6, Figure V-8). The extreme hazard zone is limited to the west by road 255 (Akureyjarvegur). Areas where flood hazards were rated as *low* (d < 0.5 m) or *moderate* (d ranging 0.5–1 m) only

represent ~10% of the flood area and are mainly located between the Rangá and Þjórsá rivers. Although depths of flooding in the manual addition to the flood area, south from Eyjafjallajökull volcano, could have been inferred to a certain degree from contiguous depth values, flood hazard in the above-mentioned area was provisionally set to *undetermined*.

Table V-6: Provisional rating of flood hazard in the Markarfljót outwash plain, using depths of flooding computed by Hólm and Kjaran (2005). The extreme hazard area (i.e. area of total devastation) represents ~40% of the flood area.

Hazard rate	Flood area, numerical simulation		Flood area, manual addition		Total	
	km²	%	km²	%	km²	%
Undetermined	0	0	33	100	33	4
Low	61	8	0	0	61	7
Moderate	33	4	0	0	33	4
High	384	47	0	0	384	46
Extreme	332	41	0	0	332	39
Total	810	100	110	100	346	100

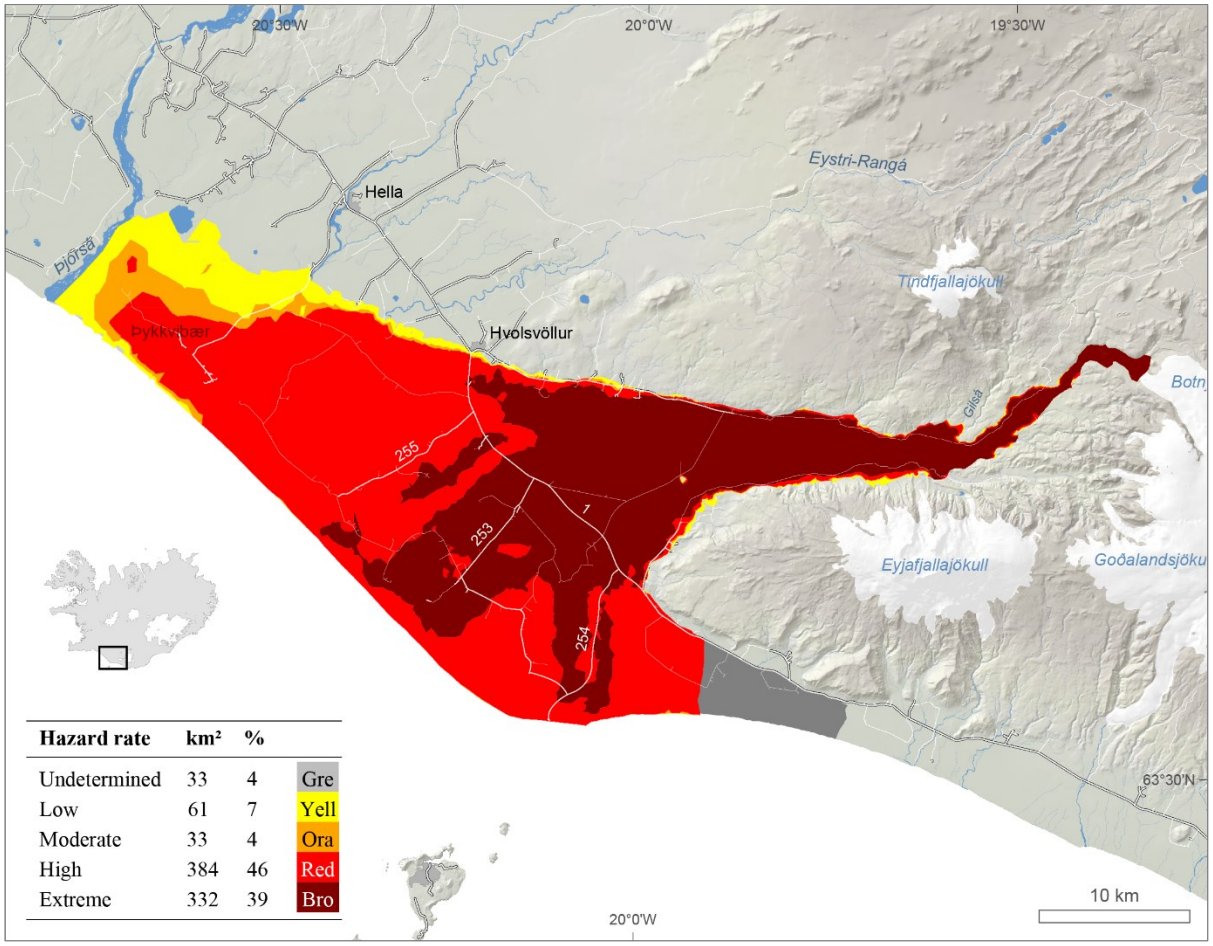

Figure V-8: Provisional rating of flood hazard in the Markarfljót outwash plain, using depths of flooding computed by Hólm and Kjaran (2005).

5.2. Öræfi district

Rating of flood hazard was performed using depth-velocity products *dv*, debris load *l,* and water temperature *t*.

5.2.1. Depth-velocity product

Based on depth-velocity products *dv*, flood hazard was rated as *high* or *extreme* on respectively ~12% (29 km^2) and ~77% (183 km^2) of the flood area identified in the numerical simulations (Table V-7). Only 10% of the computed flood area was rated as *low* or *moderate* hazard areas

5.2.2. Debris and sediments

Geomorphic evidence of past flooding events indicates that the area identified at risk of flooding in the simulations performed by Helgadóttir *et al.* (2015) is certainly exposed to flows of debris including clasts of glacier ice and boulders exceeding hundreds of tonnes. During the 1362 jökulhlaup, angular-shaped boulders weighing > 500 tons were transported by floodwaters from the Fall-jökull glacier and left interbedded with sediments, ~4 km from the glacier margin (Roberts and Gudmundsson, 2015 and references therein). It has also been reported that during the 1727 jökulhlaup many icebergs were transported to the sea (Thorarinsson, 1958). The thickness of sediments transported by floodwaters was also important enough to bury completely structures and people. At the base of Öræfajökull, modern-day exposures of sediments deposited during the 1727 jökulhlaup range from metres to tens of metres in depth. At distances exceeding 7 km from the edge of the ice cap, metre-scale sections of jökulhlaup sediments are apparent, signifying that large volumes of eruptive material and pre-existing sandur deposits were mobilised by volcanogenic floods. Throughout the same region, grain sizes range from coarse sands to boulders in excess of 5 m in diameter.

The debris index *l* was therefore set to 1 at every location of the computed flood area and of the manual addition.

Table V-7: Hazard rating of the flood area identified in the numerical simulations by Helgadóttir et al. (2015), using depth-velocity products.

Hazard rate	code	km^2	%
Low	1	4	1.7
Moderate	2	20	8.5
High	3	29	12.4
Extreme	4	183	77.4

5.2.3. Water temperature

Highly variable water temperatures can be expected at the vicinity of the glaciers should an eruption happen. It has been reported for instance that the temperature of torrents, a few kilometres from the Kotárjökull glacier margin, was warm enough days after the 1727 jökulhlaup to prevent horses from wading in waters (Thorarinsson, 1958).

At the onset of the eruption, while floodwater is in sustained contact with glacial ice, near-freezing water temperatures can be expected.

As a result, the floodwater temperature index *t* was set to 1 at every location of the computed flood area and of the manual addition.

5.2.4. Computed hazard rate

Flood hazard was finally rated as *high* or *extreme* on 164 km^2 (47%) and 183 km^2 (53%) of land, respectively (Figure V-9, Table V-8). The share of *extreme* hazard is certainly higher in reality, as the depth-velocity products could not be computed beyond the boundaries of the hydraulic model.

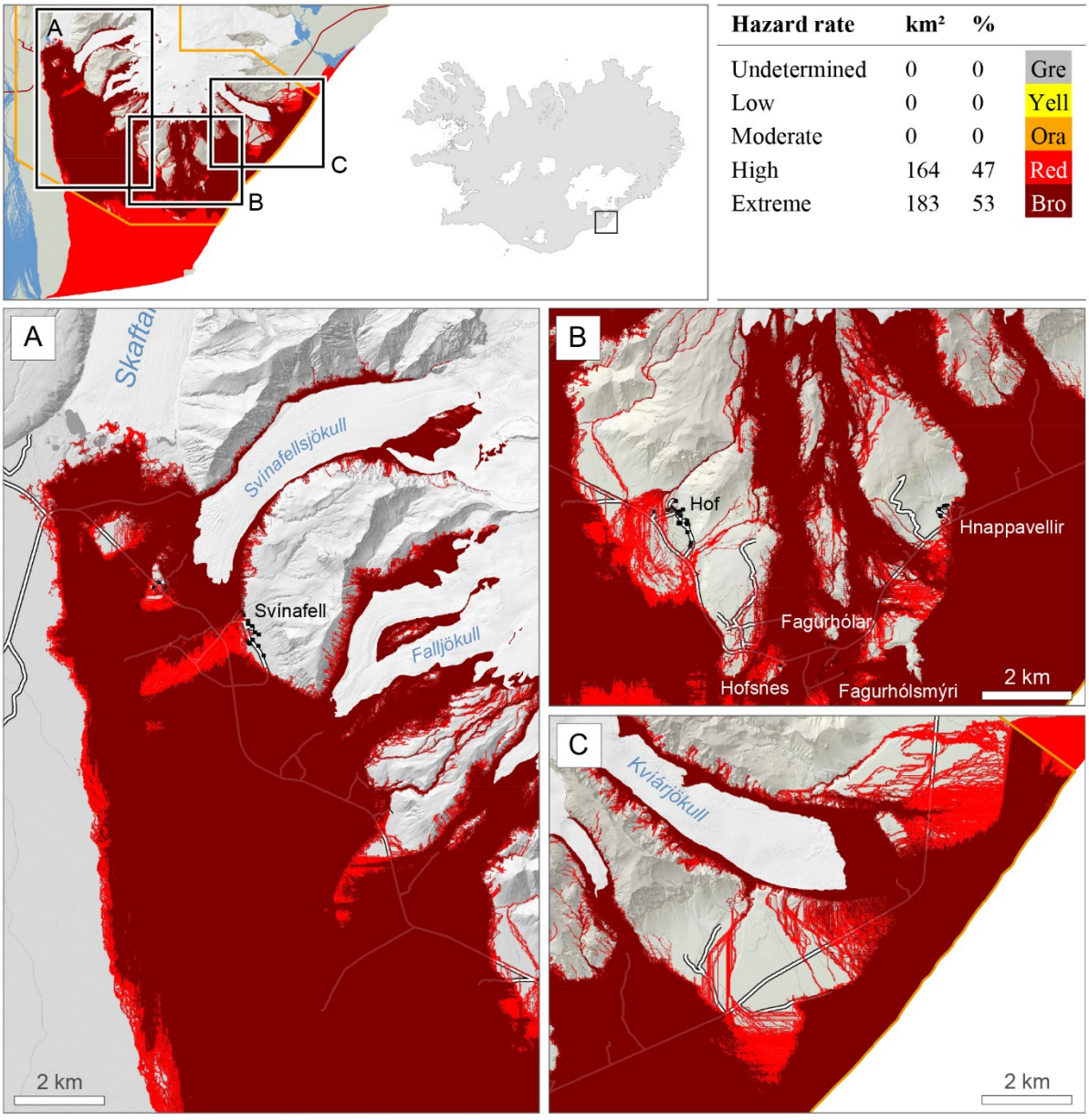

Figure V-9: Provisional rating of flood hazards due to eruptions of Öræfajökull volcano. Depths of flooding and flow velocities computed by Helgadóttir et al. (2015) were used, along with considerations on debris and water temperature. The extreme hazard area (i.e. area of total devastation) represents ~53% of the flood area.

Table V-8: Provisional rating of flood hazards due to eruptions of Öræfajökull; depths of flooding and flow velocities computed by Helgadóttir et al. (2015) were used, along with considerations on debris and water temperature. The extreme hazard area represents 53% of the flood area.

Hazard rate	Flood area, numerical simulations		Flood area, manual addition		Total	
	km^2	*%*	km^2	*%*	km^2	*%*
Undetermined	0	*0*	0	*0*	0	*0*
Low	0	*0*	0	*0*	0	*0*
Moderate	0	*0*	0	*0*	0	*0*
High	54	*23*	110	*100*	164	*47*
Extreme	183	*77*	0	*0*	183	*53*
Total	237	*100*	110	*100*	347	*100*

6. Discussion

6.1. Methodological limits

Several aspects should be considered carefully when rating of flood hazard is performed, or when use is made of flood hazard rates, using the methodology proposed.

6.1.1. Input parameters

Using alternatively depths of flooding (hydrostatic forces), velocities or dynamic pressures, and depth-velocity products does not give similar results. Using either depth of flooding or dynamic pressure alone leads to a significant downgrading of hazard rates obtained with the depth-velocity product. In the Öræfi district, the area where flood hazard is rated as extreme using depths of flooding only covers 116 km^2 of land, which is ~40% less than by using the *dv* product (Table V-9).

As the depth-velocity product takes into account both hydrostatic and hydrodynamic forces, it is assumed to reflect real conditions better than either depths of flooding or dynamic pressure, and therefore should receive precedence in the rating of flood hazard when available.

Table V-9: Spatial extent of extreme hazard areas, based on either depths of flooding or depth-velocity products.

	depths of flooding *d*	depth-velocity product *dv*
Lower threshold	6 m	7 m^2/s
Spatial extent (km^2)	116	183
Spatial extent (%)*	49	77
Spatial extent (%)**	63	100

* As share of the total flood area identified in numerical simulations

** As share of the area where flood hazard is rated as extreme according to the depth-velocity product

6.1.2. Switching between rates

Switching from *moderate* hazard to *high* hazard represents a qualitative jump in terms of injuries and fatalities: danger is for all where hazard is rated *high* while it is for some (disabled, elderly, and children) where hazard is rated *moderate*. The extreme hazard class is primarily aimed at identifying areas where 100% destruction is expected (during events or afterwards, in the recovery phase). Such information should be useful when an effort is made on quantifying monetary losses due to direct damages inflicted to physical assets (e.g. van Vesten *et al.*, 2014).

6.2. Reproducibility

The presence of life-threatening debris and temperature of floodwater were considered, along with depths of flooding and flow velocities, in a flood hazard rating methodology that account for the unique nature of jökulhlaups. The methodology was devised to be used for the delineation of flood hazard zones in Icelandic areas prone to volcanogenic floods, provided that enough information on flood hazard characteristics therein can be acquired and processed. Use of the methodology is not bound to be used in the Markarfljót outwash plain and the Öræfi district only.

As the flood hazard characteristics considered, and the thresholds retained, are also valid for tsunamis (e.g. Leone *et al.*, 2010; Valencia *et al.,* 2011) and riverine floods, including ice-jam floods (e.g. Pagneux and Snorrason, 2012) and flooding due to dam break (e.g. Karvonen *et al.,* 2000), an application of the methodology to types of floods other than jökulhlaups can also be envisaged.

7. Summary and conclusion

A semi-quantitative rating of flood hazards focusing on flood damage potential was proposed and flood hazard zones designated accordingly in the Markarfljót outwash plain and in the Öræfi district, two Icelandic regions that have experienced jökulhlaups due to subglacial eruptions in the last 1000 years.

Using alternatively depths of flooding or the product of flow velocities and flood depths on one hand, the presence of life-threatening debris and temperature of floodwater on the other (Table V-4), a distinction was made between four hazard rates:

- **Low hazard**

  Injuries or fatalities are unlikely; damages are mostly limited to furniture inside buildings.

- **Moderate hazard**

  Danger is for some, including children, the elderly and the infirm, inside and outside buildings. Damage to buildings is expected but the structural integrity of buildings remains preserved.

- **High hazard**

  All lives are in jeopardy, outside and inside inhabited buildings. The risk of drowning is significant as the wading limit for a normalised adult is reached; severe injuries or fatalities due to debris load and floodwater temperature are expected. Partial or total collapse of light buildings is expected due to scouring, buoyancy, and lateral pressures exerted against walls.

- **Extreme hazard**

  Total destruction of non-reinforced buildings is expected; structural damages to reinforced concrete dwellings are expected to a degree that does require demolition in the recovery phase.

An application of the method to the two study areas indicates a potential for significant direct economic damage and fatalities:

- **Markarfljót outwash plain**

  Based on maximum depths of flooding, flood hazard was rated as *high* or *extreme* on respectively 384 and 332 km^2 of land, i.e. 85% of the flood area (Figure V-8). Extent of the high-hazard area may increase upon

integration of flow velocities, water temperature, and debris load.

- **Öræfi district**

  Using the depth-velocity product as well as information on water temperature index and debris load, flood hazard was exclusively rated as *high* or *extreme* on 164 km^2 and 183 km^2 of land, respectively (Figure V-9).

As a first approximation of damage potential due to volcanogenic floods in the two areas, these results should be carefully considered by the local and national authorities when evacuation procedures and planning on the long term are discussed. The spatial boundary between hazard rates depends much on which and how flood characteristics are used. It should be noted, in particular, that using depths of flooding alone leads to a significant downgrading of hazard rates obtained with the depth-velocity product. As the depth-velocity product accounts for both hydrostatic and hydrodynamic forces, it is assumed to reflect real conditions better than depths of flooding alone and therefore should receive precedence in the rating of flood hazard when available.

8. Acknowledgements

The authors would like to thank Frédéric Leone, Tómas Jóhannesson, and Trausti Jónsson for their review and proof-reading of the chapter. Oddur Sigurðsson is thanked for provision of photographs.

The present work was funded by the Icelandic Avalanche and Landslide Fund, the National Power Company, and the Icelandic Road and Coastal Administration.

9. References

Abt, S. R., Whittker, R. J., Taylor, A., & Love, D. J. (1989). Human stability in a high flood hazard zone. *Water Res. Bull., 25*, 881–890.

Akbas, S. O., Blahut, J., & Sterlacchini, S. (2009). Critical assessment of existing physical vulnerability estimation approaches for debris flows. In J. P. Malet, A. Remaître, & T. A. Bogaard (Ed.), *International Conference "Landslide Processes"* (pp. 229–233). Strasbourg: CERG Editions.

Barbolini, M., Cappabianca, F., & Sailer, R. (2004). Empirical estimate of vulnerability relations for use in snow avalanche risk assessment. In C. Brebbia (Ed.), *Risk analysis IV* (pp. 533–542). Southampton: WIT Press.

Black, R. (1975). *Flood Proofing Rural Residences.* New York: Department of Agricultural Engineering, Cornell University.

Clausen, L., & Clark, P. (1990). The development of criteria for predicting dambreak flood damages using modelling of historical dam failures. In W. R. White (Ed.), *International Conference on River Flood Hydraulics* (pp. 369–380). John Wiley &Sons Ltd.

de Moel, H., van Alphen, J., & Aerts, J. (2009). Flood maps in Europe - Methods, availability and use. *Nat. Hazards Earth Syst. Sci., 9*, 289–301.

DEFRA (2006). *Flood risk to people. Phase 2.* London: Environment Agency and Department for Environment, Food and Rural Affairs.

DEFRA (2008). *Supplementary note on flood hazard ratings and thresholds for development planning and control purpose. Clarification of the Table 13.1 of FD230/TR2 and figure 3.2. of FD2321/TR1.* London: Environment Agency and Department for Environment, Food and Rural Affairs.

Dutta, D., Herath, S., & Musiake, K. (2003). A mathematical model for flood loss estimation. *Journal of Hydrology, 277*, 24–49.

Environment Canada. (1993). *Flooding: Canada Water Book* (Andrews, J. ed.). Ottawa: Economics and Conservation Branch, Ecosystem Sciences and Evaluation Directorate, Environment Canada.

EXCIMAP (2007). *Handbook on Good Practices for Flood Mapping in Europe.* (F. Martini, & R. Loat, Eds.) The Hague: Netherland Ministry of Transport, Public Works and Water Management.

Foster, D. N., & Cox, R. J. (1973). *Stability of children on roads used as floodways.* Manly vale, New South Wales, Australia: Water Research Laboratory, The University of New South Wales.

Fraser, S., Raby, A., Pomonis, A., Goda, K., Chian, S. C., Macabuag, J., Offord, M., Saito, K., and Sammonds, P. (2013). Tsunami damage to coastal defences and buildings in the March 11th 2011 Mw 9.0 Great East Japan earthquake and tsunami. *Bull. Earthquake Eng., 11*, 205–239.

French, J., Ing, R., von Allmen, S., & Wood, R. (1983). Mortality from flash floods: A review of National Weather Service Reports, 1969-1981. *Public Health Reports, 98*(6), 584–588.

Fuchs, S., Heiss, K., & Hübl, J. (2007). Towards an empirical vulnerability function for use in debris flow risk assessment. *Nat. Hazards Earth Syst. Sci., 7*, 495–506.

Gudmundsson, M. T., Högnadóttir, Þ., & Magnússon, E. (2015). Öræfajökull: Eruption melting scenarios. In E. Pagneux, M. T. Gudmundsson, S. Karlsdóttir, & M. J. Roberts (Eds.), *Volcanogenic floods in Iceland: An assessment of hazards and risks at Öræfajökull and on the Markarfljót outwash plain* (pp. 45–72). Reykjavík: IMO, IES-UI, NCIP-DCPEM.

Gudmundsson, M. T., Larsen, G., Höskuldsson, Á., & Gylfason, Á. G. (2008). Volcanic hazards in Iceland. *Jökull*, 58, 251–258.

Guðmundsson, M. T., Elíasson, J., Larsen, G., Gylfason, Á. G., Einarsson, P., Jóhannesson, T., Hákónardóttir, K. M., and Torfason, H. (2005). Yfirlit um hættu vegna eldgosa og hlaupa frá vesturhluta Mýrdalsjökuls og Eyjafjallajökli (Overview of hazards due to volcanic eruptions and volcanogenic floods on the western slopes of Mýrdalsjökull and Eyjafjallajökull). In M. T. Guðmundsson, & Á. G. Gylfason (Eds.), *Hættumat vegna eldgosa og hlaupa frá vestanverðum Mýrdalsjökli og Eyjafjallajökli (Hazard assessment of volcanic eruptions and glacial outbursts for Eyja-fjallajökull and the western outwash plain of Mýrdalsjökull)* (pp. 11–44). Reykjavík: National Commissioner of Police.

Helgadóttir, Á., Pagneux, E., Roberts, M. J., Jensen, E. H., & Gíslason, E. (2015). Öræfajökull Volcano: Numerical simulations of eruption-induced jökulhlaups using the SAMOS flow model. In E. Pagneux, M. T. Gudmundsson, S. Karlsdóttir, & M. J. Roberts (Eds.), *Volcanogenic floods in Iceland: An assessment of hazards and risks at Öræfajökull and on the Markarfljót outwash plain* (pp. 73–100). Reykjavík: IMO, IES-UI, NCIP-DCPEM.

Hólm, S. L., & Kjaran, S. P. (2005). Reiknilíkan fyrir útbreiðslu hlaupa úr Entujökli (Hydraulic model of floods from Entujökull). In M. T. Guðmundsson, & Á. G. Gylfason (Eds.), *Hættumat vegna eldgosa og hlaupa frá vestanverðum Mýrdalsjökli og Eyjafjallajökli (Hazard assessment of volcanic eruptions and glacial outbursts for Eyjafjallajökull and the western outwash plain of Mýrdalsjökull)* (pp. 197–210). Reykjavík: National Commissioner of Police.

Jonkman, S. N., & Kelman, I. (2005). An analysis of the causes and circumstances of flood deaths. *Disasters, 29*(1), 75–95.

Jonkman, S. N., & Penning-Rowsell, E. (2008). Human instability in flood flows. *Journal of the American Water Resources Association, 44*(4), 1–11.

Jóhannesson, T., Björnsson, H., Magnússon, E., Guðmundsson, S., Pálsson, F., Sigurðsson, O., Thorsteinsson, T., and Berthier, E. (2013). Ice-volumes changes, bias estimation of mass-balance measurements and changes in subglacial lakes derived by lidar mapping of the surface of Icelandic glaciers. *Annals of Glaciology, 54*(63), 63–74.

Jóhannesson, T., Björnsson, H., Pálsson, F., Sigurðsson, O., & Thorsteinsson, T. (2011). LiDAR mapping of the Snæfellsjökull ice cap, western Iceland. *Jökull, 61*, 19–32.

Karvonen, R. A., Hepojoki, A., Huhta, H., & Louhio, A. (2000). *The use of physical models in dam-break analysis. RESCDAM Final Report.* Helsinki: Helsinki University of Technology.

Keller, R. J., & Mitsch, B. (1993). *Safety aspects of the design of roadways as floodways. Final report for Urban Water Research Association, Melbourne Water Research PRoject.* Melbourne: Monash University.

Kelman, I., & Spence, R. (2004). An overview of flood actions on buildings. *Engineering Geology, 73*, 297–309.

Kemmerling, G. L. (1921). De uitbarsting van den G. Keloet in den nacht van den 19den op den 20sten mei 1919 (The eruption of Mount Kelud on the May 19–20 1919 night). *Vulkanol Mededeel, 2*.

Kreibich, H., & Dimitrova, B. (2010). Assessment of damages caused by different flood types. In D. Wrachien, D. Proverbs, C. A. Brebbia, & S. Mambretti (Eds.), *Flood Recovery, Innovation and Response II* (Vol. 133, pp. 3–11). South-ampton: WIT Press.

Kreibich, H., Piroth, K., Seifert, I., Maiwald, H., Kunnert, U., Schwarz, J., Merz, B., and Thieken, A. H. (2009). Is flow velocity a significant parmater in flood damage modelling? *Nat. Hazards Earth Syst. Sci., 9*, 1679–1692.

Leone, F., Lavigne, F., Paris, R., Denain, J. C., & Vinet, F. (2010). A spatial analysis of the December 26th, 2004 tsunami-induced damages: Lessons learned for a better risk assessment integrating buildings vulnerability. *Applied Geography, 31*(1), 363–375.

Lloyd, E. L. (1996). Accidental hypothermia. *Resuscitation, 32*(2), 111–24.

Luna, B. Q., Blahut, J., van Westen, C. J., Sterlacchini, S., van Asch, T. W., & Akbas, S. O. (2011). The application of numerical debris flow modelling for the generation of physical vulnerability curves. *Nat. Hazards Earth Syst. Sci., 11*, 2047–2060.

MATE/METL (2002). *Plans de Prévention des Risques Naturels (PPR): Risques d'inondation. Guide méthodologique (Prevention Plans against Natural Hazard Risks: Flooding Risks. Methodological guide).* Paris: La Documentation Française.

Merz, B., Kreibich, H., Scwarze, R., & Thieken, A. H. (2010). Assessment of economic damage. *Nat. Hazards Syst. Sci., 10*, 1697–1724.

Mileti, D., Bolton, P., Fernandez, G., & Updike, R. (1991). *The eruption of Nevado del Ruiz Volcano Colombia, South America, November 13, 1985.* (Commission on Engineering and Technical Systems, Ed.) Washington D.C.: National Academy Press.

Ministry for the Environment. (2000). Reglugerð 505/2000 um hættumat vegna ofanflóða, flokkun og nýtingu hættusvæða og gerð bráða-birgðahættumats (Regulation 505/2000 on the risk assessment of avalanches and shallow slides, classification and use of risk zones, and making of...). Reykjavík: Government Offices of Iceland.

Ministry for the Environment and Natural Resources. (2013). Skipulagsreglugerð 90/2013. Reykjavík: Government Offices of Iceland.

NARA (2009). Flood plain management and protection of wetlands. In *U.S. Code of Federal Regulations, Title 44, Vol. 1, Chapter 1, part 9 (pp 69–88)*.

Pagneux, E. (2015a). Öræfi district and Markarfljót outwash plain: Spatio-temporal patterns in population exposure to volcanogenic floods. In E. Pagneux, M. T. Gudmundsson, S. Karlsdóttir, & M. J. Roberts (Eds.), *Volcanogenic floods in Iceland: An assessment of hazards and risks at Öræfajökull and on the Markarfljót outwash plain* (pp. 123–140). Reykjavík: IMO, IES-UI, NCIP-DCPEM.

Pagneux, E. (2015b). Öræfajökull: Evacuation time modelling of areas prone to volcanogenic floods. In E. Pagneux, M. T. Gudmundsson, S. Karlsdóttir, & M. J. Roberts (Eds.), *Volcanogenic floods in Iceland: An assessment of hazards and risks at Öræfajökull and on the Markarfljót outwash plain* (pp. 141–164). Reykjavík: IMO, IES-UI, NCIP-DCPEM.

Pagneux, E., & Snorrason, Á. (2012). High-accuracy mapping of inundatons induced by ice-jams: a case-study from Iceland. *Hydrology Research, 43*(4), 412–421.

Parliament of Iceland. (2010). Skipulagslög 123/2010 (Planning Act 123/2010).

Penning-Rowsell, E., Johnson, C., Tunstall, S., Tapsell, S., Morris, J., Chatterton, J., & Green, C. (2005). *The Benefits of Flood and Coastal Risk Management: A Handbook of Assessment Techniques.* London: Middlesex University Press.

Reiter, P. (2000). Considerations on urban areas and floating debris in dam-break flood modelling. *RESCDAM seminar, Session 2, Mathematical and physical modelling to simulate a dam-break flood.*

Roberts, M. J., & Gudmundsson, M. T. (2015). Öræfajökull Volcano: Geology and historical floods. In E. Pagneux, M. T. Gudmundsson, S. Karlsdóttir, & M. J. Roberts (Eds.), *Volcanogenic floods in Iceland: An assessment of hazards and risks at Öræfajökull and on the Markarfljót outwash plain* (pp. 17–44). Reykjavík: IMO, IES-UI, NCIP-DCPEM.

Roberts, M. J., Sigurðsson, G., Sigurðsson, O., Pagneux, E., Jóhannesson, T., Zóphóníasson, S., Gudmundsson, M. T., Russell, A. J., Gylfason, Á. G., Höskuldsson, F., and Björnsson, B. B. (2011). The April 2010 Eruption of Eyjafjallajökull Volcano: Glacial flooding and attendant hazards. *IAVCEI Symposium Surface processes in volcanic terrains: the erosion, transport and redeposition of volcaniclastic material and their associated hazards.* Melbourne.

Russell, A. J., Tweed, F., Roberts, M. J., Harris, T. D., Gudmundsson, M. T., Knudsen, O., & Marren, P. M. (2010). An unusual jökulhlaup resulting from subglacial volcanism, Sólheimajökull, Iceland. *Quaternary Science Review*, 1363–1381.

Russo, B., Gómez, M., & Macchione, F. (2013). Pedestrian hazard criteria for flooded urban areas. *Nat. Hazards, 69*, 251–265.

Schwarz, J., & Maiwald, H. (2008). Damage and loss prediction model based on the vulnerability of building types. *4th International Symposium on Flood Defence: Managing Flood Risk, Reliability and Vulnerability.* Toronto.

Smith, D. I. (1991). Extreme floods and dam failure inundation implications for loss assessment. *Proceedings of a Seminar "Natural and Technological Hazards: Implications for the Insurance Industry"*, (pp. 149–165).

Snorrason, Á., Einarsson, B., Pagneux, E., Hardardóttir, J., Roberts, M., Sigurðsson, O., Thórarinsson, Ó., Crochet, P., Jóhannesson, T., and Thorsteinsson, T. (2012). Floods in Iceland. In Z. W. Kundzewicz (Ed.), *Changes in flood risk in Europe* (pp. 257–276). IAHS Special Publication 10.

Thorarinsson, S. (1958). The Öræfajökull eruption of 1362. *Acta Naturalia Islandica, 2*(4), 100.

Tinti, S., Tonini, R., Bressan, L., Armigliato, A., Gardi, A., Guillande, R., Valencia, N., and Scheer, S. (2011). *Handbook of tsunami hazard and damage scenarios.* Luxembourg: Publications Office of the European Union.

USBR (U.S. Department of the Interior, Bureau of Reclamation). (1988). *Downstream Hazard Classification Guidelines.* Denver: USBR.

Valencia, N., Gardi, A., Gauraz, A., Leone, F., & Guillande, R. (2011). New tsunami damage functions developed in the framework of SCHEMA project: application to European-Mediterranean coasts. *Nat. Hazards Earth Syst. Sci., 11*, 2835–2846.

Van Vesten, C., Kappes, M. S., Luna, B. Q., Frigerio, S., Glade, T., & Malet, J. P. (2014). Medium-scale multi-hazard risk assessment of gravitational processes. In T. Van Asch, J. Corominas, S. Greiving, J. P. Malet, & S. Sterlacchini (Eds.), *Mountain risks: From prediction to management and governance.* London: Springer.

Voigt, B. (1990). The 1985 Nevado del Ruiz volcano catastrophe: anatomy and restrospection. *Journal of Volcanology and Geothermal Research, 44*, 349–386.

Wilhelm, C. (1998). Quantitative risk analysis for evaluation of avalanche protection projects. *Proceedings of the 25 Years of Snow Avalanche Research* (pp. 288–293). Oslo: NGI Publications.

VI. ÖRÆFI DISTRICT AND MARKARFLJÓT OUTWASH PLAIN: SPATIO-TEMPORAL PATTERNS IN POPULATION EXPOSURE TO VOLCANOGENIC FLOODS

Emmanuel Pagneux *

* *Icelandic Meteorological Office*

1. Introduction

Characterisation of population exposure has recently gained importance in the assessment of flood hazards and is now incorporated in regulatory frameworks such as the European directive on the assessment and management of flood risks (European Parliament and Council, 2007). The EU Floods directive enjoins to make an inventory of the "inhabitants" living in areas identified at risk of flooding, but wisely does not forbid assessors to make therein further distinction between populations. Choosing which populations should be targeted in a flood exposure assessment is indeed much a matter of scale of analysis and objectives. Population exposure to floods has been assessed in recent years from various angles, such as age and disabilities (e.g. Chakraborty *et al.*, 2005; McGuire *et al.*, 2007) or socio-economic status (e.g. Gaillard *et al.*, 2001). In their assessment of variations in population exposure to lahar hazards from Mount Rainier, Wood and Soulard (2009) considered it necessary to make a distinction between residents, employees, and tourists, the last group outnumbering the first two groups in some of the counties exposed.

As in Mount Rainier, an assessment that would focus only on residents may not be fully satisfying in Icelandic areas characterised by strong seasonal patterns in population exposure due to tourist activities. In reality, it may be critical for the efficiency of the emergency response to look at spatio-temporal patterns and provide the Icelandic authorities with figures including also transient populations. Linkage of the road network in Icelandic floodplains and around is often reduced and therefore may not fit the needs for a sudden and massive emergency evacuation. The learning keys of the "full-scale" evacuation exercise organised by the authorities in the Markarfljót outwash plain in 2006 (Bird *et al.*, 2009) have been of limited value in this regard, as the exercise concerned the residents only and was performed in March, i.e. outside the high touristic season. Making a distinction between residents and transient population and quantifying their respective weight may be also necessary, as these two populations may have different understanding and perceptions of the pending hazards, show different levels of preparedness (Wisner *et al.*, 2004), and react subsequently in different manners to warnings and evacuation orders. Survey conducted in the Markarfljót outwash plain in 2009 suggests that tourists seriously lack knowledge of volcanic hazards, warning systems and emergency response procedures (Bird *et al.*, 2010).

In addition to making a distinction between residents and transients, it is useful to consider potential land accessibility loss (e.g. Leone *et al.*, 2013; Leone *et al.*, 2014) and include, in a population exposure assessment, an inventory of the populations that would be isolated as a consequence of the floods and

exposed subsequently to other hazards relating to glaciovolcanism, such as ash fall and lightning (Gudmundsson *et al.*, 2008).

In this study, a spatiotemporal analysis of population exposure to floods is performed in the Markarfljót outwash plain and in the Öræfi district (Figure VI-1), two regions of Iceland that have been subjected to severe volcanogenic floods in the last millennium.

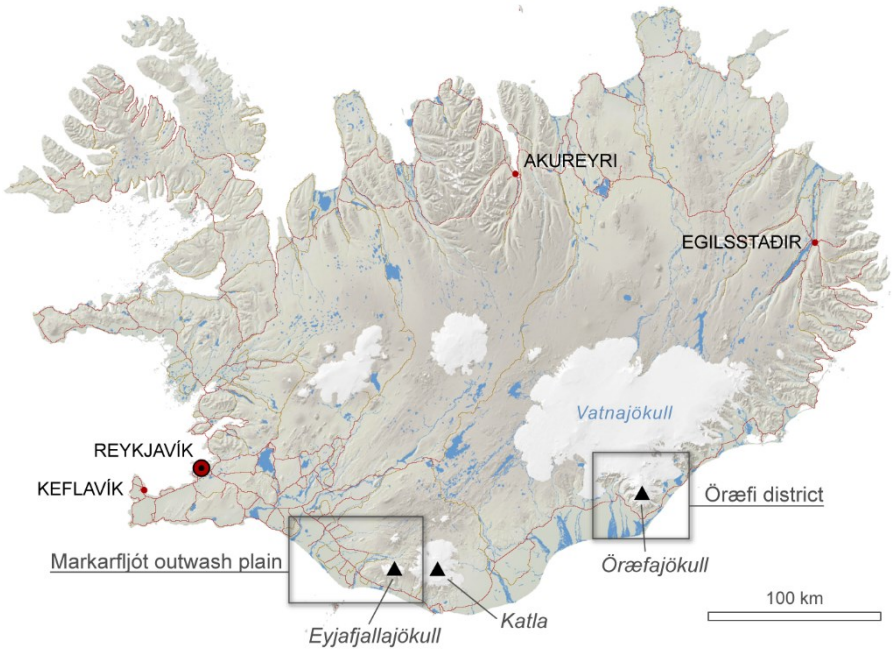

Figure VI-1: General location of the Markarfljót outwash plain and Öræfi district. Map base: Iceland Geosurvey, IMO, NLSI; Basemap: IMO.

The two regions host recreational areas that are very popular amongst Icelanders and foreign visitors during summertime. The main objective of the assessment is to provide the national and local authorities with a fair estimation, at different periods of the year and at particular locations within the two studied areas, of the likely number of residents and guests that would stand in the path of volcanogenic floods or be isolated as a consequence of the floods. Inventory of the populations exposed to floods is performed for night time, using daily overnights estimates weighted with road traffic data as an indicator. Results of the assessment in the Öræfi district are used in chapter VII (Pagneux, 2015) to estimate the time required for a full evacuation of areas at risk of flooding. Although having their importance in emergency planning, variations corresponding to demographic attributes such as age (e.g. Liu *et al.*, 2010; Scaini *et al.*, 2014), health (e.g. McGuire *et al.*, 2007) or nationality (e.g. Guðmundsson, 2014), are not addressed in the study. They could form, along with physical assets (buildings, infrastructure, and land), the subject of an extended exposure assessment coming as a sequel of the work presented hereafter.

2. Study areas

2.1. Markarfljót outwash plain

The Markarfljót outwash plain extends from the western margins of the Mýrdalsjökull ice-cap down to the Þjórsá River (Figure VI-2). The outwash plain corresponds, to a great extent, to the topographic envelope of glacial floods due to volcanic eruptions on the north-western slopes of the Mýrdalsjökull ice cap. The plain contains evidence of at least 11

volcanogenic floods having occurred before the settlement of Iceland (Larsen *et al.*, 2005). Only two jökulhlaups are known after Iceland was settled, which were caused by the Eyjafjallajökull eruptions in 1821–1823 CE (Óskarsdóttir, 2005) and 2010 CE (Snorrason *et al.*, 2012). None of these floods are known to have caused fatalities.

Hydraulic simulations performed by Hólm and Kjaran (2005) indicate that a 300,000 m^3/s flood originating from the Mýrdalsjökull ice-cap (Entujökull) would inundate an area of ~800 km^2 (Figure VI-2). Based on these simulations, Pagneux and Roberts (2015) estimated that flood hazard should be rated therein as high or extreme on 716 km^2 of land (85% of the flood area), meaning that floods could cause therein numerous fatalities and destroy or damage severely all types of habitation buildings standing in the path of the floods.

Driving through the plain is the most convenient option for moving along the south coast of Iceland and is a requirement for automobilists to reach Þórsmörk, a much popular recreational area nestled between the Mýrdalsjökull, Eyjafjallajökull, and Tindfjallajökull glaciers (Figure VI-2).

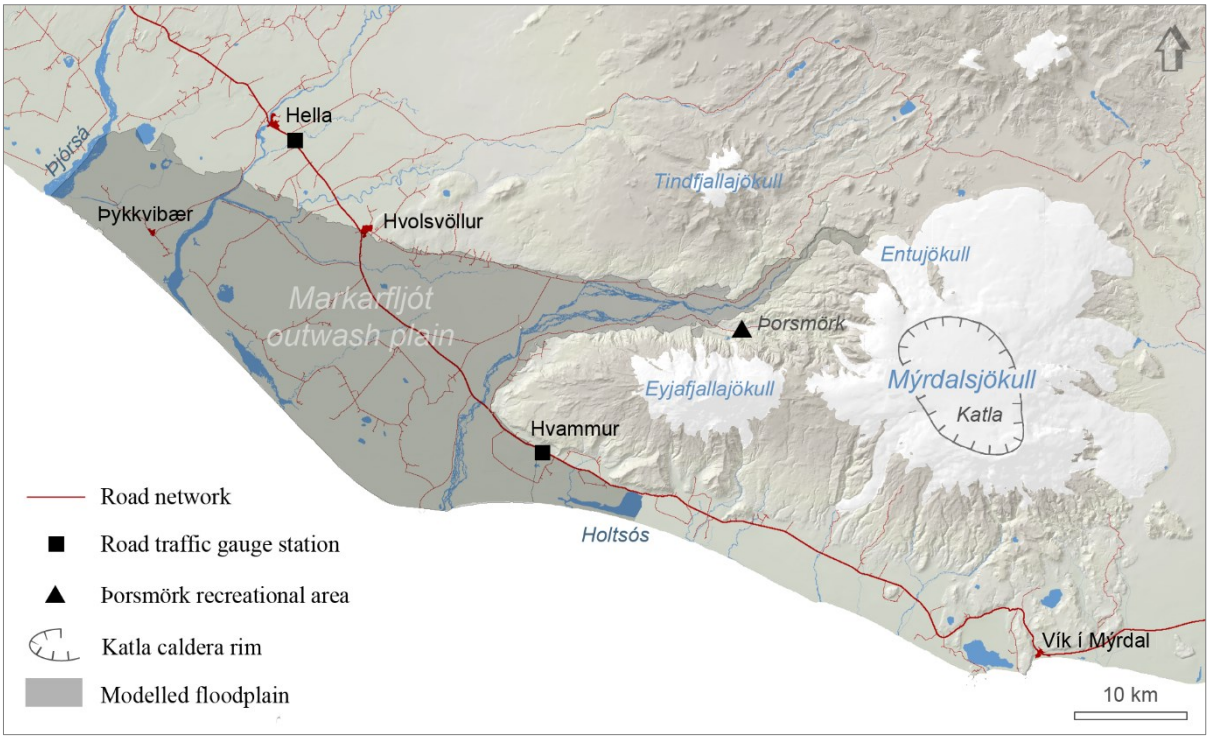

Figure VI-2: Markarfljót outwash plain. Extent of the floodplain corresponds to a simulated 300,000m^3/s flood originating from the Entujökull glacier (Hólm and Kjaran, 2005; Pagneux and Roberts, 2015). Driving through the plain is the most convenient option for moving along the south coast of Iceland and is a requirement for automobilists willing to reach Þórsmörk, a much popular recreational area nestled between the Mýrdalsjökull, Eyjafjallajökull, and Tindfjallajökull glaciers.

2.2. Öræfi district

The region bears it name — Öræfi (the "Waste land") — from the 1362 CE eruption of Öræfajökull Volcano and the resulting floods, which devastated most of the inhabited areas (Thorarinsson, 1958).

These floods are likely to have caused, in combination with ash fall, the death of about 300 individuals (Thorarinsson, 1958). Floods due to the other historical eruption of Öræfajökull, in 1727 CE, are known to have caused three fatalities (Gudmundsson *et al.*, 2008).

Numerical simulations performed by Helgadóttir *et al.* (2015) indicate that a large portion of the district, ~350 km^2 of land, is at risk of flooding should an eruption of Öræfajökull volcano occur (Figure VI-3). Using thresholds in flow velocities and depths of flooding, alongside considerations on debris and water temperature, Pagneux and Roberts (2015) have proposed to rate flood hazard therein as high or extreme, exclusively.

The district hosts now the main service centre of the Vatnajökull National Park. Located in Skaftafell, west from the volcano, the centre is safe from floods due to eruptions of Öræfajökull (Figure VI-3) but is exposed to significant tephra fall, as can be inferred from the position of the 20-cm tephra isopach of the 1362 CE eruption (Thorarinsson, 1958).

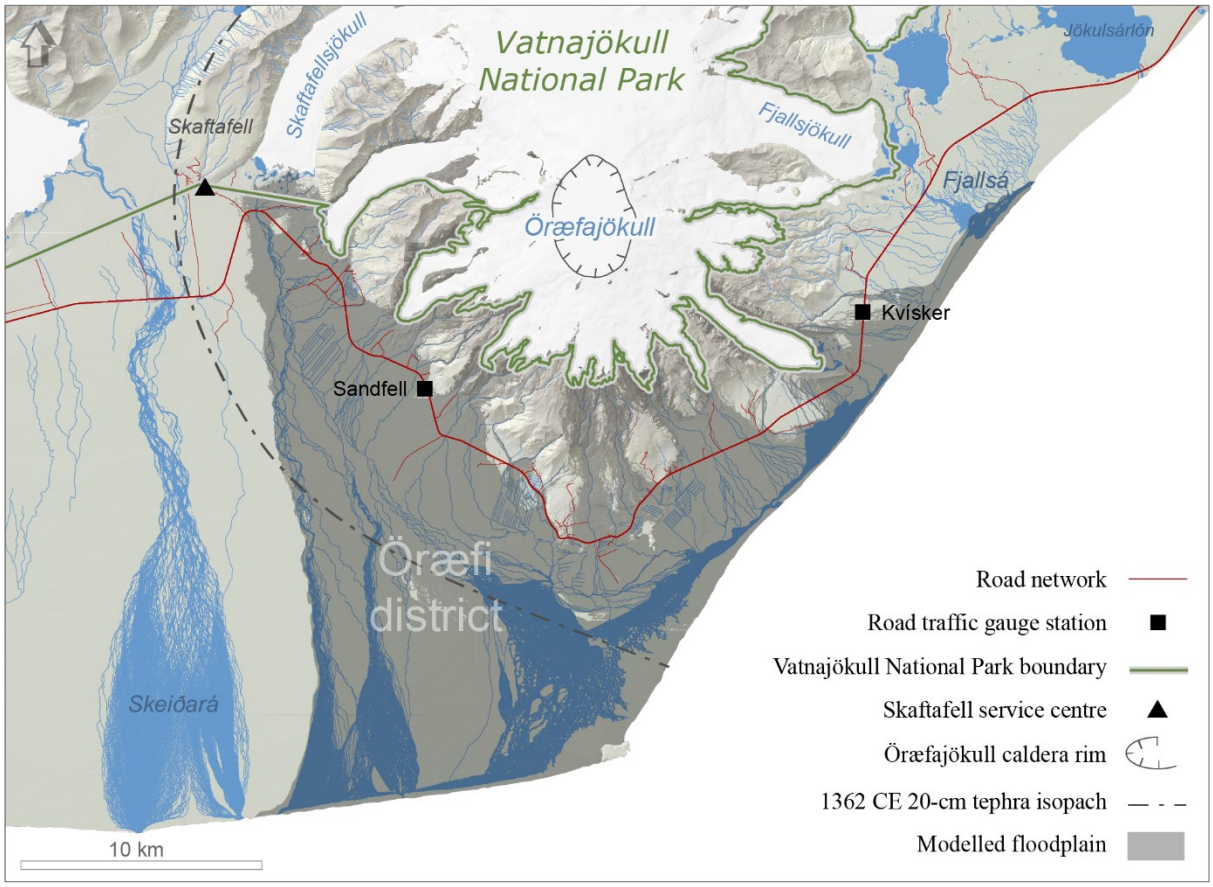

Figure VI-3: Öræfi district. The floodplain extends on ~350 km^2 of land (Helgadóttir et al., 2015). The district hosts the main service centre of the Vatnajökull National Park, located at Skaftafell, west from the volcano.

3. Methods

3.1. Populations targeted

The population was classified into residents and transient population. Transient population potentially includes the non-resident population staying overnight at given locations on a temporary basis: guests at accommodation premises, seasonal workers on worksites, people in institutional or community facilities (e.g. students in boarding schools) and public assembly structures, as well as owners and guests in secondary residences (summerhouses). Registered residents include in some cases

seasonal workers who have declared themselves as residing on their worksite.

3.2. Data sources

Data on residents were extracted from the Population Register (Table VI-1). Data on transient population were obtained from various sources, including indoor accommodation premises, camping sites, local authorities, the Icelandic Road and Coastal Administration, and Statistics Iceland, over the period 2007–2012.

3.3. Temporal analysis

Multiple scales can be used in the identification of temporal patterns. One can look for instance at month-over-month variations, interdaily variations, make a distinction between working days and weekends (Liu *et al.*, 2010) or holidays (Camarasa-Belmonte *et al.*, 2011), or between summer and winter. At a finer scale of analysis, it is also sensible to identify circadian variations in exposure, making a distinction between daytime and night time (Camarasa Belmonte *et al.*, 2011), as well as changes throughout the day on an hourly basis (Liu *et al.*, 2010).

In this study, focus of the temporal analysis was set on the assessment of seasonal patterns due to tourist activities. A distinction was also made between day time (8 a.m.–8 p.m.) and night time (8 p.m.–8 a.m.) but the analysis was restricted, for feasibility reasons, to the assessment of night-time exposure, using daily overnight estimates as an indicator.

An assessment of daytime exposure would suffer, in the two study areas, of the lack of data to work with. In the last 15 years, data collection mainly concerned the Skaftafell natural site (e.g. Sæþórsdóttir *et al.*, 2001) and was framed to be used in tourism management or conservation perspectives. Though an effort has been engaged recently on surveying other sites, such as Jökulsárlón in the Öræfi district (Guðmundsson, 2014), yet acquisition of quantitative data at a precision and a time scale relevant for disaster risk management is missing. In Skaftafell for instance, quantitative surveys conducted on a permanent basis rely on automated counters that make no distinction between ingoing and outgoing visitors, so a fair estimation of the number of visitors actually on site during daytime is not possible.

3.3.1. Constraints

Estimating daily overnights at accommodation premises, institutional and community facilities and secondary residences is much of a challenge.

An important constraint, to be added to potential deliberate misreporting, consists of the fact that premise managers are not obliged to transmit overnights figures to Statistics Iceland at a temporal resolution higher than monthly aggregates; in other words, the day-over-day variations are masked in the official statistics.

Another constraint is due to the fact that Statistics Iceland is not allowed to provide third parties with data about individual premises; data that can be delivered are aggregates showing only the types of establishment, each type covering at least five different premises. As premises of a same type may be distant to each other of tens of kilometres within the areas studied, and therefore exposed to floods in a different manner, one will easily understand that the level of temporal and spatial aggregation available at Statistics Iceland does not allow an analysis of exposure at a high spatio-temporal resolution. In addition, information is lacking on occasional overnights at institutional or community facilities, and overnights at secondary residences.

Table VI-1: Data sources.

Data	Source
Indoor accommodation capacity	Accommodation premises
Overnights at indoor accommodation premises	Accommodation premises
Overnights at camping sites	Camping sites
Overnights at institutional and community facilities	Local authorities
Regional occupation rates at accommodation premises	Statistics Iceland
Residents	Registers Iceland, Population Register
Road traffic	Iceland Road and Coastal Administration

3.3.2. Calculations

For what concerns overnights at residences, the maximum overnights were assumed to equal the number of residents registered and were therefore considered in the analysis a spatiotemporal constant.

Due to insufficient information, overnights at institutional and community facilities and at secondary residences were provisionally kept out of the calculations.

For what concerns overnights at accommodation premises, statistical and legal constraints were partly bypassed using a two-step approach. As a first step, mean daily overnights at each premise and for each month of the year were approximated by multiplying the mean daily regional occupation rate for indoor premises and the premise accommodation capacity:

$$\overline{O}(m,p) = \overline{Oc}(m) \cdot A(p),$$

Where $\overline{O}(m,p)$ is the mean daily overnight for given month m and given indoor accommodation premise p, $\overline{Oc}(m)$ is the mean daily regional occupation rate for given month m, and $A(p)$ is the accommodation capacity of indoor premise p.

Regional occupation rates applying for south Iceland (Table VI-2) were used for the estimation of overnights daily means in the Markarfljót outwash plain. For the premises located in the Öræfi district, regional occupation rates for east Iceland were used. In order to avoid overestimations, the opening period of each premise was taken into account in the calculations.

Since Statistics Iceland does not take in to account the camping sites in their calculation of regional occupation rates, the camping sites were encouraged to provide, as an addition, their own overnights figures.

As a second step, daily road traffic (Figure VI-4) was used as a proxy for calculating minimum and maximum daily overnights, for each premise and each month of the year, based on the assumption that daily overnights for both residents and transient population follow, throughout each month, variations that are close to daily road traffic.

Thus, daily variation rates were estimated from road traffic daily averages over the period 2007–2011 at relevant gauges stations in the two surveyed areas (Figure VI-2, Figure VI-3, Table VI-3), and applied to the overnight daily means in order to obtain weighted daily overnights from which monthly minima and maxima were eventually extracted:

$$Ow(d,m) = \overline{O}(m) \cdot Vtr(d),$$

Where $Ow(d,m)$ is the weighted overnight for given day d and month m, $\overline{O}(m)$ the overnight daily mean for given month m, and $Vtr(d,m)$ the road traffic variation rate for given day d and month m.

Table VI-2: Regional occupation rates (rounded %) at indoor accommodation premises over the period 2007–2011 (Source: Statistics Iceland). Strong seasonal patterns can be seen, with occupation rates jumping from ~5% in December–January to ~75% in July.

	Jan	Feb	Mar	Apr	May	Jun	Jul	Aug	Sep	Oct	Nov	Dec
Capacity 1–59 beds												
Austurland	6	7	10	11	19	45	75	69	24	11	6	4
Suðurland	4	8	10	13	19	37	58	50	20	17	8	5
Capacity 60+ beds												
Austurland	5	7	11	15	25	46	76	63	25	12	7	3
Suðurland	8	19	22	24	26	41	70	61	25	25	17	11

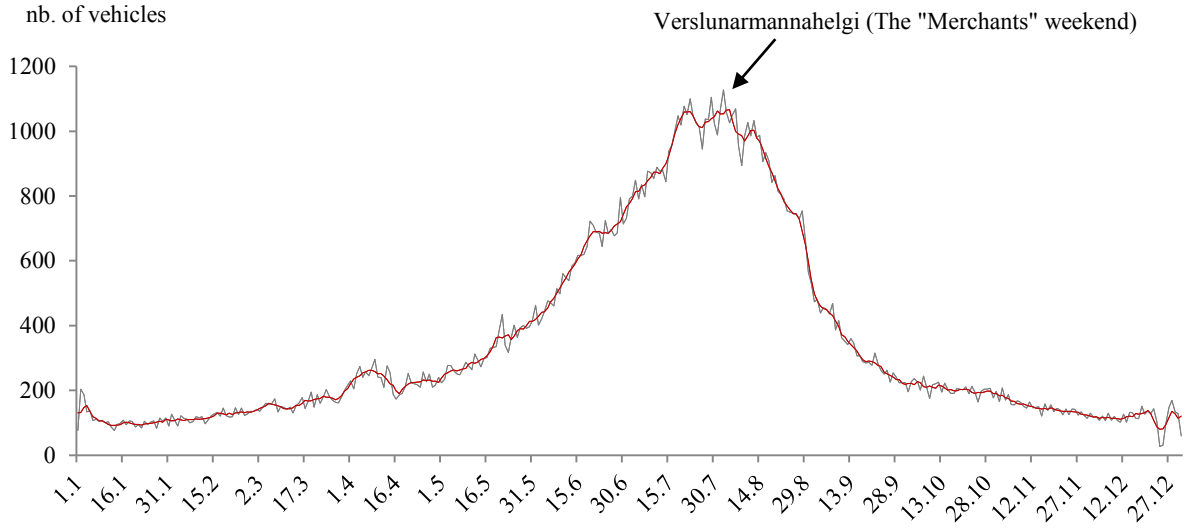

Figure VI-4: Road traffic daily averages at Sandfell gauge station, Öræfi district (2007–2011); 5-days moving averages are shown in red. The peaks in road traffic at the junction between July and August correspond to the "Merchants" weekend. Source: Iceland Road and Coastal Administration

Table VI-3: Gauging stations used to derive overnights estimates from road traffic. Source: Iceland Road and Coastal Administration.

Area surveyed	Gauge station	Lat	Long
Markarfljót outwash plain	Hvammur	63 34,689	-19 54,117
Öræfi district	Sandfell	63 56,327	-16 47,721

3.4. Spatial analysis

Estimation of overnights was limited to residences and premises located within a restricted area, herein labelled "extended flood hazard zone" (FHZ-X), which includes:

- The areas identified at risk of flooding in the simulations performed by Hólm and Kjaran (2005) and Helgadóttir *et al.* (2015), herein labelled FHZ-S;
- The manual additions to the FHZ-S made by Helgadóttir *et al.* (2015) and Pagneux

and Roberts (2015), herein labelled FHZ-M;

- The areas contiguous to the FHZ-S and FHZ-M that could be isolated - i.e. disconnected from the road network - should a flood happen, herein labelled FHZ-I.

Finally, estimates were plotted against the flood hazard rates computed by Pagneux and Roberts (2015).

4. Results

4.1. Residents

Based on the Population Register's 2012 figures, the number of residents in the Öræfi and Markarfljót Extended Flood Hazard Zones was estimated 86 and 1024, respectively.

4.2. Mean daily overnights at accommodation premises

The estimations based on accommodation capacity and regional occupation rates on one hand, on overnight figures transmitted by premise managers on the other, put a light on a strong seasonal pattern in exposure. Mean daily overnights jump from ~10 or less in January and December to ~250 and ~740 in the Öræfi and Markarfljót FHZ-Xs, respectively (Figure VI-5). The July peak represents increases of December-January figures by a factor 55 in the Öræfi FHZ-X and a factor 71 in the Markarfljót FHZ-X.

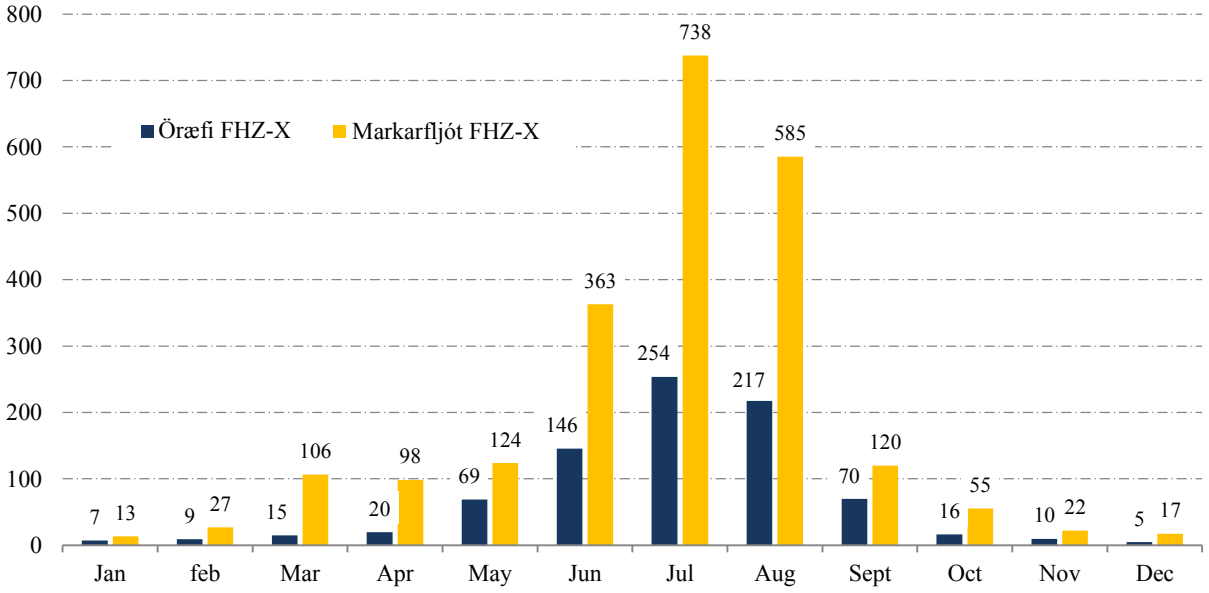

Figure VI-5: Mean daily overnights at accommodations premises in the Öræfi and Markarfljót Extended Flood Hazard Zones. For indoor accommodations, the estimates were derived from regional occupation rate and accommodation capacity. Estimation of overnights for camping sites was based on figures given by camping managers. Overnights at community facilities and summerhouses were not taken into account.

4.3. Correlation between road traffic and overnights

In the Öræfi district, overnight daily means including transient population and residents present monthly variations that are close to road traffic daily means (Figure VI-6, upper left). The correlation between month-over-month increase rates in road traffic and overnights is quite high (r^2=0.80).

Gaps can be seen between the curves during the spring and summer periods (Figure VI-6, bottom): In spring, the road traffic increases

faster than the overnights, which may be due to the fact that many premises remain closed. During the summer, in turn, the overnights increase faster than the road traffic, which may be explained by an increase in the number of passengers per vehicle. The correlation is poor from January to May (r^2=0.18) but excellent from June to December (r^2=0.96).

The all-year round correlation between month-over-month increase rates in road traffic and overnights is not as good in the Markarfljót outwash plain FHZ-X (r^2=0.65; Figure VI-7) as it is in the Öræfi district. The correlation is poor from January to May (r^2=0.03) but excellent from June to December (r^2=0.92). However, the assumption that road traffic and overnights follow similar variations looks solid enough in the studied areas and justifies therein a careful use of daily road traffic as a proxy for the estimation of minimum and maximum daily overnights for at least seven months of the year.

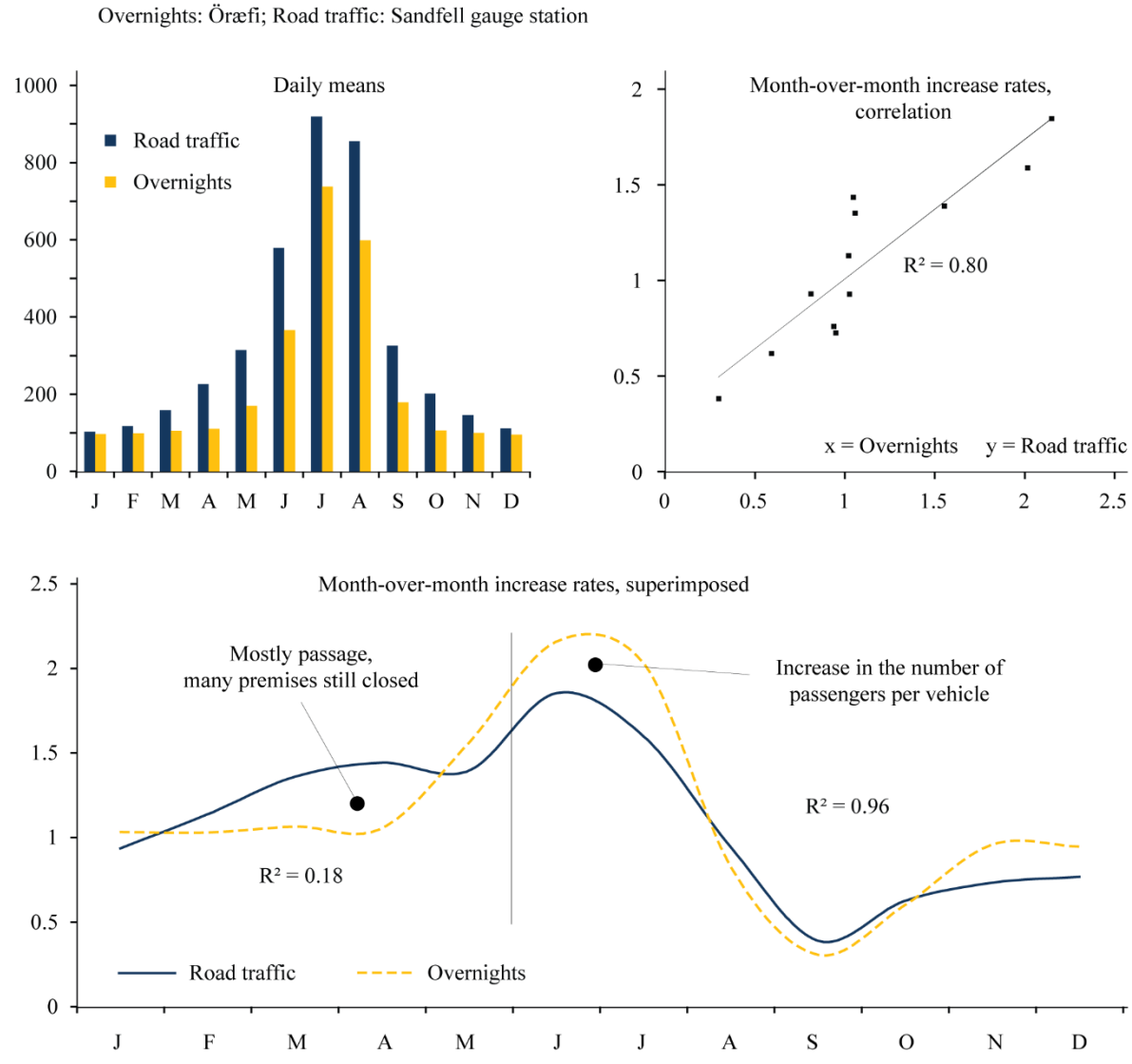

Figure VI-6: Mean daily figures for overnights in the Öræfi district (FHZ-X and surrounding settlements) and road traffic at the Sandfell gauge station (upper left) and how their respective month-over-month grow rates correlate to each other (upper right). Road traffic grows faster than overnights in spring, while overnights increase faster than road traffic during the summer (bottom).

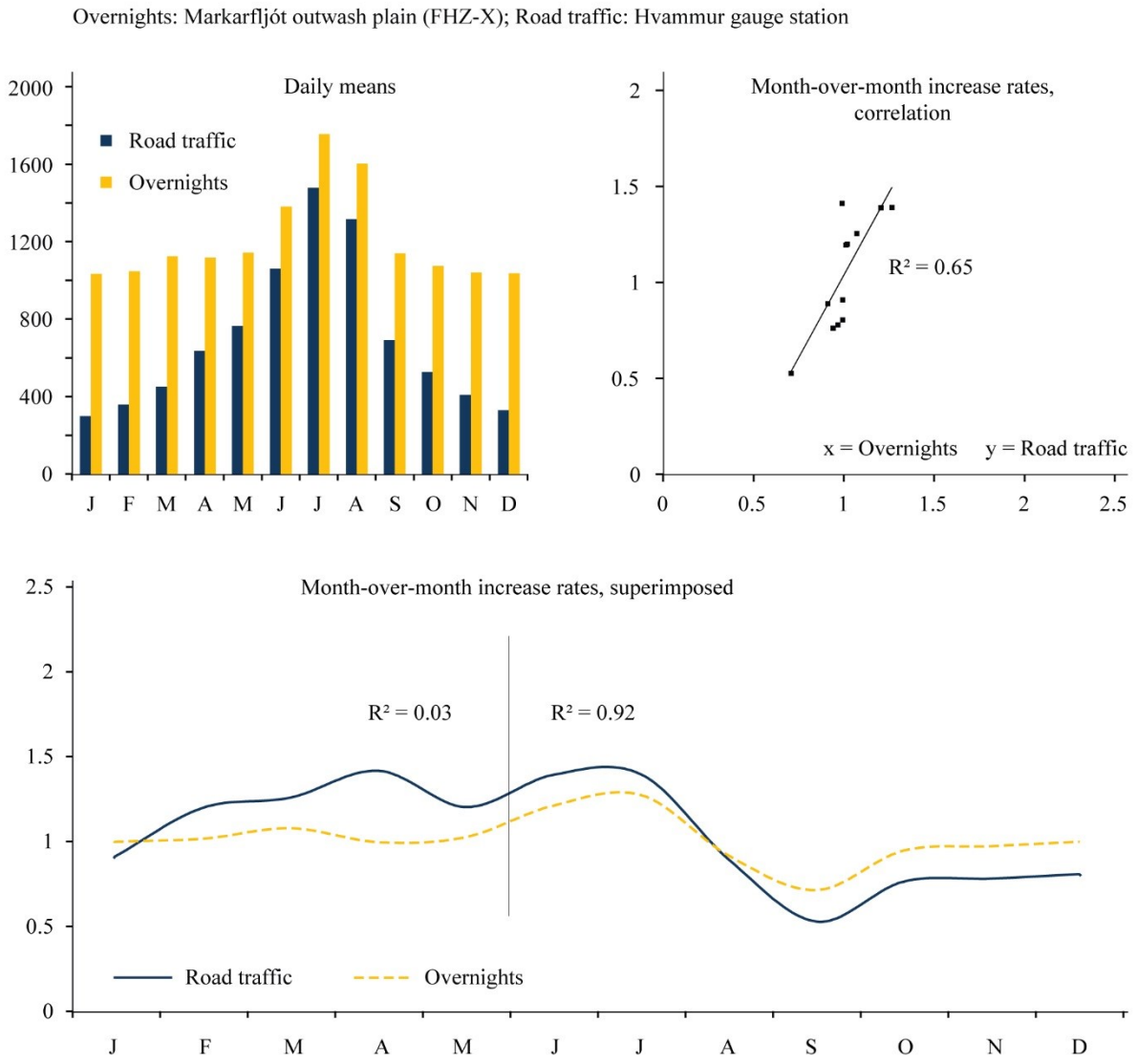

Figure VI-7: Mean daily figures for overnights in the Markarfljót outwash plain FHZ-X and road traffic at the Hvammur gauge station (upper left) and how their respective month-over-month grow rates correlate to each other (upper right).

4.4. Weighted overnights

Using road traffic as a weighting factor, daily maxima of ~370 and ~1760 overnights were found in the Öræfi and Markarfljót Extended Flood Hazard Zones, respectively (Figure VI-8, Figure VI-9). Figures in the Öræfi FHZ-X represent 45% of the daily maxima in the Öræfi district (FHZ-X and surrounding settlements), which were estimated to ~830 overnights using the same methodology.

Transient population represents a maximum of 77% of the overnights estimates in the Öræfi FHZ-X and 42% in the Markarfljót FHZ-X (Table VI-4), attained in August. The maximum daily overnights represent a maximum increase of the daily means of 22% and 9% respectively (Table VI-5).

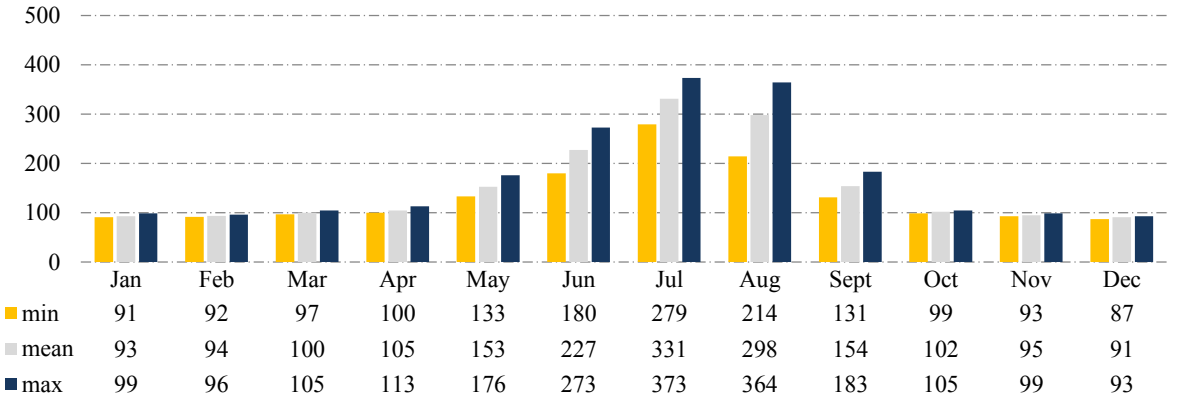

Figure VI-8: Daily overnights in the Öræfi Extended Flood Hazard Zone over the period 2007–2011. Daily road traffic was used to derive the minimum and maximum values for each month. The estimates include residents and transient population at accommodation premises (hotels, guest houses, camping sites, etc.).

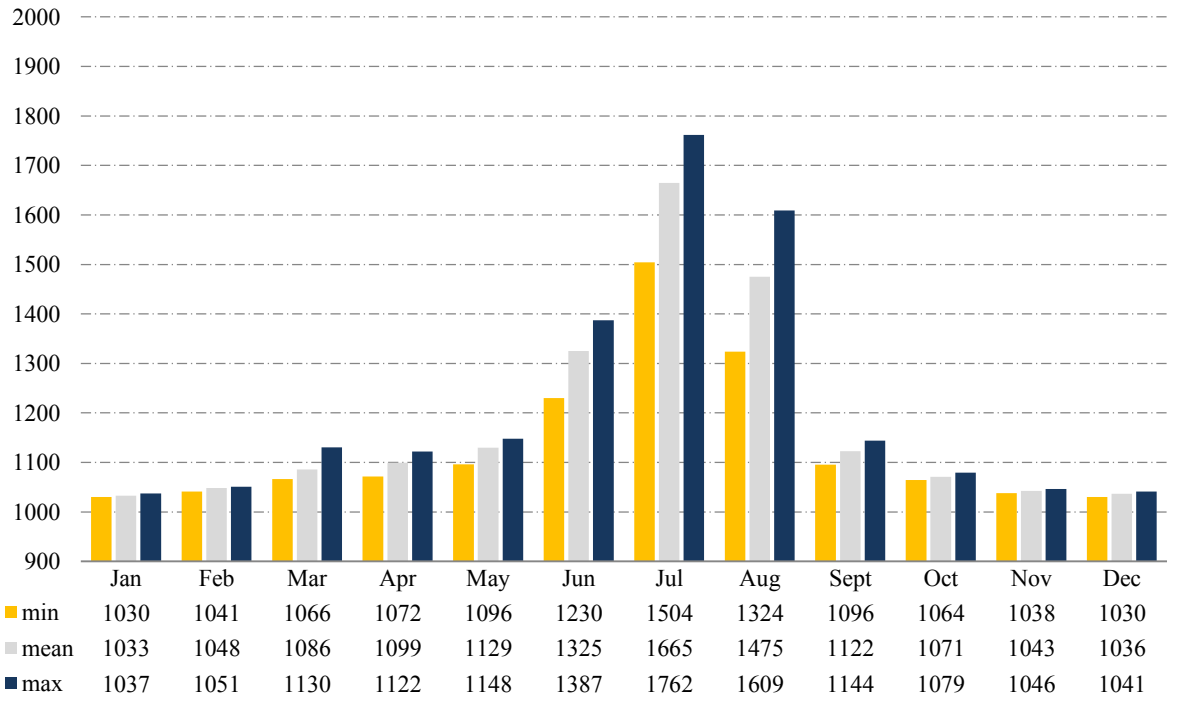

Figure VI-9: Daily overnights in the Markarfljót Extended Flood Hazard Zone over the period 2007–2011. Daily road traffic was used to derive the minimum and maximum values for each month. The estimates include residents and transient population at accommodation premises (hotels, guest houses, camping sites, etc.).

Table VI-4: Share (%) of transient population in overnights in the Öræfi and Markarfljót Extended Flood Hazard Zones (FHZ-X) over the period 2007–2011.

FHZ-X	Jan	Feb	Mar	Apr	May	Jun	Jul	Aug	Sept	Oct	Nov	Dec
Öræfi	13	10	18	24	51	68	77	76	53	18	13	8
Markarfljót	1	3	9	9	11	26	42	36	10	5	2	2

Table VI-5: Increase factor between maximum and mean daily overnight estimates.

FHZ-X	Jan	Feb	Mar	Apr	May	Jun	Jul	Aug	Sept	Oct	Nov	Dec
Öræfi	1.06	1.02	1.05	1.08	1.15	1.2	1.13	1.22	1.19	1.03	1.04	1.02
Markarfljót	1	1	1.04	1.02	1.02	1.05	1.06	1.09	1.02	1.01	1	1

4.5. Spatial distribution

4.5.1. Öræfi

A maximum of 135 overnights was found in the area identified at risk of flooding (FHZ-S), representing 36% of the maximum overnights estimates in the FHZ-X and ~20% of the transient population staying overnight therein (Table VI-6, Figure VI-10). Overnights in the high and extreme hazard zones were estimated to a maximum of ~20 and ~110 respectively (Table VI-7). A maximum of ~240 overnights was found in the FHZ-I (Table VI-8, Figure VI-10), mostly disseminated in the Svínafell (44%) and Hof (53%) settlements' clusters

Table VI-6: Maximum daily overnights in the Öræfi extended flood hazard zone (FHZ-X) and around.

Area	Residents		Guests		Overall	
	n	%	n	%	n	%
FHZ-I	65	*76*	177	*61*	242	*64*
FHZ-M	0	*0*	0	*0*	0	*0*
FHZ-S	21	*24*	114	*21*	135	*36*
FHZ-X	86	*100*	291	*100*	377	*100*
Other *	4		448		452	

* Skaftafell, Bölti, Kvísker

Table VI-7: Maximum daily overnights in the Öræfi flood hazard zone identified in the numerical simulations (FHZ-S).

Area	Flood hazard level	Residents		Guests		Overall	
		n	%	n	%	n	%
	Low	0	*0*	0	*0*	0	*0*
	Moderate	0	*0*	0	*0*	0	*0*
	High	12	*57*	11	*10*	23	*17*
	Extreme	9	*43*	103	*90*	112	*83*
FHZ-S		21	*100*	114	*100*	135	*100*

Table VI-8: Maximum daily overnights in the Öræfi FHZ-I.

Area	Sector	Residents		Guests		Overall	
		n	%	n	%	n	%
	Svínafell	16	*25*	79	*45*	95	*40*
	Hof, Litla Hof	17	*26*	98	*55*	114	*47*
	Other	32	*49*	0	*0*	32	*13*
FHZ-I		65	*100*	177	*100*	242	*100*

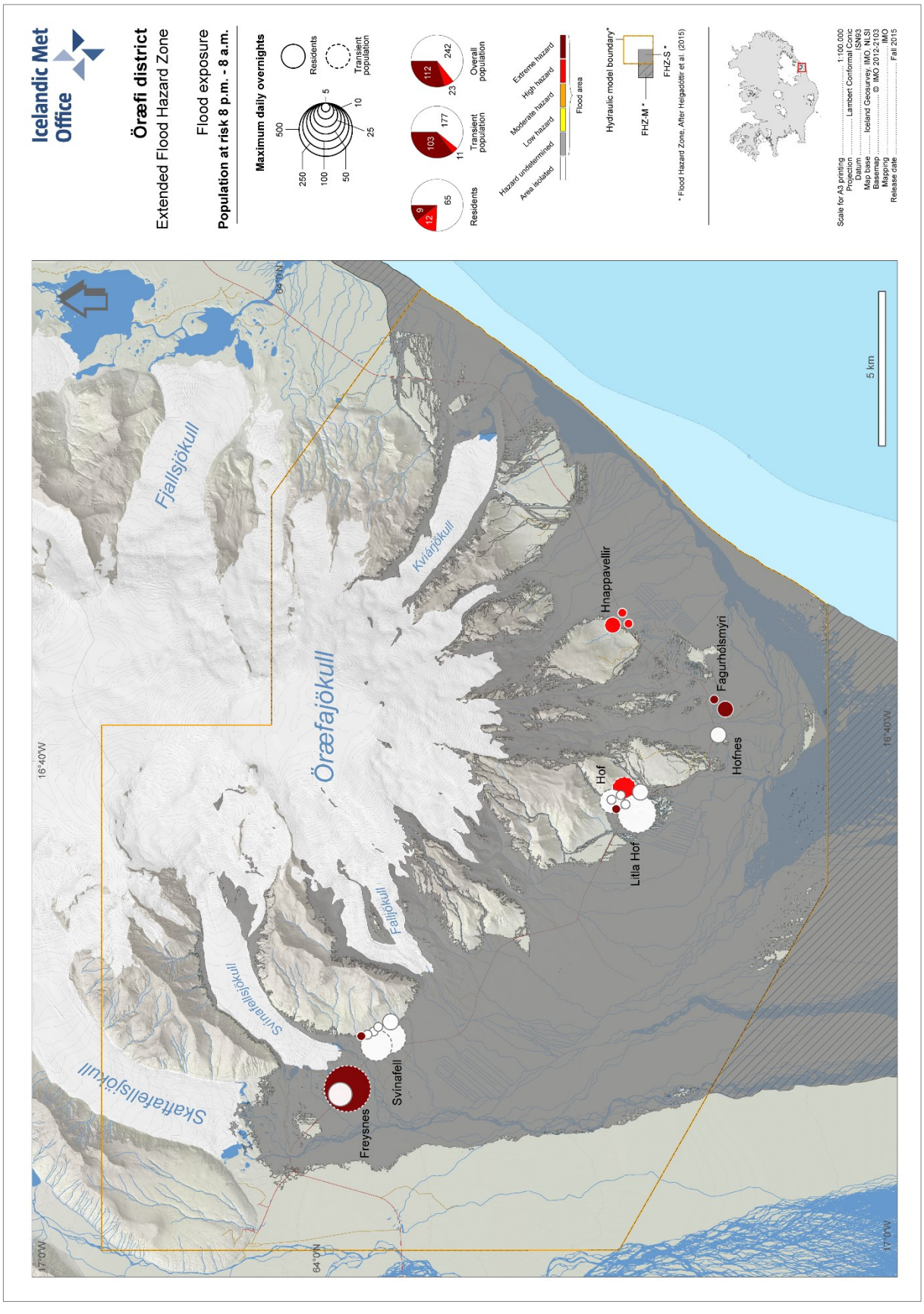

Figure VI-10: Maximum daily overnights in the Öræfi Extended Flood Hazard Zone (FHZ-X).

4.5.2. Markarfljót outwash plain

A maximum of ~1190 overnights was found in the area identified at risk of flooding (FHM-S and FHM-M), representing 80% of the residents and 50% of the transient population located in the FHZ-X (Table VI-9, Figure VI-11). Overnights in the high and extreme hazard zones proposed by Pagneux and Roberts (2015) were estimated to a maximum of ~475 and ~550 respectively (Table VI-10), i.e. 40% and 46% of the overnights in the flood area.

A maximum of ~580 overnights was found in the FHZ-I (Table VI-11), disseminated in the Fljótshlíð hillside (24%), the Þórsmörk recreational area (60%), and the north-western flank (4%) and south-western flank (12%) of Eyjafjallajökull Volcano.

Table VI-9: Maximum daily overnights in the Markarfljót extended flood hazard zone (FHZ-X).

Area	Residents		Guests		Overall	
	n	%	n	%	n	%
FHZ-I	204	*20*	372	*50*	576	*33*
FHZ-M	28	*3*	0	*0*	28	*2*
FHZ-S	792	*77*	366	*50*	1158	*66*
FHZ-X	1024	*100*	738	*100*	1762	*100*

Table VI-10: Maximum daily overnights in the Markarfljót flood area (FHM-S + FHM-M).

Area	Flood hazard level	Residents		Guests		Overall	
		n	%	n	%	n	%
FHZ-M		28	*3*	0	*0*	28	*2*
	Undetermined	28	*3*	0	*0*	28	*2*
FHZ-S		792	*97*	366	*50*	1158	*98*
	Low	49	*6*	0	*0*	49	*4*
	Moderate	22	*3*	62	*17*	84	*7*
	High	441	*54*	35	*10*	476	*40*
	Extreme	280	*34*	269	*73*	549	*46*
FHZ		820	*100*	366	*100*	1186	*100*

Table VI-11: Maximum daily overnights in the Markarfljót FHZ-I.

Area	Sector	Residents		Guests		Overall	
		n	%	n	%	n	%
	Fljótshlíð	121	*59*	20	*5*	141	*24*
	Þórsmörk	0	*0*	343	*92*	343	*60*
	North-western flank E15*	14	*7*	9	*2*	23	*4*
	South-western flank E15*	69	*34*	0	*0*	69	*12*
FHZ-I		204	*100*	372	*100*	576	*100*

* E15: Abreviation for Eyjafjallajökull

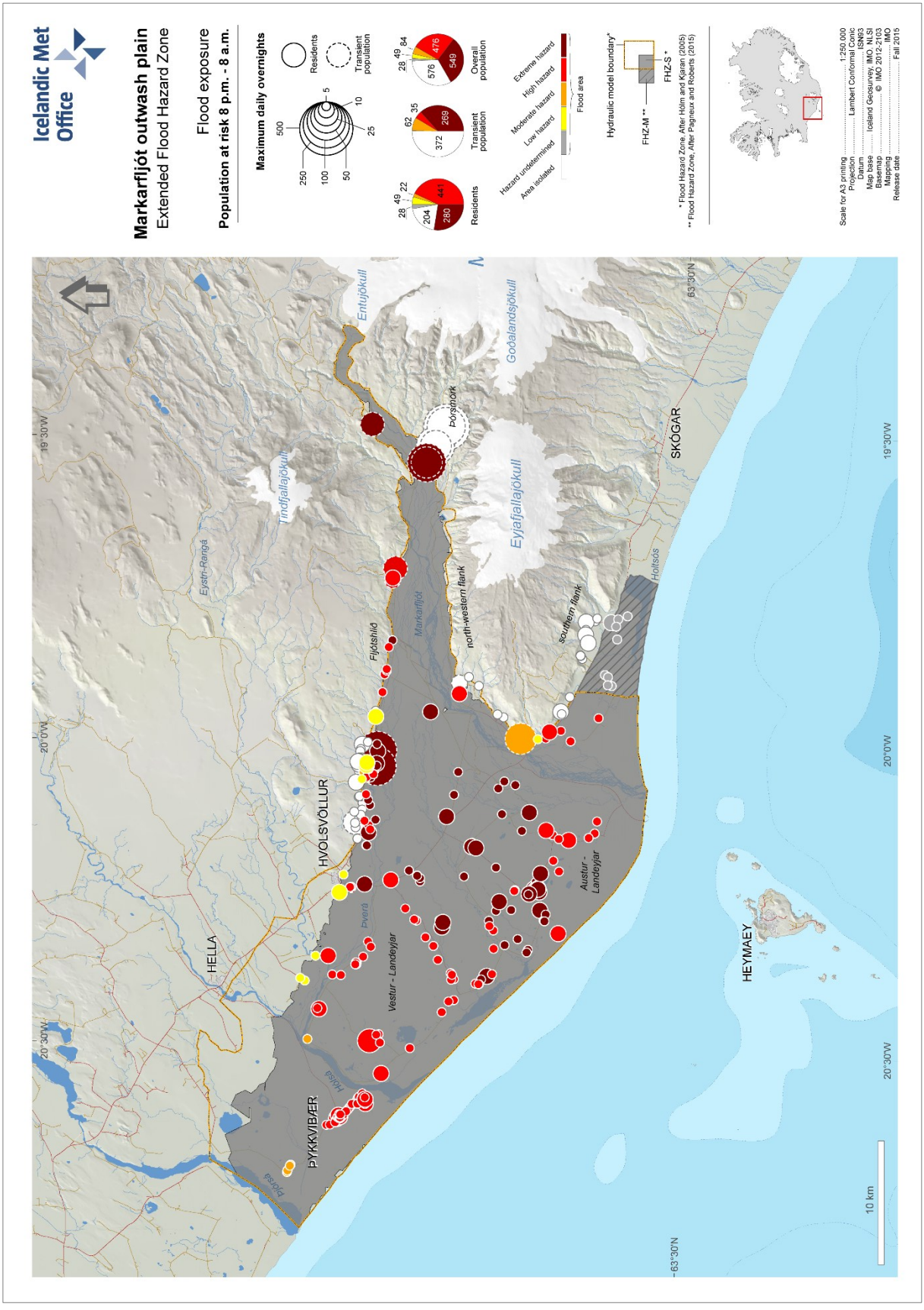

Figure VI-11: Maximum daily overnights in the Markarfljót extended flood hazard zone (FHZ-X).

5. Summary

A spatio-temporal characterisation of population exposure to floods was performed in the Markarfljót outwash plain and in the Öræfi district. The assessment consisted of an inventory of the populations — residents and transient population — exposed to floods during night time, using minimum and maximum daily overnights estimates as an indicator. Variations in daily road traffic were used as a proxy for the estimation of minimum and maximum daily overnights for each month of the year, based on the assumption that road traffic and overnights follow, in the two studied areas, similar variations.

The results indicate that exposure to floods in the two studied areas is subject to large seasonal changes. The July peak represents an increase of the December–January exposure minimum by a factor of 55 in the Öræfi district and a factor of 71 in the Markarfljót outwash plain.

A maximum of ~380 overnights was found in the Öræfi Extended Flood Hazard Zone, thereof ~135 overnights in the area identified at risk of flooding and ~245 overnights in the areas potentially isolated by floods (Figure VI-10):

- Overnights in areas potentially isolated are mostly disseminated in the Svínafell (44%) and Hof (53%) settlement clusters.
- Transients represent ~80% of the local population during the summer peak.
- Overnights in the high and extreme hazard zones proposed by Pagneux and Roberts (2015) were estimated to a maximum of ~20 and ~110, respectively.

A maximum of ~1760 overnights was found in the Markarfljót Extended Flood Hazard Zone, including ~1190 overnights in the area identified at risk of flooding and ~580 overnights in sectors potentially isolated (Figure VI-11):

- Overnights in areas potentially isolated are disseminated on the Fljótshlíð hillside (24%), the Þórsmörk recreational area (60%), and the western flank (4%) and southern flank (12%) of the Eyjafjallajökull volcano.
- Transients represent ~ 40% of the local population during the summer exposure peak.
- Overnights in the high and extreme hazard zones proposed by Pagneux and Roberts (2015) were estimated to a maximum of ~475 and ~550, respectively.

6. Recommendations

The night-time exposure figures do not account for overnights at secondary residences and at institutional or community facilities and, therefore, should be regarded as a low estimate. Caution is therefore advised in using the results, especially when it comes to make an assessment of the time available for evacuating areas exposed to volcanogenic floods, directly or indirectly.

An update of the estimations is recommended at a regular interval, e.g. every five years, such as to take into account changes in overnights at accommodation premises, whose capacity and number is likely to change in the coming years. Further research is needed on the integration of overnights at secondary residences and at institutional or community facilities, and on securing overnights at commercial accommodation premises. In that respect, changes in the rules and clauses of reporting overnights to the statistical authorities would certainly be helpful.

Further work is also needed that should focus on the characterisation of daytime exposure. Too little information is available as for now to be used in a direct or indirect counting effort. Should surveys or permanent monitoring of frequentation at visiting sites be performed in the future, it is crucial to have data collected in a way that is meaningful for the emergency response.

7. Acknowledgements

The author would like to thank Stéphanie Defossez and Tómas Jóhannesson for reviewing the chapter. Philippe Crochet is thanked for valuable feedback on methodological aspects during the framing of the research, as well as Ásdís Helgadóttir and Trausti Jónsson for proof-reading the chapter.

The present work was funded by the Icelandic Avalanche and Landslide Fund, the National Power Company, and the Icelandic Road and Coastal Administration.

8. References

Bird, D. K., Gísladóttir, G., & Dominey-Hoves, D. (2010). Volcanic risk and tourism in southern Iceland: Implications for hazard, risk and emergency response education and training. *Journal of Volcanology and Geothermal Research, 189*, 33–48.

Bird, D. K., Gísladóttir, G., & Dominey-Howes, D. (2009). Resident perception of volcanic hazards and evacuation procedures. *Nat. Hazards Earth Syst. Sci., 9*, 251–266.

Camarasa Belmonte, A. M., Soriano-García, J., & López-García, M. (2011). Mapping temporally-variable exposure to flooding in small Mediterranean basins using land-use indicators. *Applied Geography, 31*, 136–145.

Chakraborty, J., Tobin, G., & Montz, B. (2005). Population evacuation: Assessing spatial variability in geophysical risk and social vulnerability to natural hazards. *Nat. Hazards Rev., 6*(1), 23–33.

European Parliament, & Council. (2007). Directive 2007/60/EC of the European Parliament and of the Council of 23 October 2007 on the assessment and management of flood risks. *Official Journal L288*, 27–34. Retrieved from http://eur-lex.europa.eu/legal-content/EN/TXT/PDF/?uri=CELEX:32007L0060&from=EN

Gaillard, J. C., d'Ercole, R., & Leone, F. (2001). Cartography of population vulnerability to volcanic hazards and lahars of Mount Pinatubo (Philippines): A case study in Pasig-Potrero River basin (Province of Pampanga). *Géomorphologie: Relief, processus, environ-nement, 3*, 209–222.

Gudmundsson, M. T., Larsen, G., Höskuldsson, Á., & Gylfason, Á. G. (2008). Volcanic hazards in Iceland. *Jökull*, 58, 251–258.

Guðmundsson, R. (2014). *Vatnajökulsþjóðgarður. Ferðamenn 2005-2013 (Vatnajökull National Park. Tourists 2005-2013).* Report.

Helgadóttir, Á., Pagneux, E., Roberts, M. J., Jensen, E. H., & Gíslason, E. (2015). Öræfajökull Volcano: Numerical simulations of eruption-induced jökulhlaups using the SAMOS flow model. In E. Pagneux, M. T. Gudmundsson, S. Karlsdóttir, & M. J. Roberts (Eds.), *Volcanogenic floods in Iceland: An assessment of hazards and risks at Öræfajökull and on the Markarfljót outwash plain* (pp. 73–100). Reykjavík: IMO, IES-UI, NCIP-DCPEM.

Hólm, S. L., & Kjaran, S. P. (2005). Reiknilíkan fyrir útbreiðslu hlaupa úr Entujökli (Hydraulic model of floods from Entujökull). In M. T. Guðmundsson, & Á. G. Gylfason (Eds.), *Hættumat vegna eldgosa og hlaupa frá vestanverðum Mýrdalsjökli og Eyjafjallajökli (Hazard assessment of volcanic eruptions and glacial outbursts for Eyjafjallajökull and the western outwash plain of Mýrdalsjökull)* (pp. 197–210). Reykjavík: National Commissioner of Police.

Larsen, G., Smith, K., Newton, A., & Knudsen, Ó. (2005). Jökulhlaup til vesturs frá Mýrdalsjökli: Ummerki um forsöguleg hlaup niður Markarfljót. In M. T. Guðmundsson, & Á. G. Gylfason (Eds.), *Hættumat vegna eldgosa og hlaupa frá vestanverðum Mýrdalsjökli og Eyjafjallajökli* (pp. 75–98). Reykjavík: National Commissioner of Police.

Leone, F., Colas, A., Garcin, Y., Eckert, N., Jomelli, V., & Gherardi, M. (2014). The snow avalanches risk on Alpine roads network. Assessment of impacts and mapping of accessibility loss. *Journal of Alpine Research, 102*(4).

Leone, F., Peroche, M., Lagahe, E., Gherardi, M., Sahal, A., Vinet, F., Hachim, S., and Lavigne, F. (2013). Modélisation de l'accessibilité territoriale pour l'aide à la gestion de crise tsunami (Mayotte, Océan Indien, France). *Annales de Géographie, 693*, 502–524.

Liu, Y., Okada, N., Shen, D., & Kajitani, Y. (2010). Development of flood exposure map considering dynamics of urban life. *Annuals of disas. Prev. Res. Inst., 53*(B).

McGuire, L., Ford, E., & Okoro, C. (2007). Natural disasters and older US adults with disabilities: implications for evacuation. *Disasters*, 49–56.

Óskarsdóttir, S. M. (2005). *Kortlagning jökulhlaups úr Gígjökli vegna eldsumbrota í Eyjafjallajökli 1821–23 (Mapping of jökulhlaups from Gígjökull glacier due to the 1821-23 eruption of Eyjafjallajökull Volcano).* Reykjavík: University of Iceland.

Pagneux, E. (2015). Öræfajökull: Evacuation time modelling of areas prone to volcanogenic floods. In E. Pagneux, M. T. Gudmundsson, S. Karlsdóttir, & M. J. Roberts (Eds.), *Volcanogenic floods in Iceland: An assessment of hazards and risks at Öræfajökull and on the Markarfljót outwash plain* (pp. 141–164). Reykjavík: IMO, IES-UI, NCIP-DCPEM.

Pagneux, E., & Roberts, M. J. (2015). Öræfi district and Markarfljót outwash plain: Rating of flood hazards. In E. Pagneux, M. T. Gudmundsson, S. Karlsdóttir, & M. J. Roberts (Eds.), *Volcanogenic floods in Iceland: An assessment of hazards and risks at Öræfajökull and on the Markarfljót outwash plain* (pp. 101–122). Reykjavík: IMO, IES-UI, NCIP-DCPEM.

Scaini, C., Felpeto, A., Martí, J., & Carniel, R. (2014). A GIS-based methodology for the estimation of potential volcanic damage and its application to Tenerife Island, Spain. *Journal of Volcanology and Geothermal Research, 278-279*, 40–58.

Snorrason, Á., Einarsson, B., Pagneux, E., Hardardóttir, J., Roberts, M., Sigurðsson, O., Thórarinsson, Ó., Crochet, P., Jóhannesson, T., and Thorsteinsson, T. (2012). Floods in Iceland. In Z. W. Kundzewicz (Ed.), *Changes in flood risk in Europe* (pp. 257–276). IAHS Special Publication 10.

Sæþórsdóttir, A., Gísladóttir, G., Ólafsson, A., Sigurjónsson, B., & Aradóttir, B. (2001). *Þolmörk ferðamennsku í þjórgarðinum í Skaftafelli (Tolerance limit to tourism in Skaftafell).* Report, Reykjavík.

Thorarinsson, S. (1958). The Öræfajökull eruption of 1362. *Acta Naturalia Islandica, 2*(4), 100.

Wisner, B., Blaikie, P., Cannon, T., & Davis, I. (2004). *At risk: Natural Hazards, People's Vulnerability and Disasters* (2nd ed.). New York: Routledge.

Wood, N., & Soulard, C. (2009). Variations in population exposure and sensitivity to lahar hazards from Mount Rainier, Washington. *Journal of Volcanology and Geothermal Research*, 367–378.

VII. ÖRÆFAJÖKULL: EVACUATION TIME MODELLING OF AREAS PRONE TO VOLCANOGENIC FLOODS

Emmanuel Pagneux *

* *Icelandic Meteorological Office*

1. Introduction

In this study, modelling of the time available at eruption onset and of the time required for a full evacuation of areas exposed to floods due to eruptive activity of Öræfajökull Volcano is realised and evacuation routes identified.

The aim of the study is to provide the authorities in charge of the emergency response — primarily the Department of Civil Protection and Emergency Management of the National Commissioner of the Icelandic Police and the local authorities — with baseline figures for the development of an effective flood evacuation plan. When evacuation should be ordered and to which extent it should be done are key considerations laying in the background of the study. It is likely that any eruption of the volcano will be foreseen days in advance. Using seismic stations, the imminence of a volcanic eruption can be fairly approached through the detection of changes in the rate of occurrence of volcano-tectonic earthquakes and the formation of harmonic tremor, considered both seismic precursors of volcanic activity (Zobin, 2011). Assuming that eruption onset will be clearly and immediately established through detection of volcanic tremor (e.g. Vogfjörd *et al.*, 2005), the main question of interest for the emergency response is of the time available and of the time required for evacuation upon signal detection. It may be mentioned that hesitation of the authorities to order an early evacuation of the Colombian cities of Armero and Chinchina during the 1985 Nevado Del Ruiz eruption resulted in the deaths of 25,000 individuals, buried in the body of high-velocity lahars (Voight, 1990; Mileti *et al.,* 1991).

1.1. Study area

Öræfajökull is an ice-capped stratovolcano located in south-east Iceland that dominates and threatens the Öræfi district (Figure VII-1). The district is delimited to the West by the Skeiðará river and to the East by the Fjallsá river (Figure VII-2).

The volcano erupted on two occasions in historical times. The first known historical eruption occurred in 1362 CE. The eruption was highly explosive, reaching VEI 6 (Gudmundsson *et al.*, 2008), and caused massive floods on the western slopes of the volcano and in the adjacent lowland (Thorarinsson, 1958; Roberts and Gudmundsson, 2015). The ash fall and floods together resulted in the death of ~300 individuals (Thorarinsson, 1958). Following the 1362 CE eruption, the Öræfi district remained mostly uninhabited for centuries, which probably explains that the second eruption, in 1727 CE, resulted in only three fatalities, although causing floods of magnitude comparable to those of 1362 CE (Thorarinsson, 1958; Roberts and Gudmundsson, 2015).

The Öræfi district now hosts the main service centre of the Vatnajökull National Park and attracts thousands of tourists during the summer seasonal high. Estimations on night-time exposure (Pagneux, 2015) suggest a maximum of ~830 individuals staying overnight in the district, thereof 130 in the area identified at risk of flooding in the hydraulic simulations performed by Helgadóttir *et al.* (2015) and 240 in areas potentially isolated by the simulated floods.

The hydraulic simulations performed by Helgadóttir *et al.* (2015) build upon melting scenarios elaborated by Gudmundsson *et al.* (2015). Three sources of melting were considered in the scenarios: eruption in the caldera, eruptions on the flanks of the volcano, and the formation of pyroclastic density currents (PDC). The numerical simulations were performed as instant release waves flowing at the surface of the glacier using 0.05 and 0.10 $sm^{-1/3}$ average Manning roughness coefficients. Results on the extent of floods suggest that 347 km^2 of land are at risk of flooding, thereof 284 km^2 exposed to floods caused by a caldera eruption, flank eruptions, or pyroclastic density currents (Figure VII-2), 42 km^2 to floods caused by flank eruptions or pyroclastic density currents, and 21 km^2 to floods caused by pyroclastic density currents only. From the lower boundary of the release areas down to the National road, the minimum flood travel times found ranged 6 – 21 minutes.

Using thresholds in computed depths of flooding and flow velocities on one hand, considering the presence of life-threatening debris and temperature of floodwater on the other, Pagneux and Roberts (2015) have proposed to rate flood hazards in the area identified at risk of flooding as high or extreme exclusively. High hazard means that all lives are in jeopardy, outside and inside inhabited buildings. Extreme hazard means that jökulhlaups have the potential to destroy completely non-reinforced buildings and cause damage to reinforced concrete dwellings to a degree that would require demolition in the recovery phase.

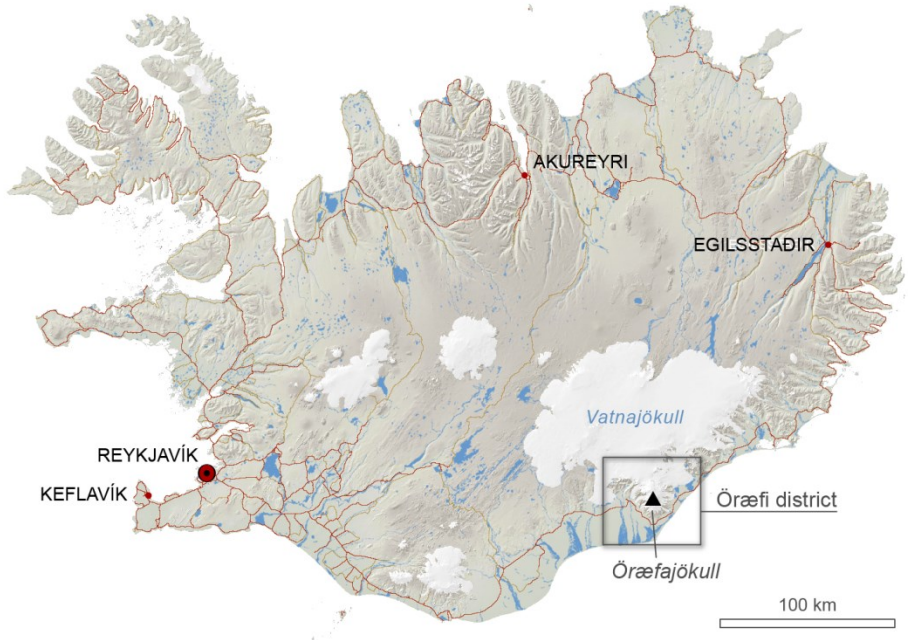

Figure VII-1: Location of the Öræfajökull ice-capped stratovolcano.

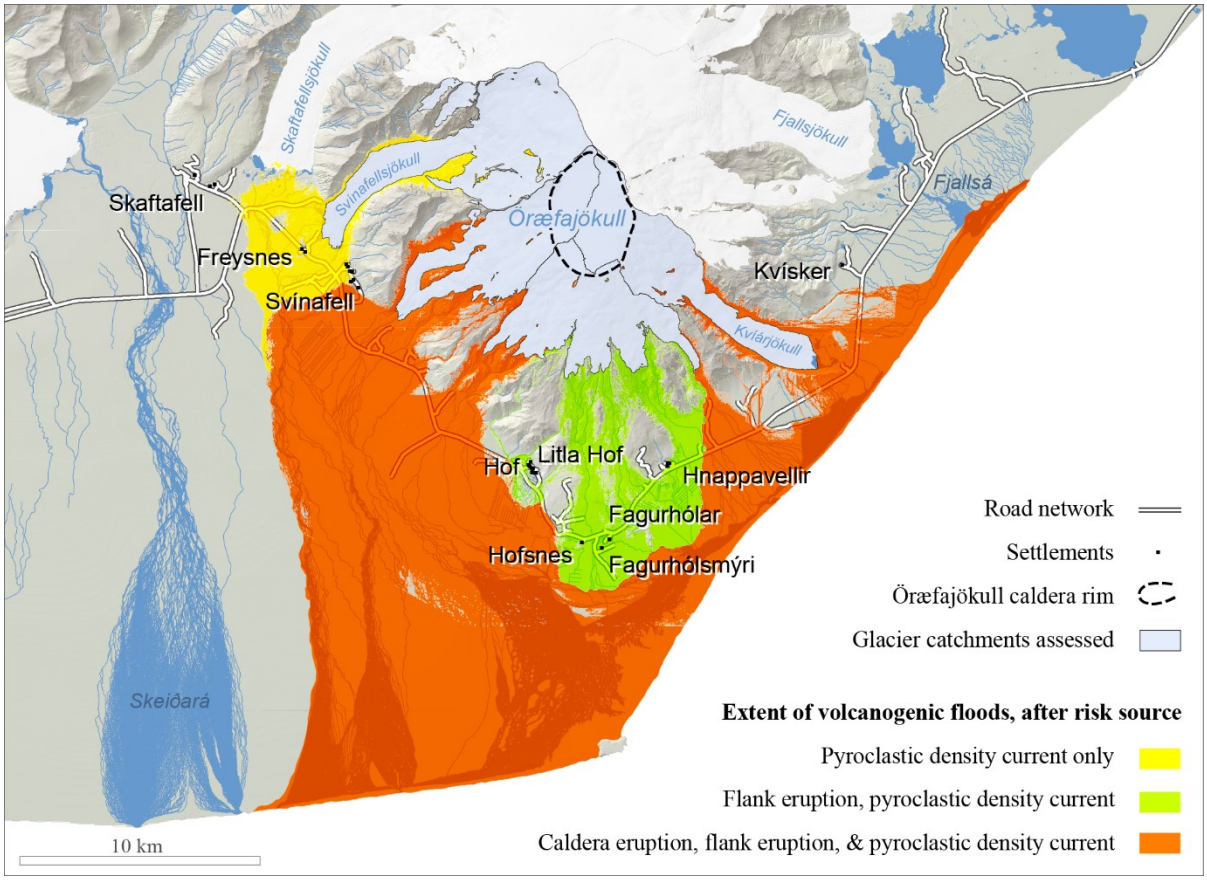

Figure VII-2: Inundation extent of scenario-based floods caused by volcanic activity of Öræfajökull volcano. Taken from Helgadóttir et al., 2015.

2. Available time for evacuation

In this study, the time available until the National road gets flooded was used as an expression of the time available for evacuation.

Estimations were made at the onset of volcanic eruptions initiated in the caldera or on the flanks of the volcano, as well as at onset of pyroclastic density currents. The melting scenarios proposed by Gudmundsson *et al.* (2015), and the results of the numerical simulations performed accordingly by Helgadóttir *et al.* (2015) were used for the estimations.

Available time in the case of floods caused by a caldera eruption (AT_{ce}) was estimated as the sum of minimum eruption onset time (EOT_{min}), minimum subglacial flood transport time ($SbTT_{min}$), and minimum transport times at onset of supraglacial flows on the volcano flanks ($SpTT_{min}$):

$$AT_{ce} = EOT_{min} + SbTT_{min} + SpTT_{min}$$

Available time in the case of floods caused by flank eruptions (AT_{fe}) was estimated as the sum of minimum eruption onset time (EOT_{min}) and minimum transport times at onset of supraglacial flows ($SpTT_{min}$):

$$AT_{fe} = EOT_{min} + SpTT_{min}$$

Available time in the case of floods caused by the formation of pyroclastic density currents (AT_{pdc}) was estimated as the sum of minimum PDC onset time (POT_{min}) and minimum transport times at onset of supraglacial flows ($SpTT_{min}$):

$$AT_{pdc} = POT_{min} + SpTT_{min}$$

The minimum subglacial flood transport time expresses the minimum time that floodwater spends migrating under the ice, on its way from the caldera eruption site to the point, on the glaciated slopes of the volcano, where the outburst is expected to turn from a pure subglacial event into a dominant supraglacial flood (Figure VII-3), and therefore does not account for the possible retention of melting water in the caldera before flood release.

The use of subglacial flow transport time was not required for the estimation of the time available for evacuation in scenarios where floods are caused by flank eruptions and the formation of pyroclastic density currents, as meltwater has its origin at the glacier's surface (Figure VII-3).

The time available at onset of the supraglacial flows ($SpTT_{min}$) was determined using the minimum surface transport times estimated by Helgadóttir *et al.* (2015) at predefined peak discharge ($SrTT_{Q_{max}}$) along with estimations of:

i. The time elapsed from the onset of supraglacial flows until the maximum discharge is reached ($t_{Q_{max}}$);
ii. The transport times at intermediate discharge ($SrTT_{Q_1}$);
iii. The time elapsed from the onset of floods until intermediary discharge (t_{Q_1}) is reached.

When $SrTT_{Q_1}$ was known or could be inferred, the minimum time effectively available at onset of any supraglacial flow was defined as

$$SpTT_{min} = \min\{SpTT_{Q_1}; SpTT_{Q_{max}}\},$$

where $SpTT_{Q_1} = SrTT_{Q_1} + t_{Q_1}$ and
$SpPT_{Q_{max}} = SrTT_{Q_{max}} + t_{Q_{max}}$

When $SrTT_{Q_1}$ could not be estimated, definition of the minimum time effectively available at onset of supraglacial flows was reduced to

$$SpTT_{min} = SpTT_{Q_{max}}$$

For each risk source (caldera eruption, flank eruption and PDC formation), the value of t_Q was determined using rising rates in the form of $Q = xt$ (where Q is discharge and t the time from onset of supraglacial flow).

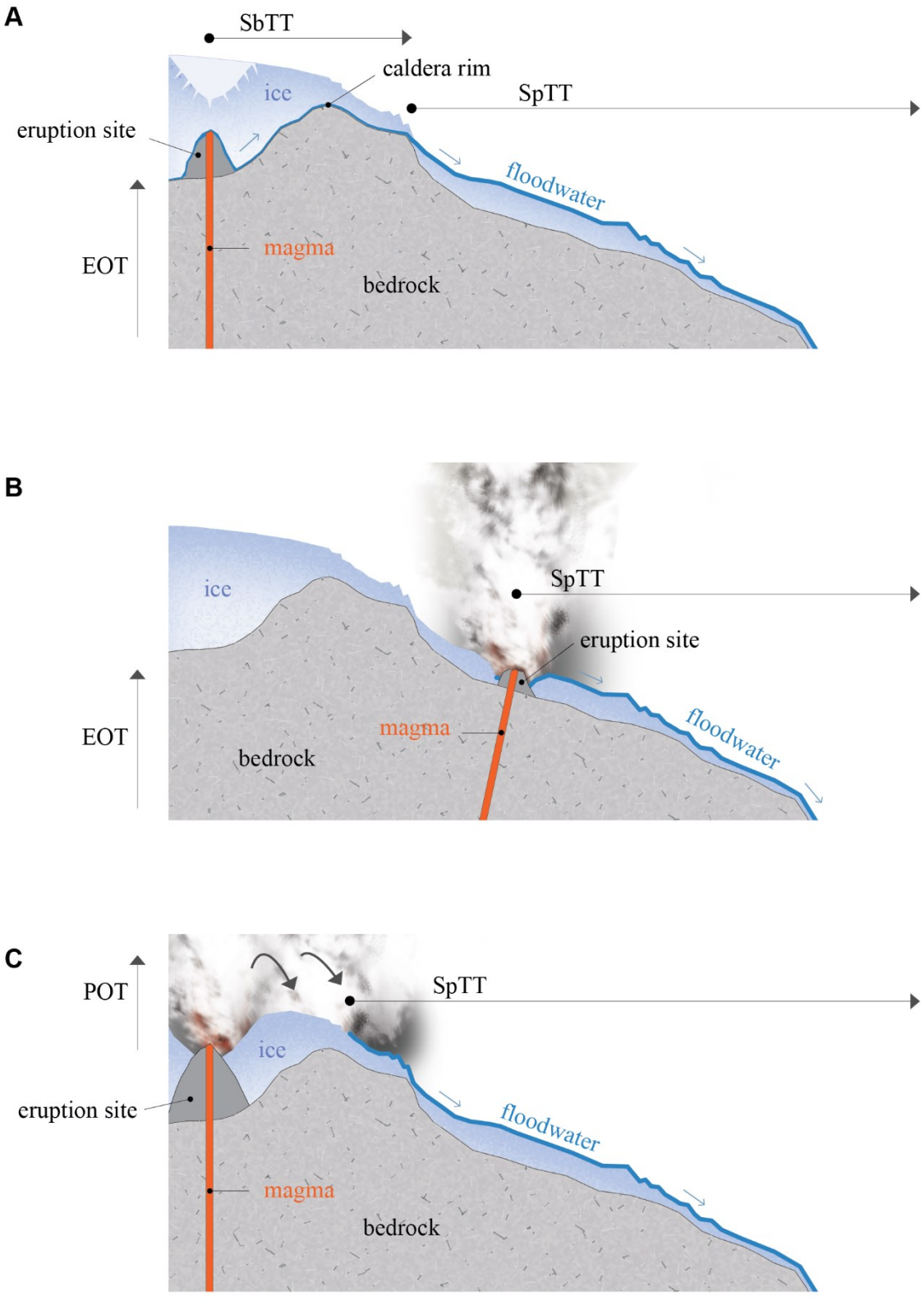

Figure VII-3: Schematic representation of the time sequences defining the time available for evacuation in the case of jökulhlaups caused by a caldera eruption (A), flank eruptions (B), and the formation of pyroclastic density currents (C). EOT: Eruption onset time; SbTT: Subglacial flow transport time; SpTT: transport time at onset of supraglacial flow; POT: Onset time of pyroclastic density current.

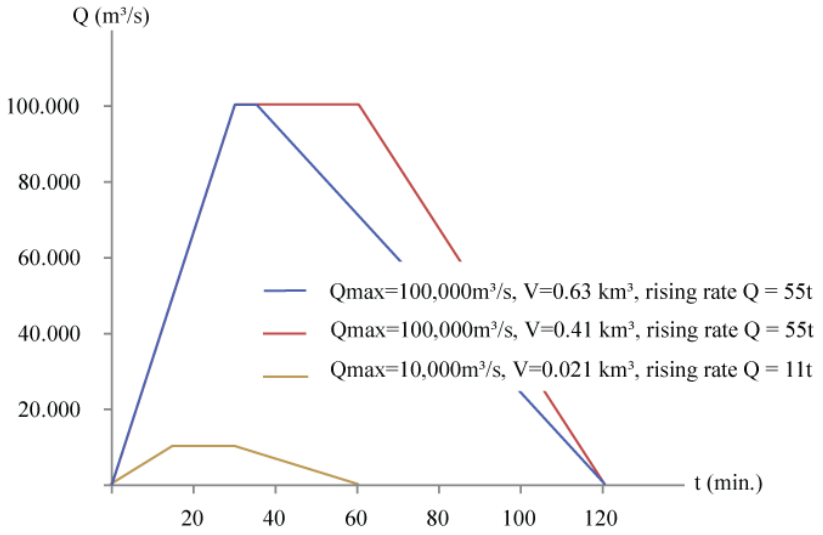

Figure VII-4: Plausible hydrographs for jökulhlaups caused by an eruption of Öræfajökull Volcano (After Gudmundsson et al., 2015). Rising rate in the concentration phase is approximated as $Q = 55t$ for catastrophic floods and $Q = 11t$ for moderate floods (Where Q is discharge and t the time from onset of supraglacial flow).

2.1. At onset of a caldera eruption

2.1.1. Eruption onset time and subglacial transport time

Gudmundsson *et al.* (2015) suggest for a caldera eruption minimum eruption onset time and minimum subglacial flood transport time of 15 and five minutes, respectively.

2.1.2. Available time at onset of supraglacial flow

There is little evidence to support the choice of a particular rising rate. Using inferences from Alaska and Iceland, Gudmundsson *et al.* (2015) suggest for catastrophic floods caused by caldera eruptions of Öræfajökull Volcano an approximate rising rate in the form of $Q = 55t$ (Figure VII-4). At such a rate, $Q_{max} = 100{,}000\ m^3/s$ is reached within 30 minutes from the onset of the flow at the glacier's surface.

Simulations of supraglacial floodwater released in the Virkisjökull - Falljökull drainage area at discharge $Q_1 = 10{,}000\ m^3/s$ and $Q_{max} = 100{,}000\ m^3/s$ alternatively (Helgadóttir *et al.*, 2015) indicate that surface transport times at discharge Q_1 represent a 2.06 increase of the transport times at discharge Q_{max}:

$$SrTT_{Q_1} = 2.06 \cdot SrTT_{Q_{max}}$$

If we assume, in every glacier catchment assessed, a rising rate $Q = 55t$ and a 2.06 increase factor in transport time between a 10,000 m^3/s discharge and a 100,000 m^3/s discharge, we find $SpTT_{Q_1}$ to be smaller than $SpTT_{Q_{max}}$ (Table VII-1):

If $Q = 55t$, $SrTT_{Q_1} = 2.06 \cdot SrTT_{Q_{max}}$, and $SpTT_{Q_1} = SrTT_{Q_1} + t_{Q_1}$

therefore $SpTT_{Q_1} < SpTT_{Q_{max}}$

As a consequence, if the rising rate is in the form of $Q = 55t$, we find $SpTT_{Q_1}$ to be a better approximation of $SpTT_{min}$ than $SpTT_{Q_{max}}$ is:

$$SpTT_{min} = SpTT_{Q_1}$$

Should in turn the maximum discharge be attained at the onset of the supraglacial flows ($t_{Q_{max}} = 0$), $SpTT_{Q_{max}}$ would be the equivalent of $SpTT_{min}$:

$$SpTT_{min} = SpTT_{Q_{max}}.$$

Table VII-1: Values of $SpTT_Q$ at discharge $Q_1 = 10{,}000m^3/s$ and $Q_{max} = 100{,}000m^3/s$ using as assumptions an increase time ratio $SrTT_{Q_1} = 2.06 \cdot SrTT_{Q_{max}}$ and a rising rate $Q = 55t$.

Glacier catchment	Discharge Q (m^3/s)	Manning n ($sm^{-1/3}$)	t_Q (min.)	$SrTT_Q$ (min.)	$SpTT_Q$ (min.)
Falljökull – Virkisjökull	10,000	0.05	3	14	**17**
		0.1		31	**34**
	100,000	0.05	30	7	37
		0.1		15	45
Kotárjökull	10,000	0.05	3	12	**15**
		0.1		27	**30**
	100,000	0.05	30	6	36
		0.1		13	43
Kvíarjökull	10,000	0.05	3	19	**22**
		0.1		41	**44**
	100,000	0.05	30	9	39
		0.1		20	50

Table VII-2: Values of $SpTT_Q$ at discharge $Q_{max} = 100{,}000m^3/s$, using $t_{Q_{max}} = 0$ as an assumption (peak discharge attained at onset of supraglacial flow).

Glacier catchment	Discharge Q (m^3/s)	Manning n ($sm^{-1/3}$)	t_Q (min.)	$SrTT_Q$ (min.)	$SpTT_Q$ (min.)
Falljökull – Virkisjökull	100,000	0.05	0	7	**7**
		0.1		15	**15**
Kotárjökull	100,000	0.05	0	6	**6**
		0.1		13	**13**
Kvíarjökull	100,000	0.05	0	9	**9**
		0.1		20	**20**

2.1.3. Computed evacuation time

Results of the calculations indicate that at onset of a caldera eruption, the minimum time available before the National road gets flooded is 26 – 29 minutes using $t_{Q_{max}} = 0$ (Figure VII-5, Figure VII-8) and 35 – 42 minutes using rising rate $Q = 55t$ (Figure VII-6, Figure VII-8).

	Manning n	EOT	SbTT	SpTT	AT
Kvíarjökull	0.10	15	5	20	**40**
	0.05	15	5	9	**29**
Kotárjökull	0.10	15	5	13	**33**
	0.05	15	5	6	**26**
Falljökull - Virkisjökull	0.10	15	5	15	**35**
	0.05	15	5	7	**27**

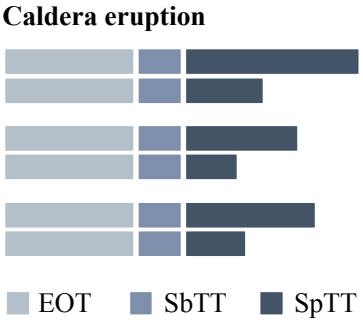

Figure VII-5: Available time at onset of a caldera eruption (AT_{ce}), before floodwater reaches the National road. $AT_{ce} = EOT_{min} + SbTT_{min} + SpTT_{min}$. Maximum discharge attained at onset of supraglacial flow ($t_{Q_{max}} = 0$) is used an assumption.

	Manning n	EOT	SbTT	SpTT	AT
Kvíarjökull	0.10	15	5	44	**64**
	0.05	15	5	22	**42**
Kotárjökull	0.10	15	5	30	**50**
	0.05	15	5	15	**35**
Falljökull - Virkisjökull	0.10	15	5	34	**54**
	0.05	15	5	17	**37**

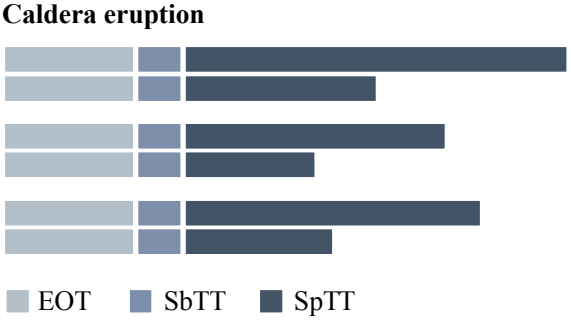

Figure VII-6: Available time at onset of a caldera eruption (AT_{ce}), before floodwater reaches the National road. $AT_{ce} = EOT_{min} + SbTT_{min} + SpTT_{min}$. An increase time ratio $SrTT_{Q_1} = 2.06 \cdot SrTT_{Q_{max}}$ and a rising rate $Q = 55t$ are used as assumptions.

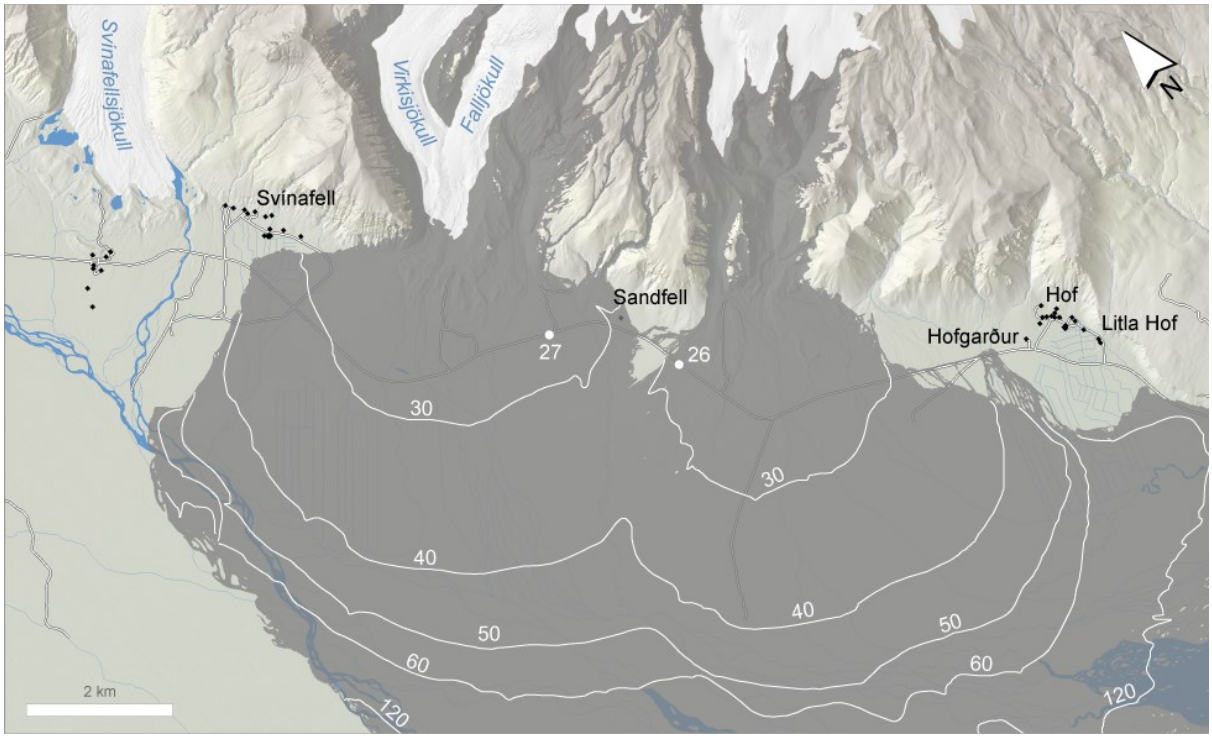

Figure VII-7: Minimum time available for evacuation (10-min isochrones) should a caldera eruption cause floods flowing down in the Falljökull – Virkisjökull and Kotárjökull drainage areas. Maximum discharge attained at onset of supraglacial flow ($t_{Q_{max}} = 0$) is used as an assumption. Inundation extent in the proglacial area is shown as a grey overlay.

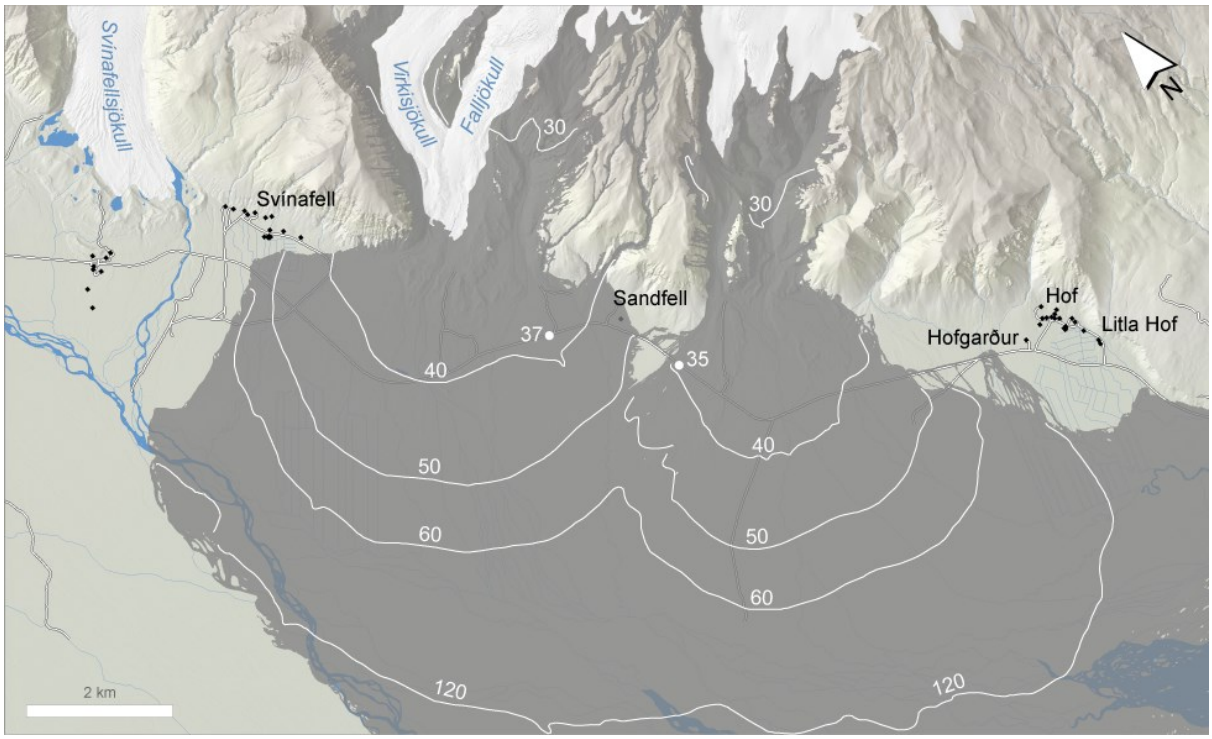

Figure VII-8: Minimum time available for evacuation (10-min isochrones) should a caldera eruption cause floods flowing down in the Falljökull – Virkisjökull and Kotárjökull drainage areas. An increase time ratio $SrTT_{Q_1} = 2.06 \cdot SrTT_{Q_{max}}$ and a rising rate $Q = 55t$ are used as assumptions. Inundation extent in the proglacial area is shown as a grey overlay.

2.2. At onset of flank eruptions

As for an eruption taking place in the caldera, Gudmundsson *et al.* (2015) suggest for flank eruptions a minimum eruption onset time (EOT_{min}) of 15 minutes.

Available time at onset of supraglacial flow was estimated using alternatively $t_{Q_{max}}$= 0 min. and $t_{Q_{max}}$ = 15 min. (approximate rising rate $Q = 11t$, see Figure VII-4).

As a comparison between $SpTT_{Q_{max}}$ and $SpTT_{Q_1}$ could not be performed, $SpTT_{Q_{max}}$ was considered the equivalent of $SpTT_{min}$ when $Q = 11t$ was used.

Results of the calculations indicate that at onset of a flank eruption, the minimum time available before the National road gets flooded is 19 – 32 minutes using $t_{Q_{max}}$= 0 (Figure VII-9, Figure VII-11) and 34 – 47 minutes using rising rate $Q = 11t$ (Figure VII-10, Figure VII-12).

	Manning n	EOT	SpTT	AT
Stígárjökull	0.10	15	9	**24**
	0.05	15	4	**19**
Kvíarjökull	0.10	15	39	**54**
	0.05	15	17	**32**
Kotárjökull	0.10	15	13	**28**
	0.05	15	6	**21**
Falljökull - Virkisjökull	0.10	15	18	**33**
	0.05	15	8	**23**

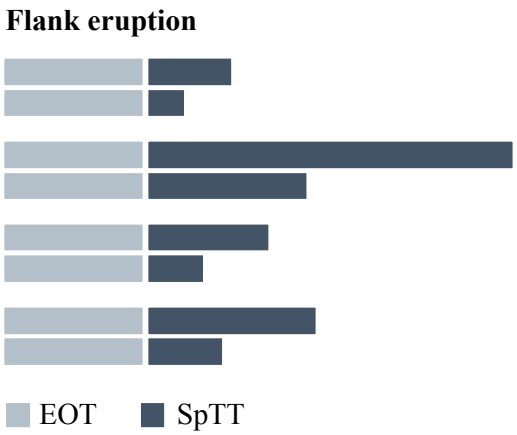

Figure VII-9: Available time at onset of a flank eruption (AT_{fe}) before floodwater reaches the National road. $AT_{fe} = EOT_{min} + SpTT_{min}$. Maximum discharge attained at onset of supraglacial flow ($t_{Q_{max}} = 0$) is used as an assumption.

	Manning n	EOT	SpTT	AT
Stígárjökull	0.10	15	24	**39**
	0.05	15	19	**34**
Kvíarjökull	0.10	15	54	**69**
	0.05	15	32	**47**
Kotárjökull	0.10	15	28	**43**
	0.05	15	21	**36**
Falljökull - Virkisjökull	0.10	15	33	**48**
	0.05	15	23	**38**

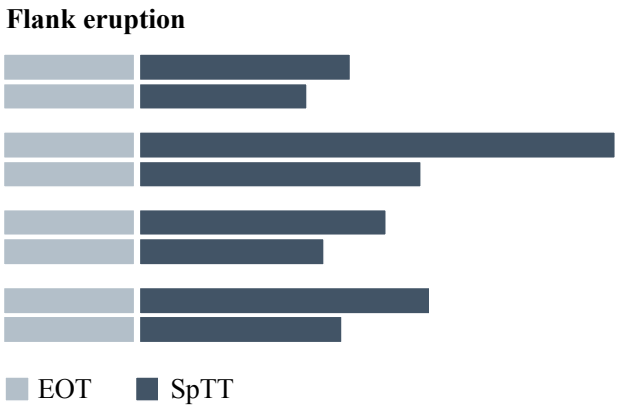

Figure VII-10: Available time at onset of a flank eruption (AT_{fe}) before floodwater reaches the National road. $AT_{fe} = EOT_{min} + SpTT_{min}$. A rising rate $Q = 11t$ is used as an assumption.

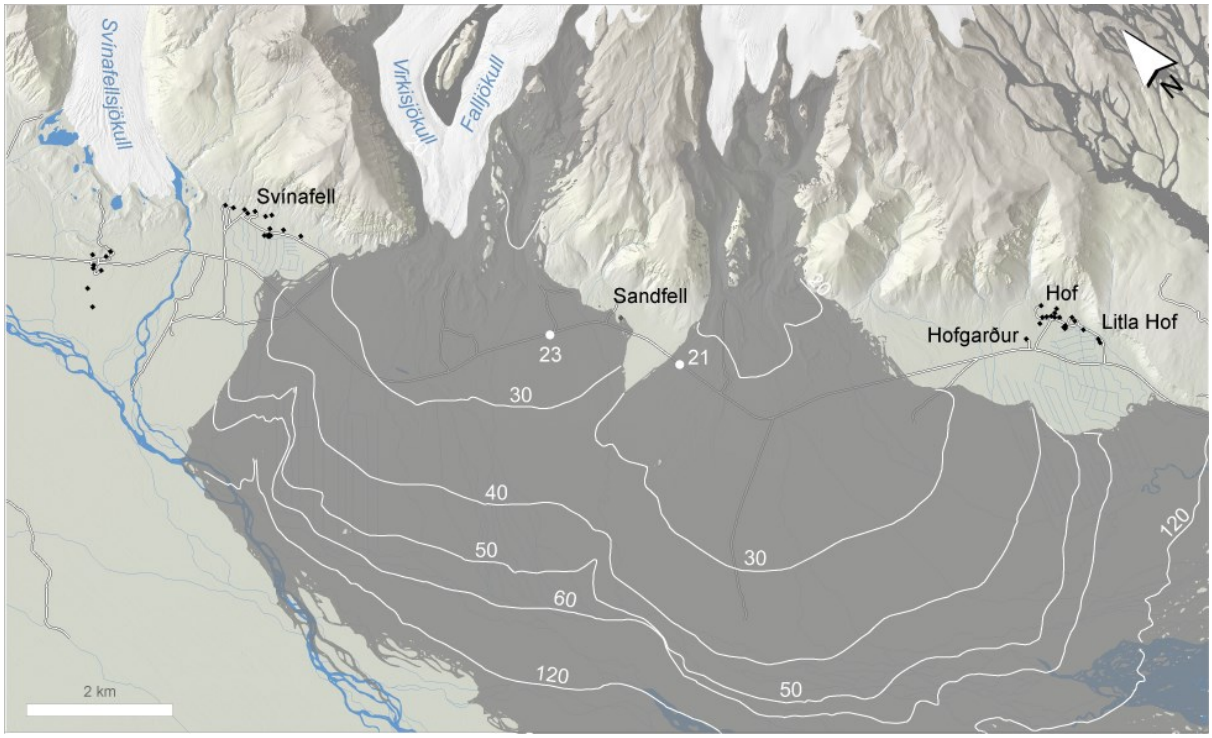

Figure VII-11: Minimum time available for evacuation (10-min isochrones) should a flank eruption cause floods in the Falljökull – Virkisjökull and Kotárjökull drainage areas. Maximum discharge attained at onset of supraglacial flow ($t_{Q_{max}} = 0$) is used as an assumption. Inundation extent in the proglacial area is shown as a grey overlay.

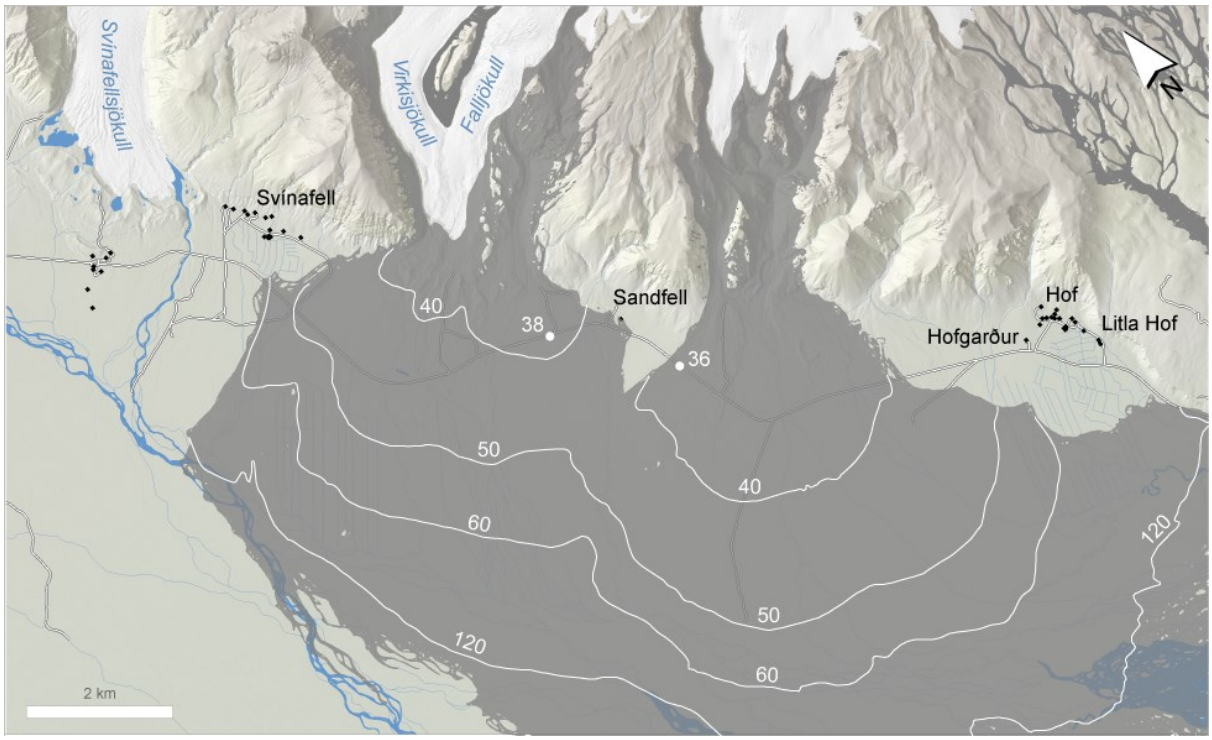

Figure VII-12: Minimum time available for evacuation (10-min isochrones) should a flank eruption cause floods in the Falljökull – Virkisjökull and Kotárjökull drainage areas. Rising rate $Q = 11t$ is used as an assumption. Inundation extent in the proglacial area is shown as a grey overlay.

2.3. At onset of pyroclastic density currents

The value of POT_{min} was fixed to 5 minutes (Gudmundsson *et al.*, 2015). Available time at onset of supraglacial flow was estimated using the assumption that all the meltwater is released instantaneously ($t_{Q_{max}}$= 0). As a consequence, $SpTT_{Q_{max}}$ was considered the equivalent of $SpTT_{min}$.

Results of the calculations indicate that the national road is cut by floodwater within a minimum of 13 minutes by Hnappavellir, on the southern slopes of Öræfajökull Volcano (Suðurhlíðar) (Figure VII-13, Figure VII-14), and 26 minutes by Freysnes, at the foot of Svínafellsjökull Glacier (Figure VII-13, Figure VII-15).

	Manning n	POT	SpTT	**AT**
Svínafellsjökull	0.10	05	51	**56**
	0.05	05	21	**26**
Suðurhlíðar	0.10	05	19	**24**
	0.05	05	08	**13**

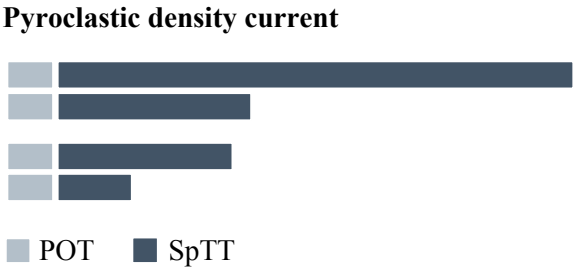

Figure VII-13: Available time at onset of a pyroclastic density current (AT_{pdc}) before floodwater reaches the National road. $AT_{pdc} = POT_{min} + SpTT_{min}$, where POT_{min} is the estimated PDC onset time (Gudmundsson et al., 2015) and $SpTT_{min}$ the minimum flood travel times at the glacier surface and on proglacial terrains for Manning n roughness coefficients 0.05 and 0.10 (Helgadóttir et al., 2015).

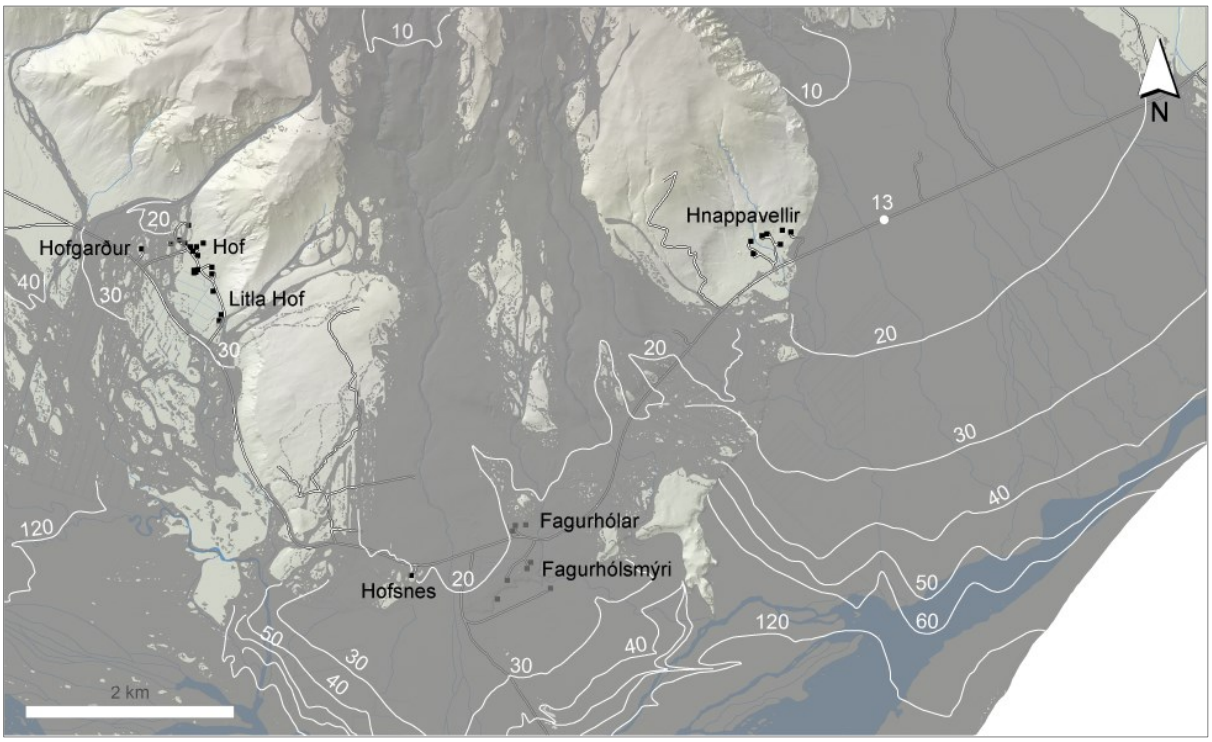

Figure VII-14: Minimum time available for evacuation (10-min isochrones) should a pyroclastic flow density current cause a flood on the southern slopes of Öræfajökull Volcano. Maximum discharge attained at onset of supraglacial flow ($t_{Q_{max}} = 0$) is used as an assumption. Inundation extent in the proglacial area is shown as a grey overlay.

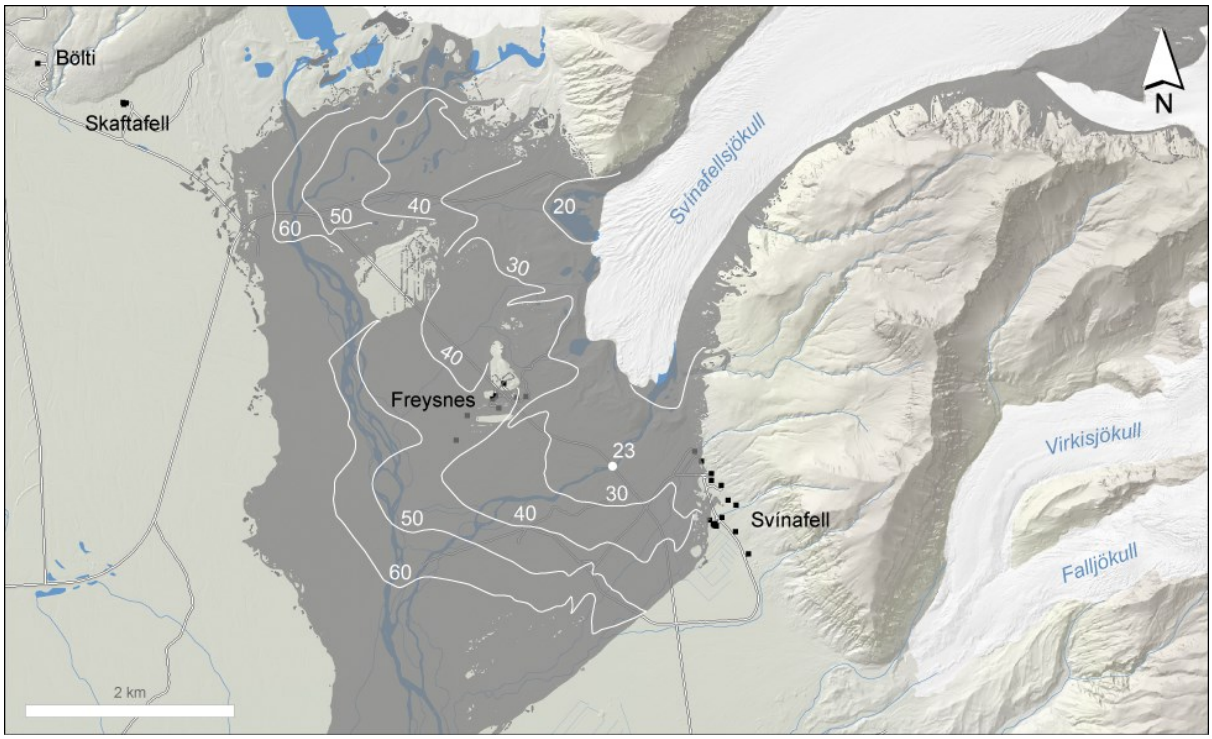

Figure VII-15: Minimum time available for evacuation (10-min isochrones) should a pyroclastic flow density current cause a flood on the slopes of Svínafellsjökull Glacier. Maximum discharge attained at onset of supraglacial flow ($t_{Q_{max}} = 0$) is used as an assumption. Inundation extent in the proglacial area is shown as a grey overlay.

3. Time required for evacuation

The notions of required safe exit time (RSET) and total evacuation time (TET) were used as expressions of the time required for evacuation. Devised by the community of fire safety engineers for timeline modelling of building evacuation (Pauls, 1980), the two notions are also used in the modelling of flood evacuation.

RSET refers in this study to the minimum time required, from departure nodes to fixed exits points placed on the National road (Table VII-3, Figure VII-16), for evacuating the proglacial terrains facing the Öræfajökull glacier catchments, including areas identified at risk of flooding in the numerical simulations performed by Helgadóttir *et al.* (2015) and adjacent terrains. The departure nodes considered in the analysis correspond to residences, accommodations premises, and the main visiting sites whose access points on the National road are located within the exit points. Although having one of its access points safely accessible in the eventuality of floods caused by an eruption of Öræfajökull Volcano, Skaftafell was included in the analysis for informative purpose.

Table VII-3: Exit points used for RSET and TET computations.

Exit points	General location	Latitude	Longitude
W1	Skaftafell	63,99064	-16,95626
E1	Kvísker	63,97284	-16,42029
E2	Jökulsárlón	64,04605	-16,17743

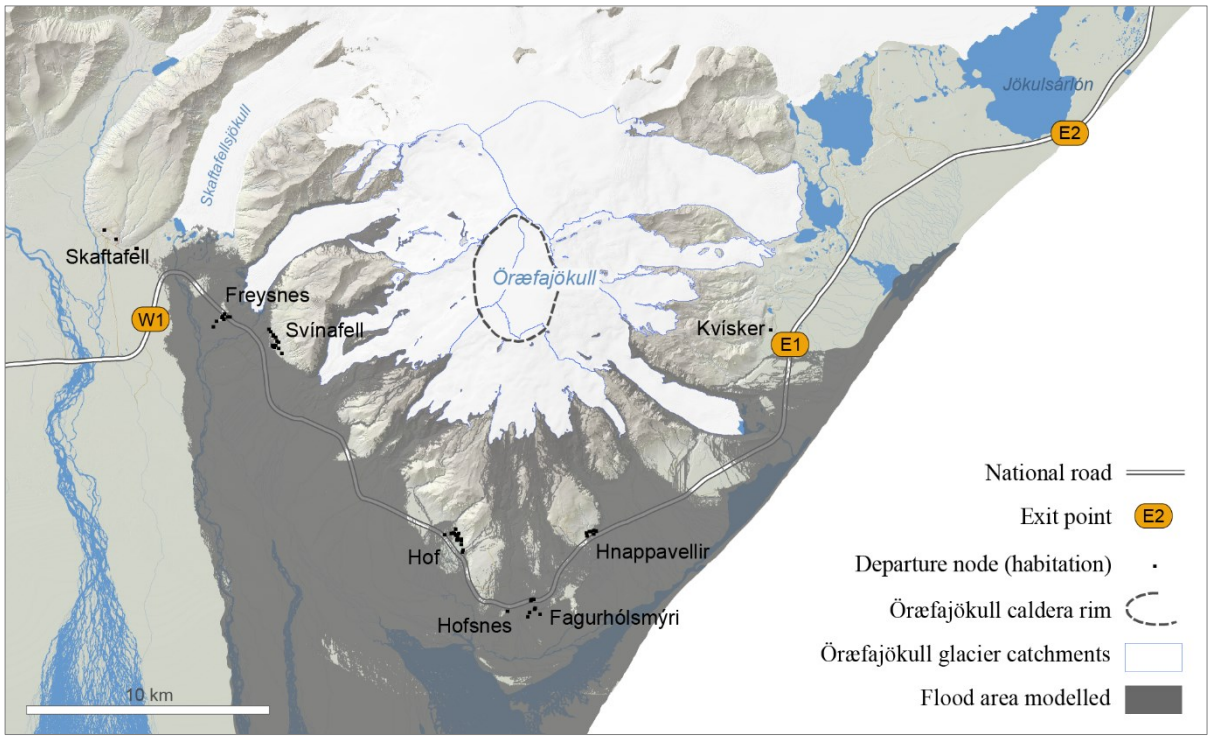

Figure VII-16: Exit points used in the estimation of required safe exit time, using the National road as a way out. Extent of the flood area is after Helgadóttir et al. (2015).

From each departure node, RSET was quantified as following:

$$RSET = RT + WT + TT$$

where RT is the response time before departure, WT the waiting time after the first element of the vehicle queue has left until the last element of the queue moves on, and TT the average travel time to exits points.

TET refers in this study to the minimum time necessary for the complete evacuation of the areas found within the exit points and should be regarded in this regard as equalling the highest of the RSET values:

$$TET = \max\{RSET_1, \dots, RSET_n\}$$

3.1. Response time before departure

Response time before departure represents in this study the time effectively spent before evacuees are ready to leave. It does include the duration of the recognition phase, i.e. the time necessary for understanding the necessity of evacuating, also termed warning acceptance factor and characterised by response inertia (Opper *et al.*, 2010), and the time effectively needed for preparation upon acceptance.

Duration of the recognition phase is likely to vary between residents and tourists, as these two populations often show different levels of awareness and knowledge of the ongoing and forthcoming events (Bird *et al.*, 2010).

For convenience, response time before departure was fixed to a 15-minute average.

3.2. Waiting time at departure

Waiting time, which is defined as the time elapsed, at departure nodes, after the first element of the vehicle queue has left until the last element of the queue moves on, was quantified using travel demand estimates and a time interval between each vehicle of the queue.

The time interval between each vehicle of the queue was fixed to a minimum of three seconds, which correspond, in optimal weather conditions, to the rounded up safe following time between vehicles (Knipling *et al.*, 1993). Travel demand was determined as the number of vehicles available for evacuation at each departure node, using estimations on the number of evacuees therefrom and estimates on the number of evacuees per vehicle.

3.2.1. Number of evacuees

Night-time exposure estimates proposed by Pagneux (2015) were used to quantify the minimum and maximum number of evacuees — residents or transients (all non-residents, such as tourists and seasonal workers, etc.) — at each departure node. Minimum figures correspond to the winter visiting respite, when residents form the main body of evacuees, while maxima correspond to the summer seasonal peak, when tourists represent a factor-9 increase of the local population (Pagneux, 2015).

3.2.2. Passengers per vehicle

There is little information available to support an estimation of the likely number of passengers per vehicle. Road traffic survey made in Berufjörður during the summer 2008 (Brynjarsson, 2009) suggests an average of 2 passengers per vehicle, without further discrimination between individual cars and passenger vehicles of a capacity >9 individuals.

In the present case, averages of 2–3 passengers for individual cars and 20–25 passengers for buses were used (Table VII-4). For each departure node, deciding on the number of passengers per vehicle was based on whether evacuees are residents or transients, and whether accommodation premises at which transients can be found offer enough beds to host groups travelling by bus.

Table VII-4: Number of passenger per vehicle, based on the type of population and of accommodation premise.

Population	Beds	car	bus
Residents		2–3	-
Accommodation premises	No group capacity	2–3	-
Accommodation premises	Group capacity	2–3	20–25

3.2.3. Computed travel demand

A maximum travel demand ranging 230–335 vehicles was found at departure nodes having access to the National road between the exit points W1 and E2 (Table VII-5). At locations where the contingent of evacuees is dominated by transients, the maximum demand was estimated to be oscillating between 25–40 vehicles (Svínafell) and 125–185 vehicles (Skaftafell). A maximum demand < 5 vehicles was found at locations where the contingent of evacuees is only made of residents.

3.2.4. Waiting time estimates

Analysing together the travel demand estimates and the time interval between vehicles (three seconds) gave a maximum waiting time < 1 minute at locations where the contingent of evacuees is only made of residents (Table VII-6). At nodes where the contingent of evacuees is dominated by non-residents (Skaftafell, Freysnes, Hof, Svínafell), minimum waiting time was estimated <2 minutes and maximum waiting time ranging 2–9 minutes.

Table VII-5: Maximum travel demand (number of vehicles) at departure nodes, based on night-time exposure figures from Pagneux (2015) and passenger-per-vehicle estimates. The share of evacuation by bus and by individual car is highly tentative.

Departure node	Transients, as maximum share of overall population			maximum travel demand (number of vehicles)
	All (%)	thereof by bus (%)	thereof by car (%)	
Skaftafell, Bölti	99.6	20	80	125 – 185
Freysnes	80.5	49	51	25 – 45
Svínafell	82	25	75	25 – 40
Hof, Litla Hof	84	17	83	40 – 55
Hofsnes	0	-	-	< 5
Fagurhólsmýri, Fagurhólar	0	-	-	< 5
Hnappavellir	0	-	-	< 5
Kvísker	0	-	-	< 5
Total				230 – 335

Table VII-6: Waiting time at departure nodes based on minimum/maximum travel demand and minimum time interval between vehicles (Safe following distance). Time values are rounded to the highest integer.

Departure node	Time interval between vehicles (seconds)	Travel demand		Waiting time (min.)	
		min	max	min	max
Skaftafell, Bölti	3	< 5	185	1	9
Freysnes	3	< 10	45	1	2
Svínafell	3	< 10	40	1	2
Hof, Litla-Hof	3	< 10	55	1	3
Hofsnes	3	< 5	< 5	1	1
Fagurhólsmýri, Fagurhólar	3	< 5	< 5	1	1
Hnappavellir	3	< 5	< 5	1	1
Kvísker	3	< 5	< 5	1	1

3.3. Average travel time to exit points

Average travel times between departure nodes and exit points were determined as the sum of average running times on road segments in optimal weather conditions and stopping times at network access points (Fitzpatrick *et al.*, 2003).

Every road segment was attributed an average running time, defined as the length of the segment considered divided by the average running speed at which a normalised vehicle traverses the segment. A normalised vehicle is defined here as every motorised vehicle — car, bus, or motorcycle — capable of reaching at least the highest mandatory or posted speed limits. Running time refers to the time a normalised vehicle spend in motion, and was estimated in this study using fixed average running speeds (Table VII-7) obtained from a combined analysis of available information on regulatory or posted speed limits (IRCA, 2010) and types of roads, including type of surface, terrain, road curvatures, segment lengths, lane widths, and bottlenecks dimensions. Stopping times, i.e. the time spent on stopping at access points and bottlenecks, was taken into account by applying a 10-percent pejoration to the average running times.

3.3.1. Types of roads

Three types of roads, either public or private, are found in the study area: C, D, and F (NLSI, 2012). Type C corresponds to double-lane roads ranging 6.5–10 metres in width, type D corresponds to single-lane roads with shoulders and types F1, F2, and F3 corresponds to mountain roads (IRCA, 2014). Surface of types C and D, which are developed on fills and are found on flat terrains, is of asphalt or compacted gravel. Mountain roads are found on flat or hilly terrains and usually entail the land surface.

3.3.2. Bottlenecks

No less than 20 bridges are present on the 85 km of the National road's stretch laying between Lómagnúpur to the west and Jökulsárlón proglacial Lagoon to the east. Half of them are single-lane structures measuring 3.2– 4.2 in width, the longest of them, on the Skeiðará river, measuring 880 m (IRCA, 2011; Figure VII-17).

The seven single-lane bridges located in the area identified at risk of flooding should an eruption of Öræfajökull volcano happen (Helgadóttir *et al.*, 2015) are not long enough to impact significantly on running speeds and travel times. In turn, any accident on the Skeiðará Bridge has the potential to interrupt totally road traffic as exemplified by the June 26 2013 event, when the bridge was closed

for more than one hour as a vehicle was stuck on the lane. Two other accidents, in 2004 and 2011, led to close the bridge temporarily. As the bridge is only 4.4 km away from the flood hazard zone identified by Helgadóttir *et al.* (2015), any closure would hinder, in the west direction, evacuation of the areas exposed to volcanogenic floods. Disuse of the Skeiðará Bridge has been planned by the Icelandic Road and Coastal Administration and will become effective upon completion, upstream, of a 70 m long double-lane bridge expected to open to traffic in the fall 2016 (Rögnvaldur Gunnarsson, personal communication). Any evacuation of the Öræfi district will certainly benefit from these improvements to the road local infrastructure.

Table VII-7: Average running speeds estimation (range) for road types C, D, and F.

Type	Description	Average running speed (range, in km/h)	Surface	Terrain
C	Double-lane road 6.5 ≤ full width ≤10 m	10 – 90	Asphalt or gravel	Flat
D	Single-lane road with shoulders	10 – 80		
F1	Mountain road	10 – 30	Earth	Flat or hilly
F2	Mountain road	10 – 20		
F3	Mountain road	10		

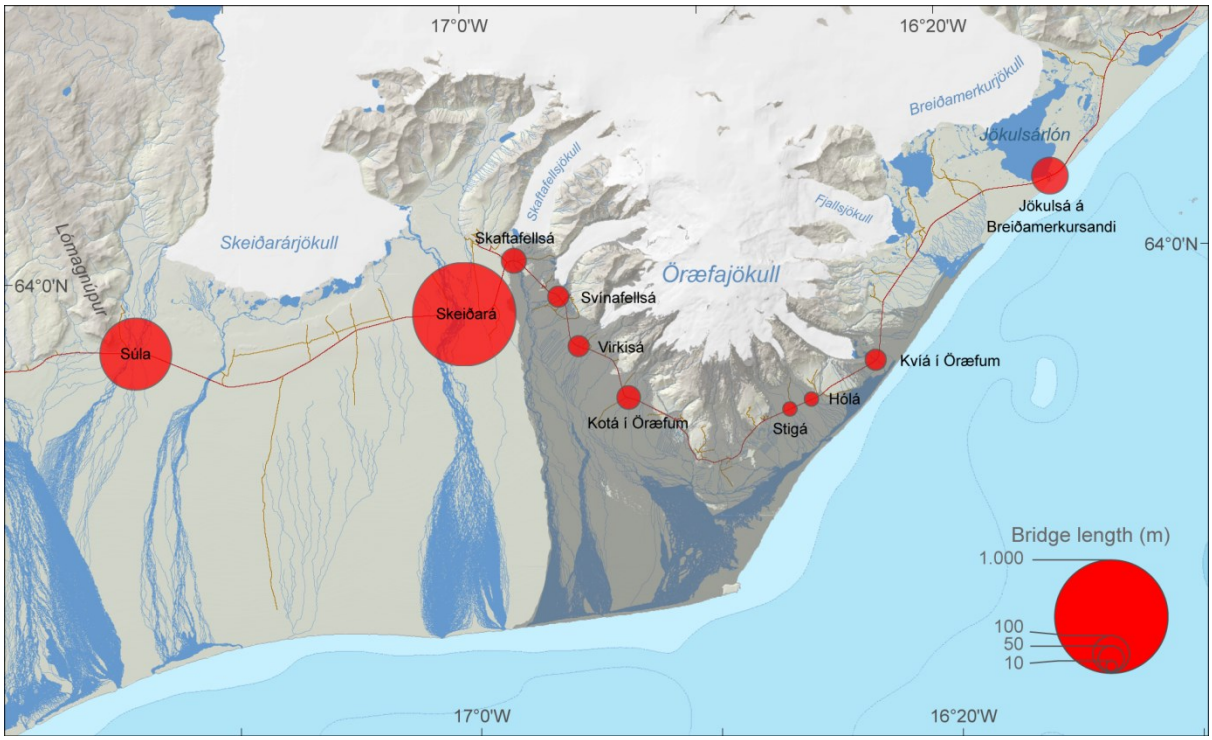

Figure VII-17: Single-lane bridges (red-filled circles) located on the Lómagnúpur - Jökulsárlón National road's segment (Source: IRCA, 2011). Seven bridges are located in the area identified at risk of volcanogenic floods (grey area) by Helgadóttir et al. (2015).

3.3.3. Computed travel times

Results of the calculations suggest that in optimal weather conditions, running times should not exceed 27 minutes on the segment W1-E1 and 37 minutes on the segment W1-E2 (Table VII-3, Table VII-8).

With the exception of Bölti and Skaftafell, all the departure nodes were found within a one-minute drive from the National road. Considering together average running times and stopping times, it was found that reaching exit point W1 should not require more than a 20-minute drive (Table VII-9). Average travel times from departure nodes to exits point E1 (Skaftafell and Kvísker excluded) and E2 (Skaftafell excluded) ranged 10–27 minutes and 21–38 minutes respectively.

3.4. Total evacuation time

Based on the sum of response time, waiting time and travel times, it appears that in optimal weather conditions, the area enclosed between exit points W1 and E1 is unlikely to be fully evacuated in less ~30 minutes (Table VII-10). A full evacuation of the area enclosed between exit points W1 and E2 should not take less than ~35 minutes.

The situation is much different from one departure node to the other. Required safe exit time was estimated to a minimum of 20 minutes from Freysnes to the nearest exit point, 32 minutes from Hof and 29 minutes from Hofsnes (Table VII-10). Similarly, evacuation from Hnappavellir to exit point E1 would take a minimum of 29 minutes, extended to 36 minutes should evacuees be required to reach exit points E2 or W1.

Table VII-8: Segments lengths, average running speeds and average running times between exits points. Values are rounded to the nearest integer.

Road segment	Segment length (km)	Average running speed (km/h)	Average running times (min.)
W1 – E1	39	88	27
E1 – E2	15	89	10
W1 – E2	54	89	37

Table VII-9: Average travel times (min.) from departure nodes to exits points W1, E1, and E2. Values are rounded to the nearest integer.

Departure node	W1	E1	E2
Skaftafell, Bölti	7	-	-
Freysnes	3	27	38
Svínafell	5	26	38
Hof, Litla-Hof	14	17	29
Hofsnes	16	14	25
Fagurhólsmýri, Fagurhólar	18	13	25
Hnappavellir	20	10	21
Kvísker	-	-	11

Table VII-10: Required safe exit times (min.), in optimal weather conditions, from departure nodes to exit points W1, E1 and E2. Values are rounded to the nearest integer.

Departure node	Exit point W1		Exit point E1		Exit point E2	
	Min	Max	Min	Max	Min	Max
Skaftafell, Bölti	24	32	-	-	-	-
Freysnes	19	20	43	44	53	54
Svínafell	21	22	42	43	53	54
Hof, Litla-Hof	30	32	33	35	44	45
Hofsnes	32	32	29	29	39	39
Fagurhólsmýri, Fagurhólar	33	33	29	29	39	39
Hnappavellir	36	36	26	26	36	36
Kvísker	47	47	-	-	27	27

As an optimal time interval of three seconds between vehicles was used (Table VII-6), seasonal changes in travel demand were found of little impact on evacuation time (Table VII-10). Any change to worse weather conditions could lead not only to a reduction of average running time but also to an increase of the safe following distance, giving incidentally more weight to seasonal patterns in travel demand. For instance, increasing the time interval between vehicles to six seconds — the recommended safe following interval in rainy conditions — would lead to a 10-minute increase for completing evacuation of Skaftafell during the summer peak.

A detailed assessment of the spatial distribution of residents and transients during daytime, comparable to what was made in Pagneux (2015) for night time exposure, is not available at present. Experience suggests that during the visiting season, the vast majority of the population can be found by day on and around the two sites of Skaftafell and Jökulsárlón, which are both located beyond the flood risk area identified in Helgadóttir *et al.* (2015). On that basis, it is reasonable to think that the population located in the areas at risk of flooding is not as important during daytime as it is during night-time. It is unlikely, however, to find at any hour of the day a departure node empty of evacuees.

4. Evacuation routes

Estimates on required safe exit times (see §2) were used to determine the shortest routes evacuees should follow, from departure nodes to the nearest exit point on road segments W1-E1 and W1-E2. The National road was divided in two routes, here referred to as the "western" and "eastern" routes.

4.1. Road segment W1-E1

Evacuees from Hof, Svínafell, and Freysnes would be required to drive west to exit point W1 (Table VII-11, Figure VII-18). E1 would be in turn the nearest exit point for evacuees located in Hofsnes, Fagurhólsmýri, and Hnappavellir. The evacuation route divide is located between the Hof and Hofsnes settlements (Figure VII-18).

4.2. Road segment W1-E2

Evacuees from Fagurhólsmýri, Hofsnes, Hof, Svínafell, and Freysnes would be required to drive west to exit point W1 (Table VII-12, Figure VII-19). E2 would be the nearest for evacuees located at Kvísker. As the evacuation route divide is located by Hnappavellir, evacuees therefrom could equally drive east or west.

Table VII-11: Required safe exit time (RSET) from departure nodes to nearest exit point on road segment W1-E1.

Departure node	Nearest exit point	RSET (min.)
Freysnes	W1	19 – 20
Svínafell	W1	21 – 22
Hof, Litla Hof	W1	30 – 32
Hofsnes	E1	29
Fagurhólsmýri, Fagurhólar	E1	29
Hnappavellir	E1	26

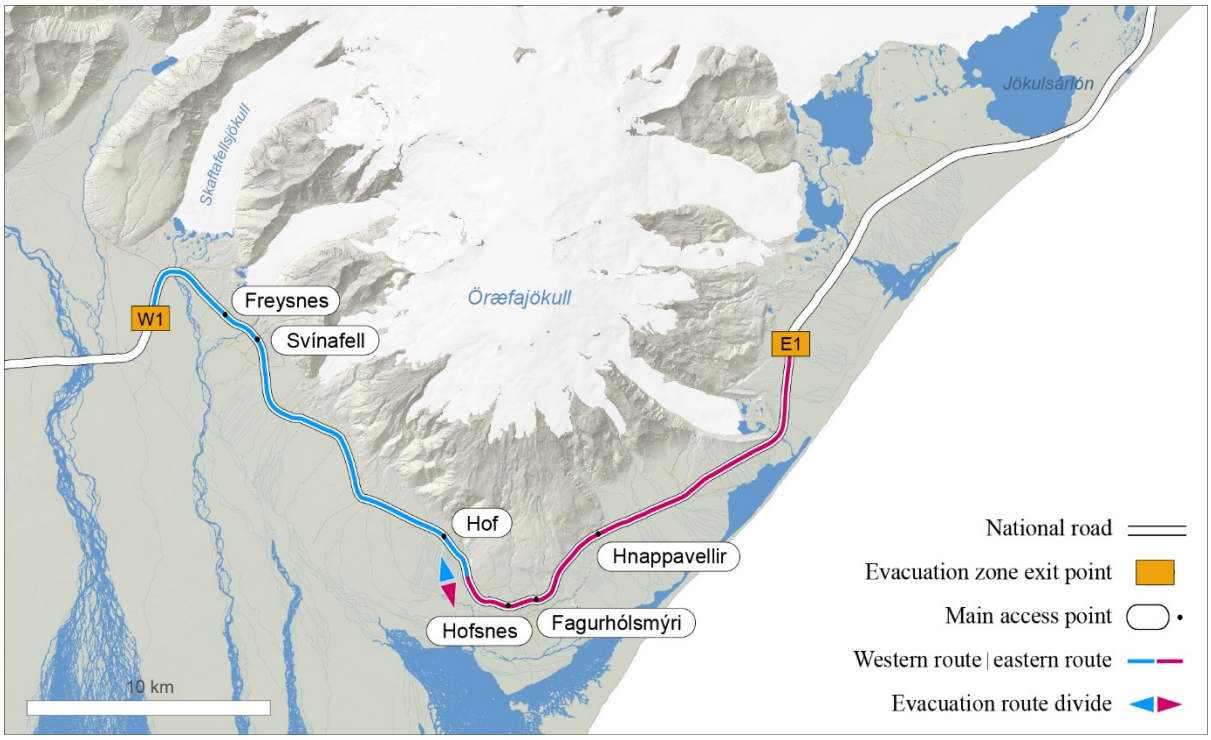

Figure VII-18: Routing of evacuation between W1 and E1 exit points.

Table VII-12: Required safe exit time (RSET) from departure nodes to nearest exit point on road segment W1-E2.

Departure node	Nearest exit point	RSET (min.)
Freysnes	W1	19 – 20
Svínafell	W1	21 – 22
Hof, Litla Hof	W1	30 – 32
Hofsnes	W1	32
Fagurhólsmýri, Fagurhólar	W1	33
Hnappavellir	W1, E2	36
Kvísker	E2	27

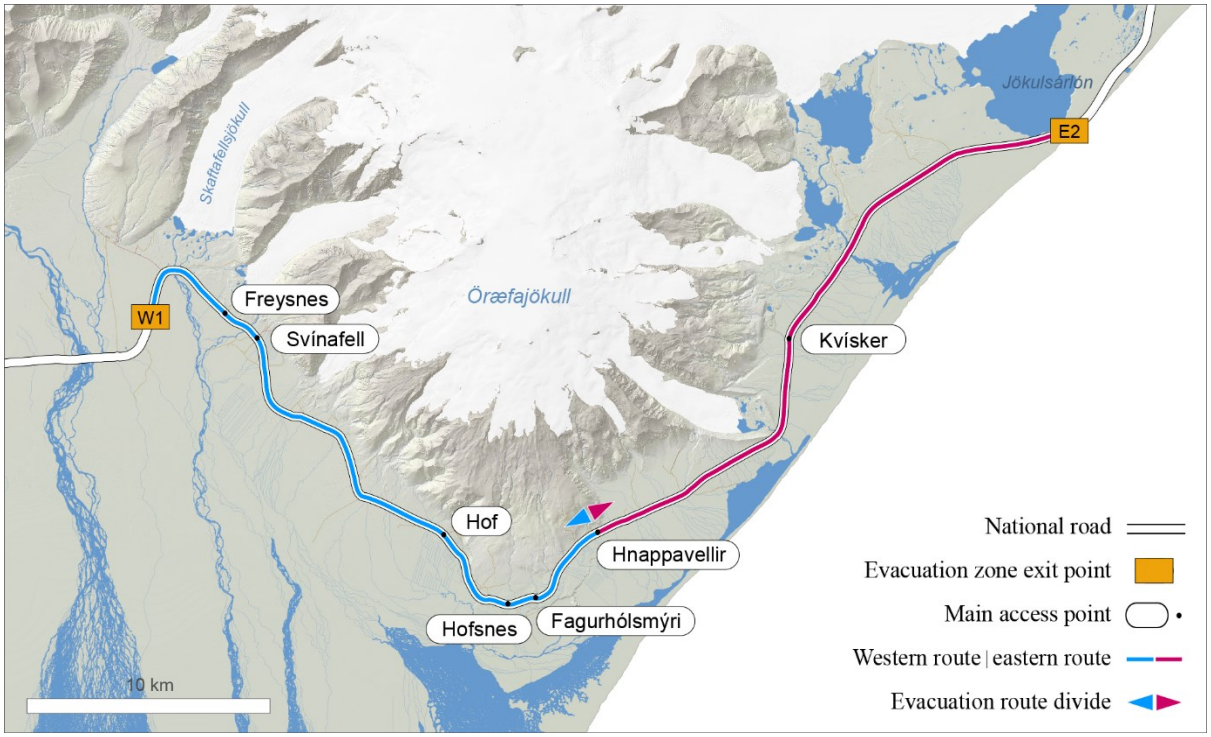

Figure VII-19: Routing of evacuation between W1 and E2 exit points.

5. Shelters

The results indicate that the time required exceeds, at eruption onset, the time actually available for a full evacuation of the areas at risk of flooding. Therefore, achieving partial or full evacuation of these areas before eruption onset may be regarded as a desirable objective. It corresponds, however, to an ideal situation where information necessary to order and secure evacuation ahead of an eruption is at hand. A situation where evacuation does not take place before an eruption starts cannot be excluded and, therefore, the possibility of sheltering in place the population that cannot evacuate in time should be considered by the authorities. Such a possibility is not investigated in this study.

6. Summary and conclusion

The time available and the time required for evacuating areas exposed to floods caused by eruptive activity of Öræfajökull Volcano was assessed, and evacuation routes determined.

Estimations on time availability were made at onset of a volcanic eruption initiated in the caldera or on the flanks of the volcano, and at onset of pyroclastic density currents. The melting scenarios elaborated by Gudmundsson *et al.* (2015), and the results of the numerical simulations performed accordingly by Helgadóttir *et al.* (2015) were used to this end. Estimation of the time required for the evacuation was quantified as the sum of response time before departure, waiting time at departure nodes, and average travel times from departure nodes to fixed exits points marking the boundaries of areas to be evacuated. Night-time exposure estimates proposed by Pagneux (2015) were used to quantify the minimum and maximum number of evacuees — residents or guests — at each departure node.

Results of the modelling suggest that areas at risk of flooding are unlikely to be successfully evacuated once an eruption has started. It was found that the National road – the only terrestrial axis of evacuation existing at present, could be flooded at multiple locations within the range of 20–30 minutes at onset of a volcanic eruption in the caldera or on the flanks (Figure VII-9 to Figure VII-12), and within 15–25 minutes at onset of a

pyroclastic density current (Figure VII-13 to Figure VII-15). In the meantime, it was found that in optimal weather conditions, a full evacuation could not be achieved in less than 30–35 minutes (Table VII-10).

As the time required for a full evacuation of the areas at risk of flooding exceeds, at eruption onset, the time actually available for the evacuation, it is crucial to rely on early precursors of volcanic activity and have the areas evacuated before eruption start. As the possibility of an eruption starting before any evacuation is initiated cannot be excluded, the feasibility of sheltering in place the populations that cannot evacuate timely should also be considered. This has to be thought of carefully, as sheltered people may no longer have the possibility to escape the district after the floods, and therefore be severely exposed to the other primary volcanic hazards that will certainly follow, such as tephra fall and lightning.

7. Acknowledgements

The author would like to thank Ágúst Gunnar Gylfason and Magnús Tumi Gudmundsson for their support during the framing of this work. Ásdís Helgadóttir, Haraldur Sigþórsson and Tómas Jóhannesson are thanked for their review and proof-reading of the chapter.

The present work was funded by the Icelandic Avalanche and Landslide Fund, the National Power Company, and the Icelandic Road and Coastal Administration.

8. References

Bird, D. K., Gísladóttir, G., & Dominey-Hoves, D. (2010). Volcanic risk and tourism in southern Iceland: Implications for hazard, risk and emergency response education and training. *Journal of Volcanology and Geothermal Research, 189*, 33–48.

Brynjarsson, F. (2009). *Berufjörður. Umferðarkönnun 17. og 19. júlí 2008 (Berufjörður: July 17–19 2008 traffic survey).* Icelandic Road and Coastal Administration. Reykjavík: Icelandic Road and Coastal Administration.

Fitzpatrick, K., Carlson, P., Brewer, M., & Wooldridge, M. D. (2003). *Design speed, operating speed, and posted speed practices.* Washington D.C.: Transportation Research Board of the National Academies.

Gudmundsson, M. T., Högnadóttir, Þ., & Magnússon, E. (2015). Öræfajökull: Eruption melting scenarios. In E. Pagneux, M. T. Gudmundsson, S. Karlsdóttir, & M. J. Roberts (Eds.), *Volcanogenic floods in Iceland: An assessment of hazards and risks at Öræfajökull and on the Markarfljót outwash plain* (pp. 45–72). Reykjavík: IMO, IES-UI, NCIP-DCPEM.

Gudmundsson, M. T., Larsen, G., Höskuldsson, Á., & Gylfason, Á. G. (2008). Volcanic hazards in Iceland. *Jökull*, 58, 251–258.

Helgadóttir, Á., Pagneux, E., Roberts, M. J., Jensen, E. H., & Gíslason, E. (2015). Öræfajökull Volcano: Numerical simulations of eruption-induced jökulhlaups using the SAMOS flow model. In E. Pagneux, M. T. Gudmundsson, S. Karlsdóttir, & M. J. Roberts (Eds.), *Volcanogenic floods in Iceland: An assessment of hazards and risks at Öræfajökull and on the Markarfljót outwash plain* (pp. 75–102). Reykjavík: IMO, IES-UI, NCIP-DCPEM.

IRCA (2010). *Þjóðvegir í þéttbýli. Leiðbeiningar 2010 (National roads intersecting urban areas. Guidelines 2010).* Icelandic Road and Coastal Administration.

IRCA (2011). *Brúaskrá. Brýr á þjóðvegum (Bridge Register. Bridges on the National road).* Retrieved 5 5, 2014, from http://www.vega-gerdin.is/Vefur2.nsf/Files/Bruaskra-a-thjodv/$file/Bruaskra-a-tjodvegum.pdf

IRCA (2014). *Vegtegundir (Road types).* Retrieved 5 5, 2014, from http://www.vegagerdin.is/vega-kerfid/vegtegundir

Knipling, R., Mironer, M., Hendricks, D., Tijerina, L., Everson, J., Allen, J., & Wilson, C. (1993). *Assessment of IVHS countermeasures for collision avoidance.* US Department of Transportation. Washington: National Highway Traffic Safety Administration.

Mileti, D., Bolton, P., Fernandez, G., & Updike, R. (1991). *The eruption of Nevado del Ruiz Volcano Colombia, South America, November 13, 1985.* (Commission on Engineering and Technical Systems, Ed.) Washington D.C.: National Academy Press.

NLSI (2012). IS 50V Geodatabase. (version 3.4). National Land Survey of Iceland.

Opper, S., Cinque, P., & Davies, B. (2010). Timeline modelling of flood evacuation operations. *Procedia Engineering, 3*, 175–187.

Pagneux, E. (2015). Öræfi district and Markarfljót outwash plain: Spatio-temporal patterns in population exposure to volcanogenic floods. In E. Pagneux, M. T. Gudmundsson, S. Karlsdóttir, & M. J. Roberts (Eds.), *Volcanogenic floods in Iceland: An assessment of hazards and risks at Öræfajökull and on the Markarfljót outwash plain* (pp. 123–140). Reykjavík: IMO, IES-UI, NCIP-DCPEM.

Pagneux, E., & Roberts, M. J. (2015). Öræfi district and Markarfljót outwash plain: Rating of flood hazards. In E. Pagneux, M. T. Gudmundsson, S. Karlsdóttir, & M. J. Roberts (Eds.), *Volcanogenic floods in Iceland: An assessment of hazards and risks at Öræfajökull and on the Markarfljót outwash plain* (pp. 101–122). Reykjavík: IMO, IES-UI, NCIP-DCPEM.

Pauls, J. (1980). Building evacuation: research findings and recommendations. In D. V. Canter (Ed.), *Fires and human behaviour* (pp. 251–276). Chichester: J. Wiley.

Roberts, M. J., & Gudmundsson, M. T. (2015). Öræfajökull Volcano: Geology and historical floods. In E. Pagneux, M. T. Gudmundsson, S. Karlsdóttir, & M. J. Roberts (Eds.), *Volcanogenic floods in Iceland: An assessment of hazards and risks at Öræfajökull and on the Markarfljót outwash plain* (pp. 17–44). Reykjavík: IMO, IES-UI, NCIP-DCPEM.

Thorarinsson, S. (1958). The Öræfajökull eruption of 1362. *Acta Naturalia Islandica, 2*(4), 100.

Vogfjörd, K. S., Jakobsdóttir, S. S., Gudmundsson, G. B., Roberts, M. J., Ágústsson, K., Arason, T., Geirsson, H., Karlsdóttir, S., Hjaltadóttir, S., Ólafsdóttir, U., Thorbjarnardóttir, B., Hafsteinsson, G., Sveinbjörnsson, H., Stefánsson, R., and Jónsson, T. V. (2005). Forecasting and monitoring a subglacial eruption in Iceland. *EOS, 86*(26), 245–248.

Voigt, B. (1990). The 1985 Nevado del Ruiz volcano catastrophe: anatomy and restrospection. *Journal of Volcanology and Geothermal Research, 44*, 349–386.

Zobin, V. M. (2011). *Introduction to Volcanic Seismology* (2nd ed.). Amsterdam: Elsevier Science.

Volcanogenic floods in Iceland
An assessment of hazards and risks at Öræfajökull and on the Markarfljót outwash plain

Icelandic Meteorological Office
Bústaðavegur 7–9
108 Reykjavik
Iceland
Web: en.vedur.is
Tel.: +354 522 6000

Institute of Earth Sciences, University of Iceland
Sturlugata 7
101 Reykjavik
Iceland
Web: earthice.hi.is
Tel.: +354 525 4492

National Commissioner of the Icelandic Police
Department of Civil Protection and Emergency Management
Skúlagata 21
101 Reykjavik
Iceland
Web: almannavarnir.is
Tel.: +354 444 2500

Front-cover photograph: Glacial outburst flood caused by summit eruption of Eyjafjallajökull Volcano on April 14 2010 © Haukur Hlíðkvist Ómarsson

ISBN 978-9979-9975-7-3